Università degli Studi del Piemonte Orientale

"Amedeo Avogadro"

Department of Pharmaceutical Sciences

Ph.D. in **Chemistry and Biology**

XXXII cycle 2016-2019

Involvement of ionic channels in chemically-induced neurotoxicity: examples of different molecular mechanisms

SSD Bio 09

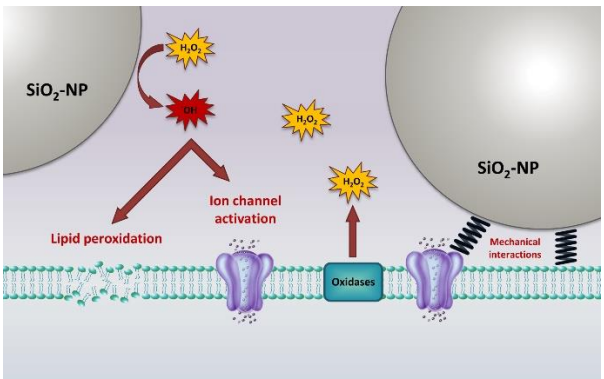

DOTTORANDA

MARIANNA DIONISI

TUTOR

PROF. CARLA DISTASI

COORDINATORE DEL DOTTORATO

PROF. LUIGI PANZA

Contents

Chapter 1

Introduction

Neurotoxicity is defined as "an adverse change in the structure or function of the nervous system that results from exposure to a chemical, biological or physical agent"[1]. This is a very general term that includes the wide variety of adverse effects elicited by an external agent acting directly on the central nervous system (brain, spinal cord, optic nerves), and/or on the peripheral nervous system (motor, sensory and/or autonomic components and end organs), and/or indirectly via peripheral organs[1]. The objective of the research project I pursued during my PhD training was the study of possible molecular targets and mechanisms involved in two specific cases of neurotoxicity, widely documented but not completely understood: 1) the potential neurotoxicity induced by Silica Nanoparticles (SiO_2) and 2) the Oxaliplatin (OHP)-induced neurotoxicity.

1.1 Nanoparticles and potential neurotoxicity

Nanomaterials (NMs) are defined as materials having at least one dimension in the range of 1–100 nm. Based on their structure, nanomaterials can be categorized into: 1) zero-dimensional (nanoparticles and quantum dots); 2) one-dimensional

(nanofibers, nanotubes, and nanowires); 3) two-dimensional (graphene and graphene oxide); and 4) three-dimensional nanomaterials, generally known as bulk nanomaterials, which consist of equiaxed nanometer sized grains, and characterized by three arbitrary dimensions which are not confined to the nanoscale. In this context, it should be noted that these categories are not so restrictive and some materials can be positioned on the margin of two of these categories[2].

The International Organization for Standardization (ISO) has defined Nanoparticles (NPs) as nano-objects with all three external dimensions in the nanoscale (https://www.iso.org/standard/51240.html). These NPs can differ in sizes and shapes (such as spheres, cylinders, cubes, triangles, rings, or disks with various dimensions) and for nature (organic, inorganic and carbon based).

At the nanoscale, the inorganic matter present chemical and physical properties that are not present when the same materials are analyzed at a micro-macroscopic scale. The increased surface area, optical properties (such as quantum effects and increased absorption efficiency), uniformity, quantum confinement (a phenomenon that causes spontaneous properties of semi-conductivity) and increased reactivity are just some example of the most important properties acquired[2].

These findings are the reason of the increasing applications of engineered NPs. NPs have been successfully applied not only to traditional manufacturing (i.e. catalysis, energy, electronics, cosmetics and personal care products), but also to emerging pharmaceutical and biomedical fields (I.e. imaging, diagnosis, drug delivery, and cancer immunology)[3].

However, the expansion of the use of NPs has raised great public attention because of potential toxicity concerns in animals and humans. Being their dimensions

comparable to those of common subcellular and molecular structures from biological material, this fact allows NPs to interact with tissues and cells and to induce unknown and/or not always well understood alterations of their functions[4]. The main cellular entrance routes are endocytosis based, and usually these require the activation of a trigger according to the cellular machinery involved in the internalization processes [5]. However, recent reports are available regarding a direct permeation of NPs through plasma membrane[6,7].

The plasma membrane represent the first site of interaction between nanoobjects and the cell before any internalization process is initiated. Therefore, the highly organized lipids and proteins of which it is composed are likely targets. In neurons (and glial cells), the main modulators of neuronal activity and of its changes in responses to external stimuli are located in the plasma membrane. It is therefore to be expected that in these tightly regulated and highly responsive cells, NPs can induce significant and potentially damaging effects by interfering with transporters and channels, receptors for neurotransmitters and neurohormones [4].

While a significantly expanded literature, especially in the last decade, on potential toxicity induced by NPs on living beings is available, the amount of data about harmful effects on central nervous system (CNS) still remains less abundant than on other tissues[4].

SiO_2 NPs

Amorphous silica powders, conversely to crystalline forms, are considered biocompatible and thus they are widely used in a large range of industrial applications, from food to catalysis. Depending on which kind of application is

considered, the size range of the powder particles can vary and, in some cases, may also include a fraction of nanometric particles[8].

Stober was the pioneer in developing a system of chemical reactions for the synthesis of spherical monodisperse micron size silica particles. From then on, the method is known as “Stober synthesis”. Many modifications have constantly been added to the Stober synthesis to yield monodisperse, ordered, nanosized silica particles. Manipulating the reaction parameters resulted in particles with different shapes and sizes, produced ad hoc to be used in various fields, including nanomedical applications ranging from drug delivery to cell tracking and subcellular imaging. On the basis of the performances required, they can be used as either produced or functionalized at the surface of the object[8,9].

The control of Ca^{2+} homeostasis is a key point for neuronal physiological and pathological processes. Any single step in neuronal function is linked to a tight control of intracellular Ca^{2+} levels and all the mechanisms involved in the regulation of this parameter. For several kinds of nanomaterials, such as Ag, ZnO, TiO_2, hydroxyapatite, quantum dots (QDs), Au and PM10, alterations of intracellular Ca^{2+} concentration $[Ca^{2+}]_i$ have been reported[9].

Although the data for SiO_2 NPs are still more scarce[9], oscillatory and reversible changes in $[Ca^{2+}]_i$ have been observed following perfusion of neuronal cells with the silica NPs[10]. In the same work, even if the NPs could be internalized, and so the intracellular organelles could represent potential targets, the Ca^{2+} imaging data supported the hypothesis of the existence of an influx from the extracellular medium as, apparently, the exclusive Ca^{2+} pathway (Fig. 1). This work suggests that target(s) that mediate the interaction with neurons should also be searched on the plasma membrane, as primary gate for all cellular interactions with the external milieu[10].

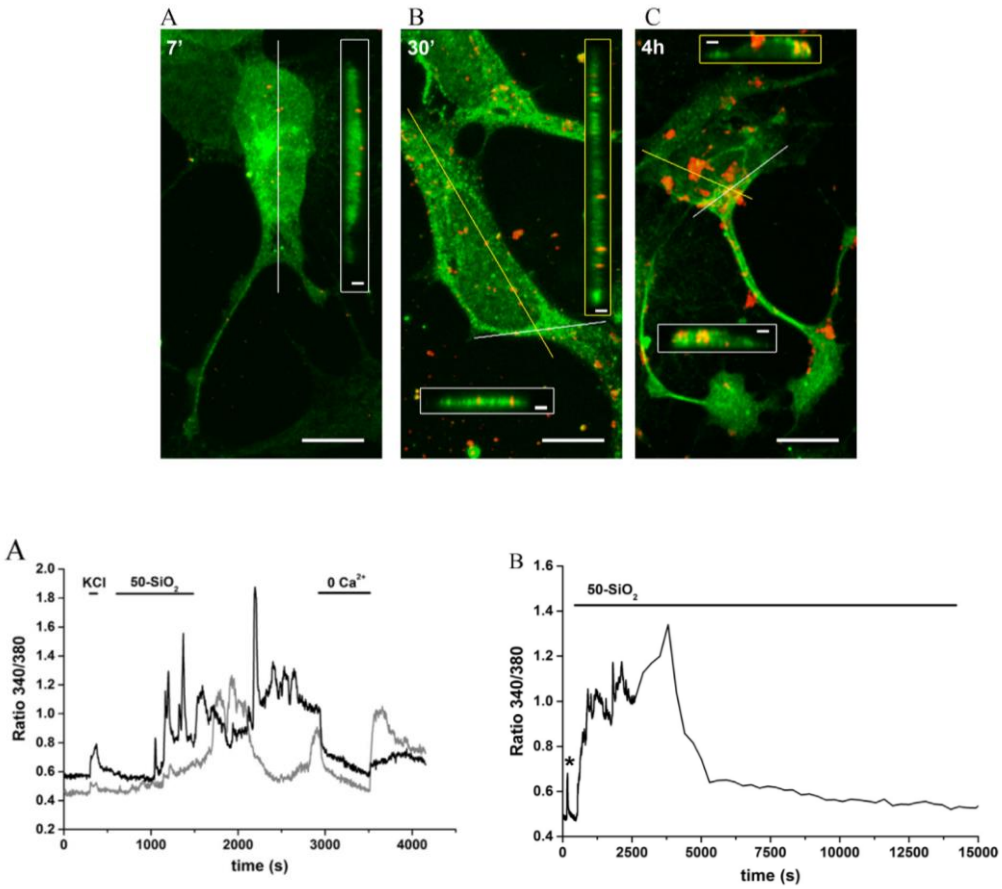

Figure 1. Upper panel. Time course of incorporation of cyanine-doped fluorescent silica NPs into GT1–7 cells. 3D reconstructions of XYZ confocal stacks. Cells were stained with a FITC conjugated with an anti-β-Tubulin III antibody. **Lower panel.** A) Perfusion with an extracellular Ca^{2+}-free solution completely and reversibly abolished the NPs-induced Ca^{2+} signals B) Reversibility of the NPs-induced increases in [Ca2+]i.(adapted from Gilardino *et al.* 2015).

1.2 Chemotherapy-induced peripheral neuropathy (CIPN)

Cancer presents an enormous global disease burden. However, the availability of sensitive tests and diagnostic methods to detect cancer at an early stage and the use of increasingly effective treatments (including chemotherapeutic agents), are improving the cancer survival rates[11].

The antineoplastics commonly used for the treatment of many types of cancers, alone or in combination with surgery and radiation therapy, belong to platinum-based antineoplastics (particularly oxaliplatin (OHP) and cisplatin), vinca alkaloids (particularly vincristine and vinblastine), epothilones (ixabepilone), taxanes (paclitaxel, docetaxel), proteasome inhibitors (bortezomib) and immunomodulatory drugs (thalidomide) (Tab. 1) . However, despite their efficacy, these agents are associated with significant, debilitating and sometimes even devastating side effects. The reduction of chemotherapy doses or even their cessation may be necessary thereby limiting its effectiveness[11,12].

One of the most relevant side effects caused by platinum-based antineoplastic agents is a condition known as chemotherapy-induced peripheral neuropathy (CIPN). Predominant CIPN is characterized by sensory symptoms, which usually develop first, characterized by paresthesias, dysesthesias, tingling and numbness especially in the hands and feet. Pain and sensory abnormalities may persist after the cessation of chemotherapy, in some cases even for years. Frequently, then sensory symptoms, motor and autonomic symptoms (including weakness, cramps, gait dysfunction, sweating abnormalities, constipation, and light-headedness) can also be encountered. The life quality of cancer patients developing CIPN can be profoundly affected. In the most severe cases, CIPN can lead to paresis, complete patient immobilization and severe disability [11].

Table 1. Cancer therapy, mechanism of action and side effects of antineoplastic drugs that induce CIPN, as reviewed in [11,13,14].

Antineoplastics	Cancer therapy	Mechanism of action	Side effects
platinum-based (cisplatin, carboplatin and oxaliplatin)	solid tumors (see Tab. 2)	mitochondrial damage, altered expression and function of ion channels (Na^+, K^+, TRP), activation of microglia and astrocytes	neuroinflammation, altered excitability of peripheral neurons
vinca alkaloids (vincristine, vinblastine, vinorelbine and vindesine)	Hodgkin and non–Hodgkin lymphoma, testicular cancer and non–small cell lung cancer	microtubule disruption, induction of changes of large axons and DRG neurons, attraction and activation of immune cells	neuroinflammation, altered excitability of peripheral neurons
taxanes (paclitaxel, docetaxel and cabazitaxel)	ovarian cancer, breast cancer, non-small cell lung cancer and prostate cancer	microtubule disruption, mitochondrial damage, altered expression and function of ion channels (Na^+, K^+, TRP), activation of microglia and astrocytes	neuroinflammation, altered excitability of peripheral neurons
proteasome inhibitors (bortezomib and carfilzomib)	myeloma and lymphoma	attraction and activation of T-lymphocytes and monocytes, mitochondrial damage, increase in sphingolipid metabolism within astrocytes	neuroinflammation, altered excitability of peripheral neurons
immunomodulatory drugs (Thalidomide)	multiple myeloma	downregulation of TNF-α, inhibition of NF-kB, antiangiogenic effects (inhibition of b-FGF and VEGF)	altered excitability of peripheral neurons

Oxaliplatin-induced peripheral neuropathy

Platinum-based chemotherapeutics are third generation agents widely used for the treatment of several types of solid tumors (Tab. 2) . Among these, OHP is indicated for the treatment of the digestive tract tumor (advanced colorectal, esophageal, stomach, liver and pancreatic cancers)[11].

Essentially, OHP toxicity is associated to the ability of the drug to interact with DNA and to induce alterations able to stop DNA replication and cell cycle, as well as to inhibit the mechanisms of DNA repair and, finally, to induce cell death through apoptosis. In particular, the PlatinumII atom center, released by the drug hydrolysis together with other metabolites (i.e. oxalate), is able to form DNA adducts, intra/inter-strand DNA cross-links and also DNA-protein cross-links. Thus, the DNA double helix structure is completely distorted and the replication is prevented causing an inhibition of proliferation[15].

It is necessary remember that the metal-based molecules, such as OHP and, in general, all platinum-based drugs, are biologically active molecules and, for this reason, they can bind, not only nucleic acids, but also to other important biological entities such as proteins, enzymes and hormones. Thus, they can interfere with the functionality of normal intracellular organelles (particularly mitochondria); influence signalling and neurotransmission by altering intracellular homeostasis and affecting the activity of membrane receptors and ion channels; or cause neuroinflammation by inducing the release of pro-inflammatory cytokines and activating apoptosis[11,15].

Despite OHP shares the typical chronic syndrome with others platinum compounds, during or immediately after its administration, the onset of an acute syndrome has

been observed in the majority of patients (85%–95%). This acute peripheral neurotoxicity, which appears to be unique for OHP treatments, is characterized by an altered cold sensitivity and by a neuronal hyperexcitability that can be resolved in hours or days after the onset[12,16]. Since the acute neurotoxicity rarely causes an early discontinuation of the treatment, mechanistic studies are usually directed to elucidate the chronic form of neurotoxicity. Despite no solid proof of a relationship between the two kinds of neurotoxicity has been given yet, it has been reported that patients with more complicated acute symptoms usually show a more severe type of chronic neurotoxicity[15].

The pathomechanism by which OHP damages the nervous system structures seems to be multifactorial, but the hypothesis concerning its effect on ion channels and Ca^{2+} signalling remains mainly related to the acute form of OHP neurotoxicity. A dysregulation of voltage-gated Na^{+} channels and the alteration of Ca^{2+} signalling seems to be the most accepted explanation. However, the mechanisms at the basis of ion channel dysfunction are not sufficiently clarified[15]. The understanding of the pathogenesis of the acute form OHP neuropathy can not be longer considered a second aim.

Table 2. Cancer therapy, side effects and main mechanisms of neurotoxicity of Platinum-based antineoplastics, as reviewed in [11,12,15].

Platinum-based antineoplastics	Cancer therapy	Side effects	Main Mechanisms of neurotoxicity
Cisplatin	testicular, ovarian, bladder, lung (small-cell and non-small-cell) cancer, sarcomas, solid tumors of head and neck	neurotoxicity (paresthesias and/or numbness in a stocking and glove distribution, sensory ataxia in the most severe cases), nephrotoxicity, ototoxicity, severe nausea and vomiting, mild hematologic toxicity	nuclear DNA damage, mitochondrial DNA damage and oxidative stress
Carboplatin	ovarian, lung, and breast cancer	hematologic toxicity (thrombocytopenia and anemia), neurotoxicity (less frequent and less severe)	nuclear DNA damage, mitochondrial DNA damage and oxidative stress
Oxaliplatin	advanced and metastatic colorectal cancer (in combination with 5-fluorouracil/leucovorin),esophageal, stomach, liver and pancreatic cancers	peripheral neurotoxicity (acute and chronic form), hematologic toxicity (neutropenia, thrombocytopenia), nausea/vomiting, and diarrhea	nuclear DNA damage, mitochondrial DNA damage and oxidative stress, altered calcium homeostasis

1.3 Features facilitating neurotoxicity

The nervous system is organized in networks in which different cell types of many anatomic locations can communicate via electric and chemical signals. The sheer complexity of the system makes it highly vulnerable.

Despite the nervous system is armed with compensating mechanisms, a widespread lesion induced by a given toxicant may correspond to a leak of functional capacity. Especially during development when the basic structures of the brain are forming, a chemical disruption of this tightly regulated process can have profound structural and functional (including behavioral) consequences for life[17].

For this reason, the nervous system is protected by the blood–brain barriers (BBBs). These barriers act effectively to retard the transfer of charged and large molecular weight compounds from circulation to nervous tissue, but do not provide protection to the BBB against lipid soluble agents or toxins that may damage and render porous. Furthermore, there are some regions that are not completely protected by BBB, including areas involved in the neuroendocrine activity (i.e. hypothalamus, pineal), as well as motor and sensory nerve terminals, and thus may represent potential points of entry for toxins[18].

Metabolism and Neuronal Structure

To maintain this extraordinary complexity, the highly differentiated cells of the CNS need a large amount of energy. More in detail, the high metabolic rate required includes the maintaining of the synapses, the restoring of ion gradients across the cell membranes for the generation of action potentials, the synthesis and packaging

of neurotransmitters in vesicles, the axonal transport, and, of course, all the "normal" cell requirements[19].

In comparison to other cell types, neurons have an exceptional cellular morphology with long projections called axons. Whereas most cells are measured in micrometers, neurons can extend their axons and dendrites for millimeters, centimeters, and, in the case of human peripheral nerves up to a meter (their length can exceed the diameter of the cell body by a factor of >100,000)[20,21].

Reflecting the functional heterogeneity presented in neuronal segments, each part of a neuron (dendrites, soma, axon, presynaptic segment) might have quite different energy demands. For this reason, mitochondria, that are thought to arise from the cell soma, are distributed along the cellular body in a more orderly way than in other cells, adapting to the local requirement of energy.

As for others organelles, anterograde and retrograde mitochondrial trafficking is supported by cytoskeletal transport mechanisms primarily by microtubule-based motors—kinesins and dynein[20]. This process, together with the maintaining of neuronal excitability, covers about the 60–80% of the ATP consumption in the CNS. The remaining 10–20% is invested in the neurotransmission, which includes synthesis and packaging of neurotransmitters in vesicles and the transport to presynaptic endings[19]. The high dependence of neurons on oxidative phosphorylation, as the major source of energy, makes them extremely vulnerable to substances that are able to interfere with the mitochondrial respiratory chain[19].

The capacity of some platinum-based chemotherapeutic, such as OHP and cisplatin[15,22], to bind mitochondrial DNA (mDNA) and form mDNA adducts may affect the replication and transcription of mDNA, resulting in the synthesis of abnormal proteins and the following damage on the mitochondrial activity.

Otherwise, the interruption of the respiratory chain function can also derived in an abnormal accumulation of substances inside the mitochondria, as in the case of NPs after the interaction with cells[23–25]. In any case, the impairment of the mitochondrial physiological function is followed by a decrease in the cellular metabolism and, thus, an increase in the production of ROS (reactive oxygen species) that, most likely, reaches the oxidative stress condition, often accompanied by the degeneration of the organelle itself and the inevitable cell death[4,11,26].

Furthermore, neurons are susceptible to any, direct or indirect, impairment to the normal cytoskeleton structure. The stress on the axonal transport system is so high that non-critical perturbations for other cell types can cause degeneration in neurons. It has been reported the role of several kinds of NPs in perturbing the cytoskeletal architecture in cells of the CNS, as observed, for example, for Ag NPs, which affect key cytoskeletal proteins β-tubulin and F-actin in rat cortical neurons [27].

Ion Channels and Neurotrasmission

The proper functioning of ion channels in the membrane is necessary for preserving the neuronal excitability. An elevated active transport maintains unequally distributed the ions on each side of the axonal membrane. In this way, the axonal membrane separates areas of unequal electrochemical potential, generating a resting potential. In this condition, the internal compartment results negative because the majority of Na^+ selective channels are closed and the K^+ selective channels open and close occasionally. However, this situation completely changes

in the presence of a stimulation, during which voltage-dependent Na^+ selective channels start to open making the membrane permeable to mainly Na^+ ions and thus the internal compartment of the cells more positive (depolarization). Right after, Na^+ selective channels start to inactivate and voltage-dependent K^+ selective channels to open, bringing the membrane back to resting levels, ready to restart the generation of another electrical signal. In order to avoid the accumulation of Na^+ (but also Ca^{2+} and Cl^-) in the neuronal cytosol, and of K^+ to the extracellular space, the combination of ATPase (Na^+-K^+ ATPases and Ca^{2+} ATPases) activity and K^+ buffering of astrocytes acts to restore and maintain neuronal excitability. When a nerve impulse reaches a terminal branch of an axon, it depolarizes the synaptic boutons. Here, a second type of transmission by means of the cellular release of special messenger chemicals (neurotransmitters) initiates. The amount of secretion is related to the degree of depolarization, which, in turn, is a function of the number of nerve impulses that reach a synaptic bouton[17]. Thus, any disturbance in the neuronal and glial functioning affects the membrane excitability and, as consequence, the release of neurotransmitters.

Before any internalization process is initiated, the plasma membrane represents the first site of interaction between nanoobjects and cell. Thus, receptors for neurotransmitters and neurohormones, transporters, channels and lipids that composed the plasma membrane, may represent possible targets of this interaction[4]. Large amounts of data support the hypothesis that ionic channels can be modulated in different ways by several kinds of NPs. Among these, there are Na^+, K^+, Ca^{2+} voltage operated channels [28–30], but also members of the highly heterogeneous family of Transient Receptors Potentials channels (TRP)[10], as well as members of large-conductance non-selective channels (i.e. Connexin and Pannexin)[31].

In a similar way, the hyperexcitability observed following a single administration of OHP may be partially induced by the altered action of Na^+ channels (Na_V)[32,33], TRP channels[34,35] and members of the two-pore domain potassium channels K_2P subfamily[36,37], as main players in the transduction of the thermal, chemical and noxious stimuli in the peripheral nervous system.

The BBB

The physical BBB has evolved for preventing the entrance of various toxic compounds in the brain and thus preserving its homeostatic microenvironment. The BBB comprises three parts: 1) the arachnoid barrier, composed by three layers of connective tissue that are collectively termed the meninges (dura mater, arachnoid mater and pia mater) and are present in the brain as well as in the spinal cord; 2) the blood–cerebrospinal fluid barrier (BCSFB), which comprises the epithelial cells that surround the specialized vascular tissue (choroid plexus) present in each lateral ventricles of the brain, where the cerebrospinal fluid (CSF) originates; and 3) the BBB itself, which is the closest to the neurons. The BBB is formed by brain microvessel endothelial cells (BMECs), which separate the blood in the capillaries from the interstitial fluid (ISF) in the brain compartment. Tight junctions, adherent junctions, apicobasal polarity, and a luminal surface-bound glycocalyx provide to BBB with unique properties that make it a physically imposing gateway that control the penetration of any molecule to brain. Different types of cells (i.e. neurons, BMECs, vascular smooth muscle cells, astrocytes, microglia, pericytes, oligodendrocytes, mast cells), constituting all together the

neurovascular unit (NVU), are in constant cross-talk to each other. They create a very complex interdependence that dynamically regulates the permeability of the BBB and, thus, preserves the optimal functioning of the CNS[38].

However, it is not completely impermeable for all substances since there is directed transport by diffusion of lipophilic substances through cell membranes, and paracellular passage of water-soluble substances across tight junctions[21]. Furthermore, not all the neurons in the body are protected. In the peripheral nervous system the lack of the BBB, that is supplied by capillaries with fenestrated walls, allows the free passage of molecules between the bloodstream and the extracellular fluid. This explains, in part, why sensory neurons located in the dorsal and trigeminal root ganglion (DRG and TG) may represent the main target of chemotherapeutic agents like platinum-based drugs. Moreover, many studies have shown a new neuropsychological syndrome associated with cancer treatment/chemotherapy-induced cognitive impairment.

A direct action of chemotherapeutics on BBB endothelial cells (EC) has not been demonstrated. However, *in vitro* administration of OHP induces significant changes in the junctional and cytoskeletal apparatus of endothelial cells, and these alterations in the BBB may be associated with higher concentrations of OHP in the brain, what probably contributes to the development of a chronic form of pain[11] .
A consistent set of data, both *in vivo* and *in vitro* assays, confirms that many types of NPs can reach the CNS by two main pathways: 1) by crossing the BBB when either orally administered or injected (transcellular diffusion, paracellular diffusion, receptor-mediated transcytosis, adsorptive-mediated transcytosis), 2) or through the nasal epithelium to the olfactory bulb and the brain, when inhaled[3]. The initial uncertainty about the accessibility of NPs to the central CNS is probably because of the lower amount of data on potential NP-induced neurotoxicity, respect to

literature dedicated to describe the interaction between NMs on other tissues and cells[4].

1.4 Mechanisms of Neurotoxicity

Among the possible mechanisms by which external agents can trigger a neuronal damage, the oxidative stress, the dysregulation of Ca^{2+} and pH homeostasis have a high impact on the functional modulation of the proteins that govern the resting membrane potentials, that set the threshold for firing action potential, that influence the duration and/or shape of an action potential and that synchronize neuronal activity. Even small perturbations in these regulatory pathways can lead to serious pathological events, including apoptosis and cell death. Even more, all these mechanisms appear to be mutually interconnected to each other[39].

Formation of ROS

The term ROS is used to describe a variety of molecules and free radicals derived from molecular oxygen. The main sources of intracellular ROS are mitochondria, endoplasmic reticulum (ER), peroxisomes, microsomes, and a family of cell membrane enzymes namely nicotinamide adenine dinucleotide phosphate (NADPH) oxidases (NOX).

MITOCHONDRIAL ROS SOURCES Mitochondrial electron-transport system represent the main intrinsic source of ROS. During the generation of ATP and water, the individual complexes of the respiratory chain mediate the transfer of the electrons from the reducing equivalents NAD(P)H and FADH2

(Flavin adenine dinucleotide) to molecular oxygen. Since mitochondria are not thermodynamically perfect machines, some of these electrons inevitably escape the physiological default pathway[40,41]. The one-electron reduction of molecular oxygen operated by complex I (NADH ubiquinone oxidoreductase) and complex III (co-enzyme Q, bc1complex, and uniquinone/cytochrome c reductase) activity in the mitochondrial matrix and intermembrane space, respectively, generate the first ROS element: the superoxide anion (O^{2-}). Once in the intermembrane space, O^{2-} can be converted, spontaneously or by the catalysis of an enzyme family known as SOD (superoxide dismutase), into a more stable form, hydrogen peroxide (H_2O_2). However, further reactions may lead to the formation of hydroxyl radicals (OH), through the Fenton or Haber-Weiss reactions[42,43].

NON-MITOCHONDRIAL ROS SOURCES In addition to the mitochondrial electron transport, other cellular systems are able to generate ROS, including NADPH oxidases, xanthine oxidase, nitric oxide synthases, cyclooxygenases and lipoxygenases. Among them, NADPH oxidases, originally discovered in neutrophils, which play a key role in the microbicidal activity, are a distinct ROS producing family of enzymes. They are multi-subunit membrane-bound enzymes, expressed at the cell surface and intracellular organelles, that catalyze the reduction of oxygen into superoxide (O_2^-) by using NADPH as an electron donor and oxygen as an electron acceptor. Thus, whereas the other oxidoreductases, mentioned above, only produce ROS as by-products along with their specific catalytic pathways, NADPH oxidases can be considered as “professional” ROS producers. Recently, seven different homologues have been identified in mammalian cells[44]. It should be noted that in many tissues their expression

is not constitutive (i.e. neurons), but Nox-dependent ROS generation can be stimulated by a large collection of chemical, physical, environmental, and biological factors. These findings suggest that NADPH oxidase is an important component of the cellular stress signal transduction network, a sort of cellular "alarm system", that can alert and prime the cells either to be adapted to the stress or to undergo apoptosis[40].

For most organ systems, including the CNS, only uncontrolled levels of ROS are deleterious. Regulated ROS generation has key functions in physiology and intracellular signaling pathways, such as inhibition of protein tyrosine phosphatases, activation of certain redox-sensitive transcription factors, and modulation of the functions of some ion channels[45]. Therefore, to maintain the concentration of these oxidants at non-toxic levels, many enzymatic mechanisms, as well as nonenzymatic components with antioxidant capacity that derive directly from the dietary (i.e. β-carotene, ascorbate (vitamin C), α-tocopherol (vitamin E)), are present [42].

SOD enzyme removes superoxide ions to form hydrogen peroxide. The cytosolic form of this enzyme contains Cu^{+} and Zn^{+} (CuZn–SOD), while the mitochondrial form contains Mn (Mn–SOD). H_2O_2 produced this way can be removed by glutathione peroxidase or catalase, both of which are haem-containing enzymes[42]. Due to the close proximity to the electron transport chain, the major locus for free radical production, and the lack of protective histones, the mitochondrial DNA (mtDNA) is, therefore, the principal cellular target of oxidative stress. Although the presence of DNA-repairing enzymes, ROS can impair the mtDNA that, in turn, may induce a decrease of cellular metabolism through the disruption of electron transport (many electron carriers are synthetized from mitochondrial

chromosome), mitochondrial membrane potential, ATP generation and an increased production of ROS[46].

The stimulation of lipid peroxidation is another important factor that may contribute to the suppression of mitochondrial metabolism. The uncontrolled formation of lipid peroxides exerts its toxic effect through two general mechanisms: first, affecting the composition, structure and dynamics of cellular membranes, since they are important for the maintaining of the membranes integrity; second, being highly reactive compounds that may react with proteins and DNA, contributing, in this way, to the propagation and generation of new ROS[47].

Mitochondria are one of the internal organelles involved in the regulation of Ca^{2+} homeostasis. A tight correlation between the oxidative stress and calcium signal disruption is markedly evidenced by the Ca^{2+}-dependent mitochondrial permeability transition (MPT). When intracellular Ca^{2+} rise and the retention capacity of the mitochondria is exceeded, the protein channels, commonly known as the permeability transition pores (PTP), open. The efflux of Ca^{2+} causes drastic changes in mitochondrial ultrastructure and functional activity. The result is a mitochondrial failure, which can lead to necrosis due to ATP depletion, or, if MPT induction occurs in a subpopulation of mitochondria, to caspase-mediated apoptosis[46].

Ca^{2+} Signalling

Ca^{2+} regulates many divergent cellular processes, including, but not limited to, muscle contraction, exocytosis and gene transcription. Signals that have a widely different spatial and temporal profiles, from microseconds, for Ca^{2+} triggering

exocytosis at the synaptic junction, to hours, for gene transcription and cell proliferation.

This versatility emerges from the use of an heterogenous molecular array of components that constitute the complex toolkit of Ca^{2+} signalling. Pumps, channels, exchangers and binding proteins tightly control changes in free cytosolic Ca^{2+} concentration $[Ca^{2+}]_c$, that in resting conditions is maintained around the value of 10-100 nM (Fig. 2). While internal and external sources of Ca^{2+} are used by the cells to generate Ca^{2+} signals [48,49].

Ca^{2+}-entry mechanisms When the permeability of the plasma membrane to Ca^{2+} changes, the ions enter the cell from the outside, where the $[Ca^{2+}]$ is around 2 mM. The large electrochemical gradient across the plasma membrane is guaranteed by the activity of the Ca^{2+}-ATPase (PMCA) and of the Na^+/Ca^{2+} exchanger (NCX), that removes Ca^{2+} from the cytoplasm in order to restore the resting state[50].

There are various entry channels, each of them characterized by widely different properties. Voltage-operated Ca^{2+} channels (VOCCs), found mainly in excitable cells, generate rapid Ca^{2+} fluxes that mediate fast cellular responses such as muscle contraction or exocytosis at the synaptic endings. Furthermore, there are also channels modulated by ligands, that can be external ligands, as in the case of NMDA (N-methyl-D-aspartate) receptors (NMDARs) that respond to glutamate and, for this reason, belonging to the class of Receptor-operated channels (ROCs); or they can be internal ligands, as in the case of channels gated by cyclic-nucleotides, found mainly in sensory systems, that belong to the class of second-messenger-operated channels (SMOCs).

Moreover, other types of stimuli are translated by different channels. Many of them belong to the superfamily of TRP channels, composed by 28 members, encoded by up to 28 different genes and one pseudogene generally characterized by a low conductance that allow them to operate over much longer time scales without swamping the cell with too much Ca^{2+} [48].

Ca^{2+} release from internal stores Other important sources for Ca^{2+} signalling are represented by the internal stores. The principal organelle responsible to rapid rise of Ca^{2+} is the ER, or its muscle equivalent, the sarcoplasmatic reticulum (SR). The release from such store is controlled principally by Ca^{2+} itself, but also, by several other messengers, such as inositol-1,4,5-trisphosphate (Ins(1,4,5)P3), cyclic ADP ribose (cADPR), nicotinic acid adenine dinucleotide phosphate (NAADP) and sphingosine-1-phosphate (S1P)[48]. Since little is known about the channels opened by NAADP and S1P, in this section, the focus will be on Ryanodine (RYR) and Inositol (1,4,5) trisphosphate (Ins (1,4,5) P_3R) receptors. These two channels are often mediators of Ca^{2+} signal amplification. In general, at low concentrations of Ins (1,4,5) P_3, they have a bell-shaped Ca^{2+} dependence. Therefore, at low concentrations of cytosolic Ca^{2+} (100-300 nM) they take part to the so-called Ca^{2+}-induced Ca^{2+} release (CICR) process, but, when the concentration of cytosolic Ca^{2+} rises over 300 nM, they are closed[51].

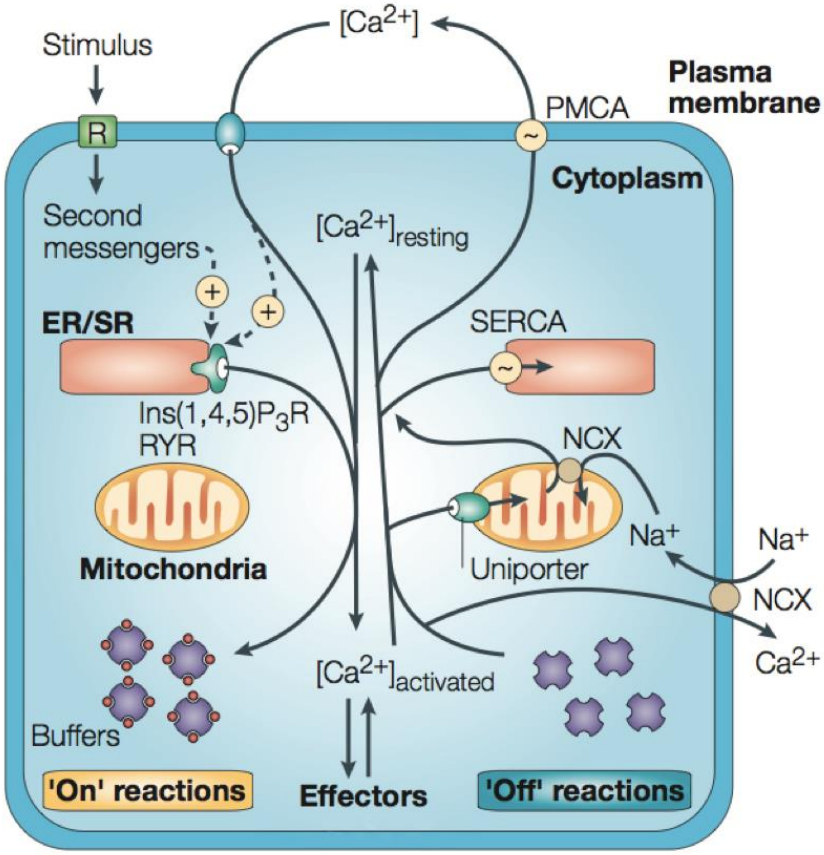

Figure 2. **Overview of the calcium homeostasis and signaling mechanisms**. $Ca2^{+}$ signalling can be divided into "on" and "off" reactions. During the "on" reactions, the $[Ca^{2+}]i$ increases as a consequence of Ca^{2+} entry from the external environment or through the release from intracellular stores. Most of this Ca^{2+} (shown as red circles) is bound to buffers and effectors. During the "off" reactions, Ca^{2+} leaves the effectors and buffers and is removed from the cell by various exchangers and pumps. The Na^{+}/Ca^{2+} exchanger (NCX) and the plasma-membrane Ca^{2+}-ATPase (PMCA) extrude Ca^{2+} to the outside, whereas the sarco(endo)plasmic reticulum Ca^{2+}-ATPase (SERCA) pumps Ca^{2+} into the ER. Mitochondria also have an active function: they rapidly sequester Ca^{2+} through a uniporter, and then slowly release it back into the cytosol (adapted from Berridge, Bootman, et al. 2003).

A unique array of channels can be found in each cell type, in order to create a perfect "toolkit" able to generate a Ca^{2+} signalling systems that differ in terms of spatial and temporal properties.

The cytosolic buffers proteins are essential for shaping the amplitude, as well as the duration of Ca^{2+} signals. They are molecules that serve as Ca^{2+} ion chelators that present appropriately spaced acidic side-chain residues (i.e. glutamate, aspartate) and/or backbone carbonyl groups, in which a Ca^{2+} ion may fit in. This evolutionarily well-conserved protein families differ in the way the Ca^{2+} ions are bound[52].
In the neurons, for example, high concentration of buffers like parvalbumin and calbindin, belonging to the EF-hand cytosolic protein family, limits the spatial spreading of local Ca^{2+} signals. This is particularly important to maintain confined the signal in the synapses in which different types of channels are strategically located[51].

pH Homeostasis

The intracellular pH represents another fundamental parameter that can affect a wide range of biological processes, including membrane excitability, intercellular communication, signal transduction and vesicle trafficking. The ionization state and, therefore, the structure and function of virtually all proteins of the cells depend on pH. Not surprisingly, dynamic and sustained mechanisms have been evolved to maintain long-term pH homeostasis[53].

Under physiological conditions, the extracellular pH is slightly alkaline (~7.3–7.4), while the cytosolic pH is slightly more acidic (7.2). The tendency of cells to acidify can be explained by 1) the electrical potential across the membrane and 2) the acid equivalents produced during metabolic reactions. Being more negative inside, the cells promote the uptake of the positively charged protons and, at the same time, the efflux through specific pathway of the negatively charged bases. Furthermore, the continuous generation of acid equivalents during metabolic reactions, like ATP

production by glycolysis and oxidative phosphorylation in the cytoplasm and in the mitochondria, respectively, can boost the gradual accumulation of free H^+ [54].

Although the cells have a high buffer capacity, characterized by various intracellular weak acids and bases that protect them from rapid and localized pH changes, active processes are needed to promote the protons extrusion from the cytosol across the plasma membrane in sustained stress situations. A steady state condition is maintained when a balance between the rate of acid loaders (JL, i.e., rate of acid influx/generation or alkali efflux/consumption) and the rate of acid extrusion (JE, i.e., rate of acid efflux/consumption or alkali influx/generation) is achieved[55,56] (Fig. 3).

ACID LOADERS Mammalian cells are continuously exposed to CO_2, which being uncharged, can cross the biological membrane and enter into the cells. Once inside, CO_2 can combine with H_2O to form H_2CO_3, most of which dissociates very slowly to form HCO_3^- and H^+. Most cells have a specific enzyme, carbonic anhydrase, that catalyzes the conversion of CO_2+H_2O to H_2CO_3, accelerating the acidification process of the cell. Although HCO_3^- is an effective proton buffer, it is negatively charged and, as well as OH^-, can passively exit to the cell and then contribute to the instauration of a chronic intracellular acid load[53].

The main acid loader that is involved in the J_L is the Cl^-/HCO_3^- exchanger (Anion Exchanger AE, encoded by the SLC4A gene). AE3 is the most expressed exchanger in the CNS and, as the other members of the family, mediates the electroneutral exchange of one Cl^- for one HCO_3^-. Generally, Cl^- concentration inside the cells is lower than extracellularly, so the inward gradient of Cl^- provides the driving force for a net efflux of HCO_3^- [54]. Thus, since acid loaders, at least in theory, work without the direct input of energy,

if the gradient driving transport reverses, the acid-base transporters can switch the direction of net transport[53].

Finally, the electrogenic Na^+/HCO_3^- cotransporter will be explained in the next paragraph in detail since this same protein can either operate as acid loader and acid extruder.

ACID EXTRUDERS The extrusion of acid equivalents is an active process that tends to raise the intracellular pH an to restore it after an acid loading, for example, after an intense neuronal activity[55]. The membrane associated vacuolar H^+-ATPase (V-ATPase), firstly found in association with endosomal membranes, but also distributed in the plasma membrane of specialized cell types (i.e. phagocytes and osteoclasts[54]), is a pump that uses the energy of ATP hydrolysis to extrude cytosolic H^+ into the extracellular space.

The net extrusion of H^+ or the influx of HCO_3^- can be also accomplished by a secondary active transport. In this context, the main acid extruders are the Na^+-H^+ antiporters or exchangers (NHE) from the SLC9 family of solute carriers and the Na^+-coupled HCO_3^- transporters (NCBTs) in the SLC4 family. NHEs use, in an electro-neutral manner, the inwardly directed electrochemical Na^+ gradient generated by Na^+/K^+-ATPases to export H^+. Until now, nine different isoforms of NHE exchangers have been identified and all of them are broadly expressed in the CNS.

Among the acid-extruding HCO_3^- transporters, the six mammalian NBCTs are the predominant. They translocate Na^+ and HCO_3^- both in the same direction, but the coupling stoichiometry varies among members of this family. In particular, several Na^+-driven HCO_3^- (or CO_3^{2-}) operate as acid extruders (NBCn1 and NCBn2), with a Na^+: HCO_3^- stoichiometry of 1:2, while

others, as acid loaders (NCBe1 and NCBe2), if Na^+:HCO_3^- stoichiometry is 1:3[53,54].

NBCn1 and NCBn2 are electroneutral isoforms, what means that they are unaffected by the transmembrane potential, and perhaps the magnitude and directionality of transport is dependent solely of the combined chemical gradients of Na^+ and HCO_3^-.

Conversely, for the electrogenic NBCe1 and NBCe2, the driving force depend of the electrical potential, as well as the concentration of HCO_3^- and Na^+ on either side of the membrane. Therefore, for example in the case of renal proximal tubule, in which the electrical component outstrips the driving force of the concentration gradients, the net direction of transport is outward, resulting in a cytosolic acidification.

Finally, the Na^+-driven Cl^-/HCO_3^- exchanger that mediates the electroneutral exchange of one Na^+ plus two HCO_3^- equivalents for one Cl^-. This was the first transporter ever to be studied as a pH_i regulator[53].

A straight correlation between the excitability of the neurons and pH changes exists. Membrane proteins, such as channels, transporters, receptors and even ATPase pumps have intracellular and extracellular moieties that result in pH sensitivity. The direction of the responses evoked by pH changes depends on the individual components that are responsible for dictating overall excitability in each neuron. For this reason, there are neurons that exhibit hyperexcitability following an acidification of the cytosol (i.e. chemosensitive neurons), while others could exhibit a decrease in the excitability[55].

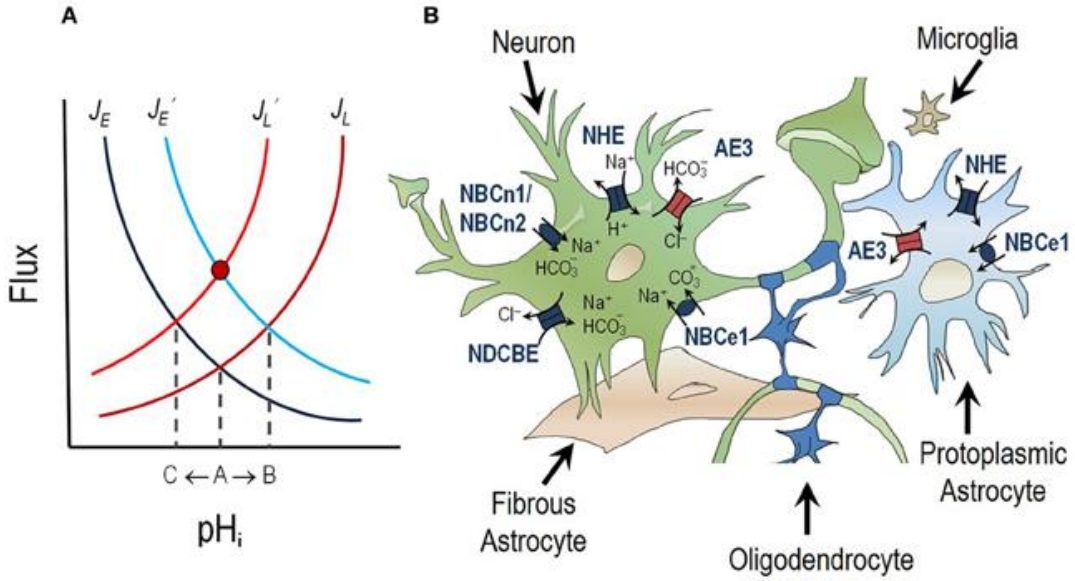

Figure 3. pH regulation in the CNS. (A) pHi dependence on the balance between the rate of acid extrusion (JE) and the rate of acid loading (JL). Steady-state of pHi is achieved when $J_E = J_L$ (intersection of dark-blue and dark-red lines: point A). A shift to a more alkaline value (intersection of light-blue and dark-red lines: point B) follows an J_E increase (J'_E). Conversely, a shift to a more acidic value (intersection of dark-blue and light-red lines: point C) follows an J_L increase (J'_L). If the rise in J_E is matched by an equal increase in J_L ($J'_E = J'_L$) there will be no net change in pHi (red circle). (B) Acid loaders (red) and acid extruders (dark blue) in neurons, astrocytes and oligodendrocytes (Ruffin, et el. 2014).

1.5 Ionic channels involved

TRP channels

The TRP superfamily is a very heterogenous class of ion channels displaying a great diversity of ion selectivity, modes of activation, and physiological functions[57]. Despite this variability, all the members of this family share a typical protein structure consisting of six putative transmembrane segments (S1 to S6) that assemble in tetramers (homo- or heterotetramers) to form the functional channel. Each subunit contributes to selectivity filter and to ion-conducting pore with a reentrant loop located between S5 and S6. They also have an intracellular amino and carboxyl termini that result variable in length and in domains.

From protein homology, TRP channels can be divided into seven subfamilies: TRPA, TRPC, TRPM, TRPML, TRPN, TRPP and TRPV[58]. They are expressed in all cellular membranes, with the exception of the nuclear envelope and mitochondria, of virtually all cell types. The majority are located in the plasma membrane, where they mediate the transport of ions[59]. Although they are defined as non selective Ca^{2+}-permeable cation channels, the variety of homo/heteromultimerizations that can be achieved, makes the overall picture of TRP channel ion selectivity more complex. Most TRPs show little preference for Ca^{2+} over Na^{+}, some others (i.e. TRPC1, TRPM1 and TRPP2) are completely non-selective cation channels, and both Ca^{2+}-selective (i.e. TRPV5 and TRPV6) and Na^{+}-selective (i.e. TRPM4 and TRPM5) are present in the superfamily[57].

Regarding the regulation of their activity, a lot of mechanisms have been described. The mechanism(s) through which a given TRP is activated and regulated cannot be predicted reliably on the basis of its subfamily assignment. Members of this family that are considered sensors for the temperature, are also sensitive to a large

number of exogenous and endogenous ligands. The heat-sensitive TRPV1 can be also activated by capsaicin (the pungent extract of hot peppers), as well as the cold receptor TRPM8 by menthol (derived from the mint plant Mentha piperita), and TRPV4 directly by bisandrographolide (derived from the plant Andrographis paniculata)[59]. The recurring topic is that most TRP channels are activated through a diversity of mechanisms[60].

Initially considered as rather insensitive to voltage, it is well documented now, that the mid-point activation of TRPs, evoked for example by temperature or ligands, can undergo to a voltage-dependent shift of even several millivolts magnitude[61]. This intrinsic voltage dependence regards mainly TRPs involved in sensory perception[59]. However, in some cases there are similarities among subfamily members, as all TRPC channels that are sensitive to membrane phospholipids, like phosphatidylinositol (4,5) bisphosphate (PtdIns (4,5) P_2).

The modulation by phospholipids can be direct or indirect. The great number of membrane-associated proteins sensitive to the levels of PtdIns (4,5) P_2 can, in turn, affect the activity of TRP channels[62]. The hydrolysis of PtdIns (4,5) P_2 operated by phospholipases C (PLCs) can be activated by two different pathways: 1) G protein–coupled receptors (GPCRs) and 2) tyrosine kinases receptors. Once the hydrolysis of PtdIns (4,5) P_2 is obtained, two important signaling molecules are produced: 1) diacylglycerol (DAG) and 2) inositol (1,4,5) trisphosphate (IP3)[58,59]. DAG can affect the TRP channel opening directly or indirectly, by producing several metabolites of (i.e.). While IP_3, which activates IP_3 receptors (IP_3R) on the ER membrane, evokes a release of Ca^{2+} from intracellular stores responsible of the activity modulation of TRP (store-operated Ca^{2+} entry (SOCE) or capacitative Ca^{2+} entry (CCE))[57]. Additional activation mechanisms include phosphorylation by PKA, PKC and PKG, that sensitize them by other stimuli; changes in extracellular and intracellular pH; ROS production; mechanical stimuli and changes in osmolarity[58,63–67].

Detecting and responding to this wide variety of external environment stimuli make their contribution essential for several physiological processes, ranging from pure sensory (chemosensation, thermosensation, nociception, mechanosensation and photoreception) and homeostatic (such as reabsorption and osmoregulation of Ca^{2+} and Mg^{2+}) functions to many other motile functions, such as muscle contraction and vasomotor control. Thus, an increasing number of evidences suggest the implication of several TRP channels in a wide range of diseases in humans, following either mutations in the encoding gene or an acquired mechanism.

Genetically and pharmacological evidences have confirmed the involvement of these channels in the generation and transduction of pain (TRPV1,TRPA1,TRPM8); in the activation of central and peripheral reflex responses, including cough, mucus secretion and bronchospasm, in the mammalian respiratory tract following the interaction with irritant and/or inflammatory stimuli (TRPV1, TRPA1, TRPM8, TRPV4, TRPC6); in the skin, where they control a variety of biological processes such as itch, regulation of barrier function, keratinocyte differentiation, hair growth, inflammation and wound healing, being expressed both on neuronal and non-neuronal cells (TRV1, TRPV3, TRPA1); in CNS disorders, like learning and memory formation through regulation of synaptic plasticity (TRPC6), or neurodegenerative disorders, Guamanian amyotrophic lateral sclerosis (ALS-G) and Parkinsonism dementia (TRPM2, TRPM7), or in axonal and neuronal degeneration in Multiple Sclerosis (MS, TRPM4) and in cardiac hypertrophy associated with arrythmias, decompensation and sudden death (TRPC1, TRPC3, TRPC6)[68].

Large conductance channels: Connexins and Pannexins

Gap junctions (GJs) were primarily known as mediators of direct intracellular communication. When two hemichannels (HCs), belonging of two neighboring cells, interact together, a GJ is formed. These junction put directly in contact the cytosolic compartments of adjacent cells allowing the flux of several small molecules, such as ATP, glutamate and prostaglandins, as well as ions, including Ca^{2+}. Each hemichannel is composed of 6 connexin (Cx) proteins, all of which consist of 4 transmembrane domains, 2 extracellular loops (EL), 1 cytoplasmic loop (CL), 1 cytoplasmic C-terminal tail (CT) and 1 cytoplasmic N-terminal tail. Now, it is clear that Cx HCs are not only structural precursors of GJs but themselves, alone, can provide a circuit for communication, albeit between the cytosol and the extracellular environment[69]. Although Cx- based GJC and hemichannels share similar structure, they differ in their localization (inside or outside the contacting zone with others cells), opening and closing regulation and their roles in cellular processes[70]. Usually, while the GJs are open in physiological conditions, Cx HCs are typically closed, because of their low open probability, which would be enough to participate in several cellular processes. For example, Cx46 and Cx50 hemichannels openings seem to have a crucial role in the lens, an avascular tissue in which the microcirculatory homeostasis depends on nutrient, electrolyte and water flow through these plasmalemmal channels. In human CNS, where 11 out 21 Cx isoforms have been identified, are differently distributed between astrocytes, oligodendrocytes, microglia and neurons. Here, hemichannels activity has been correlated to release of precursor or signaling molecules such as Nicotinamide adenine dinucleotide (NAD^+), ATP, adenosine, IP_3 and glutamate. The opening of Cx43 hemichannels, which represents also the most abundantly expressed connexin in the human body, and the following release of ATP have been observed

in astrocytes in which it seems to be involved in the Ca^{2+} wave propagation mediated by an extracellular paracrine signaling component [71].

However, in the presence of several type of stimuli such as increases in membrane depolarization, an increase in intracellular Ca^{2+} concentration or a decrease in extracellular Ca^{2+} concentration, mechanical stimulation, changes in the Cx phosphorylation status, oxidative stress, pH, ischemia/reperfusion insults, fatty acid overload and in the inflammatory conditions the Cx- hemichannels open probability increases. When the hemichannel activity becomes too high and uncontrolled, cell viability diminishes. In this cases, they form "leaky hemichannels" and/or their number at the plasma membrane increase dramatically up to enhance cell membrane permeabilization, enough to cause an accelerated cell death[70]. In addition of a possible abnormal connexin hemichannel activity that could be considered as a gain-of-function mutation, many connexins undergo to loss of gap junction function owing to trafficking deficiencies (i.e. gap junction plaque formation), channel malformation (non-functional or communication-deficient channels) or the genesis of aberrant hemichannel activity. At least the half part of the total human connexin genes identified can be linked to inherited human diseases including neuropathies, deafness, skin diseases, oculodentodigital dysplasia (ODDD) and cardiac arrhythmias [69,70,72].

In 2000, a novel class of Cx-like proteins, with similar membrane topology to the connexins but without forming GJs, has been identified. The Panx family consists of three members, namely Panx1, Panx2, Panx3. Panx1 is the most widely represented one in diverse tissues and cell types, while the other two are mainly expressed respectively in the CNS and, in skin and skeletal tissues. Similar to Cx hemichannels, Panx ones are implicated in a wide variety of physiological and pathological contexts. Although Panx channels are opened at positive potential, a wide number

of triggers that promote their opening at membrane resting potential, has been identified[69,73]. Large amount of data refers their activation following the intracellular Ca^{2+} increments, the phosphorylation mediated by Src family kinase or by other types of kinases (i.e. c-Jun NH2-terminal kinase (JNK); protein kinase G), the ATP binding to purinergic P2 receptors (such as P2Y receptors), the oxygen deprivation (in erythrocytes and neurons), the elevation of extracellular potassium or a mechanical stress (in various cell types)[74].

Both reversible (i.e. G-protein-coupled receptor) and irreversible (caspase-mediated cleavage) forms of channel activation induce a progressive channel opening, characterized by a robust macroscopic currents across the plasma membrane of individual cells (ion- and large-molecule transport) that presents at least five open substates (corresponding to 5, 25, 30, and 90% of the fully open unitary conductance, ranging from ∼300 pS to >500 pS)[74].

The involvement of pannexins in the induction of inflammation has been reported in multiple publications. There are many evidences that support the idea that Panx1 and its associated P2X receptors are essential for upstream regulation of inflammasomes and proteolytic activation of Casp1 and Casp11. This has been reported in many cell types, however a strong demonstration has been only supplied for inflammasome regulation in the CNS and in the retina[75].

Two-pore domains (K_2P) channels

The two- pore domain are the third major family of K^+ channels, along with voltage-gated (K_V) and inwardly rectifying (Kir). They are structurally different to the others K^+ channels. While voltage-gated K_V channels and inwardly rectifying Kir channels assemble as tetramers and each subunit symmetrical contribute to the ion permeation pathway through a single copy of P-domain, the K_2P have two pore domains (P1 and P2) in tandem per subunit and four transmembrane domains (TM1–TM4). A large extracellular cap-domain linked to the P1 from TM1, stabilized by an apical disulphide bridge, can be considered as the most prominent structural motif of K_2P. The steric hindrance created by the specific position of the cap-domain seems to modulate the gating of the K_2P channels, rendering them less sensitive to classical toxin peptides and pore blocking molecules like tetraethyl-ammonium ions that, instead, act on other classes of K^+ selective channels.

In mammals, K_2P derive from 15 genes and can be classified in six subfamilies: TWIK (weak inward rectifiers), TREK (lipid and mechanosensitive channels), TASK (acidification-inhibited), TALK (alkalinization-activated), THIK (inhibited by halo-thane), and TRESK (spinal cord channels)[76]. They are called leak or background channels for their primary function, which is to maintain hyperpolarized resting the membrane potential of virtually every excitable and non-excitable eukaryotic cell. Increasing evidence suggests that the activity of these ion channels can be also modulated by a great variety of stimuli, including changes in membrane tension, voltage, temperature, oxygen-tension, extracellular and intracellular pH, phospholipids, and other signaling molecules arising from G-protein–coupled receptor activation[76,77]. Although they do not have a conventional voltage-sensor, a voltage-dependence has been shown in most K_2P channels, except for TWIK-1. A

recent work provides a possible explanation of the voltage-dependence of K_2P[78]. The intriguing hypothesis relies crucially on the movement of the permeant ion, along the selectivity filter (SF), and therefore on its electrochemical potential difference. Only a depolarization would push ions into the SF, otherwise empty. Once fully occupied, it become permeant in outward direction. High occupancy would not be reached by forcing ion movement in the inward direction; under these conditions, the SF would become inactive. Many stimuli including intracellular acidification , lipids, membrane tension can affect the voltage- dependence[78].

K_2P channels are expressed throughout the body and each type of channels have a different expression profile. It is well established that several members of this family are highly expressed in DRG and TG neurons[77]. Therefore, an increasing number of evidences is revealing their central role in the transduction of noxious stimuli by modulating the somatosensory excitability. The painful stimuli activate various classes of cationic ion channels like ASIC, TRPV1 and TRPA1 in the peripheral nerve terminals, in which they induce a depolarization of the membrane potential. Voltage-dependent Na^+ channels generate an action potential when the threshold is reached. The leak K^+ channels are able to prevent the generation of an action potential hyperpolarizing the membrane potential. Thus, these channels operate a counteraction by decreasing conduction fidelity across the axon or by limiting the release of neurotransmitter[79]. Further evidences are provided, for example, by less amplitude current required to elicit an action potential in cells derived by TRESK-1 knockout mice; or the mechanical and thermal hypersensitivity showed by both TREK-1- and TRAAK-deficient mice in response to a chronic inflammation. On the contrary, the overexpression of TRESK channels reduces mechanical and thermal hypersensitivity in response to nerve injury[80].

The implication of these channels in the regulation of multiple types of pain, such as inflammatory, neuropathic, mechanical and thermal, migraine and cancer pain, make them possible molecular targets for the development of pain therapeutic strategies. However, the pharmaceutical design is restrained by 1) the broad range of transcript processing and post-translational modification mechanisms (phosphorylation, SUMOylation, glycosylation) and 2) the high capacity of heterodimerization of specific pairs of subunits. The result of these mechanisms is a high rate of diversification of channels, with completely distinct physiological and pharmacological properties by combining the functional properties of single constituent. However, the lack of structural data remains the first most prominent bottleneck in the development of drugs that act at K_2P channels[77,80,81].

1.6 Neurotoxicity screening

Traditionally, the paradigms for hazard identification and risk assessment requires an animal-based experimental approach. In the last years, a change towards new approaches using integrate in silico and *in vitro* testing to identify the mechanisms of toxicity is occurring. Many practical and scientific considerations support this evolution, first of all the increase of safety testing reliability by reducing the need for animals and by lowering the costs with the implementation of high-throughput methods[82].

The endpoints commonly used for *in vitro* neurotoxicity testing can be divided into three categories: 1) viability read-outs, 2) morphological read-outs and 3) functional read-outs. The first step is, essentially, to identify which are the compounds that cause toxicity in one or more cell types and to individuate which is

the lower concentration that can affect the viability of the cells. Thus, biochemical assays are usually chosen for monitoring the irreversible cell damage by measuring the level of energy metabolism, using ATP as indicator[83]; by quantifying the reduction in resazurin or tetrazolium salts (i.e. MTT, MTS, XTT or WST) in viable cells[84]; by evaluating the level of lactate dehydrogenase (LDH) from dead cells[85]; or by measuring markers of the apoptosis, such as cleaved caspase-3 or the accumulation of p53, for the evaluation of the degree of proliferation of cells exposed to neurotoxicants[86].

Once established the sub-cytotoxic concentrations that can be used, morphological and functional read-outs are evaluated. At this point, the common endpoints considered are neuronal differentiation (i.e. by measuring neurite outgrowth and biomarker expression), spontaneous electrical activity of neuronal networks, cell communication, migration and synaptogenesis.

The distinction between morphological and functional read-outs is often not so evident. Largely, it depends on the analytical method used for measuring the endpoints at each specific case[21].

Electrophysiological screens

The perturbation of neuronal excitability induces substantial and rapid disruption of the nervous system functions. For this reason, the physiological assessment is a key factor when potentially-neurotoxic compounds are considering. To monitor and evaluate the eventual disruption of ion channels, receptors and other critical determinants of neuronal electrical activity, highly optimized analytical methods are needed[87].

Multielectrode arrays (MEAs), recently developed, are a useful tool for functional neurotoxicity screening. By interfacing microelectrodes with neurons, MEA platforms provide non-invasive, spatio-temporal information of the network activity of a population of neurons during development, as well as any functional effects of acute and chronic treatment paradigms. One of the major advantages of this technology is the possibility of long-term monitoring (up to weeks and/or months) of a cell population electrical behavior[88,89]. Moreover, the availability of multiwell MEA plates has allowed increased throughput, offering the ability to perform complete concentration-effect curves of several compounds on cell populations exposed to the same culture conditions[87,90].

Developed by Neher and Sakmann over 40 years ago, the patch-clamp technique remain the gold standard for the study of ion channel activity at the single molecule level (microscopic current) and at the cellular level (macroscopic current)[91]. Actually, automated patch-clamp (APC) systems has been developed, but they have not replaced the traditional patch-clamp technique, rather represent a very useful tool during the initial stages of pharmaceutical lead compound development[21].

Outline of the Project

The objective of this thesis project was focused on the study of the possible molecular targets and mechanisms involved in two specific cases of neurotoxicity, widely documented but not completely understood: 1) the potential neurotoxicity induced by Silica Nanoparticles (SiO_2) and 2) the Oxaliplatin (OHP)-induced neurotoxicity.

This Ph.D. thesis comes out in the form of collection of papers. They are presented progressively, each one corresponding to a single chapter (those from 2 to 4). In turn, in chapter 5 it is described a concluded set of experiments partially conducted during my visiting period in the Laboratory of Molecular and Cell Biology at the Instituto de Investigación, Desarrollo e Innovación en Biotecnología Sanitaria de Elche (IDIBE) (Spain), coordinated by Prof. Antonio Ferrer Montiel. All together, this is the scientific production, strictly related to my Ph.D. research program, I contributed to during the “Chemistry and Biology” Ph.D. three years course: The studies were conducted in the Laboratory of Cellular Physiology and Biophysics at the Department of Pharmaceutical Sciences of the University of Piemonte Orientale "A. Avogadro", under the supervision of my tutor Prof. Carla Distasi.

This research was conducted in collaboration with the Laboratory of Pharmacology at the Department of Pharmaceutical Sciences of the University of Piemonte Orientale "A. Avogadro", coordinated by Prof. Armando Genazzani, and the Laboratory of Physiology, coordinated by Prof. Davide Lovisolo..

During these last 3 years Prof. Carla Distasi has been active within different research lines in the field of neurophysiology. Among the most important ones, to highlight the study of the impact of chemical agents on the Central Nervous System from an

electrophysiological perspective in order to characterize the molecular targets and the mechanisms underlying the toxicity induced by different types of engineered nanoparticles, i.e. TiO_2 and SiO_2 NP, and by the administration of platinum-based chemotherapeutic agents.

Before starting my Ph.D. studies, it had been already described that amorphous 50 nm SiO_2 nanoparticles (NPs), developed by the group of Prof. Gianmario Martra, (Dept. of Chemistry, University of Turin) and tested by Prof. Lovisolo and his team (Dept. of, University of Turin), can be made fluorescent by hybridization with cyanine dyes and safely incorporated into neurons and other cell types[10]. At non-toxic doses (20 µg mL^{-1}), 50 nm SiO_2 NPs elicit increases in the intracellular Ca^{2+} concentration in a neuroendocrine cell line GT1-7. These signals are fully dependent on Ca^{2+} influx by means of different types of Ca^{2+} permeable channels, and are completely reversible even in the continuous presence of NPs.

My role in this field consisted in assessing 1) the possible molecular targets correlated with cytosolic Ca^{2+} signals observed following the administration of 50 nm SiO_2 NPs and 2) investigating the Ca^{2+} mobilizing mechanisms involved in these processes (see section 1.4 and 1.5).

Under the supervision of Prof. Carla Distasi and Prof. Lovisolo, I performed patch clamp measurements, which combined with long-term recordings of electrical activity with multielectrode arrays, provided evidence that these SiO_2 NPs evoke a transient depolarization of the membrane potential, leading to a modulation of action potential firing without any change in gene expression. These results were published in 2018 in the journal *Scientific Reports* (quoted in full in Chapter 2) as:

> *C. Distasi, F. A. Ruffinatti, M. Dionisi, S. Antoniotti, A. Gilardino, G. Croci, B. Riva, E. Bassino, G. Alberto, E. Castroflorio, D. Incarnato, E. Morandi, G. Martra, S. Oliviero, L. Munaron & D. Lovisolo (2018)* "**SiO_2 nanoparticles**

modulate the electrical activity of neuroendocrine cells without exerting genomic effects." *Sci. Rep.* **8**, 1–12

In view of a safe and effective use of these tools in biomedical applications, the next step was to provide a detailed electrophysiological characterization of the responses elicited by NPs in GT1-7 neuronal cells. Ca^{2+} imaging data on cell populations and electrophysiological recordings pointed out three classes of channels as the major components of the observed Ca^{2+} signals following the administration of 50 nm SiO_2 NPs: TRPV4, Cx and Panx-like channels. All these channels are known to be involved in a wide spectrum of physiological and pathological processes and characterized by multiple activation mechanisms (see Section 1.5 and 1.6). In this specific case, the most relevant mechanism is likely related to the production of reactive species, since we have shown that lipid peroxidation is significantly increased after 30 min of NP exposure and that preincubation with the antioxidant N-acetyl-L-cysteine (NAC) strongly reduced the increase in NP-induced $[Ca2+]_i$. Furthermore, a relevant issue in the interpretation of these data is the finding that their activation has been observed also in excised membrane patches (outside out configuration) suggesting the implication of a direct membrane-delimited pathway. This fact does not exclude the coexistence of more than one mechanism, being all the three group of channels involved, for example, in the transduction of cell stretch and mechanical pressure.

These results were published in 2019 in the journal *Nanomedicine* as:

Carla Distasi, Marianna Dionisi*, Federico Alessandro Ruffinatti, Alessandra Gilardino, Roberta Bardini, Susanna Antoniotti, Federico Catalano, Eleonora Bassino, Luca Munaron, Gianmario Martra & Davide Lovisolo* (2019) "**The interaction of SiO_2 nanoparticles with the neuronal cell membrane: Activation of ionic channels and calcium influx.**" *Nanomedicine* **8**, 575–594

where * means that these two authors contributed equally to this work. In particular, I contributed by performing and analyzing whole cell and inside-out patch patch clamp experiments. Chapter 3 quotes in full this article

In parallel I also addressed the problem of OHP induced peripheral neurotoxicity (OIPN). In particular, given that intracellular Ca^{2+} related-events appears to play an important role in the onset of OIPN, we focused on the TRP family members (TRPV1, TRPA1, TRPM8) that are known to participate in the transduction of noxious stimuli. Ca^{2+} imaging experiments, performed by Dr. Beatrice Riva (Dept. Pharmaceutical Sciences, University of Piemonte Orientale "A. Avogadro"), showed that an acute treatment with OHP (6 h, 0,1 μg/mL) reduced the responses to capsaicin (TRPV1 agonist), but significantly enhanced the responses to icilin (TRPA1-M8 agonist). By using specific antagonist (BCTC, TRPV1-M8 antagonist; HC-030031, TRPA1 antagonist), we demonstrated that these increased responses in treated neurons exerted by icilin were mediated by a TRPA1-dependent mechanism. In parallel, we observed a significant OHP-induced acidification of intracellular pH (pH_i) in DRG cells both *in vitro* and *in vivo*. Since in our conditions, no changes in the levels of channel expression can be correlated with such enhanced responses, we investigated a pH-dependent hyperactivation of the channel. The electrophysiological patch clamp experiments in the cell attached mode, performed and analyzed by my supervisor and me, demonstrated that. In particular, we observed that when pH_i is restored in treated DRG neurons the hyperactivity of TRPA1 is normalized. All these results were published in 2018 in the journal *Scientific Reports* (quoted in full in Chapter 4) as:

> *Beatrice Riva, Marianna Dionisi, Alberto Potenzieri, Alessia Chiorazzi, Celia Cordero-Sanchez, Roberta Rigolio, Valentina Alda Carozzi, Dmitry Lim, Guido Cavaletti, Paola Marmiroli, Carla Distasi & Armando A. Genazzani (2018)* "**Oxaliplatin induces pH acidification in dorsal root ganglia neurons."** *Sci. Rep.* **8**, 1–12

Being pH_i an essential parameter in cellular homeostasis, it is likely that OHP-induced intracellular pH_i changes do not affect solely TRPA1 but also other types of channels. Several evidences of this hypothesis are presented in Chapter 5. In particular, I combined electrophysiological recordings at both single cell level (patch clamp technique) and at population level (multielectrode arrays, MEAs), as well as quantitative real-time polymerase chain reaction (qRT-PCR), to investigate the potential involvement of K_2P channels. Indeed, these channel proteins are known to play a key role in preserving and maintaining the neuronal excitability. Transient increments of expression levels, observed at 6 h post OHP-treatment, and the hyperactivity recorded in cell attached configuration of TREK-family members, confirmed the effective involvement of these channels in the OIPN. In this regard, the resultant hyper-excitability observed in OIPN could be interpreted as the effect of multiple adjustments on different molecular targets whose activity is altered by changes in the pH induced by chemotherapeutic agent.

Concluding remarks are drawn in Chapter 6 by joining information from all the previous works in order to provide an integrated view about the ionic channels and the main mechanisms involved in the chemically-induced neurotoxicity.

References

1. Chepelev, N. L., Moffat, I. D., Bowers, W. J. & Yauk, C. L. Neurotoxicity may be an overlooked consequence of benzo[a]pyrene exposure that is relevant to human health risk assessment. *Mutat. Res. - Rev. Mutat. Res.* **764**, 64–89 (2015).

2. Teleanu, D., Chircov, C., Grumezescu, A., Volceanov, A. & Teleanu, R. Impact of Nanoparticles on Brain Health: An Up to Date Overview. *J. Clin. Med.* **7**, 490 (2018).

3. Ge, D. *et al.* The neurotoxicity induced by engineered nanomaterials. *Int. J. Nanomedicine* **14**, 4167–4186 (2019).

4. Lovisolo, D., Dionisi, M., A. Ruffinatti, F. & Distasi, C. Nanoparticles and potential neurotoxicity: focus on molecular mechanisms. *AIMS Mol. Sci.* **5**, 1–13 (2018).

5. Bannunah, A. M., Vllasaliu, D., Lord, J. & Stolnik, S. Mechanisms of nanoparticle internalization and transport across an intestinal epithelial cell model: Effect of size and surface charge. *Mol. Pharm.* **11**, 4363–4373 (2014).

6. Lin, J. & Alexander-Katz, A. Cell membranes open 'doors' for cationic nanoparticles/ biomolecules: Insights into uptake kinetics. *ACS Nano* **7**, 10799–10808 (2013).

7. Zanella, D. *et al.* The direct permeation of nanoparticles through the plasma membrane transiently modifies its properties. *Biochim. Biophys. Acta - Biomembr.* **1861**, 182997 (2019).

8. Narayan, R., Nayak, U. Y., Raichur, A. M. & Garg, S. Mesoporous silica nanoparticles: A comprehensive review on synthesis and recent advances. *Pharmaceutics* **10**, 1–49 (2018).

9. Ariano, P. *et al.* Interaction of spherical silica nanoparticles with neuronal cells: Size-dependent toxicity and perturbation of calcium homeostasis. *Small* **7**, 766–774 (2011).

10. Gilardino, A. *et al.* Interaction of SiO<inf>2</inf> nanoparticles with neuronal cells: Ionic mechanisms involved in the perturbation of calcium homeostasis. *Int. J. Biochem. Cell Biol.* **66**, 101–111 (2015).

11. Zajaczkowską, R. *et al.* Mechanisms of chemotherapy-induced peripheral neuropathy. *Int. J. Mol. Sci.* **20**, (2019).

12. Aromolaran, K. A. & Goldstein, P. A. Ion channels and neuronal hyperexcitability in chemotherapy-induced peripheral neuropathy: Cause and effect? *Mol. Pain* **13**, 1–24 (2017).

13. Grisold, W., Cavaletti, G. & Windebank, A. J. Peripheral neuropathies from chemotherapeutics and targeted agents : *Neuro. Oncol.* **14**, 45–54 (2012).

14. Park, S. B. *et al.* <CA CANCER J CLIN 2013_Park_peripheral neuropathy cisplatin.pdf>. *CA Cancer J. Clin.* **63**, 419–437 (2013).

15. Chiorazzi, A., Semperboni, S. & Marmiroli, P. Current view in platinum drug mechanisms of peripheral neurotoxicity. *Toxics* **3**, 304–321 (2015).

16. Paola Marmiroli, Guido Cavaletti, Valentina Carozzi, Beatrice Riva, Dmitry Lim, A. A. G. Calcium-related Neurotoxicity of Oxaliplatin: Understanding the Mechanisms to Drive Therapy. Current Medicinal Chemistry Volume 22, Issue 32 , (2015).

17. Kaufman, M. A. *Environmental Neurotoxicology. The Committee on Neurotoxicology and Models for Assessing Risk, Board on Environmental Studies and Toxicology, Commission on Life Sciences, National Research Council . The Quarterly Review of Biology* vol. 69 (1994).

18. Harris, J. B. & Blain, P. G. Neurotoxicology: What the neurologist needs to know. *Neurol. Pract.* **75**, (2004).

19. Kann, O. & Kovács, R. Mitochondria and neuronal activity. *Am. J. Physiol. - Cell Physiol.* **292**, (2007).

20. Schwarz, T. L. Mitochondrial trafficking in neurons. *Cold Spring Harb. Perspect. Med.* **3**, 1–16 (2013).

21. Schmidt, B. Z. *et al.* In vitro acute and developmental neurotoxicity screening: an overview of cellular platforms and high-throughput technical possibilities. *Arch. Toxicol.* **91**, 1–33 (2017).

22. Podratz, J. L. *et al.* Cisplatin induced Mitochondrial DNA damage in dorsal root ganglion neurons. *Neurobiol. Dis.* **41**, 661–668 (2011).

23. Lee, J., Giordano, S. & Zhang, J. Autophagy, mitochondria and oxidative stress: Cross-talk and redox signalling. *Biochem. J.* **441**, 523–540 (2012).

24. Luo, Y. H. *et al.* Cadmium-based quantum dot induced autophagy formation for cell survival via oxidative stress. *Chem. Res. Toxicol.* **26**, 662–673 (2013).

25. Xia, T., Kovochich, M., Liong, M., Zink, J. I. & Nel, A. E. Cationic Polystyrene Nanosphere. *ACS Nano* **2**, 85–96 (2008).

26. Yang, Z. *et al.* A review of nanoparticle functionality and toxicity on the central nervous system. *Nanotechnology, Brain, Futur.* 313–332 (2013) doi:10.1007/978-94-007-1787-9_18.

27. Xu, F., Piett, C., Farkas, S., Qazzaz, M. & Syed, N. I. Silver nanoparticles (AgNPs) cause degeneration of cytoskeleton and disrupt synaptic machinery of cultured cortical neurons. *Mol. Brain* **6**, 1 (2013).

28. Hong, F. *et al.* Suppression of neurite outgrowth of primary cultured hippocampal neurons is involved in impairment of glutamate metabolism and NMDA receptor function caused by nanoparticulate TiO<inf>2</inf>. *Biomaterials* **53**, 76–85 (2015).

29. Liu, Z., Ren, G., Zhang, T. & Yang, Z. The inhibitory effects of nano-Ag on voltage-gated potassium currents of hippocampal CA1 neurons. *Environ. Toxicol.* **26**, 552–558 (2011).

30. Tang, M. *et al.* Mechanisms of unmodified CdSe quantum dot-induced elevation of cytoplasmic calcium levels in primary cultures of rat hippocampal neurons. *Biomaterials* **29**, 4383–4391 (2008).

31. Wei, H. *et al.* Ultrafine carbon black induces glutamate and ATP release by activating connexin and pannexin hemichannels in cultured astrocytes. *Toxicology* **323**, 32–41 (2014).

32. Lolignier, S. *et al.* The Nav1.9 Channel Is a Key Determinant of Cold Pain Sensation and Cold Allodynia. *Cell Rep.* **11**, 1067–1078 (2015).

33. Argyriou, A. A. *et al.* Voltage-gated sodium channel polymorphisms play a pivotal role in the development of oxaliplatin-induced peripheral neurotoxicity: Results from a prospective multicenter study. *Cancer* **119**, 3570–3577 (2013).

34. Ta, L. E. *et al.* Transient Receptor Potential Vanilloid 1 is essential for cisplatin-induced heat hyperalgesia in mice. *Mol. Pain* **6**, 1–15 (2010).

35. Zhao, M. *et al.* Acute cold hypersensitivity characteristically induced by oxaliplatin is caused by the enhanced responsiveness of TRPA1 in mice. *Mol. Pain* **8**, 1–11 (2012).

36. Poupon, L. *et al.* Targeting the TREK-1 potassium channel via riluzole to eliminate the neuropathic and depressive-like effects of oxaliplatin. *Neuropharmacology* **140**, 43–61 (2018).

37. Descoeur, J. *et al.* Oxaliplatin-induced cold hypersensitivity is due to remodelling of ion channel expression in nociceptors. *EMBO Mol. Med.* **3**, 266–278 (2011).

38. Furtado, D. *et al.* Overcoming the Blood–Brain Barrier: The Role of Nanomaterials

in Treating Neurological Diseases. *Adv. Mater.* **30**, (2018).

39. Görlach, A., Bertram, K., Hudecova, S. & Krizanova, O. Calcium and ROS: A mutual interplay. *Redox Biol.* **6**, 260–271 (2015).

40. Nayernia, Z., Jaquet, V. & Krause, K. H. New insights on NOX enzymes in the central nervous system. *Antioxidants Redox Signal.* **20**, 2815–2837 (2014).

41. Demaurex, N. & Scorrano, L. Reactive oxygen species are NOXious for neurons. *Nat. Neurosci.* **12**, 819–820 (2009).

42. Genestra, M. Oxyl radicals, redox-sensitive signalling cascades and antioxidants. *Cell. Signal.* **19**, 1807–1819 (2007).

43. Dayem, A. A. *et al.* The role of reactive oxygen species (ROS) in the biological activities of metallic nanoparticles. *Int. J. Mol. Sci.* **18**, 1–21 (2017).

44. Brandes, R. P., Weissmann, N. & Schröder, K. Nox family NADPH oxidases: Molecular mechanisms of activation. *Free Radic. Biol. Med.* **76**, 208–226 (2014).

45. Bedard, K. & Krause, K. H. The NOX family of ROS-generating NADPH oxidases: Physiology and pathophysiology. *Physiol. Rev.* **87**, 245–313 (2007).

46. Ott, M., Gogvadze, V., Orrenius, S. & Zhivotovsky, B. Mitochondria, oxidative stress and cell death. *Apoptosis* **12**, 913–922 (2007).

47. Gaschler, M. M. & Stockwell, B. R. Lipid peroxidation in cell death. *Biochem. Biophys. Res. Commun.* **482**, 419–425 (2017).

48. Berridge, M. J., Bootman, M. D. & Roderick, H. L. Calcium signalling: Dynamics, homeostasis and remodelling. *Nat. Rev. Mol. Cell Biol.* **4**, 517–529 (2003).

49. Raffaello, A., Mammucari, C., Gherardi, G. & Rizzuto, R. Calcium at the Center of Cell Signaling: Interplay between Endoplasmic Reticulum, Mitochondria, and Lysosomes. *Trends Biochem. Sci.* **41**, 1035–1049 (2016).

50. Zecchini, E. & Pinton, P. NIH Public Access. **1787**, 1342–1351 (2010).

51. Berridge, M. J., Lipp, P. & Bootman, M. D. 2000-Review-Calcium Signalling. **1**, (2000).

52. Schwaller, B. Ca2+ buffers. *Handb. Cell Signaling, 2/e* **2**, 955–962 (2010).

53. Boron, W. F. Regulation of intracellular pH. *Am. J. Physiol. - Adv. Physiol. Educ.* **28**, 160–179 (2004).

54. Casey, J. R., Grinstein, S. & Orlowski, J. Sensors and regulators of intracellular pH. *Nat. Rev. Mol. Cell Biol.* **11**, 50–61 (2010).

55. Ruffin, V. A., Salameh, A. I., Boron, W. F. & Parker, M. D. Intracellular pH regulation by acid-base transporters in mammalian neurons. *Front. Physiol.* **5 FEB**, 1–11 (2014).

56. Deitmer, J. W., Theparambil, S. M., Ruminot, I. & Becker, H. M. The role of membrane acid/base transporters and carbonic anhydrases for cellular pH and metabolic processes. *Front. Neurosci.* **9**, (2015).

57. Montell, C. The TRP superfamily of cation channels. *Sci. STKE* **2005**, (2005).

58. Ramsey, I. S., Delling, M. & Clapham, D. E. A i trp c. *October* (2006) doi:10.1146/annurev.physiol.68.040204.100431.

59. Nilius, B. & Owsianik, G. The transient receptor potential family of ion channels. *Genome Biol.* **12**, (2011).

60. Venkatachalam, K. & Montell, C. TRP Channels TRP: Transient Receptor Potential. *Annu Rev Biochem.* **76**, 387–417 (2007).

61. Nilius, B. *et al.* Gating of TRP channels: A voltage connection? *J. Physiol.* **567**, 35–44 (2005).

62. Nilius, B., Mahieu, F., Karashima, Y. & Voets, T. Regulation of TRP channels: A voltage-lipid connection. *Biochem. Soc. Trans.* **35**, 105–108 (2007).

63. Hong, Z. *et al.* Enhanced oxidative stress is responsible for TRPV4-induced neurotoxicity. *Front. Cell. Neurosci.* **10**, 1–8 (2016).

64. Becker, D., Blase, C., Bereiter-Hahn, J. & Jendrach, M. TRPV4 exhibits a functional role in cell-volume regulation. *J. Cell Sci.* **118**, 2435–2440 (2005).

65. Wang, Y. Y., Chang, R. B., Allgood, S. D., Silver, W. L. & Liman, E. R. A TRPA1-dependent mechanism for the pungent sensation of weak acids. *J. Gen. Physiol.* **137**, 493–505 (2011).

66. Dhaka, A. *et al.* TRPV1 is activated by both acidic and basic pH. *J. Neurosci.* **29**, 153–158 (2009).

67. Startek, J. B., Boonen, B., Talavera, K. & Meseguer, V. TRP channels as sensors of chemically-induced changes in cell membrane mechanical properties. *Int. J. Mol. Sci.* **20**, (2019).

68. Kaneko, Y. & Szallasi, A. Transient receptor potential (TRP) channels: A clinical perspective. *Br. J. Pharmacol.* **171**, 2474–2507 (2014).

69. Willebrords, J., Maes, M., Crespo Yanguas, S. & Vinken, M. Inhibitors of connexin and pannexin channels as potential therapeutics. *Pharmacol. Ther.* **180**, 144–160

(2017).

70. Retamal, M. A. Connexin and Pannexin hemichannels are regulated by redox potential. *Front. Physiol.* **5 FEB**, 1–9 (2014).

71. Giaume, C., Leybaert, L., Naus, C. C. & Sáez, J. C. Connexin and pannexin hemichannels in brain glial cells: Properties, pharmacology, and roles. *Front. Pharmacol.* **4 JUL**, 1–17 (2013).

72. Patel, D., Zhang, X. & Veenstra, R. D. Connexin hemichannel and pannexin channel electrophysiology: How do they differ? *FEBS Lett.* **588**, 1372–1378 (2014).

73. Chiu, Y.-H., Schappe, M. S., Desai, B. N. & Bayliss, D. A. Revisiting multimodal activation and channel properties of Pannexin 1. *J. Gen. Physiol.* **150**, 19–39 (2018).

74. Bond, S. R. & Naus, C. C. The pannexins: Past and present. *Front. Physiol.* **5 FEB**, 1–24 (2014).

75. Makarenkova, H. P., Shah, S. B. & Shestopalov, V. I. The two faces of pannexins: New roles in inflammation and repair. *J. Inflamm. Res.* **11**, 273–288 (2018).

76. Niemeyer, M. I., Cid, L. P., Gonzalez, W. & Sepulveda, F. V. Gating, Regulation, and Structure in K2P K+ Channels: In Varietate Concordia? *Mol. Pharmacol.* **90**, 309–317 (2016).

77. Gada, K. & Plant, L. D. Two-pore domain potassium channels: emerging targets for novel analgesic drugs: IUPHAR Review 26. *Br. J. Pharmacol.* **176**, 256–266 (2019).

78. Schewe, M. *et al.* A Non-canonical Voltage-Sensing Mechanism Controls Gating in K2P K+Channels. *Cell* **164**, 937–949 (2016).

79. Li, X. Y. & Toyoda, H. Role of leak potassium channels in pain signaling. *Brain Res. Bull.* **119**, 73–79 (2015).

80. Waxman, S. G. & Zamponi, G. W. Regulating excitability of peripheral afferents: Emerging ion channel targets. *Nat. Neurosci.* **17**, 153–163 (2014).

81. Levitz, J. *et al.* Heterodimerization within the TREK channel subfamily produces a diverse family of highly regulated potassium channels. *Proc. Natl. Acad. Sci.* **113**, 4194–4199 (2016).

82. Radio, N. M. & Mundy, W. R. Developmental neurotoxicity testing in vitro: Models for assessing chemical effects on neurite outgrowth. *Neurotoxicology* **29**, 361–376 (2008).

83. Posimo, J. M. *et al.* Viability assays for cells in culture. *J. Vis. Exp.* **2**, 1–14 (2014).

84. Präbst, K., Engelhardt, H., Ringgeler, S. & Hübner, H. Colorimetric Proliferation Assays. *Basic Color. Prolif. Assays MTT, WST, Resazurin* **1601**, 1–17 (2017).

85. Kumar, P., Nagarajan, A. & Uchil, P. D. Analysis of cell viability by the lactate dehydrogenase assay. *Cold Spring Harb. Protoc.* **2018**, 465–468 (2018).

86. Tong, Z. Bin *et al.* Characterization of three human cell line models for high-throughput neuronal cytotoxicity screening. *J. Appl. Toxicol.* **37**, 167–180 (2017).

87. McConnell, E. R., McClain, M. A., Ross, J., LeFew, W. R. & Shafer, T. J. Evaluation of multi-well microelectrode arrays for neurotoxicity screening using a chemical training set. *Neurotoxicology* **33**, 1048–1057 (2012).

88. Wheeler, B. C. & Nam, Y. In Vitro Microelectrode Array Technology and Neural Recordings. *Crit. Rev. Biomed. Eng.* **39**, 45–61 (2012).

89. Newberry, K. *et al.* Development of a spontaneously active dorsal root ganglia assay using multiwell multielectrode arrays. *J. Neurophysiol.* **115**, 3217–3228 (2016).

90. Massobrio, P., Tessadori, J., Chiappalone, M. & Ghirardi, M. In vitro studies of neuronal networks and synaptic plasticity in invertebrates and in mammals using multielectrode arrays. *Neural Plast.* **2015**, (2015).

91. Neher, E. & Sakmann, B. Single-channel currents recorded from membrane of denervated frog muscle fibres. *Nature* **260**, 799–802 (1976).

92. Plant, L. D. A Role for K2P Channels in the Operation of Somatosensory Nociceptors. *Front. Mol. Neurosci.* **5**, 1–11 (2012).

93. Lamas, J. A., Rueda-Ruzafa, L. & Herrera-Pérez, S. Ion Channels and Thermosensitivity: TRP, TREK, or Both? *Int. J. Mol. Sci.* **20**, (2019).

94. Zhao, M. *et al.* Acute cold hypersensitivity characteristically induced by oxaliplatin is caused by the enhanced responsiveness of TRPA1 in mice. *Mol. Pain* **8**, 1–11 (2012).

95. Alloui, A. *et al.* TREK-1, a K+ channel involved in polymodal pain perception. *EMBO J.* **25**, 2368–2376 (2006).

96. Noël, J. *et al.* The mechano-activated K±channels TRAAK and TREK-1 control both warm and cold perception. *EMBO J.* **28**, 1308–1318 (2009).

97. Riva, B. *et al.* Oxaliplatin induces pH acidification in dorsal root ganglia neurons. *Sci. Rep.* **8**, 1–12 (2018).

98. Patel, A. J. *et al.* A mammalian two pore domain mechano- gated S- like K +

channel. *EMBO J.* **17**, 4283–4290 (1998).

99. Braun, G., Lengyel, M., Enyedi, P. & Czirják, G. Differential sensitivity of TREK-1, TREK-2 and TRAAK background potassium channels to the polycationic dye ruthenium red. *Br. J. Pharmacol.* **172**, 1728–1738 (2015).

100. Lesage, F., Terrenoire, C., Romey, G. & Lazdunski, M. Human TREK2, a 2P Domain Mechano-sensitive K+Channel with Multiple Regulations by Polyunsaturated Fatty Acids, Lysophospholipids, and Gs, Gi, and GqProtein-coupled Receptors. *J. Biol. Chem.* **275**, 28398–28405 (2000).

101. Renn, C. L. *et al.* Multimodal assessment of painful peripheral neuropathy induced by chronic oxaliplatin-based chemotherapy in mice. *Mol. Pain* **7**, 29 (2011).

102. Marmiroli, P. *et al.* Susceptibility of different mouse strains to oxaliplatin peripheral neurotoxicity: Phenotypic and genotypic insights. *PLoS One* **12**, 1–25 (2017).

103. Noël, J., Sandoz, G. & Lesage, F. Molecular regulations governing TREK and TRAAK channel functions. *Channels* **5**, 402–409 (2011).

104. Kang, D., Choe, C., Cavanaugh, E. & Kim, D. Properties of single two-pore domain TREK-2 channels expressed in mammalian cells. *J. Physiol.* **583**, 57–69 (2007).

105. Fernández-Fernández, D. *et al.* Activation of TREK currents by riluzole in three subgroups of cultured mouse nodose ganglion neurons. *PLoS One* **13**, 1–24 (2018).

106. Kang, D., Choe, C. & Kim, D. Thermosensitivity of the two-pore domain K+ channels TREK-2 and TRAAK. *J. Physiol.* **564**, 103–116 (2005).

107. Kang, D. & Kim, D. TREK-2 (K 2P 10 . 1) and TRESK (K 2P 18 . 1) are major background K ƨ channels in dorsal root ganglion neurons. **2**, 138–146 (2006).

108. Feng, X. *et al.* Central nervous system toxicity of metallic nanoparticles. *Int. J. Nanomedicine* **10**, 4321–4340 (2015).

109. Golbamaki, N. *et al.* Genotoxicity of metal oxide nanomaterials: Review of recent data and discussion of possible mechanisms. *Nanoscale* **7**, 2154–2198 (2015).

110. Wang, Z. *et al.* Silver nanoparticles induced RNA polymerase-silver binding and RNA transcription inhibition in erythroid progenitor cells. *ACS Nano* **7**, 4171–4186 (2013).

111. Lehman, S. E. *et al.* Silica nanoparticle-generated ROS as a predictor of cellular toxicity: mechanistic insights and safety by design. *Environ. Sci. Nano* **3**, 56–66 (2016).

112. Wu, Q. F. *et al.* Activation of transient receptor potential vanilloid 4 involves in hypoxia/reoxygenation injury in cardiomyocytes. *Cell Death Dis.* **8**, e2828 (2017).

113. White, J. P. M. *et al.* TRPV4: Molecular conductor of a diverse orchestra. *Physiol. Rev.* **96**, 911–973 (2016).

114. Chuang, H. H. & Lin, S. Oxidative challenges sensitize the capsaicin receptor by covalent cysteine modification. *Proc. Natl. Acad. Sci. U. S. A.* **106**, 20097–20102 (2009).

115. Andersson, D. A., Gentry, C., Moss, S. & Bevan, S. Transient receptor potential A1 is a sensory receptor for multiple products of oxidative stress. *J. Neurosci.* **28**, 2485–2494 (2008).

116. Nazıroğlu, M. Activation of TRPM2 and TRPV1 Channels in Dorsal Root Ganglion by NADPH Oxidase and Protein Kinase C Molecular Pathways: a Patch Clamp Study. *Journal of Molecular Neuroscience* vol. 61 425–435 (2017).

117. Descoeur, J. *et al.* Oxaliplatin-induced cold hypersensitivity is due to remodelling of ion channel expression in nociceptors. *EMBO Mol. Med.* **3**, 266–278 (2011).

118. Miyake, T. *et al.* Cold sensitivity of TRPA1 is unveiled by the prolyl hydroxylation blockade-induced sensitization to ROS. *Nat. Commun.* **7**, (2016).

119. Piechotta, P. L. *et al.* The pore structure and gating mechanism of K2P channels. *EMBO J.* **30**, 3607–3619 (2011).

120. Potenzieri, A. *et al.* Oxaliplatin-induced neuropathy occurs through impairment of haemoglobin proton buffering and is reversed by carbonic anhydrase inhibitors. *Pain* **161**, 405–415 (2020).

121. Bucci, E., Fronticelli, C. & Ragatz, B. The proton-binding behavior of human hemoglobin and its subunits in their native state. *J. Biol. Chem.* **243**, 241–249 (1968).

Chapter 2

SiO_2 nanoparticles modulate the electrical activity of neuroendocrine cells without exerting genomic effects

C. Distasi[*+1], *F.A. Ruffinatti*[+1,6§], *M. Dionisi*[1], *S. Antoniotti*[2,6], *A. Gilardino*[2,6], *G. Croci*[2], *B.Riva*[1], *E. Bassino*[2], *G. Alberto*[3,6], *E. Castroflorio*[4], *D. Incarnato*[2,5], *E. Morandi*[2,5], *G. Martra*[3,6], *S. Oliviero*[2,5], *L. Munaron*[2,6], *D. Lovisolo*[2]

1. Dept. of Pharmaceutical Sciences, University of Piemonte Orientale "A. Avogadro", Novara, Italy 2. Dept. of Life Sciences and Systems Biology, University of Torino, Italy 3. Dept. of Chemistry, University of Torino, Italy 4. Center for Synaptic Neuroscience , Istituto Italiano di Tecnologia, Genova, Italy 5. Human Genetics Foundation, Torino, Italy 6. NIS Interdepartmental Center, University of Torino, Italy

+These two Authors contributed equally to the work

Abstract

Engineered silica nanoparticles (NPs) have attracted increasing interest in several applications, and particularly in the field of nanomedicine, thanks to the high biocompatibility of this material. For their optimal and controlled use, the understanding of the mechanisms elicited by their interaction with the biological target is a prerequisite, especially when dealing with cells particularly vulnerable to

environmental stimuli like neurons. Here we have combined different electrophysiological approaches (both at the single cell and at the population level) with a genomic screening in order to analyze, in GT1-7 neuroendocrine cells, the impact of SiO_2 NPs (50 $\pm$ 3 nm in diameter) on electrical activity and gene expression, providing a detailed analysis of the impact of a nanoparticle on neuronal excitability. We find that 20 μg mL^{-1} NPs induce depolarization of the membrane potential, with a modulation of the firing of action potentials. Recordings of electrical activity with multielectrode arrays provide further evidence that the NPs evoke a temporary increase in firing frequency, without affecting the functional behavior on a time scale of hours. Finally, NPs incubation up to 24 hours does not induce any change in gene expression.

2.1 Introduction

The fast development of nanoparticles (NPs) designed and engineered to be employed as tools for targeting to specific cells and tissues and for drug delivery has opened an entire new field in both basic science and medical applications. A preliminary, albeit essential, phase was devoted at addressing the concerns about their potential toxicity *in vitro* and, more relevantly, *in vivo*. A huge amount of papers[1-3] has evidenced the parameters (size, concentration, surface properties, etc.) that can determine the presence or absence of toxic effects, thus providing the rational background for designing safe and biocompatible nanotools. The next step is to switch the focus on the more subtle effects that can arise from a prolonged presence of NPs in contact with cells, and to understand the mechanisms that underlie the interaction between objects at the nanoscale and their cellular

and molecular targets. This task is particularly relevant when the target is represented by single nerve cells or by complex neuronal networks.

Engineered silica NPs have encountered a rapid diffusion in several applications in the last decade[4], specifically in nanomedicine, thanks to the high biocompatibility of this material[5]. We have reported that amorphous 50 nm SiO_2 NPs can be made fluorescent by hybridization with cyanine dyes and can be safely incorporated into neurons[6] and other cell types[7]. In a previous paper, we have shown that 50 nm SiO_2 NPs, at non-toxic doses, elicit increases in the intracellular calcium concentration, $[Ca^{2+}]_i$, in a neuroendocrine cell line, GT1-7 cells[8]. These signals are fully dependent on calcium influx, carried through different types of calcium permeable channels, and are completely reversible even in the continuous presence of NPs. A few other papers[3, 9-11] have reported that NPs of different composition can elicit changes in neuronal $[Ca^{2+}]_i$. This is a relevant topic, since perturbations of intracellular calcium homeostasis, even if reversible, can significantly affect neuronal excitability. Electrical activity is the most distinctive functional feature of neuronal cells, and the issue of the potential effects of NPs on the electrical behaviour of neurons and on the ionic channels that underlie it, while still only partially investigated, has attracted increasing interest in recent years, particularly in the light of their value as tools for nanoneuromedicine. Most of these studies deal with the effects of NPs on the properties of a specific channel (see e.g. Refs 12,13). Recently, a few excellent reviews, focused on the potential medical applications of NPs[14-16], have provided a comprehensive picture of the available knowledge about NPs and neuronal ionic channels; some of them also report the effects on action potential firing. Interestingly, both excitatory[17] and inhibitory[18,19] effects have been observed.

A further level of complexity that needs to be addressed stems from the finding that changes in the pattern of neuronal electrical activity may have effects on the expression of relevant genes, particularly when calcium influx is involved[20,21]. In the perspective of using SiO_2 NPs, both *in vitro* and *in vivo*, for applications such as drug delivery[22] or cell tracking[23] in neuronal cells and tissues, it is of the outmost importance to analyze at the cellular level the functional changes induced by the interaction with the NPs, and to investigate whether these changes have stable and long-lasting outcomes on the neuronal phenotype. We have addressed this issue by means of an integrated approach, combining patch-clamp recordings from single neuroendocrine cells and sensory neurons in culture with population recordings by means of multielectrode arrays (MEAs), spanning a time scale from early responses (min) after acute NPs application to hours. In addition, by means of a genomic approach, we have investigated the potential effects of the changes in neuronal activity on gene expression.

2.2 Materials and Methods

Materials. Unless otherwise specified, materials were obtained from Sigma Aldrich.

Synthesis of silica NPs. Synthesis and characterization of the SiO_2 nanoparticles have been described in previous papers[6, 8]. Briefly, bare silica nanoparticles were synthesized by the reverse microemulsion technique; in particular, a reverse microemulsion was prepared by mixing 75.0 mL of cyclohexane, 18.85 g of Triton X-100, 18.0 mL of n-hexanol and 5.4 mL of deionized H_2O in a round bottom flask. After 30 min of equilibration at room temperature and continuous gentle magnetic stirring, 1.0 mL of tetraethylorthosilicate (TEOS) was added; after further 10 min of equilibration, reaction was started by the addition of 0.7 mL of NH_3 (28-30%) and

continued overnight at room temperature under magnetic stirring. After 16 hrs, reaction was interrupted by the addition of acetone; then particles were extracted by centrifugation at 10,000 rpm for 20 min and finally washed twice with ethanol and several times with deionized water until complete removal of surfactant. The nanoparticles were stored in water suspension (1 mg mL^{-1}) at room temperature.

High resolution transmission electron microscopy (HRTEM). Micrographs of nanoparticles were acquired using a 3010 Jeol instrument operated at 300 kV. Samples were prepared by spreading a droplet of the corresponding suspensions in MilliQ H_2O (1.0 mg mL^{-1}) on a copper grid coated with a lacey carbon film and then letting water to slowly evaporate to limit particle agglomeration. The mean particle diameter was calculated as $d_m = \Sigma d_i n_i / \Sigma n_i$ (n_i= number of particles of diameter d_i) by measuring the size of ca. 300 particles.

Dynamic Light Scattering (DLS). DLS measurements were performed in a 90Plus Particle Size Analyzer (Brookhaven Instruments) at a laser wavelength of 660 nm, a detection angle of 90°, and 293 K. Samples were prepared by suspending NPs in Milli-Q water (pH 5.5, concentration: 0.1 mg mL^{-1}). DLS plots are reported in number distribution.

GT1-7 cell cultures. GT1-7 cells, an immortalized line derived from highly differentiated mouse gonadotropin-hormone releasing hormone (GnRH) neurons (generously donated by Prof. P.L. Mellon), were maintained in Dulbecco's Modified Eagle's medium (DMEM) supplemented with 10% fetal bovine serum (FBS, Lonza), gentamycin (50 µg mL^{-1}), and glutamine (2 mM) at 310 K, in a humidified atmosphere of 5% CO_2 in air. For patch-clamp experiments, cells were plated at the density of 9,000 cells cm^{-2} on uncoated plastic dishes (Corning). After 24 hrs, medium was changed to 0.5% FBS supplemented with 1/50 of B27 (Invitrogen) to

improve survival and differentiation, then switched to 0.5% FBS alone for 4-6 days for patch-clamp experiments (a protocol similar to that described in Ref. 25) or 8-15 days for multielectrode arrays (MEAs) experiments. Plating density was increased to 20,000-30,000 cells/cm^2 both for genomic experiments, in order to have a sufficient amount of cells for RNA extraction, and for recordings on MEAs, to reach a higher surface of microelectrodes covered by cells.

Isolation and Primary Cell Culture of Mouse Dorsal Root Ganglion Neurons. Mice were purchased from Charles River (Segrate, Italy). The care and husbandry of mice were in conformity with the institutional guidelines in compliance with national (D. L.vo 26/2014, Gazzetta Ufficiale della Repubblica Italiana, n.61, March 14th 2014) and international laws and policies (European Union directive 2010/63/UE; Guide for the Care and Use of Laboratory Animals, U.S. National Research Council, 1996). Adult Balb-C mice (5/10-wk-old) were euthanized under deep isoflurane-induced anaesthesia. The procedures were approved by the local animal-health and ethical committee (Università del Piemonte Orientale) and were authorized by the national authority (Istituto Superiore di Sanità; authorization number N. 22/2013).

DRG were aseptically removed and collected in a dish containing cold F12 (Nutrient Mixture F12 Ham) medium. Working under a dissecting microscope and using fine forceps, the surrounding membrane was gently teased away from each DRG; nerves and sheath were cut. All desheathed DRG were then transferred into a sterile 35 mm dish containing collagenase from clostridium hystoliticum 0.125% and DNase in F12 medium and incubated at 310 K for 1 hour. After incubation, DRG were triturated using a tip p1000. Myelin and nerve debris were eliminated by centrifugation trough a bovine serum albumin (BSA) cushion. Cell pellet was re-suspended in Bottenstein and Sato medium (BS) (30% F12, 40% DMEM (Dulbecco's Modified Eagle's medium, 30% Neurobasal A medium (Life Technologies, Italy), 100

X N2 supplement (Life Technologies, Italy), penicillin 10 U/mL and streptomycin 100 mg/mL, supplemented with Recombinant Human β-NGF, Recombinant Murine GDNF and Recombinant Human NT3 (Peprotech, USA) and plated onto 35 mm Petri dish pre-coated with laminin. Two days after, electrophysiological patch clamp measurements were performed on DRG neurons of all soma sizes.

Exposure to NPs. Prior to the experiments, cells were switched to the appropriate extracellular medium (either DMEM or standard physiological solution, both serum-free). NPs, stored in a stock solution (1 mg mL^{-1} in water) were sonicated for 20 min before final dilution. For all protocols except patch-clamp, the NPs were administered by substituting the extracellular solution with an identical one containing a stable suspension of NPs at the final desired concentration.

Incorporation of nanoparticles. For conventional transmission electron microscopy (TEM), GT1-7 cells were treated for 1 and 2 hours with NPs and then fixed with 1.2 % glutaraldehyde in 66 mM sodium cacodylate buffer, post-fixed in 1% OsO_4, 1.5% $K_4Fe(CN)_6$, 0.1 M sodium cacodylate, *en bloc* stained with 1% uranyl acetate, dehydrated, and flat embedded in epoxy resin (Epon 812, TAAB). After baking for 48 hrs, the glass coverslip was removed from the Epon block by thermal shock. Cells were identified by means of a stereomicroscope, excised from the block and mounted on a cured Epon block for sectioning using an EM UC6 ultramicrotome (Leica Microsystem, Vienna). Ultrathin sections (70-90 nm thick) were collected on copper mesh grids and observed with a JEM-1011 microscope (Jeol, Tokyo, Japan) operating at 100 kV and equipped with an ORIUS SC1000 CCD camera (Gatan, Pleasanton, CA). For each experimental condition, at least 100 images were acquired at 10,000 to 15,000× magnification and analyzed using the ImageJ software[37].

Si^{2+} uptake was quantified by using inductively coupled plasma mass spectrometry (ICP-MS; element-2; Thermo-Finnigan, Rodano (MI), Italy). GT1-7 cells were seeded at the initial density of 20.000 cells cm^{-2} in DMEM 10% FCS. The following day, the medium was changed with DMEM 0.5% FCS supplemented with B27 to improve survival and differentiation. Afterward, cells were incubated with SiO_2 NPs (20 μg mL^{-1}) added to DMEM 0.5% FCS for 1 and 24 hrs. After the treatments cells were washed for three times with PBS solution, detached with Trypsin, recounted and collected into an appropriate conical tube and centrifuged (5 minutes at 1000 rpm). The supernatant was discarded and the pellet was analyzed with ICP-MS. Sample digestion was performed with concentrated HNO_3 (70%, 1 mL) under microwave heating at 433 K for 20 minutes (Milestone MicroSYNTH Microwave labstation). Control measurements were performed as above but omitting nanoparticles; values were below the sensitivity of the instrument.

Electrophysiology - Patch-clamp. Conventional whole cell patch-clamp recordings were performed in the current clamp mode at 295-298 K. Cells were continuously superfused with a standard physiological solution of the following composition (in mM): NaCl, 154; KCl, 4; $CaCl_2$, 2; $MgCl_2$, 1; 4-(2-hydroxyethyl)-1-piperazine ethane sulfonic acid (HEPES), 5; glucose, 5.5; and NaOH (pH 7.35). Composition of the pipette solution was (in mM): KCl, 15; $CaCl_2$, 3; $MgCl_2$, 3; Hepes, 5; KAsp, 118; EGTA, 5; Na_2ATP, 5; pH to 7.3 with KOH. Pipettes had a resistance of 2-5 MΩ. NPs were dispersed in the solutions at the required concentration. Solutions were applied by means of a microperfusion system connected to a set of five syringes containing the control and test solutions; the perfusion pipette was located at several tens of microns away from the cell to be recorded, in order to minimize mechanical perturbations. Correction for junction potential was performed analogically. Data were collected with an Axopatch 200B amplifier (Molecular Devices, USA) using

Clampex 10.2 and Axoscope 10.2 software. Step protocols, in the voltage clamp mode, were applied to check cell functionality. In the presence of NPs, whole cell recordings lasted from 5 to 30 min, durations comparable to those obtained in control experiments in the absence of NPs.

Electrophysiology - Multielectrode Arrays (MEAs). Extracellular GT1-7 action potentials were recorded by means of a commercial 60-channel multi-electrode array (MEA) setup. A description of the experimental apparatus is provided in Supplementary Methods online. An external T-control unit (TC02) kept the temperature of the socket surface at 310 K. The digitalized output-data coming from the USB-ME64 unit were acquired, monitored and recorded on a PC through MC_Rack software (Version 4.6.2, Multi Channel Systems MCS GmbH). To reduce the data file size, only upward (positive) and downward (negative) spike cutouts from each of the available recording electrodes were stored. These waveforms consisted of 1 ms pre-spike and 2 ms post-spike fragments respect to the point of threshold crossing. Threshold was fixed at ±6 standard deviations from baseline noise (typically around 15 µV peak-to-peak). A channel was considered active if it recorded at least 30 spikes in 5 hrs. In general, according to the technical specifications of the device, one electrode does not correspond to a single cell. Rather, each electrode can detect all the electrical signals originating in the spatial region surrounding it, within a radius of tens of micrometers. Waveforms drawn from each active channel were finally transformed into time stamps using NeuroExplorer (Nex Technologies, USA). The same software was used also to make raster plots and rate histograms.

Survival assay. Cytotoxicity was evaluated by counting cells with a Burker chamber at 24 hours after incubation in DMEM medium supplemented with B27 without FBS

either in the presence or in the absence of the NPs. Data are expressed as number of cells/cm^2.

RNA-Seq analysis. GT1-7 cells, plated in 10 cm Petri dishes and kept in 0.5% FBS for 4 days, were shifted to DMEM without FBS to prevent adsorption of serum proteins to NPs and either treated or not (control cells) with 20 μg L^{-1} NPs for 30 min, 1, 6 and 24 hrs. Cells were then washed with ice cold PBS and lysed with TriReagent (Sigma), 1 mL per dish, harvested with a scraper and stored at 193 K until RNA extraction. RNA was purified as previously described[38]. RNA integrity measurements were performed using Fragment Analyzer™ (Advanced Analytical). All samples had RNA Quality Number (RQN) greater than 9.8. RT-qPCR was performed using the SuperScript III Platinum One-Step Quantitative RT-PCR System (Invitrogen) following the manufacturer's instructions. Library preparation was performed using Illumina TruSeq RNA prep-kit following manufacturer's instructions. Reads were mapped using TopHat2[39] and RPKM were calculated using cuffdiff tool from Cufflinks software package[40]. Data analysis and plotting was performed using custom R scripts[41]. RNA-seq data has been deposited on Gene Expression Omnibus database under the accession GSE98032.

Statistical analysis. Particle size evaluated by TEM is given as mean ± SD. Unless otherwise specified, all other data are expressed as means ± SEM. For analysis of NP-cell internalization, differences were assessed by a Mann-Whitney U test; for ICP-MS measurements and cell survival assays, differences were checked by a *t*-test (after normality had been verified through a Shapiro-Wilk test); in the analysis of MEAs recordings, to compare the differences in firing rate, a paired-samples sign test was used.

Data availability. The RNA-seq data has been deposited on Gene Expression Omnibus database under the accession GSE98032. All other datasets generated and

analysed during the current study are available from the corresponding author on reasonable request.

2.3 Results

SiO_2 NPs interact with the cell membrane and are incorporated in endocytic compartments

In agreement with previous studies[5, 6] TEM and DLS analysis (Fig. 1) indicated that the lab made SiO_2 were in the form of nanospheres with a narrow size distribution (mean diameter 50 $\pm$ 3 nm). When suspended in water they mainly exhibited a hydrodynamic diameter similar to what observed in TEM images, indicating that they suffered a very limited aggregation.

In order to analyze the distribution of nanoparticles on the cell membrane, we imaged by electron microscopy GT1-7 cells exposed for 1 or 2 hours to 20 µg mL^{-1} NPs. Ultrastructural analysis (Fig. 2a,b) reveals that the NPs were present on the plasma membrane (NP density for 1 hour treated cells: 2.60 ± 0.61 NPs μm^{-2}; 2 hours treated cells: 9.20 ± 0.39 NPs μm^{-2}; Fig. 2c) suggesting that they can interact with membrane channels at times shorter than 1 hour. Following the interaction with the plasma membrane, nanoparticles could be internalized inside the cell. Intriguingly, free nanoparticles were never imaged either in the cytoplasm of the GT1-7 cells or inside mitochondria, Golgi apparatus, endoplasmic reticulum or nucleus, but always inside membranous endocytic-like structures, indicating a possible induction of endocytosis after the interaction with the plasma membrane. A quantitative assessment of NPs incorporation in GT1-7 cells was performed by means of the ICP-MS technique (Fig. 2d). It can be seen that at 1 hour of incubation,

a detectable amount of NPs could be measured (0.43 ± 0.16 pg/cell), that was significantly increased at 24 hours (1.35 ± 0.31 pg/cell).

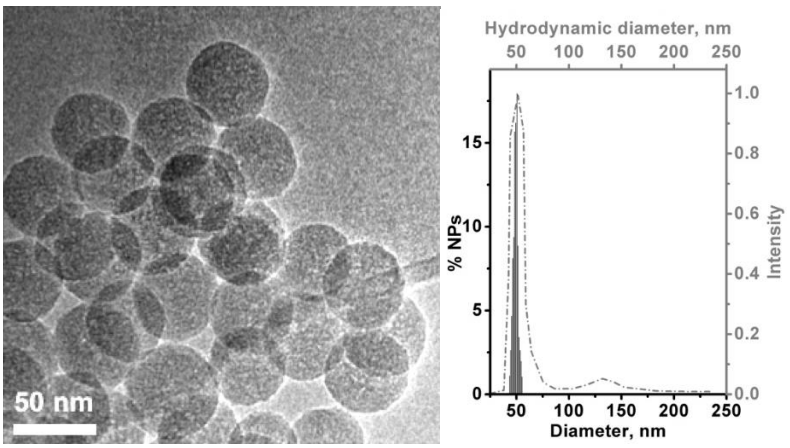

Fig. 1. **Characterization of the lab-made silica NPs**. Left: representative TEM image (original magnification: ×50k). Right: related particle size distribution by TEM data (histogram; values on the left Y and bottom X axes) and hydrodynamic diameters by DLS in water (dashed-dotted line; values on the right Y and top X axes).

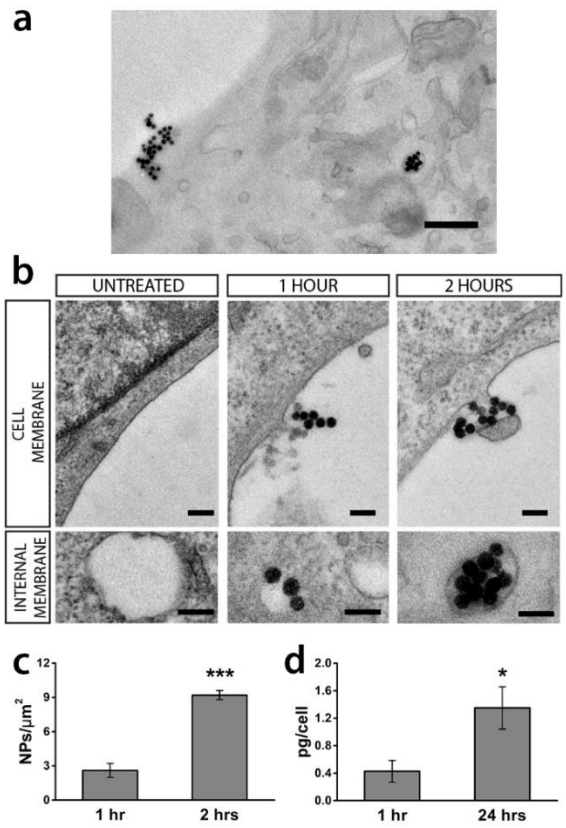

Fig. 2. Interaction with the plasmamembrane of GT1-7 cells and internalization of 50 nm SiO_2 NPs. (**a**) Low magnification TEM image of a GT1-7 cell with NPs on the plasmamembrane and in a vescicle (2 hours incubation). Scale bar: 500 nm. **(b)** After either 1 or 2 hours of incubation, small agglomerates of NPs could be observed in association with the plasmamembrane; some of them were already incorporated into endocytic vesicles. Scale bars: 100 nm. (**c**) NPs density obtained by TEM images at 1 and 2 hrs of incubation. Mann-Whitney U test; *** $p < 0.0001$ two-tailed, n = 3. **(d)** Quantitative assessment of internalization at 1 and 24 hours of incubation by means of ICP-MS. *t*-test, * $p = 0.037$ two-tailed, n = 4.

SiO_2 NPs elicit depolarizing responses in GT1-7 cells and adult mouse sensory neurons

When bathed in physiological Tyrode solution, GT1-7 cells showed different patterns of electrical activity as recorded in patch clamp experiments, in current clamp mode. Out of 32 cells, 19 had a stable resting potential (Fig. 3a,b), 10 cells

showed small oscillations (Fig. 3d); in three cells firing of full-sized action potential was detected (Fig. 3c). Average V_m was -69.7 ± 2.2 mV.

The 50 nm SiO_2 NPs were used at the concentration of 20 μg mL^{-1}, that in previous experiments had been shown to be non-toxic[6] and to elicit strong and long-lasting but reversible $[Ca^{2+}]_i$ oscillations[7]. When NPs were added to the extracellular Tyrode solution, they elicited a depolarizing response (average ΔV = 40.1 ± 3.1 mV) in 28 out of 32 cells. In most cells, after transient firing of one or few full action potentials, the membrane potential either showed oscillatory activity with small spikes

(Fig. 3a) or was stabilized at the depolarized value (Fig. 3b,c), without showing further oscillations and/or spikes, probably because of a strong inactivation of voltage dependent Na^+ and Ca^{2+} channels. In two cells firing activity was markedly increased for longer times (Fig. 3d).

The depolarizing response was in general irreversible, at least for the duration of the recordings (up to 20 min). The functional state of the cells, checked by transiently switching to the voltage clamp mode and recording responses to voltage stimulation protocols appeared to be preserved (an example, related to the response of Fig 3b, is shown in Supplementary Fig. S1 online).

In 2 experiments, cells were first challenged with a lower dose (0.5 μg mL^{-1}) and subsequently with 20 μg mL^{-1}. Supplementary Fig. S2 online shows that the lower dose induced a small and reversible depolarization, while the response to the higher one was stronger and oscillatory.

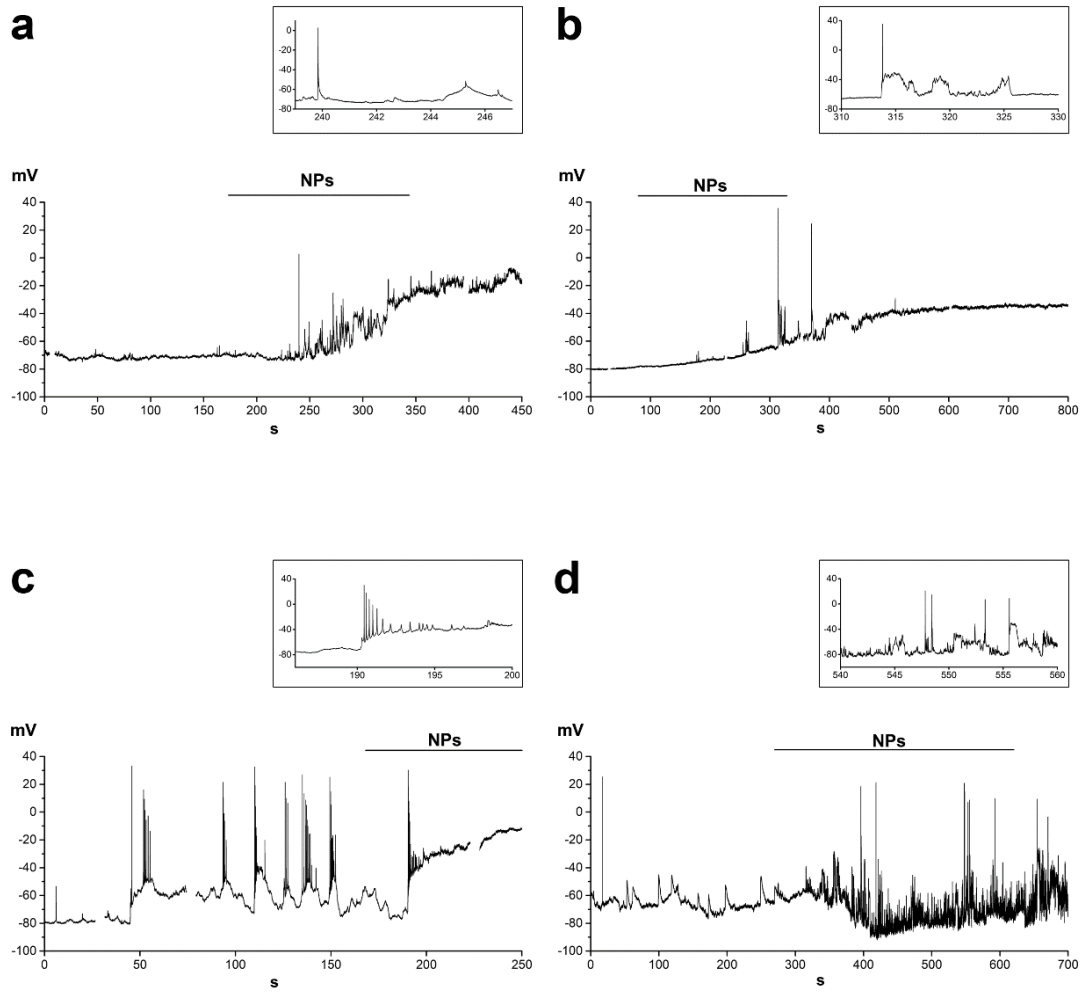

Fig. 3. Four examples of the changes in electrical activity recorded from single cells in response to 20 µg mL^{-1} SiO_2 NPs. Insets show expanded segments at the times indicated. Traces were blanked in correspondence to the application of the voltage clamp protocols as shown in Supplementary Fig. S1 online.

These findings were confirmed by recordings from another neuronal model, primary cultures of DRG sensory neurons from adult mice. DRG neurons had a stable resting potential of -60.7 ± 1.5 mV (n=20), ranging from -72.0 mV to -47.0 mV. Only 30% of neurons generated sporadic spontaneous activity. In all cells challenged with 20 μg mL^{-1} 50 nm SiO_2 NPs (n=8), we recorded a depolarizing response (average ΔV = 37.8 ± 3.0 mV, ranging from 27.5 to 53.8 mV). In most cells, the membrane potential shifted to a depolarized value without firing any action potential, as shown in Fig. 4a. The remaining two neurons, prior to the V_m stabilization at the depolarized value, fired one or a few action potentials in response to fast and transient V_m changes above threshold (Fig. 4b).

SiO_2 NPs transiently increase the electrical activity of GT1-7 cells in long lasting recordings

To provide further information on the electrical activity elicited by the NPs on a longer time scale, comparable to the duration (several hours) of the calcium imaging experiments reported in a previous paper[7] and at a population level with a non-invasive approach, we performed extracellular recordings from GT1-7 cells cultured on MEAs.

Full recordings sampled at 25 kHz (Fig. 5a) were filtered using a voltage threshold (see Methods) in order to extract extracellular action potential (EAP) waveforms from raw data (Fig.5b), and build raster plots (Fig. 5c, lower) and rate histograms (Fig. 5c, upper). Rate histograms represent the time course of the firing rate and they can be used to highlight how the electrical activity clusters in time.

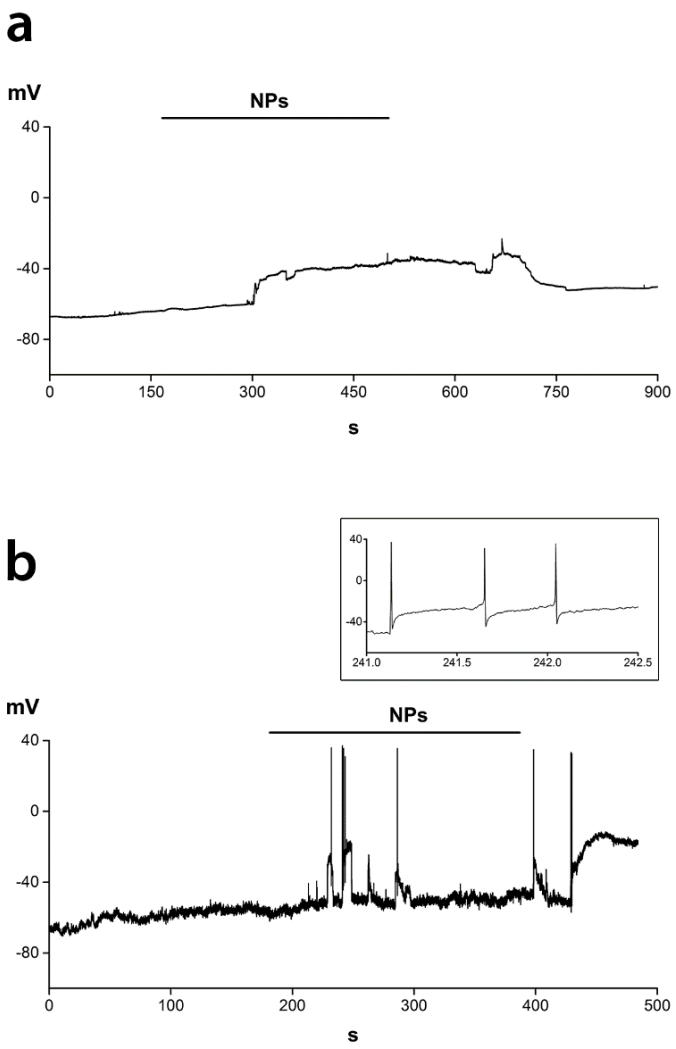

Fig. 4 Current clamp recordings from mouse DRG neurons. **(a,b**) Two examples of changes in Vm induced by 20 µg mL^{-1} SiO_2 NPs. Inset in **b** shows action potential firing at expanded time scale.

In our experiments, both under control condition and in presence of NPs, GT1-7 cells exhibited a characteristic firing pattern, in which active and resting phases alternated with an irregular period ranging from 5 to 15 min (Fig. 5c). This is in good agreement with the reported behavior of GT1-7 cells described in literature[24].

Over 24 different MEAs, just 7 (about 30% of the total) showed a sustained electrical activity in at least one MEA electrode. For each of these experiments, an average of 3 out of 59 electrodes (5%) recorded non-sporadic activity, resulting in a total of 21 independent long duration recordings. Half of them were silent channels under control conditions (standard physiological solution) that started to show electrical activity only after 20 μg mL^{-1} NPs administration (Fig. 5e, *e.g.* Exp7, Ch71+). Conversely, the other half presented some degree of spontaneous activity already under control conditions and the effect of NPs on these channels apparently consisted in a modulation of the number of EAPs recorded (Fig. 5e, *e.g*. Exp4, Ch82–), confirming the heterogeneity already observed in current clamp experiments.

In order to quantify the overall effects of NPs on GT1-7 firing rate, distinguishing between early and long lasting effects, we firstly decided to measure the average number of EAPs within two temporal windows of equal length (200 s), placed just before (Δt_{pre}) and immediately after (Δt_{post}, Fig. 5e) NPs administration. Within these temporal borders, active channels changed their firing rate according to Fig. 5d.

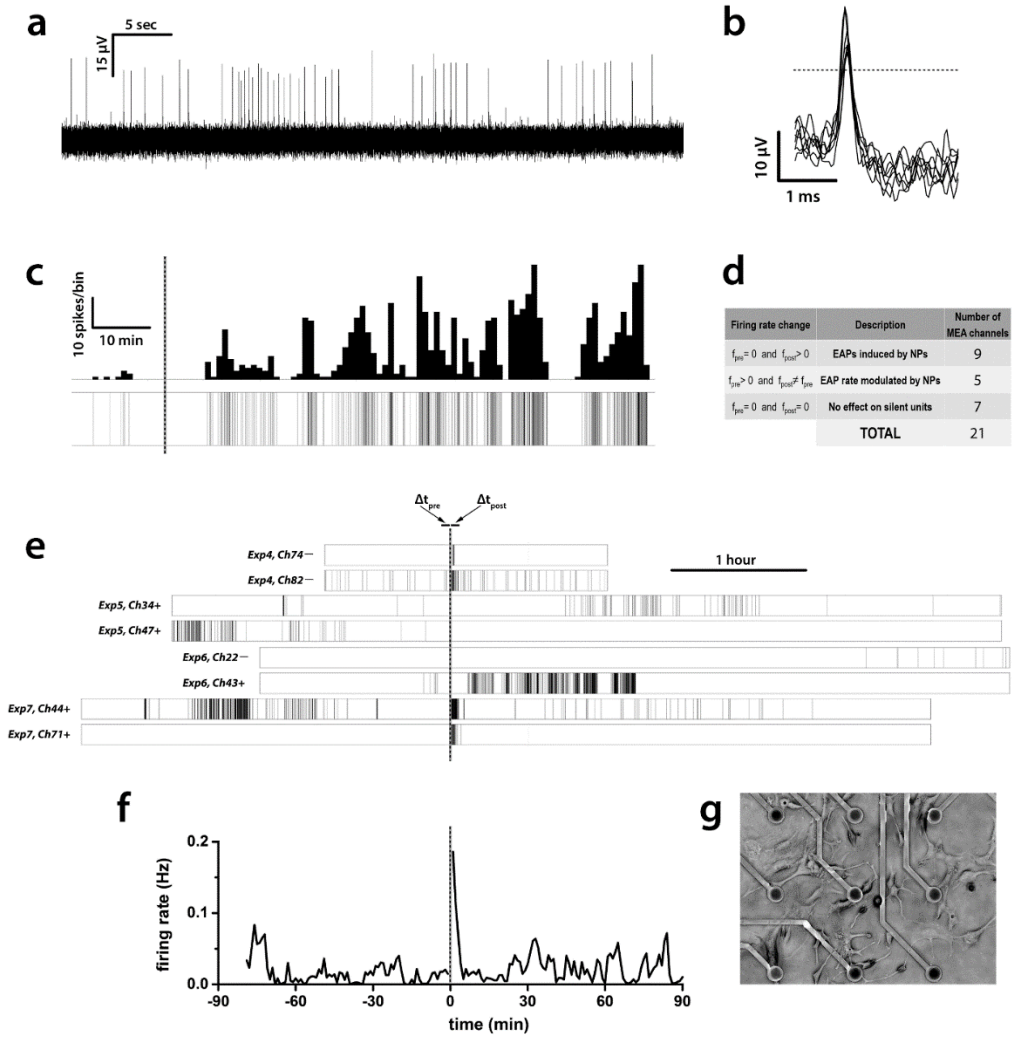

Firing rate change	Description	Number of MEA channels
$f_{pre}=0$ and $f_{post}>0$	EAPs induced by NPs	9
$f_{pre}>0$ and $f_{post}\neq f_{pre}$	EAP rate modulated by NPs	5
$f_{pre}=0$ and $f_{post}=0$	No effect on silent units	7
	TOTAL	21

Fig. 5. MEA recordings. (**a**) A representative raw signal featuring many EAPs, as displayed by the acquisition software MC_Rack (sampling frequency: 25 kHz). (**b)** 7 superimposed waveforms consisting of upward EAPs extracted from raw data. Each cutout extends from 1 ms before to 2 ms after the point where the signal crosses the threshold (horizontal dashed line) with a negative slope. Threshold was fixed at ±6 standard deviations from the baseline noise. (**c**) A representative raster plot (lower trace) and the corresponding rate histogram (upper trace) of an active channel (the same shown in (e): Exp6, Ch43+). Bin size: 60 s. 10 spikes/bin ≈ 0.17 Hz. Dashed line is the time of NPs administration. (**d**) Schematic overview of the early changes induced by 20 µg mL^{-1} SiO_2 NPs in GT1-7 EAP rate. Table refers only to the short temporal window (Δt_{pre}+Δt_{post}) as shown in (e). (**e**) 8 complete raster plots (representative of 21) from the 7 experiments featuring the active channels used for the analysis. On the left side of each raster are the experiment number and the channel reference. Symbols + and – represent the direction (upward or downward respectively) of the EAPs detected. Dashed line is the time of medium change. (**f**) Global rate histogram resulting from the

average of the rate histograms of all the 21 active units. Here, too, the dashed line is the time of medium change and NPs administration. **(g)** Low magnification image of GT1-7 cells pated on MEAs.

Overall, the average firing rate under control conditions (average spontaneous activity) was $\langle f_{pre} \rangle = 0.014 \pm 0.011$ Hz, that increased to $\langle f_{post} \rangle = 0.095 \pm 0.038$ Hz after NPs addition. The maximum value for GT1-7 firing rate we recorded (using a 1 min binning) was $f_{max} = 1.02$ Hz, but both f_{max} and $\langle f_{post} \rangle$ are possibly underestimated because of the blind spot (about 15 seconds) in MEA recording due to medium substitution. To compare the differences in firing rate in the two conditions, a paired-samples sign test was used. The sign test is a non-parametric alternative to the paired-samples *t*-test and Wilcoxon signed-rank test, being our distribution of differences $\Delta f = f_{post} - f_{pre}$ neither normal nor symmetrical.

NPs elicited a statistically significant median increase in firing rate compared to the spontaneous electrical activity ($p = 4.883 \cdot 10^{-4}$ two-tailed, n = 21). Different choices for window length (*e.g.* $\Delta t = 400$ s, $\Delta t = 500$ s) led to the same conclusions, even though *p*-values showed a clear increasing trend as window length increased ($p = 0.002$ for $\Delta t = 400$ s; $p = 0.013$ for $\Delta t = 500$ s), thus confirming the transient nature of the effect on the firing rate elicited by NPs.

In particular, after about 10 min from NPs administration, this effect on GT1-7 firing rate was no more detectable in any of the channels taken into account, even if nearly half of them still showed some kind of electrical activity after 1 hour or more. The late firing rate of this portion of channels, such as their percentage respect to the total of the active channels used for the analysis, were comparable to the ones measured under control condition. A global firing rate histogram (Fig. 5f) was drawn by averaging the full rate histograms from all the 21 active channels. It shows that,

after the short and early phase already discussed, electrical activity indeed recovered to control levels and was preserved in time, thus providing evidence that 50 nm SiO_2 NPs, at the concentration of 20 μg mL^{-1}, do not exert long lasting effects on neuronal function. Fig. 5g shows an image of the GT1-7 cells plated onto the MEAs.

Incubation with NPs up to 24 hours does not affect gene expression

To further characterize the effect of SiO_2 NPs treatment, and evaluate whether it could induce a transcriptional response, we performed RNA-Seq in GT1-7 cells at various time points following treatment with 20 μg mL^{-1} NPs. RNA-Seq analysis of the samples at 30 min, 1, 6 and 24 hrs showed very high correlation (R > 0.99, Pearson Correlation Coefficient) between treated and untreated cells for the entire timescale of the analysis (Fig. 6), revealing that the SiO_2 NPs do not induce a detectable transcriptional response.

Since these experiments were performed in the absence of FBS, and since the lack of toxicity of the concentration of 20 μg mL^{-1} has been tested in a previous paper[6] in the presence of 0.5% FBS, we repeated the survival assay at 24 hours on cells cultured in DMEM without FBS. Supplementary Fig. S3 online shows that also under these conditions the NPs did not affect cell survival.

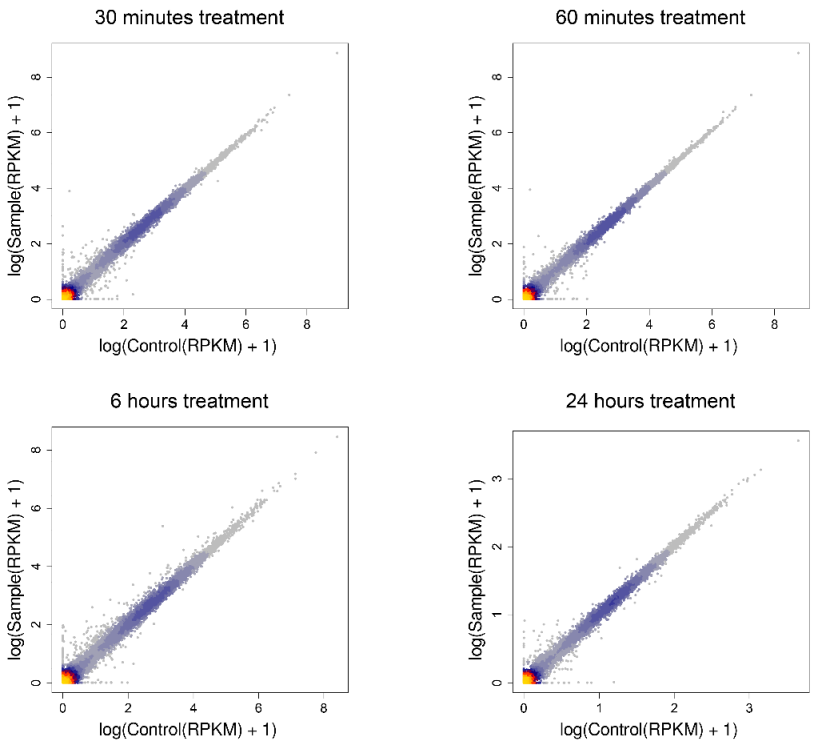

Fig 6. Lack of detectable transcriptional responses to incubation with SiO_2 NPs. Scatter plot with heat density of pairwise expression level comparison between treated and untreated (20 µg mL^{-1} of 50 nm SiO_2 NPs) cells at 30 minutes, 1, 6 and 24 hrs post-treatment. Gene expression values (per kb per million total reads, RPKM) in log scale. Dots indicate each gene expressed in the two samples.

2.4 Discussion

The data presented in this paper show that our nanoparticle model, 50 nm SiO_2 NPs, non-toxic at the size and concentration employed, induces fast changes in membrane potential and modulates the electrical activity of GT1-7 cells. MEAs recordings provide evidence for a transient increase in the firing rate of action potentials, without inducing long lasting alterations on the time scale of a few hrs. This is in agreement with previous observations[8] that the increases in $[Ca^{2+}]_i$

induced by the presence of these NPs were transient and reversible. These findings are not limited to a specific experimental model. We have observed similar responses to 50 nm SiO_2 NPs with single cell recordings from primary adult neurons that have electrical properties quite different from GT1-7 cells: the latter, in varying percentages according to culture conditions, are able to generate spontaneous electrical activity, either sporadic or in bursts[25]; DRG neurons, on the other hand, even if representing an heterogeneous population of different sensory cells, have a very limited and sporadic spontaneous electrical activity[26].

Interestingly, ultrastructural and ICP-MS data provide evidence for an interaction with the plasma membrane followed by the activation of an endocytic process. It is of relevance that in the culture medium, NPs form very small agglomerates, as reported by dynamic light scattering (DLS) data in a previous paper[8].

A very recent paper[27], combining a complex set of experimental approaches with numerical simulations, has reported that different kinds of nanoobjects (Quantum Dots, Quantum Rods, Fe_2O_3 NPs of different shape) elicit an increase in electrical activity in cultured rat hippocampal neurons. The most relevant and novel findings are: i) the responses are size-and shape independent; ii) electrical charge is the crucial parameter: negative NPs adhere to the neuronal plasmamembrane, cause a depolarization and increase firing, neutral and positive ones do not; iii) NPs interact only with active neurons. While in the present paper we did not characterize the dependency of the responses from these parameters, in a previous paper we have shown that SiO_2 NPs with a negative ζ potential elicited increases in $[Ca^{2+}]_i$, while positively charged (aminated) ones had no effect. In the above paper, we reported a size dependency; however the size range (50-200 nm) was broader than the range (5-75 nm) tested in Ref. 25. While the issue of dependency of interaction with the plasmamembrane from the negative surface charge of NPs finds support in the data

from several other laboratories (see e.g. Refs. 28, 29), the independency from size needs further investigation. Finally our experiments show that, in both GT1-7 and DRG neurons, the firing activity is not a requisite for SiO_2 NPs-neuronal membrane interaction.

The fact that electrical activity in neurons may have effects on gene transcription (the "excitation-transcription" paradigm[14,15]), mainly because of its link to changes in $[Ca^{2+}]_i$, were the rational for carrying out the analysis of the whole transcriptome. Interestingly, we found that the treatment with SiO_2 NPs does not induce a detectable transcriptional response at all time points analyzed, and this deserves further comments.

The issue of the effects of NPs on the target cell genome has attracted increasing interest in the last decade, the main focus being on potential genotoxic effects. Several comprehensive reviews are available[30-32]; in general, evidence for DNA damage induced by SiO_2 NPs is limited, and confined to relatively high doses (in most cases over 100 μg mL^{-1}). Most of the reported effects are cell- and nanoparticle size specific (the smaller being in general more genotoxic), thus requiring great caution when trying to derive general conclusions. Data based on neuronal models are more scarce, and limited to the pheocromocytoma cell line, PC12 cells. Here the reports are conflicting: it has been found[33] that 20 nm SiO_2 NPs at the concentration of 500 μg mL^{-1} did not alter chemokine and NF-κB levels in microglial cell, but only induce a small increase in the secretion of inflammatory chemokines; the supernatant from these cells, when applied to PC12 cells, did not induce cytotoxicity nor changes in a few marker genes. On the other hand, with 50 μg mL^{-1} of 25 nm NPs, other Authors[34] found activation of reactive oxygen species (ROS) and aggregation of α–synuclein, a potential early Parkinsons' Disease marker. Finally another group[35], using 20 and 50 nm NPs, report that they affect viability in

a time dependent way at concentrations starting from 50 μg mL^{-1} for the former and from 100 μg mL^{-1} for the latter; both induced significant increases of ROS starting from 25 μg mL^{-1}. A likely explanation for these discrepancies can be based on the different sizes employed, and, more relevantly, from the different experimental protocols: in the first two cases the NPs were administered to PC12 cells in the presence of 10% FBS, while in the latter stimulation was performed on cells in 0.1% FCS. This comparison points to another key issue in analyzing toxicity and genotoxicity induced by NPs: it has been reported that the toxic doses can change even of a few orders of magnitude when evaluated in the presence or in the absence of serum[32]. The finding that in our experimental conditions, the lack of genomic effects is paralleled by a lack in reduction of cell survival, even in the absence of FBS, strengthens the conclusion that the use of these particles is particularly safe and opens to the possibility of employing them as markers for cell tracking and/or carriers for drug delivery. This is, to our knowledge, the first detailed description of the changes in electrical activity of neurons following exposure to a nanoparticle, and of its evolution in time. The transient nature of these effects can explain the absence of long term outcomes on cell fate.

References

1. D. Napierska, D. et al. Size-dependent cytotoxicity of monodisperse silica nanoparticles in human endothelial cells. *Small* **5**, 846-53 (2009).

2. Park M. V. et al. In vitro developmental toxicity test detects inhibition of stem cell differentiation by silica nanoparticles. *Toxicol. Appl. Pharmacol*. **240**, 108-116 (2009).

3. Ariano, P. et al. Interaction of spherical silica nanoparticles with neuronal cells: Size-dependent toxicity and perturbation of calcium homeostasis. *Small* **7**, 766-774 (2011).

4. van Schooneveld, M. M. et al. Transcript assembly and quantification by RNA-Seq reveals unannotated transcripts and isoform switching during cell differentiation. *Nano Lett.* **8**, 2517-2525 (2008).

5. Izak-Nau, E. et al. Interaction of differently functionalized fluorescent silica nanoparticles with neural stem- and tissue-type cells. *Nanotoxicology* **8**, 138-148 . (2014)

6. Miletto, I. et al. Highly bright and photostable cyanine dye-doped silica nanoparticles for optical imaging: photophysical characterization and cell tests. *Dyes Pigment*s **84**, 121-127 (2010).

7. Accomasso, L. et al. Fluorescent silica nanoparticles improve optical imaging of stem cells allowing direct discrimination between live and early-stage apoptotic cells. *Small* **8**, 3192-3200 (2012).

8. Gilardino, A. et al. Interaction of SiO_2 nanoparticles with neuronal cells: Ionic mechanisms involved in the perturbation of calcium homeostasis. *Int. J. Biochem. Cell. Biol*. **66**, 101-111 (2015).

9. Haase, A. et al. Effects of silver nanoparticles on primary mixed neural cell cultures: Uptake, oxidative stress and acute calcium responses, *Toxicol. Sci.* **126**, 457-468 (2012).

10. Nyitrai, G. et al. Polyamidoamine dendrimer impairs mitochondrial oxidation in brain tissue. *J. Nanobiotechnology* **11**, 9 (2013).

11. Lovisolo, D., Gilardino, A. & Ruffinatti, F. A. When neurons encounter nanoobjects: spotlight on calcium signaling. *Int. J. Environ. Res. Public Health* **11**, 9621-9637 (2014).

12. Liu, Z., Liu, S., Ren, G., Zhang, T. & Yang, Z. Nano-CuO inhibited voltage-gated sodium current of hippocampal CA1 neurons via reactive oxygen species but independent from G-proteins pathway. *J. Appl. Toxicol.* **31**, 439-445 (2011).

13. Shan, D., Xie, Y., Ren, G. & Yang, Z. Inhibitory effect of tungsten carbide nanoparticles on voltage-gated potassium currents of hippocampal CA1 neurons. *Toxicol. Lett*. **209**, 129-135 (2012).

14. Polak, P. & Shefi O. Nanometric agents in the service of neuroscience: Manipulation of neuronal growth and activity using nanoparticles. *Nanomedicine* 11, 1467-1479 (2015).

15. Colombo, E., Feyen, P., Antognazza, M.R., Lanzani, G. & Benfenati, F. Nanoparticles: A Challenging Vehicle for Neural Stimulation. *Front Neurosci*. **10**:105 (2016).

16. Kang, Y. et al. Potential Links between Cytoskeletal Disturbances and Electroneurophysiological Dysfunctions Induced in the Central Nervous System by Inorganic Nanoparticles. *Cell Physiol Biochem*. **40**,1487-1505 (2016).

17. Jung, S.et al. Intracellular gold nanoparticles increase neuronal excitability and aggravate seizure activity in the mouse brain. *PLoS One* **9**:e91360 (2014).

18. Gramowski, A. et al. Nanoparticles induce changes of the electrical activity of neuronal networks on microelectrode array neurochips. *Environ Health Perspect.* **118**, 1363-1369 (2010).

19. Liu, Z., Ren, G., Zhang, T. & Yang, Z. Action potential changes associated with the inhibitory effects on voltage gated sodium current of hippocampal CA1 neurons by silver nanoparticles. *Toxicology* **264**, 179-184 (2009).

20. Dolmetsch, R. Excitation-transcription coupling: signaling by ion channels to the nucleus. *Sci STKE* **166**, PE4 (2003).

21. Ma, H., Groth, R. D., Wheeler, D. G., Barrett, C.F. & Tsien, R. W. Excitation-transcription coupling in sympathetic neurons and the molecular mechanism of its initiation. *Neurosci. Res*. **70**, 2-8 (2011).

22. Rosenholm, J. M., Sahlgren, C. & Lindén, M. Multifunctional mesoporous silica nanoparticles for combined therapeutic, diagnostic and targeted action in cancer treatment. *Curr. Drug Targets* **2**, 1166-1186 (2011).

23. Montalti, M., Prodi, L., Rampazzo, E. & Zaccheroni, N. Dye-doped silica nanoparticles as luminescent organized systems for nanomedicine. *Chem. Soc.Rev*. **43**, 4243-4268 (2014).

24. Nunemaker, C.S. et al. Long-term recordings of networks of immortalized GnRH neurons reveal episodic patterns of electrical activity. *J. Neurophysiol.* **86**, 86-93 (2001).

25. Martinez-Fuentes, A.J., Hu, L., Krsmanovic, L.Z. & Catt KJ. Gonadotropin-releasing hormone (GnRH) receptor expression and membrane signaling in early embryonic GnRH neurons: role in pulsatile neurosecretion. *Mol Endocrinol.* **18**, 1808-1817 (2004).

26. Newberry,K., et al. Development of a spontaneously active dorsal root ganglia assay using multiwell multielectrode arrays. *J Neurophysiol.* **115**, 3217–3228 (2016).

27. Dante, S. et al. Selective Targeting of Neurons with Inorganic Nanoparticles: Revealing the Crucial Role of Nanoparticle Surface Charge. *ACS Nano* **11**, 6630-6640 (2017).

28. Bewersdorff, T., Vonnemann, J., Kanik, A., Haag, R. & Haase, A. The influence of surface charge on serum protein interaction and cellular uptake: studies with dendritic polyglycerols and dendritic polyglycerol-coated gold nanoparticles. *Int J Nanomedicine* **12**, 2001-2019 (2017).

29. Liu, Q., Li, H., Xia, Q., Liu, Y. & Xiao, K. Role of surface charge in determining the biological effects of CdSe/ZnS quantum dots. *Int J Nanomedicine* **10**, 7073-7088 (2015).

30. Magdolenova, Z. et al. A review of in vitro and in vivo studies with engineered nanoparticles. *Nanotoxicology* **8**, 233-278 (2014).

31. Kwon, J. Y. et al. Undetactable levels of genotoxicity of SiO_2 nanoparticles in in vitro and in vivo tests. *Int. J. Nanomedicine* **9** Suppl. 2, 173-178 (2014).

32. Golbamaki, N. et al. Genotoxicity of metal oxide nanomaterials: review of recent data and discussion of possible mechanisms. *Nanoscale* **7**, 2154-2198 (2015).

33. Xue, Y., Wu, J. & Sun, J. Four types of inorganic nanoparticles stimulate the inflammatory reaction in brain microglia and damage neurons in vitro. *Toxicol. Lett.* **214**, 91-98(2012) .

34. Xie, H. & Wu, J. Silica nanoparticles induce alpha-synuclein induction and aggregation in PC12-cells. *Chem. Biol. Interact*. **258**, 197-204 (2016).

35. Wang, F. et al. Oxidative mechanisms contribute to nanosize silican dioxide-induced developmental neurotoxicity in PC12 cells. *Toxicol. In Vitro* **25**, 1548-1556 (2011).

36. Gonzalez, L. et al. Co-assessment of cell cycle and micronucleus frequencies demonstrates the influence of serum on the in vitro genotoxic response to amorphous monodisperse silica nanoparticles of varying sizes. *Nanotoxicology* **8**, 876-884 (2014).

37. Rasband, W. S. ImageJ, U.S. National Institutes of Health, Bethesda, MD, USA. http://rsb.info.nih.gov/ij/ (1997-2007).

38. Incarnato, D., Neri, F., Anselmi, F. & Oliviero, S. Genome-wide profiling of mouse RNA secondary structures reveals key features of the mammalian transcriptome. *Genome Biol.* **15**, 491 (2014).

39. Kim, D. et al. TopHat2: accurate alignment of transcriptomes in the presence of insertions, deletions and gene fusions. *Genome Biol.* **14**, R36 (2013).

40. Trapnell, C. et al. Transcript assembly and quantification by RNA-Seq reveals unannotated transcripts and isoform switching during cell differentiation. *Nature Biotechnol.* **28**, 511-515 (2010).

41. R Core Team, R: A Language and Environment for Statistical Computing. R Foundation for Statistical Computing. Vienna, Austria, url: https://www.R-project.org/ (2016).

Ackowledgements

We wish to thank Prof. Fabio Benfenati and prof. Armando Genazzani for helpful advice and comments. This work was supported by the Fondazione CRT (call "Richieste ordinarie 2014", project n. 2014.1041) and by funds of the University of Piemonte Orientale ("Bando Ricerca Locale 2015").

Author contributions

C.D. and F.A.R. shared first authorship; C.D., M.D., D.L. and L.M. performed and analyzed the patch clamp experiments; S.A. and A.G. prepared the GT1-7 cultures; B.R. prepared the DRG cultures; A.G. performed the survival assays; F.A.R. and G.C. performed and analyzed the MEA experiments; G.A. and G.M performed nanoparticle synthesis and characterization; E.C. analyzed the localization of the nanoparticles; D.I., E.M. and S.O. performed the genomic analysis; E.B performed the ICP-MS measurements; D.L. and C.D. designed the experiments and wrote the paper. All authors reviewed and approved the manuscript.

Chapter 3

The interaction of SiO_2 nanoparticles with the neuronal cell membrane: activation of ionic channels and calcium influx

Carla Distasi[+,,1], Marianna Dionisi[+,1], Federico Alessandro Ruffinatti[1], Alessandra Gilardino[2], Roberta Bardini[2], Susanna Antoniotti[2], Federico Catalano[3], Eleonora Bassino[2], Luca Munaron[2], Gianmario Martra[3,4], Davide Lovisolo[2]*

[1]Dept. of Pharmaceutical Sciences, University of Piemonte Orientale "A. Avogadro", Via Bovio 6, 28100, Novara, Italy [2]Dept. of Life Sciences and Systems Biology, University of Torino, via Accademia Albertina 23, 10123 Torino, Italy [3]Dept. of Chemistry, Torino, University of Torino, Via P. Giuria 9, 10125, Italy [4]NIS Interdepartmental Center, University of Torino, Italy

+These two Authors contributed equally to the work

Abstract

Aim: To clarify the mechanisms of interaction between SiO_2 nanoparticles (NPs) and the plasmamembrane of GT1–7 neuroendocrine cells, with focus on the activation of calcium-permeable channels, responsible for the long lasting calcium influx and modulation of the electrical activity in these cells. **Materials & methods**: Non-toxic doses of SiO_2 NPs were administered to the cells. Calcium imaging and patch clamp

techniques were combined with a pharmacological approach. **Results**: TRPV4, Connexins and Pannexin-like channels are the major components of the NP-induced inward currents. Pre-incubation with the antioxidant N-acetyl-L-cysteine strongly reduced the $[Ca^{2+}]_i$ increase. **Conclusion**: These findings suggest that SiO_2 NPs directly activate a complex set of calcium-permeable channels, possibly by catalyzing free radicals production.

Keywords: Neuronal cells, silica nanoparticles, TRPV4, connexin, pannexin, free radicals, calcium, patch clamp, single channel

3.1 Introduction

SiO_2 nanoparticles (NPs) are among the most promising tools in the field of nanomedicine because of their good biocompatibility [1,2] and have already been employed in several applications from drug delivery [3,4] to cell tracking and imaging [5,6]. A previous research [7] provided evidence for the possibility to incorporate at nontoxic doses dye-doped fluorescent silica NPs, displaying high yield and extremely stable photoemission, into neuronal cells. These properties are particularly attractive for imaging application in nanoneuromedicine, that deals with highly sensitive and delicate biological material, both at the cell and at the organ level. In this context, the understanding of the mechanisms of interaction between the NPs and their targets as well as of the cellular and molecular responses elicited by these interactions is a prerequisite to the rational design of safe and efficient nanotools for both laboratory and clinical applications. At the nanoscale, the exploration of the laws that govern the interaction between inorganic particles and biological structures such as membrane proteins is still moving its first steps. A

lot of information has to be gathered to set on solid ground the generalized use of nanoparticles in basic and applied biology, and specifically in the highly sensitive field of neuroscience. One of the crucial parameters known to be affected by the interaction of nanoobjects with cells is the intracellular free calcium concentration, $[Ca^{2+}]_i$, controlling a plethora of signaling pathways, particularly in neuronal cells [8,9]. Nontoxic doses of 50 nm SiO_2 NPs were found to elicit strong and oscillatory increases in $[Ca^{2+}]_i$ in a neuronal cell line, GT1–7 cells; these signals are reversible even in the continued presence of NPs [10], fully dependent on calcium influx, and carried at least partially through Transient Receptor Potential V4 (TRPV4) channels even if other, up to now unidentified channels are involved. Indeed, the first and critical step of the interaction between these nanoobjects and the cell resides at the plasmamembrane and its rich inventory of proteins that mediate the responses to the changes in the extracellular environment. Among this inventory, a key role is played by ionic channels, and specifically calcium permeable ones, that can activate both fast responses and long term intracellular signalling mechanisms [8,9]. In spite of their functional relevance, few reports are available regarding the effects of NPs on neuronal calcium permeable channels [10]; most of them have been obtained by means of a calcium imaging approach that, even if useful for a phenomenological description of the process on a population scale, cannot provide a complete and detailed biophysical characterization of the properties of the multiple influx pathways activated by the NPs. The adequate approach is electrophysiology, but data about patch clamp recordings from cells, and particularly neurons, exposed to acute applications of NPs are quite scarce and limited; most of them refer to effects on a specific current, isolated from the whole cellular response [11-13]. Recently [14] single cell patch clamp measurements combined with long term recordings of electrical activity with multielectrode arrays have provided evidence that, at nontoxic concentrations, SiO_2 NPs evoke a transient depolarization of the

membrane potential, leading to a modulation of action potential firing, without any change in gene expression. Here, a new contribution to the knowledge of the interaction of NPs with the neuronal membrane is presented, focusing on the molecular targets involved and on the membrane-delimited mechanisms responsible of their activation.

3.2 Materials and methods

Materials. Lab-made silica nanoparticles, in the bare form (i.e. SiO_2-50 nm NP) and functionalized at their surface with amino groups (i.e. NH_2-SiO_2-55 nm NP) were prepared following the procedure reported in [8] and [11], respectively. In brief, in both cases SiO_2 NPs were prepared by the reverse microemulsion technique, using tetraethylorthosilicate (TEOS) as source of silica. For the functionalization, (3-Aminopropyl) triethoxysilane (APTS) was added to the microemulsion after the formation of NP. Microparticles were purchased from Corpuscular Inc., www.microspheresnanosphere.com

Characterization of (nano)particles. Size and shape of SiO_2 NPs were determined by transmission electron microscopy (Jeol 3010, operated at 300 kV). Samples were prepared by dropping of aqueous suspensions of the NPs on TEM grids, supporting a lacey carbon film, and waiting until dryness. Histograms of the size distribution of NPs were obtained by measuring ca. 200 particles, and the mean particle diameter (d_m) was calculated as $d_m = \Sigma d_i n_i / \Sigma n_i$, where n_i was the number of particles of diameter d_i. The results are indicated as d_m ± standard deviation. Microparticles were imaged by SEM (Zeiss EVO 50), observing an aliquot of the sample fixed on a conventional stub through a carbon conducting biadhesive tape.

Dynamic light scattering (DLS) measurements, providing hydrodynamic radius values, were carried out with a 90Plus Par-ticle Size Analyzer, laser wavelength 660 nm, detection angle 90°, T = 20 °C). Materials were suspended (0.1 mg mL^{-1}) in the relevant aqueous media indicated in Table 1. Measurements were repeated in triplicate. In presence of large agglomerates in the micrometer range, in some cases significant differences among repeated measurements occurred, because of the much more complex scattering behaviour [15]. The same samples were used for ζ-potential measurements by electrophoretic light scattering (ELS; Zetasizer Nano-ZS , Malvern Instruments). Results are reported as mean value ± standard deviation of five separate measurements each resulting from 10 runs.

Cell culture. GT1–7 cells, an immortalized line derived from highly differentiated mouse gonadotropin-hormone releasing hormone (GnRH) neurons (generously donated by Prof. P.L. Mellon), were plated either on glass 32 mm cover-slips coated with 100 μg mL^{-1} poly-l-lysine (for calcium imaging experiments) or, for electrophysiological experiments, on uncoated plastic dishes (Falcon, Becton Dickinson) at densities of 10,000 cells cm^{-2}. The cells were maintained in Dulbecco's Modified Eagle's medium (DMEM) supplemented with10% heat-inactivated fetal bovine serum (FBS; Lonza), gentamycin (50 μg mL^{-1}), and glutamine (2 mM) at 37 °C, in a humidified atmosphere of 5% CO_2 in air and then switched for 1 day to 0.5% FBS supplemented with B27 (Invitrogen), and subsequently for 3-4 days to 0.5% FBS, to improve survival and differentiation.

Electrophysiology - Patch clamp. Conventional whole cell patch clamp recordings were performed at 22-25 °C in the voltage clamp mode. In a first set of recordings, the cells were continuously superfused with a standard physiological Tyrode

solution of the following composition (in mM): NaCl, 154; KCl, 4; $CaCl_2$, 2; $MgCl_2$, 1; 4-(2-hydroxyethyl)-1-piperazine ethane sulfonic acid (HEPES), 5; glucose, 5.5; NaOH to pH 7.35. Composition of the pipette solution was (in mM): KCl, 15; $CaCl_2$, 3; $MgCl_2$, 3; 4(2hydroxyethyl) -1-piperazine ethane sulfonic acid (HEPES), 5; KAsp, 118; EGTA, 5, Na_2ATP, 5, KOH to pH 7.35. Pipettes had a resistance of 2-5 MΩ. In a second set, in order to abolish or reduce the contribution of currents through K^+ channels, the extracellular solution had the following composition (in mM): NaCl, 134; tetraethylammonium chloride (TEACl), 20; KCl, 4; $CaCl_2$, 2; $MgCl_2$, 1; 4(2hydroxyethyl) 1 piperazine ethane sulfonic acid (HEPES), 5; glucose, 5.5; NaOH to pH 7.35. Composition of the pipette solution was (in mM): CsCl, 20; $CaCl_2$, 0.08; $MgCl_2$, 1; 4(2hydroxyethyl) 1 piperazine ethane sulfonic acid (HEPES), 10; Aspartic Acid, 100; CsOH, 100; Na_2ATP, 4; pH 7.35. A few control experiments were performed using DMEM as an extracellular medium.

NPs (sonicated for 20 min prior to the preparation of the suspensions) and other agents were dispersed in the solutions at the required concentration. Solutions were applied by means of a microperfusion system connected to a set of five syringes containing the control and test solutions; the perfusion pipette was located at several tens of microns away from the cell to be recorded, in order to minimize mechanical perturbations.

Correction for junction potential was performed analogically. Data were collected with an Axopatch 200B amplifier (Molecular Probes, USA) using Clampex 10.2 and Axoscope 10.2 software and sampled at 10 kHz and 1 kHz respectively. Current voltage (I-V) relationships were obtained from protocols designed to inactivate the voltage-dependent inward currents expressed in these cells (see Fig. S-8 of the Supplementary Materials, hereafter SM). In the presence of NPs, whole cell recordings lasted from 5 to 40 minutes, durations comparable to those obtained in control experiments in the absence of NPs.

For single channel outside out experiments, patch pipettes, with a resistance of 5-7 MΩ, were filled with the Cs-aspartate solution used for whole cell experiments. In preliminary experiments with the extracellular solution containing 20 mM TEACl, we observed gigaseal (2-10 GΩ) rupture very soon after NPs perfusion. In order to increase the duration of the experiments, since it has been reported that NPs are less agglomerated when they are suspended in DMEM [10], we added MEM supplements (Sigma) to the above solution. A control test (by means of dynamic light scattering, DLS, see Methods of the SM and Table 1) showed that agglomeration was lower in this solution than in Tyrode solution, even if greater than previously reported for DMEM [6]. Actually, this condition enhanced the stability of the gigaseals, although the duration of the outside out patch recordings was significantly shorter in the presence of 20 μg mL^{-1} of NPs (median and interquartile range: M_{NP} = 158 s, IQR_{NP} = [99; 216] s, n = 14 cells) than in the presence of pharmacological agents in similar experiments with the TRPV4 agonist GSK1016790A (M_{GSK} = 346 s, IQR_{GSK} = [260; 687] s, n = 28 cells, *p*-value = 0.022, π = 0.77, Mann-Whitney *U* test, two-tailed, unpaired). Data were filtered at 1 kHz and digitized continuously at a sampling frequency of 1 kHz with PClamp Axoscope software. Steady state voltage clamp and ramp protocols from -120 mV to 100 mV were applied and digitized at 10 or 20 kHz with PClamp Clampex software. Data analysis was performed with OriginPro 9.1 software (OriginLab, USA). To obtain the I-V relationship and the reversal potential of the mean current activated by the agonists, we subtracted, if not otherwise specified, the average of at least ten current traces recorded in control conditions during ramp application (red curves in the figure insets), from the average current recorded in the presence of the agonist (black curves in the figure insets). Single channel I-V was obtained by subtracting the baseline (current ramp during closed or blocked state of the

channel, red curves in the insets) from a current ramp recorded during channel opening (black curves in the insets).

Calcium imaging. Cells were loaded with the Fura-2 acetoxymethyl ester (2.5 M, 45 min, 37 °C) and subsequently shifted to a standard physiological Tyrode solution of the following composition (in mM): NaCl, 154; KCl, 4; $CaCl_2$, 2; $MgCl_2$, 1; 4-(2-hydroxyethyl)-1-piperazineethanesulfonic acid (HEPES), 5; glucose, 5.5; and NaOH (pH 7.35). The NPs were sonicated and dispersed in the Tyrode solution at the required concentration. The solutions were applied with a microperfusion system. Cells were imaged every 3 s at 37 °C using a monochromator system attached to an inverted microscope with a 20× objective (SFluor, Nikon). Images were acquired using an enhanced CCD camera (PCO) and the Metafluor software (Universal Imaging Co.).

Assessment of lipid peroxidation. GT1–7 cells were seeded at the initial density of 35,000 cm^{-2} in 96 well plates in DMEM supplemented 10% FBS (Lonza). The medium was changed with DMEM plus 0.5% FBS supplemented with B27 (Invitrogen) for 24 hrs and substituted with DMEM 0.5% FBS for three days. Lipid peroxidation was analysed using the Click-iT® Lipid Peroxidation Imaging kit (ThermoFisher). The Click-iT® Lipid Peroxidation Imaging Kit-Alexa Fluor® 488 leverages copper-catalyzed click chemistry and the linoleamide alkyne (LAA) reagent (alkyne-modified linoleic acid) for detection of lipid peroxidation-derived protein modifications in fixed cells. Details are given in Methods of the SM.

Statistical data analysis. All samples were first tested for normality (Shapiro-Wilk test) and for homogeneity of variance (Levene's test). Mean and standard error of the mean (SEM), rather than median (or trimmed mean) and interquartile range

(IQR), depending on the skewness of data distribution, were used as measures of central tendency and dispersion respectively, as detailed along the text. When possible, statistical significance was assessed by parametric tests, otherwise non-parametric alternatives were used as specified case by case. In any case, all statistical tests were among unpaired samples, two-tailed and a *p*-value < 0.05 was considered statistically significant. Sample size was chosen to ensure a statistical power π at least equal to 0.8 or to satisfy a particular statistical sensitivity criterion. In particular, the power actually achieved (in the case of null hypothesis rejection) or the required effect size as a measure of statistical sensitivity (in the case of rejection failure) are provided for each test. Single channel current amplitudes are represented as mean ± standard deviation (SD), estimated by fitting the amplitude histograms to a sum of Gaussian functions (OriginPro 9.1).

3.3 Results

Silica particles

The nanoparticles mainly considered in this work were of bare silica, highly homogeneous in spherical shape and in diameter, of 50 ± 2 nm, of the type already used in previous investigations [7,10,14]. These nanoparticles will be labeled as SiO_2-50 nm NPs. Moreover, selected cell tests were also carried out using two other types of SiO_2 spherical particles: i) nanoparticles functionalized with $–NH_2$ groups, in order to impart different surface properties, namely in terms of ζ-potential, with only a quite limited change in size [11] (55 ± 3 nm; hereafter: NH_2-SiO_2-55 nm NPs), and ii) commercial microparticles about 2 μm in size [10]. TEM and SEM images of the three types of particles are shown in Fig. S-1 of SM. The material features

relevant for this work (ζ-potential, size and dispersion/agglomeration state in the media used for presenting the particles to the cells) are listed in Table 1.

SiO_2 NPs elicit long lasting inward currents in GT1–7 cells

In the voltage clamp mode, the holding potential was set at -50 mV (close to the reversal potential for Cl^- ions with standard Tyrode extracellular and K^+ aspartate intracellular solutions, see Materials and methods), in order to exclude any contribution of Cl^- ions to the NP-induced currents. In these conditions the inward currents could be univocally ascribed to influx of cations into the cell. In 34 cells perfusion with SiO_2-50 nm NPs (20 μg mL^{-1}) induced the activation of an inward current, characterized by a noisy behavior (Fig. 1A,C); peak current density, expressed as median and interquartile range, was: M = -7.80 pA pF^{-1}, IQR = [-14.80; -4.35] pA pF^{-1} (n = 34 cells). Information about the currents was obtained by subtracting the current-voltage (I-V) relationship recorded in control conditions from the one recorded during the response. The I-V curves of the NP-activated currents of Fig. 1A,C are shown respectively in Fig. 1B,D. In most cases, the I-V curves showed a more or less marked outward rectification; the reversal potential (V_{rev}) was analyzed in 16 cells and was M = -1.7 mV, IQR = [-12.4; +8.7] mV (Table 2). Openings of large conductance single channels were clearly detectable in most of the cells (19 out of 34 cells, Figure 1C, inset). The amplitude histogram of the elementary events is shown in Fig. 1E. The currents were only partially reversible after NP removal, at least for the duration of the recordings (up to 30 minutes).

When the cells were challenged with 2 µm SiO_2 microparticles (to assess the role of size), no current was recorded (n = 5 cells, Table 2 and Fig. 1F). Similarly, perfusion with NH_2-SiO_2-55 nm NPs (to assess the role of surface charge) failed to induce an inward current in 7 out of 12 cells (Fig. 1F); in 5 cells, either sporadic events and/or low amplitude inward currents could be observed (Table 2 and Fig. S-2 in the SM). These findings are in agreement with previous data [10] obtained with a calcium imaging approach, and provide evidence for a lack of nonspecific perturbation of the cell membrane following exposition to the SiO_2 NPs. The above protocol was repeated with a lower concentration of the same SiO_2 NPs (0.5 µg mL^{-1}): in 5 out of 29 cells, no detectable change in the current baseline was observed; in the other 24 cells, the NPs elicited currents of similar time course, but with a significantly lower peak current density (Table 2; *p*-value = 0.0008, π = 0.99, Mann-Whitney *U* test). An example is shown in Fig. S-3 of the SM.

It has been previously shown [10] that the calcium signals could be also recorded when the NPs were dispersed in DMEM medium, in which the agglomeration is sharply reduced (Table 1). This finding was confirmed in electrophysiological experiments: when dissolved in DMEM, SiO_2-50 nm NPs (20 µg mL^{-1}) elicited and inward current similar to those observed in Tyrode solution (n = 5 cells). A representative recording is shown in Fig. S-4 of the SM.

In order to better characterize the inward current, a further set of experiments was performed on cells bathed in an external solution containing 20 mM tetraethylammonium (TEA) and internally perfused with a pipette solution in which K^+ was substituted with Cs^+ (see Materials and methods), to block outward currents through K^+-selective channels. Fig. 2A,C shows two typical experiments out of 31 similar recordings. In these conditions the I-V relationships of NP-activated currents were in most cases linear (Fig. 2B); V_{rev} was M = -2.8 mV, IQR = [-10.0; +5.5] mV (n = 26 cells).

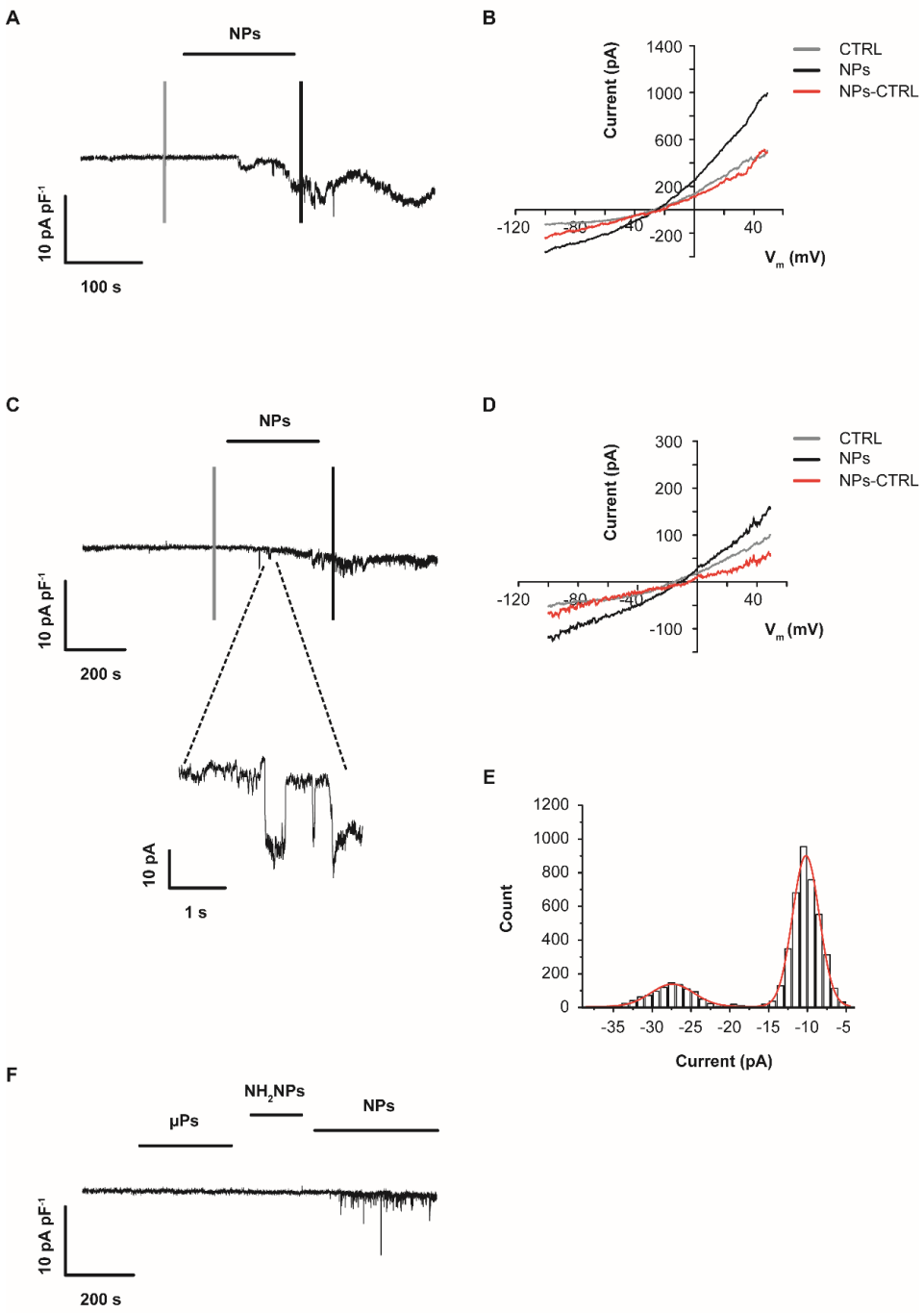

Figure 1. SiO_2-50 nm NPs activate inward currents in GT1–7 cells. (A,C) Two examples of whole cell currents recorded following administration of 20 µg mL^{-1} of SiO_2-50 nm NPs. Voltage clamp recordings, V_{hold} = -50 mV. Inset in **(C)**: a large conductance event observed during a whole cell recording. **(B,D)** I-V relationships obtained from the experiments in **(A,C)**. The red curves were

obtained subtracting the currents activated by the voltage ramps applied before NP administration (gray) from those recorded during the response (black). **(E)** Amplitude histogram of the large conductance events shown in the inset of **(C)**: the resulting amplitude is 17.2 pA. **(F)** Stimulation with either SiO_2 microparticles (diameter 2 µm) or NH_2-SiO_2-55 nm NPs failed to induce an inward current; subsequent administration of plain SiO_2-50 nm NPs elicited a response.

Median peak current density was significantly lower than in Tyrode solution (Table 2; *p*-value = 0.001, π = 0.99, Mann-Whitney *U* test; since the same control group of peak amplitudes in Tyrode solution has been used twice, *p*-values have been corrected for multiple comparisons). The response was only partially reversible. Single channel opening events could again be resolved (Fig. 2C). The amplitude histogram of the elementary events in shown in Fig. 2D.

Table 2

Particles	Extra/Intra-Cellular Solutions	N° Cells	N° Responsive Cells	Current Density (pA pF^{-1})		I-V	V_{rev} (mV)	
				Median	**IQR**		**Median**	**IQR**
NP (20 µg mL^{-1})	Tyrode/KAsp	34	34	-7.8	[-14.8; -4.4]	Outward rectification	-1.7	[-12.4; +8.7]
	TyrodeTEA/CsAsp	31	31	-4.7	[-6.2; -2.3]	Linear	-2.8	[-10.0; +5.5]
NP (0.5 µg mL^{-1})	Tyrode/KAsp	29	24	-4.2	[-5.2; -1.5]	Outward rectification	-	-
µP (20 µg mL^{-1})	Tyrode/KAsp	5	0	-	-	-	-	-
NH_2-NP (20 µg mL^{-1})	Tyrode/KAsp	12	5	-1.7	[-2.0; -0.9]	-	-	-

Effects of channel blockers

The currents activated by the NPs, both in physiological solutions and in the presence of K^+ channel blockers, showed some peculiar features, such as an irregular evolution in time, a marked noisy behavior and the occurrence of single channel unitary events of amplitude of about 10 pA in whole cell configuration. These features point to a complex process involving the activation of multiple channel types. It has been shown [10] that the NPs-induced calcium signal could be reduced by TRPV4 blockers. As for openings of the large conductance channels recorded in whole cell configuration, potential candidates are, among others, members of the connexin (Cx) and/or pannexin (Panx) families. Both connexins and pannexins form high conductance multimeric membrane channels. In addition, Cxs assemble to form vertebrate gap junctions for direct intercellular communication. Cx and Panx families share similar membrane topology and in part pharmacologic and gating properties, but not sequence homology. Cx and Panx plasma membrane channels allow the exchange of ions and signaling molecules between the cytoplasm and the extracellular medium, including calcium ions, ATP and large size molecules and play important roles in health and desease, such as neuroinflammation and neuropathic pain [16-21]. Among connexins, GT1–7 cells express at least Cx26 and Cx43 [22], two proteins that can form gap junctions as well as hemichannels. Panxs are widely expressed in the nervous system [18, 23-27] but to our knowledge no data are currently available for GT1–7 neuronal cells. Interestingly, in a different experimental model (cultured cortical astrocytes), it has been reported [28] that ultrafine carbon black activates Cx43 and Panx1 channels.

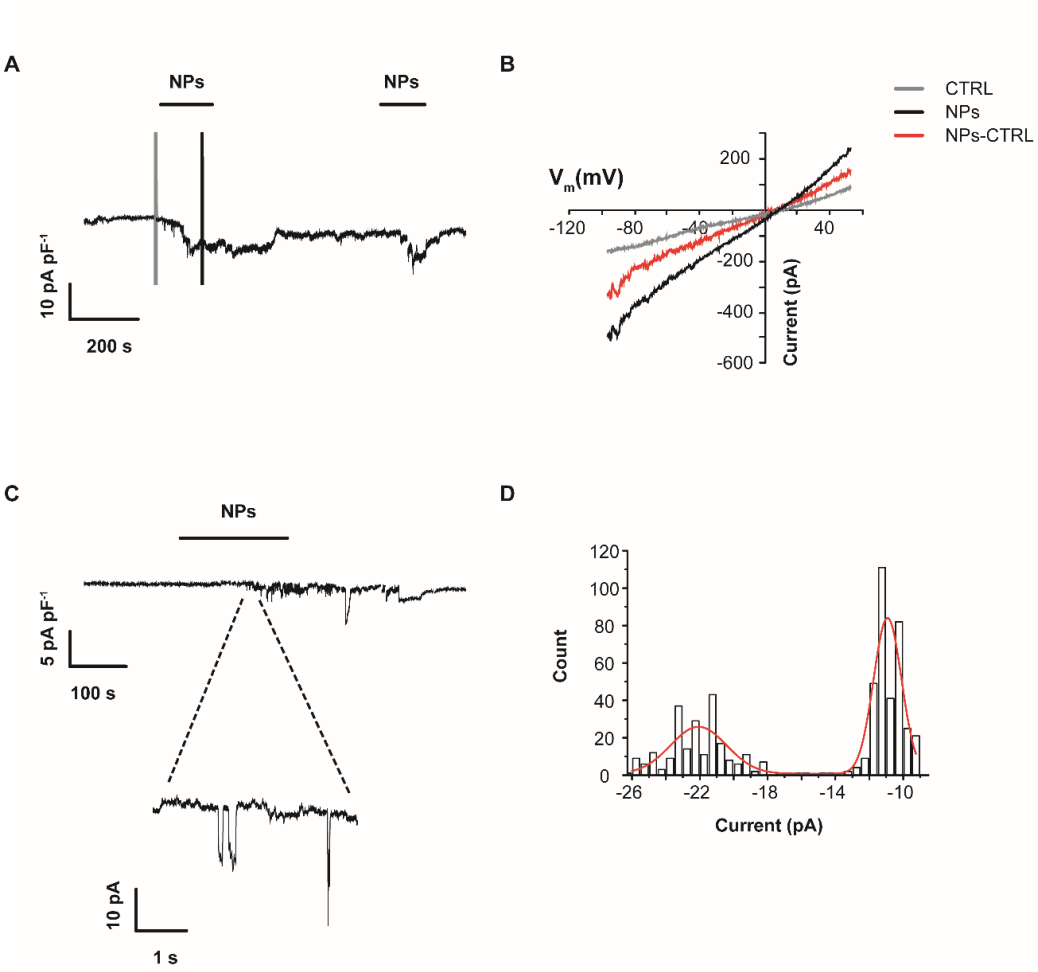

Figure 2. Inward currents activated by SiO_2-50 nm NPs in the presence of block of K+ selective channels. (A,C) Two examples of whole cell currents recorded following administration of 20 µg mL^{-1} of SiO_2 NPs. Voltage clamp recordings, V_{hold} = -50 mV. Inset in **(C)**: large conductance events observed during a whole cell recording. **(B)** I-V relationships obtained from the experiment in **(A)**. The red curve was obtained subtracting the current activated by the voltage ramps applied before NP administration (gray) from the one recorded during the response (black). **(D)** Amplitude histogram of the large conductance events shown in the inset of **(C)**: the resulting amplitude is 11 pA.

In order to evaluate the involvement of these channels, we used a pharmacological approach. We preliminary analyzed the effects of these blockers on NP-induced calcium signals by means of calcium imaging experiments on cell populations. As a first step we tested the activity of Gd^{3+}, a known inhibitor of TRPVs and other calcium permeable channels [29] and of several connexins [30, 31]. Its effectiveness on pannexins is controversial: some Authors [32] reported lack of blockade of dye uptake through Panx1, while others [33] ascribed a reduction in ATP release from lymphocytes to Gd^{3+} block of Panx1. Since it is known that polyvalent ions can induce nanoparticle agglomeration in suspension [34] we preliminarily checked the aggregation effects by Dynamic Light Scattering at different concentrations of Gd^{3+}. Concentrations in the range 50-100 µM are used by some Authors [30, 33, 35, 36]. As can be seen in Table 1, agglomeration was strongly increased by 100 µM Gd^{3+}, above the detection range of the instrument. At 10 µM, a more detailed analysis revealed a bimodal distribution: while a very small fraction of extremely agglomerated NPs was present, the majority were even less agglomerated than in normal Tyrode (Table 1). For these reasons we employed 10 µM Gd^{3+}, a concentration still compatible with the blocking activity on TRPV and Cx channels [31, 37]. In the presence of 10 µM Gd^{3+}, NPs failed to induce a detectable increase of $[Ca^{2+}]_i$ (4 experiments, 354 cells). Upon blocker removal and in the continued presence of the NPs, we observed a strong $[Ca^{2+}]_i$ increase (Fig. 3A, upper and low). A second approach was to combine Ruthenium Red (RR), another blocker of several types of TRP channels including TRPVs [38], and carbenoloxone (CBX), inhibitor of Cxs and Panx1 channels [16, 32, 39]. Specifically, we used 50 µM CBX and 5 µM RR [28, 40. 41]. No relevant change in $[Ca^{2+}]_i$ levels was detected upon addition of the drugs to the medium. On the other hand, the $[Ca^{2+}]_i$ increase induced by SiO_2-50 nm NPs was strongly reduced but not totally abolished in some cells.

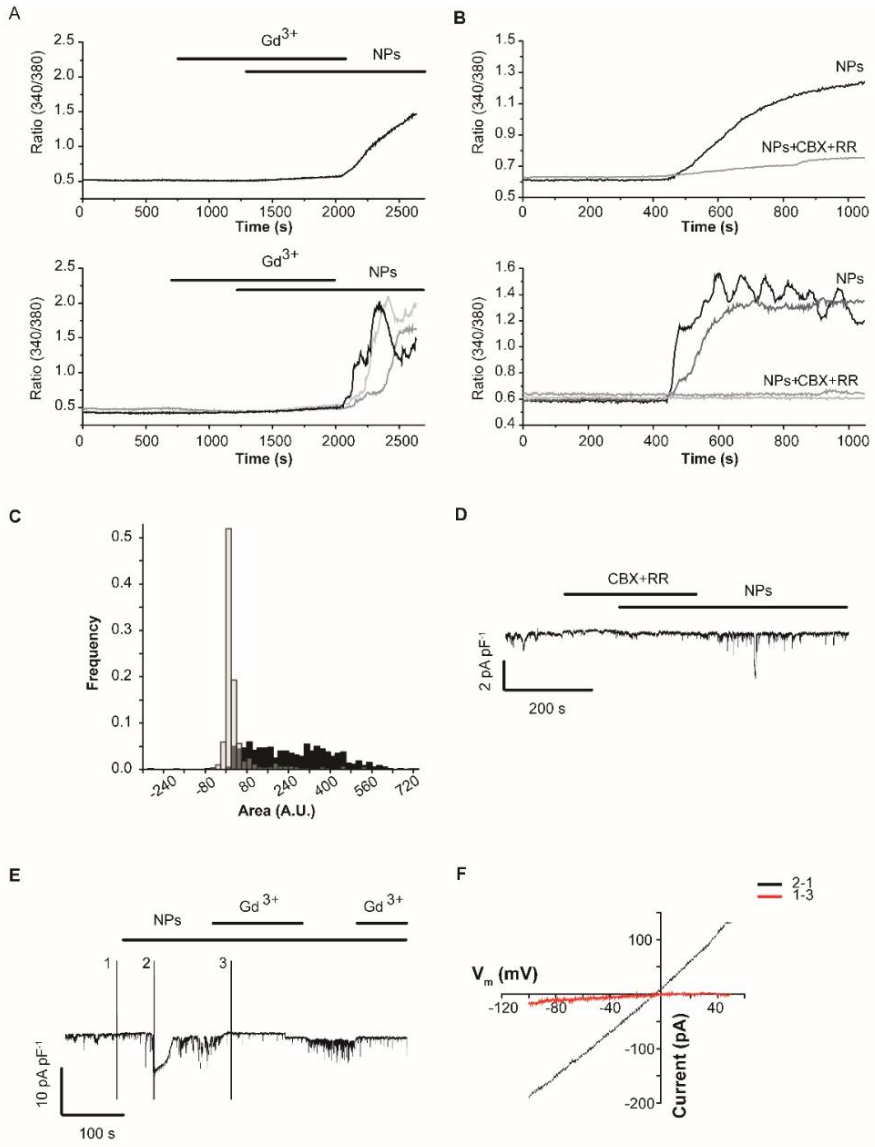

Figure 3. Effects of channel blockers on the increases in $[Ca^{2+}]_i$ and on the ionic currents activated by SiO_2-50 nm NPs. (A) Gd^{3+} (10 µM) completely abolished the NP-induced increase in $[Ca^{2+}]_i$. Upper: Average response (105 cells) from one experiment representative of 4 (total 354 cells). Lower: three individual traces from the same experiment. **(B)** The combination of 5 µM RR and 50 µM CBX strongly reduced the NP-induced increase in $[Ca^{2+}]_i$. Upper: the comparison of the average of 457 cells from 6 control experiments in which the NPs were administerd in the absence of the blockers (black) and the average of 693 cells from 6 experiments in which cells were preincubated with the blockers prior to NP administration (gray). Lower: two representative traces from one control experiment and one with the blockers. **(C)** Frequency histograms of the areas between the curve of $[Ca^{2+}]_i$ response to

NPs and the reference baseline. Black bars: areas measured in control condition (SiO_2 NPs alone). Transparent gray bars: areas measured during NP administration in the presence of CBX and RR blockers. In most of the tested cells NPs did not induce any calcium signal when administered after CBX and RR preincubation. **(D)** Reversible block of the NP-activated inward current by 5 μM RR and 50 μM CBX. **(E)** Reversible block of the NP-activated inward current by 10 μM Gd^{3+}. **(F)** I-V relationships of the currents activated by the NPs in the absence (black) and in the presence of Gd^{3+} (red).

For this reason we performed a quantitative analysis by evaluating the area under the curves representing the time courses of the cytosolic calcium concentration after NP administration. Responses induced by the NPs in the presence of RR and CBX (693 cells from 6 different experiments) were compared with a control group (response in the sole presence of NPs; 457 cells from 6 different experiments). The average $[Ca^{2+}]_i$ increases in the two conditions are compared in Fig. 3B, upper; individual traces from one control experiment and one performed in the presence of the blockers are in Fig. 3B, lower. For both conditions, areas were evaluated within an integration time interval of 10 minutes starting from the onset of the averaged response and represented by frequency histograms in Fig. 3C. Statistical analysis confirmed that the combined administration of 50 μM CBX and 5μM RR exerted a strong and significant reduction in $[Ca^{2+}]_i$ increase following NP administration (Mann-Whitney *U* Test, *p*-value = $1.4 \cdot 10^{-126}$, $\pi = 0.99$, effect size $r = 0.71$). Further analytical and statistical details are provided in Methods of the SM.

The same blockers were tested in whole cell patch clamp experiments, with the same intracellular and extracellular solutions as in Figure 2. Fig. 3D shows that in the presence of CBX and RR the current was completely and reversibly abolished (n = 5 cells). Fig. 3E,F shows an example (out of 11 cells) of reversible block of the NP-activated current following the acute application of 10 μM Gd^{3+}.

Biophysical characterization of NPs-activated channels: TRPV4

In order to shed more light on the biophysical properties of the NP activated channels, we performed experiments in the outside-out patch configuration. To confirm that NPs activate TRPV4 channels, we used GSK1016790A, a selective TRPV4 agonist [42] with Cs^+-aspartate solution in the pipette and TEA chloride solution with added MEM supplements in the bath (see Materials and methods). Fig. 4A shows the simultaneous activation of TRPV4 channels at V_{hold}= -50 mV in response to 500 nM GSK1016790A. The I-V curve, shown in Figure 4B, is outwardly rectifying with a V_{rev} = -8 mV, as expected for the cationic TRPV4 current [43-45]. Examples of single channel inward currents and the corresponding amplitude histograms are plotted in Fig. 4C (same experiment as in Fig. 4A). Current amplitudes from the traces were respectively -2.2, -1.9 and -1.7 pA, in agreement with previous studies. Fig. 4D shows an example of single channel I-V obtained from another outside-out experiment, in the presence of a lower concentration (25 nM) of the agonist. The resulting outward rectifying I-V curve shows a V_{rev} of -4 mV and current amplitudes of -1.8 pA at -50 mV and of +8.1 pA at +100 mV. Moreover, we obtained similar results for both mean patch current and single channel unitary current in experiments in which we applied RR to block the GSK1016790A activated currents (Fig. S-5A,B of the SM). Finally, current amplitudes at -50 mV and +100mV and reversal potential were respectively -2.3 ± 0.4 pA, +9.5 ± 0.7 pA and -2.4 ± 4.2 mV (n = 9 cells). In conclusion, in our experimental conditions, TRPV4 single channel conductance for outward and inward currents values are respectively 90-100 pS and 40-50 pS (Table 3).

Table 3

Channels	Agonist	N° patches	Current Amplitude at -50 mV (pA)	Current Amplitude at +100 mV (pA)	I-V	Single channel conductance (pS)	V_{rev} (mV)
TRPV4	GSK1016790A	9	-2.3 ± 0.4	+9.5 ± 0.7	Outward rectification	≈100 pS (at 100 mV)	-2.4 ± 4.2
	NPs	11	-2.2 ± 0.2	+11.0 ± 1.1	Outward rectification	≈50 pS (at -50 mV)	+3.2 ± 2.4
CONNEXINS	NPs	13	-	-	Linear	221.0 ± 4.4 (n=8); 317.7 ± 8.2 (n=5)	+2.2 ± 2.0; +2 ± 3.0
PANNEXINS	NPs	5	-	-	Outward rectification	685.0 ± 23.8 (at -50mV)	-0.6 ± 2.1

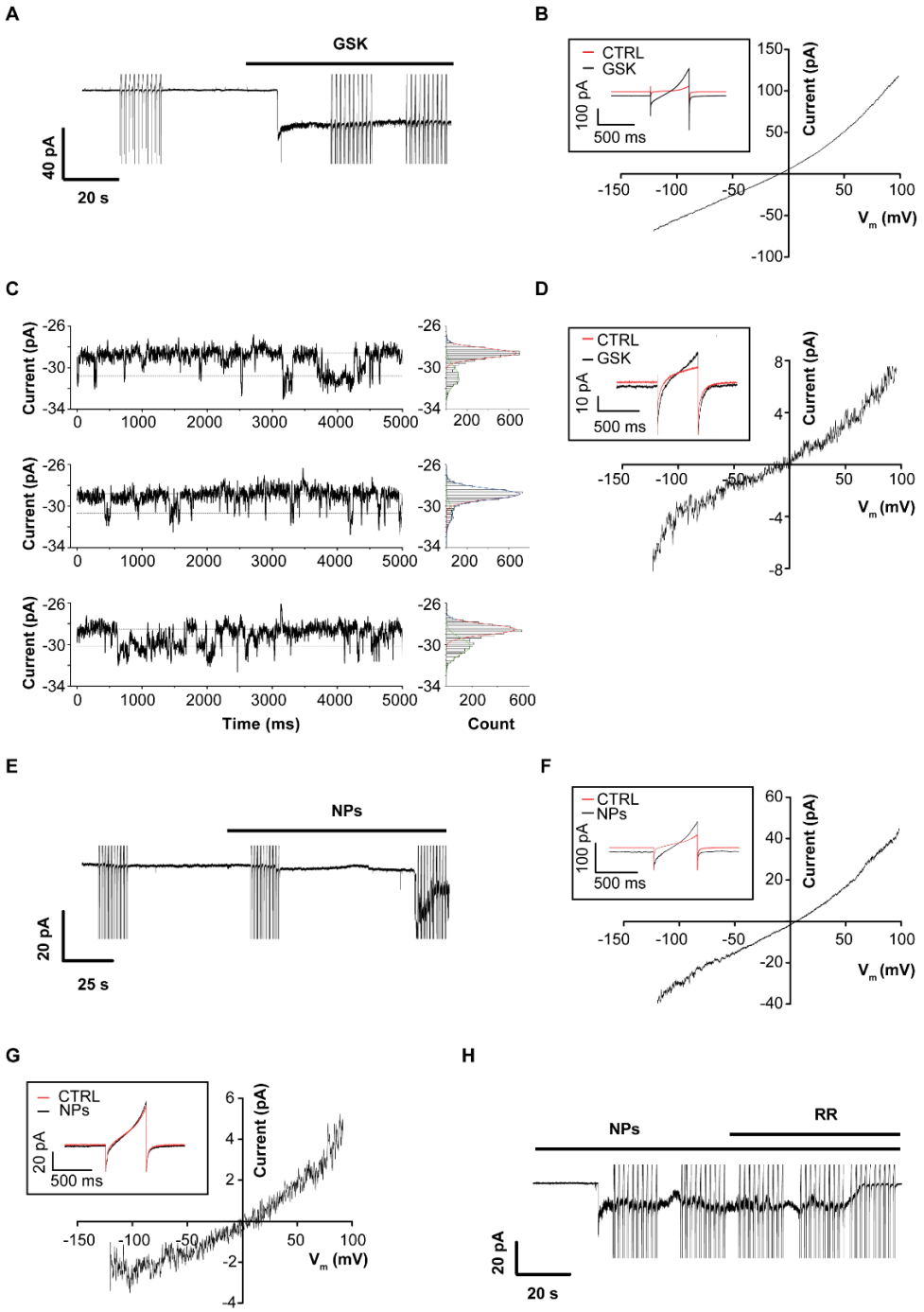
A
GSK
40 pA
20 s
B
CTRL
GSK
100 pA
500 ms
Current (pA)
V_m (mV)
C
Current (pA)
Time (ms)
Count
D
CTRL
GSK
10 pA
500 ms
Current (pA)
V_m (mV)
E
NPs
20 pA
25 s
F
CTRL
NPs
100 pA
500 ms
Current (pA)
V_m (mV)
G
CTRL
NPs
20 pA
500 ms
Current (pA)
V_m (mV)
H
NPs
RR
20 pA
20 s

Figure 4. SiO_2-50 nm NPs open TRPV4 channels in outside-out patches. (A) Currents activated by the TRPV4 specific agonist GSK1016790A (500 nM) at V_{hold}= -50 mV. **(B)** I-V relationship of the patch average current obtained subtracting the red trace to the black trace shown in the inset. **(C)** Examples of TRPV4 single channel currents and the corresponding amplitude histograms. **(D)** Single channel I-V relationship obtained subtracting the red trace (inset, baseline) from the black trace recorded in the presence of GSK1016790A (25 nM). **(E)** Currents activated by 20 μg mL^{-1} SiO_2 NPs at V_{hold} = -50 mV. **(F)** I-V relationship of the patch average current activated by SiO_2 NPs obtained subtracting the red trace from the black trace shown in the inset. **(G)** Single channel I-V relationship obtained subtracting the red trace (baseline) from the black trace shown in the inset. **(H)** Ruthenium red (5 μM) blocked NP-activated TRPV4 channels.

Subsequently we challenged outside-out patches with 20 μg mL^{-1} SiO_2 NPs. Fig. 4E shows the activation of a cationic inward current at V_{hold} = -50 mV. Importantly, this result obtained on isolated patches provides strong evidence that NPs act via a membrane-delimited mechanism to activate ionic channels.

Furthermore, we obtained the I-V relationship and the reversal potential of the average patch NP-activated current (Fig. 4F). The resulting curve showed a V_{rev} = 4.5 mV; Fig. 4G shows the single channel I-V relationship obtained from the same patch (i_{-50} = -1.8 pA, i_{100} = 6.3 pA, V_{rev} = 5 mV). The NP-activated inward current was blocked by RR (Fig. 4H). Figure S-5C,D of the SM shows the I-V relationship of respectively the mean patch current and the single channel current blocked by RR.

Finally, amplitude at -50 mV and +100 mV and reversal potential of the single channel currents were respectively of -2.15 ± 0.2 pA, 11.0 ± 1.1 pA and 3.2 ± 2.4 mV (n = 11 cells, Table 3). These values do not significantly differ from those obtained for TRPV4 (Welch's *t*-test, *p*-value = 0.67, statistical sensitivity = 1.17 pA at π = 0.8 for comparison at -50 mV, *p*-value = 0.25, statistical sensitivity = 4.06 pA at π = 0.8 for comparison at +100 mV), suggesting that TRPV4 channels are actually one the calcium-permeable channel types that are activated, via a membrane-delimited mechanism, by SiO_2-50 nm NPs in GT1–7 neuronal cells.

Large conductance nonselective channels

Whole cell and calcium imaging experiments showed that Gd^{3+} or RR+CBX block almost completely the NP-activated inward currents and calcium influx. These data point to the involvement of connexins and pannexins as the main large-conductance calcium-permeable channels activated in response to NPs. In the absence of NPs in the external solution, large conductance nonselective channel activity was detected in 5 out of 42 outside-out experiments. An example is shown in Fig. S-6 of the SM.

On the other hand, large conductance channel activity in response to NPs perfusion was measured in the majority of the experiments (in 3 out of 4 with 0.5 μg mL^{-1} and in 13 out 14 with 20 μg mL^{-1}). Fig. 5A shows an example of the channel activation in the presence of 0.5 μg mL^{-1} NPs. Here and in the trace with an expanded time scale (Fig. 5B), the activation of unitary single channel events of -12 pA was suddenly followed by a steep activation of additional inward currents of about -67 pA and then of -34 pA. Fig. 5C shows the single channel I-V relationship obtained during the opening of the channel of unitary current amplitude of -12 pA: the conductance was 233 pS and the reversal potential +0.5 mV. Finally, the best fit of the amplitude histogram distribution of the single channel trace shown in the inset (Fig. 5D; same events as shown at the end of the record of Fig. 5B) indicates a fully open state of -34 pA (about 680 pS; see below) and two current sub-levels. In a second set of experiments we analyzed the responses to 20 μg mL^{-1} NPs. Fig. 5E shows a series of bursts of single channel currents recorded in the presence of 20 μg mL^{-1} NPs and of the TRPV4 antagonist HC-067047 [46] in the bath solution (10 μM), which well illustrates several sub-conductance states and loop-gating events, i.e. transitions between an open and the fully closed state that occur through a number of meta-

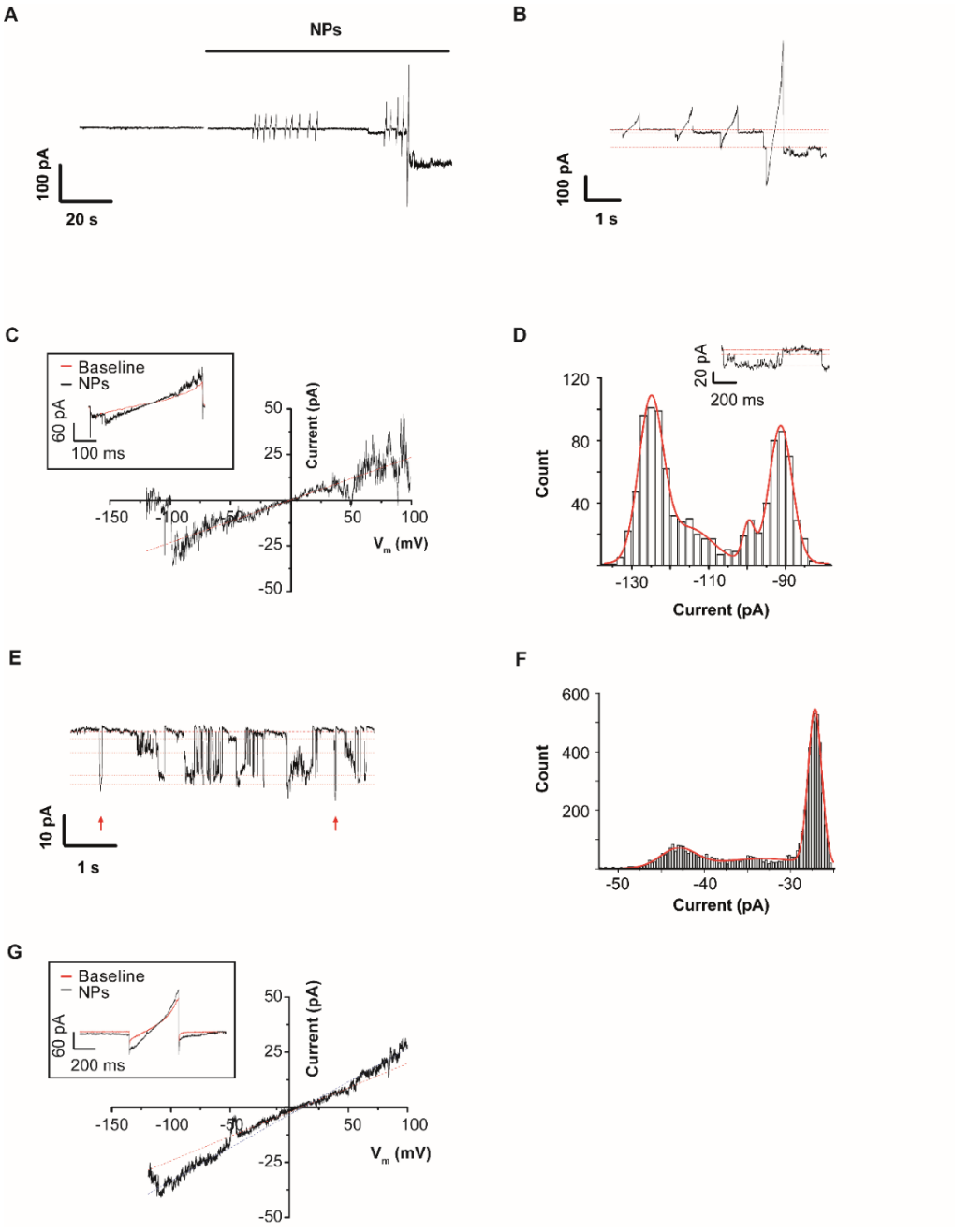

Figure 5. SiO2-50 nm NPs open large conductance channels in outside-out patches. (**A**) Currents activated by 0.5 µg mL-1 SiO2 NPs at Vhold = -50 mV. (**B**) Single channels currents recorded between and during the last 4 voltage ramps of (**A**) in more expanded scales. Red lines indicate the main current levels. (**C**) Single channel I-V relationship obtained by subtracting from the second current

ramp (inset, black trace) of (**B**) the first one (inset. red trace). The dotted red line represents the regression line obtained by fitting the curve from -50 mV to +40 mV. (**D**) Amplitude histogram, fitted by the sum of 4 gaussian curves, of the single channel trace shown in the inset. (**E**) Single channel currents activated in response to 20 µg mL-1 SiO_2 NPs at Vhold = -50 mV and (**F**) the corresponding amplitude histogram. (Arrows indicate single channel events of about -20 pA). (**G**) I-V relationship of the channel in (**E**), obtained by subtracting the baseline from a current ramp recorded during channel opening (respectively red and black trace in the inset).

stable intermediate conductance states with a slow, measurable time course [47, 48].

The best fit of the amplitude histogram distribution (Fig. 5F) of the single channel trace indicates a main open state of -15.9 pA, but single channel events of -20 pA and even larger could be detected (arrows in Fig. 5E). Fig. 5G, obtained from the same experiment as in Fig. 5E, shows the single channel I-V relationship. The curve was fitted with two regression lines yielding a conductance state of 300 pS (blue line) and another of 220 (red line). In 5 experiments, NPs activated also channels of higher conductance (see also above, Fig. 5B) and with different biophysical properties. Fig. 6A shows a current trace, recorded in the presence of 20 µg mL^{-1} NPs and 5 µM RR. The I-V relationship in Fig. 6B shows a strong outward rectification for $V_m > 50$ mV and $V_{rev} = -7.8$ mV. In the expanded traces shown in the lower part of Fig. 6A single channel openings could be observed, with a current amplitude of -29 pA (687 pS) at $V_m = -50$ mV (red lines).

In conclusion, the data provide evidence that SiO_2 NPs activate most frequently channels with a conductance in the range of 200-250 pS and in the range of 300-350 pS (Table 3). These data are in agreement with those reported in previous papers for Cx43 and Cx26 [49-53]. In addition, we also recorded nonselective channels with an outwardly rectifying I-V relationship, with a very large conductance in the range of 600-700 pS at -50 mV (Table 3), properties comparable to those described for Panx channels [25, 48, 54, 55].

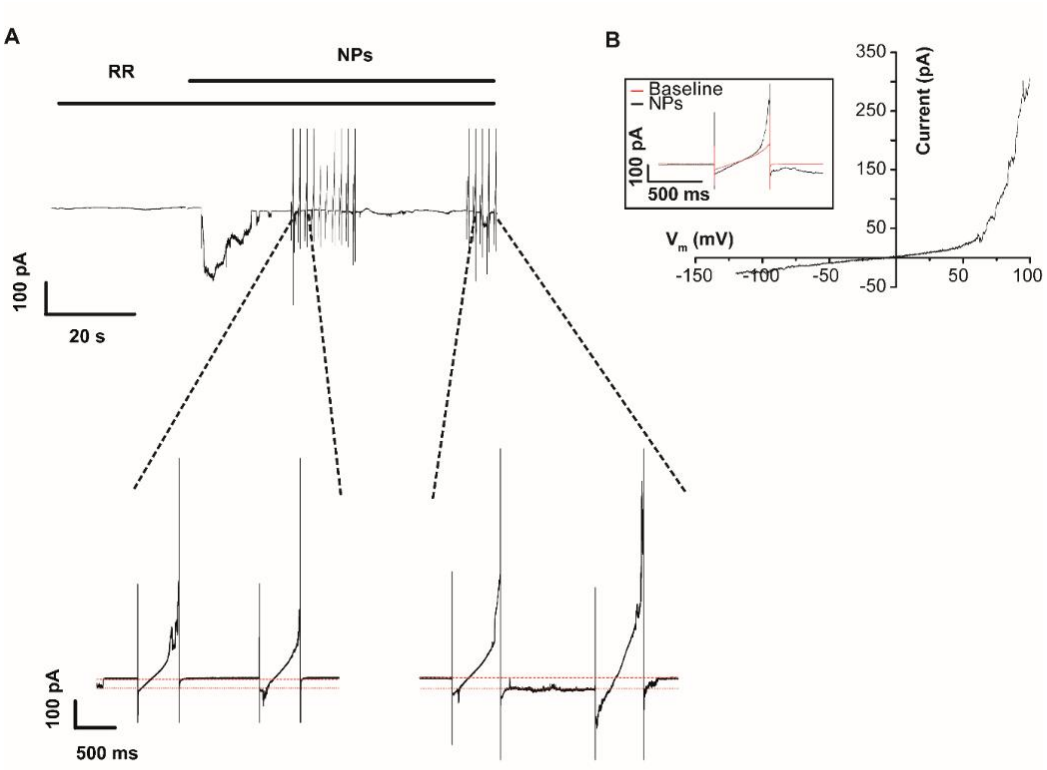

Figure 6. SiO_2-50 nm NPs open Panx-like channels in outside-out patches. (A) Currents activated by 20 µg mL^{-1} SiO_2 NPs at V_{hold} = -50 mV in the presence of 5 µM RR. Lower traces are single channels currents recorded between and during the voltage ramps in more expanded scales. **(B)** I-V relationship obtained by subtracting the baseline (red trace, inset) from the averaged current obtained from the ramps shown in **(A)** (black trace, inset).

SiO_2 NPs induce lipid peroxidation in GT1-7 cells

Production of free radicals, and in particular lipid peroxidation, has been reported to be activated by the interaction of several kinds of NPs with different cell types [56-58]; this pathway may be in turn involved in the activation of some of the channels we described in the previous sections. To investigate this potential mechanism, GT1–7 were treated with SiO_2-50 nm NPs (20 µg mL^{-1}, 30 minutes), and the changes in lipid peroxidation were evaluated by means of the Click-iT® Lipid Peroxidation Imaging kit (see Materials and methods). As shown in Fig. 7A, the treatment triggered a significant increase (*p*-value = 0.003) in lipid peroxidation over the basal value, while cell preincubation with 1 mM of the antioxidant N-acetyl-L-cysteine (NAC) significantly reduced (*p*-value = 0.045) the response (Welch's *F*-test, π = 0.98, Games-Howell post hoc test, n = 17 for each condition, from 3 or 4 technical replicates in 5 biological replicates).

These protocols were performed by adding the NPs to the culture medium in the culture dish, differently from all the other experiments in which the NPs were administered by microperfusion. A set of control tests (Methods and Fig. S-7 in the SM) allowed to confirm that there was no significant difference in the actual NP concentration.

Preincubation with NAC affects the calcium increases induced by SiO_2 NPs

To evaluate the effects of NAC on calcium signals induced by SiO_2 NPs we performed further calcium imaging experiments in which GT1–7 cells were challenged with 20 μg mL^{-1} SiO_2 after 30 min of preincubation with 1 mM NAC. Specifically, we recorded $[Ca^{2+}]_i$ time course from 434 NAC-preincubated cells (from 7 experiments) and compared the responses elicited by NPs with the same set of control traces already used to assess the effect of RR and CBX. NAC preincubation caused a strong reduction of NP-induced calcium signals, as shown by the average traces in Fig. 7B; Fig. 7C shows 4 representative traces from 2 different experiments (one in control conditions and one with NAC preincubation). The area between each trace and its baseline was evaluated by the same approach previously described; Fig. 7D shows the frequency distributions of the areas measured in the two experimental conditions. Similarly to what observed with RR/CBX blockers, the effect of NAC as compared to the control condition was striking, leading to a nearly complete suppression of the response in most of the observed cells (Mann-Whitney *U* Test, *p*-value = $9.1 \cdot 10^{-82}$, $\pi = 0.99$, effect size $r = 0.64$). Further analytical and statistical details are provided in Methods of the SM.

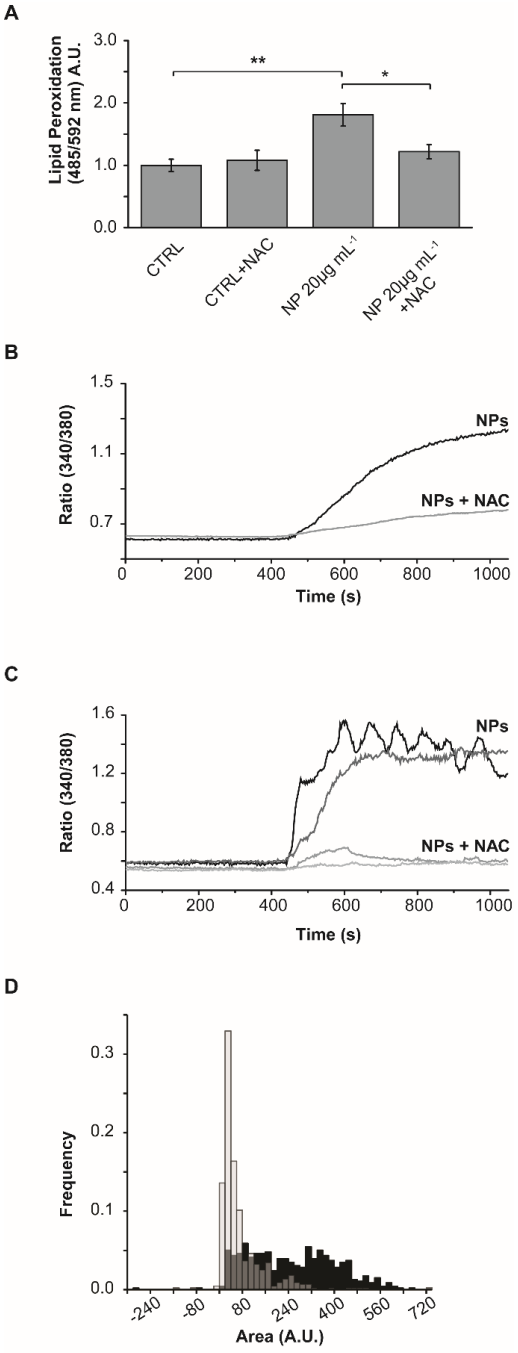

Figure 7. SiO_2-50 nm NPs induce lipid peroxidation and this pathway is strongly involved in NP-activated calcium influx. **(A)** 30 min preincubation of GT1–7 cells with 1 mM NAC prevented the increase in lipid peroxidation induced by 20 µg mL^{-1} SiO_2 NPs (**p*-value = 0.045, ***p*-value = 0.003, Welch's *F*-test and Games-Howell post hoc test, error bars = s.e.m.). **(B)** Preincubation with NAC

strongly reduced the calcium influx induced by NPs as can be seen from the comparison between the average of 434 cells from 7 experiments with NAC (gray trace) and the average of the same control traces already used as reference for RR and CBX blockers (black trace, 457 traces from 6 experiments). **(C)** Two representative traces from one control experiment compared with two from one experiment with NAC. **(D)** Frequency histograms of the areas between the curve of $[Ca^{2+}]_i$ response to NPs and the reference baseline. Black bars: areas measured in control condition (SiO_2 NPs alone). Transparent gray bars: areas measured during NP administration after NAC preincubation.

3.4 Discussion

The detailed and quantitative assessment of the physiopathological responses elicited by nanoparticles in cells and tissues is the prerequisite for determining which properties (in terms of composition, surface, size) have to be selected in view of a safe and effective use of these tools in biomedical applications. In neurons, interaction of the NPs with the plasmamembrane can represent a critical factor profoundly affecting cell functionality, particularly by modulating the activity of ionic channels. In spite of their functional relevance, few reports are available regarding the effects of NPs on neuronal channels, in particular at the single channel level, due to the challenges posed by the technique: most refer to inhibition of voltage-dependent Na^+ and K^+ channels [11, 12, 59], while increases in I_{Na} and I_K by ZnO NPs have been reported at a relatively high concentration (100 μg mL^{-1}) [60]. As reported in the Introduction, a previous work [10] provided evidence that SiO_2-50 nm NPs, at nontoxic doses, activate in the GT1–7 neuroendocrine cell line strong and long lasting increases in $[Ca^{2+}]_i$, at least in part dependent on the activation of the calcium permeable channel TRPV4, an integrator of different physical and chemical stimuli [61], and only marginally affected by blockers of

voltage dependent calcium channels. Therefore, the object of the present work was to provide direct evidence, using the patch clamp electrophysiological approach, for the involvement of TRPV4 and to identify the other channels responsible of the NP-activated calcium influx.

In whole cell experiments we have found that SiO_2-50 nm NPs (0.5 and 20 μg mL^{-1}) elicit inward currents showing a noisy behavior, with partial reversibility (Figs. 1, 2, S-3). The reversal potential, near 0 mV, suggests the involvement of nonselective conductances. The striking observation of single unitary macroscopic events even in the whole cell configuration pointed to the activation of large conductance channels. A pharmacological approach, by means of blockers of TRPV4 channels and of the connexin and pannexin families of large conductance nonselective channels allowed to dissect the contribution of the different channel types (Fig. 3). By combining calcium imaging on cell populations with whole cell and single channel recordings evidence is provided that the three major components of the inward currents elicited by the interaction of the NPs with the neuronal plasma membrane are carried by TRPV4 channels and Cx and Panx-like channels (Figs. 4, 5, 6). All three classes of channels described above are known to be involved in a wide spectrum of physiological and pathological processes [25, 46] and characterized by multiple activation mechanisms. In the present case the most relevant is likely related to the production of reactive species, since we have shown that lipid peroxidation is significantly increased after 30 minutes of NP exposure and that preincubation with the antioxidant NAC strongly reduced the NP-induced [Ca2+]i increase (Fig. 7). The detection and measurement of lipid peroxidation is one of the evidence most frequently cited to support the involvement of free-radical reactions in cellular responses [62]. ROS are involved in the activation of TRPV4 [63]; moreover, ROS production has been observed downstream of TRPV4-mediated calcium influx [64-67], thus providing a potential amplification mechanism. In

addition, some Cxs and Panxs have been reported to open in response to generation of ROS and other reactive species [18, 68, 69].

A relevant issue in the interpretation of these data is the finding that their activation has been observed also in excised membrane patches, pointing to membrane-delimited pathways. One explanation is based on the existence of plasmamembrane, constitutively active oxidases that generate oxides/peroxides in the extracellular medium [70, 71]; a recent paper [72] has reported that SiO_2 NPs can generate $^{\cdot}HO$ in the presence of H_2O_2. Therefore, channels present in an excised patch can be activated by the reactive species produced either locally or in the surrounding environment, derived from the whole cell population. Interestingly, the Authors reported that in contrast with bare SiO_2 NPs, aminated NPs did not catalyze ROS production: this is in agreement with a previous observation that aminated NPs failed to induce detectable increases in $[Ca^{2+}]_i$ [10] and to activate inward currents in most cells tested. Additionally, more than one mechanism may coexist, in particular for TRPV4: as discussed above, its activation could lead to intracellular ROS production, thus explaining the strong contribution of this pathway to the observed cellular responses. The obvious candidate is mechanotransduction, following membrane stretch due to the interaction with the NP. TRPV4 is a polymodal channel, that can give an integrated response to different chemical and physical stimuli [73]. It is involved in the transduction of cell stretch and mechanical pressure, even if it is still controversial whether it is activated directly by deformation of the membrane or by the ensuing release of some membrane component that in turn acts on the channel [74-76]. Mechanosensitivity has been reported also for Panx channels [77].

The data presented in this paper can be related to the findings of Ref.14, that show that in primary sensory neurons these nanoparticles elicited the same modulation of electrical excitability as in GT1-7 cells. The picture has to be broadened to

encompass other neurologically relevant nanomaterials. Interestingly, one of such materials, graphene, has attracted the interest of several groups for its potential biomedical applications, and it has been shown to affect astrocyte function and morphology [78] and neuronal excitability, at concentrations that do not impair cell viability. The effects on neurons are mediated by modulation of several types of ionic channels in hippocampal and cortical neurons, such as synaptic excitatory and/or inhibitory ones [79,80] or of K^+ currents by an indirect mechanism, due to the depletion of extracellular K^+ ions because of ion adsorption on the graphene surface [81]. The understanding of the biophysical mechanisms underlying these interactions is only at the beginning, and future research will provide useful information for the design of safe and efficient tools for nanomedicine.

Conclusions

In the present paper we report the detailed electrophysiological characterization of the ionic currents activated by the interaction of nanoparticles with the neuronal plasmamembrane and identify the major channel types involved. Combining whole cell and single channel recordings with calcium imaging we show that the response can be ascribed to two major components carried respectively by TRPV4 and large conductance channels and point to the involvement of free radicals production as one of the key actors in this process.

A peculiar feature of the results presented in this paper is that they have been obtained at NP concentrations that we have previously shown to be nontoxic [10, 14, 82]; a key question is whether the same molecular actors may underlie toxicity at higher doses, given the potential amplification pathways described above. In this light, recently [83] it has been reported that SiO_2 NPs inhibit TRPV4 following its activation with the agonist GSK1016790A in airway epithelial cells; however, these

findings were obtained with smaller (10 nm) particles with a ζ-potential of 20 mV; of greater relevance, the concentrations used in native cell (100-3000 μg mL^{-1}) have been shown to be well above the threshold for toxicity [82]. It is quite reasonable that at such high doses the interaction of the NPs with the membrane involves radically different mechanisms. In any case, the information presented here may be of general value, particularly for cells of the nervous system, since a similar pathway has been reported for Panx1 activation by Carbon Black NPs in astrocytes [28].

References

Papers of special note have been highlighted as: • of interest; •• of considerable interest

[1] Malvindi MA, Brunetti V, Vecchio G, Galeone A, Cingolani, R, Pompa PP. SiO_2 nanoparticles biocompatibility and their potential for gene delivery and silencing. *Nanoscale* 4, 486-495 (2012).

[2] Izak-Nau E, Kenesei K, Murali K *et al*. Interaction of differently functionalized fluorescent silica nanoparticles with neural stem- and tissue-type cells. *Nanotoxicology* 8, 138-148 (2014).

[3] Rosenholm, J. M;. Sahlgren, C.; Lindén, M. Multifunctional mesoporous silica nanoparticles for combined therapeutic, diagnostic and targeted action in cancer treatment. *Curr. Drug Targets* 2, 1166-1186 (2011).

[4] Zhang S, Chu Z, Yin C, Zhang C, Lin G, Li Q. Controllable drug release and simultaneously carrier decomposition of SiO_2-drug composite nanoparticles. *J. Am. Chem. Soc.*135, 5709-5716 (2013).

[5] Montalti M, Prodi L, Rampazzo E, Zaccheroni N. Dye-doped silica nanoparticles as luminescent organized systems for nanomedicine. *Chem. Soc. Rev.* 43, 4243-4268 (2014).

[6] Wei Z, Wu Y, Zhao Y, Mi L, Wang J, Wang J *et al*. Multifunctional nanoprobe for cancer cell targeting and simultaneous fluorescence/magnetic resonance imaging. *Anal. Chim. Acta* **2016**, 938, 156-164.

[7] Miletto I, Gilardino A, Zamburlin P *et al*. Highly bright and photostable cyanine dye-doped silica nanoparticles for optical imaging: photophysical characterization and cell tests. *Dyes Pigments* 84, 121-127 (2010).

[8] Clapham DE. Calcium signaling. *Cell* 131, 1047-1058 (2007).

[9] Lovisolo D, Gilardino A, Ruffinatti FA. When neurons encounter nanoobjects: spotlight on calcium signalling. *Int. J. Environ. Res. Public Health* 11, 9621-9637 (2014).

[10] Gilardino A, Catalano F, Ruffinatti FA *et al*. Interaction of SiO_2 nanoparticles with neuronal cells: Ionic mechanisms involved in the perturbation of calcium homeostasis. *Int. J. Biochem. Cell Biol.* 66, 101-111 (2015).

[11] Liu Z, Ren G, Zhang T, Yang Z. Action potential changes associated with the inhibitory effects on voltage-gated sodium current of hippocampal CA1 neurons by silver nanoparticles. *Toxicology* 264, 179-184 (2009).

[12] Shan D, Xie Y, Ren G, Yang Z. Inhibitory effect of tungsten carbide nanoparticles on voltage-gated potassium currents of hippocampal CA1 neurons. *Toxicol. Lett.* 209, 129-135 (2012).

[13] Busse, M.; Stevens, D.; Kraegeloh, A *et al*. Estimating the modulatory effects of nanoparticles on neuronal circuits using computational upscaling. *J. Nanomedicine* 8, 3559-3572 (2013).

[14] Distasi C, Ruffinatti FA, Dionisi M *et al*. SiO_2-nanoparticles modulate the electrical activity of neuroendocrine cells without exerting genomic effects. *Sci. Rep*. 8, 2760 (2018).

- **Silica nanoparticles, at nontoxic doses, transiently increase neuronal firing without affecting functional behavior and gene expression**

[15] Orts-Gil, G.; Natte, K.; Drescher, D *et al*. Characterisation of silica nanoparticles prior to in vitro studies: from primary particles to agglomerates. *J. Nanopart. Res*. 13, 1593-1601 (2011).

[16] Ambrosi C, Gassmann O, Pranskevich JN *et al*. Pannexin1 and Pannexin2 channels show quaternary similarities to connexons and different oligomerization numbers from each other. *J. Biol. Chem.* 285, 24420-24431 (2010).

[17] Chandrasekhar A, Bera AK. Hemichannels: permeants and their effect on development, physiology and death. *Cell Biochem. Funct.* 30, 89-100 (2012).

[18] Orellana JA, Martinez AD, Retamal MA. Gap junction channels and hemichannels in the CNS: regulation by signaling molecules. *Neuropharmacology* 75, 567-582 (2013).

[19] Penuela S, Gehi R, Laird DW. The biochemistry and function of pannexin channels. *Biochim. Biophys. Acta* 1828, 15-22 (2013).

[20] Isakson BE, Thompson RJ. Pannexin-1 as a potentiator of ligand-gated receptor signaling *Channels (Austin)* 8, 118-123 (2014).

[21] Patel D, Zhang X, Veenstra RD. Connexin hemichannel and pannexin channel electrophysiology: how do they differ? *FEBS Lett.* 588, 1372-1378 (2014).

[22] Bose S, Leclerc GM, Vasquez-Martinez R, Boockfor FR. Administration of connexin43 siRNA abolishes secretory pulse synchronization in GnRH clonal cell populations. *Mol. Cell Endocrinol.* 314, 75-83 (2010).

[23] Bruzzone R, Hormuzdi SG, Barbe MT, Herb A, Monyer H. Pannexins: a family of gap junction proteins expressed in brain. *Proc. Natl. Acad. Sci. USA* 100, 13644-13649 (2003).

[24] Vogt A, Hormuzdi SG, Monyer H. Pannexin1 and Pannexin2 expression in the developing and mature rat brain. *Brain Res. Mol. Brain Res.* 141, 113-120 (2005).

[25] Cheung G, Chever O, Rouach N. Connexons and pannexons: newcomers in neurophysiology. *Front. Cell Neurosci.* 8, 348 (2014).

[26] Shestopalov VI, Slepak VZ. Molecular pathways of pannexin1-mediated neurotoxicity. Molecular pathways of pannexin1-mediated neurotoxicity. *Front. Physiol.* 5, 23 (2014).

[27] Swayne LA, Bennett SA. Connexins and pannexins in neuronal development and adult neurogenesis. *BMC Cell Biol.* 7 Suppl 1, 10 (2016).

[28] Wei H, Deng F, Chen Y, Qin Y, Hao Y, Guo X. Ultrafine carbon black induces glutamate and ATP release by activating connexin and pannexin hemichannels in cultured astrocytes. *Toxicology* 323, 32-41 (2014).

- **Provides evidence, by dye uptake essay, of carbon black ability to activate pannexin and connexin channels.**

[29] Alexander SP, Striessnig J, Kelly E *et al*. The concise guide to Pharmacology 2017/18: Voltage-gated ion channels. *Br. J. Pharmacol.* 174 Suppl 1, S160-S194 (2017).

[30] Stout CE, Costantin JL, Naus CC, Charles AC. Intercellular calcium signaling in astrocytes via ATP release through connexin hemichannels. *J. Biol. Chem.* 277, 10482-10488 (2002).

[31] Vergara L, Bao X, Cooper M, Bello-Reuss E, Reuss L. Gap-junctional hemichannels are activated by ATP depletion in human renal proximal tubule cells. *J. Membr. Biol.* 196, 173-184 (2003).

[32] Hansen DB, Ye ZC, Calloe, K. Activation, permeability, and inhibition of astrocytic and neuronal large pore (hemi)channels. *J. Biol. Chem.* 289, 26058-26073 (2014).

[33] Woehrle T, Yip L, Manohar M *et al*. Hypertonic stress regulates T cell function via pannexin-1 hemichannels and P2X receptors. *J. Leukoc. Biol.* 88, 1181-1189 (2010).

[34] Israelachvili JN. *Intermolecular and Surface Forces*. Academic Press, London, UK (1996).

[35] Kondo RP, Wang SY, John SA, Weiss JN, Goldhaber JI. Metabolic inhibition activates a non-selective current through connexin hemichannels in isolated ventricular myocytes. *J. Mol. Cell Cardiol.* 32, 1859-1872 (2000).

[36] Lee JH, Park C, Kim SJ *et al*. Different uptake of gentamicin through TRPV1 and TRPV4 channels determines cochlear hair cell vulnerability. *Exp. Mol. Med.* 45:e12 (2013).

[37] Yang F, Zhou L, Wang D, Yang LL, Yuan GR, Huang QY. Suppression of TRPV4 channels ameliorates anti-dipsogenic effects under hypoxia in the subfornical organ of rats. *Sci. Rep.* 6, 30168 (2016).

[38] Patapoutian A, Peier AM, Story GM, Viswanath V. ThermoTRP channels and beyond: mechanisms of temperature sensation. *Nat. Rev. Neurosci*. 4, 529-539 (2003).

[39] Seminario-Vidal L, Okada SF, Sesma JI *et al*. Rho signaling regulates pannexin 1-mediated ATP release from airway epithelia. *J. Biol. Chem.* 286, 26277-26286 (2011).

[40] Bai JZ, Lipski J. Involvement of TRPV4 channels in Aβ(40)-induced hippocampal cell death and astrocytic Ca(2+) signalling. *Neurotoxicology* 41,64-72 (2014).

[41] Mueller-Tribbensee SM, Karna M, Khalil M, Neurath MF, Reeh PW, Engel MA. Differential Contribution of TRPA1, TRPV4 and TRPM8 to Colonic Nociception in Mice. *PLoS One* 10:e0128242 (2015).

[42] Thorneloe KS, Sulpizio AC, Lin Z *et al*. N-((1S)-1-{[4-((2S)-2-{[(2,4-dichlorophenyl)sulfonyl]amino}-3-hydroxypropanoyl)-1-piperazinyl]carbonyl}-3-methylbutyl)-1-benzothiophene-2-carboxamide (GSK1016790A), a novel and potent transient receptor potential vanilloid 4 channel agonist induces urinary bladder contraction and hyperactivity: Part I. *J. Pharmacol. Exp. Ter.* 326, 432-442 (2008).

[43] Watanabe H, Vriens J, Suh SH, Benham CD, Droogmans G, Nilius B. Heat-evoked activation of TRPV4 channels in a HEK293 cell expression system and in native mouse aorta endothelial cells. *J. Biol. Chem*. 277, 47044-47051 (2002).

[44] Cao DS, Yu SQ, Premkumar LS. Modulation of transient receptor potential Vanilloid 4-mediated membrane currents and synaptic transmission by protein kinase C. *Mol. Pain* 5, 5 (2009).

[45] Feetham CH, Nunn N, Lewis R, Dart C, Barrett-Jolley R. TRPV4 and K(Ca) ion channels functionally couple as osmosensors in the paraventricular nucleus. *Br. J. Pharmacol*. 172, 1753-1768 (2015).

[46] Everaerts W, Zhen X, Ghosh D *et al*. Inhibition of the cation channel TRPV4 improves bladder function in mice and rats with cyclophosphamide-induced cystitis. *Proc. Natl. Acad. Sci. U S A* 107, 19084-19089 (2010).

[47] Bao L, Locovei S, Dahl G. Pannexin membrane channels are mechanosensitive conduits for ATP. *FEBS Lett*. 572, 65-68 (2004).

[48] Oh S, Bargiello TA. Voltage regulation of connexin channel conductance. *Yonsei Med. J.* 56, 1-15 (2015).

[49] Contreras JE, Sáez JC, Bukauskas FF, Bennett MV. Gating and regulation of connexin 43 (Cx43) hemichannels. *Proc. Natl. Acad. Sci. U S A* 100, 11388-11393 (2003).

[50] Kang NJ, Lee KM, Kim JH *et al*. Inhibition of gap junctional intercellular communication by the green tea polyphenol (-)-epigallocatechin gallate in normal rat liver epithelial cells. *J. Agric. Food Chem.* 56, 10422-10427 (2008).

[51] Carnarius C, Kreir M, Krick M *et al*. Green fluorescent protein changes the conductance of connexin 43 (Cx43) hemichannels reconstituted in planar lipid bilayers*. J. Biol. Chem*. 287, 2877-2886 (2012).

[52] Valiunas V. Cyclic nucleotide permeability through unopposed connexin hemichannels. V. *Front. Pharmacol*. 4, 75 (2013).

[53] Sanchez HA, Villone K, Srinivas M, Verselis VK. The D50N mutation and syndromic deafness: altered Cx26 hemichannel properties caused by effects on the pore and intersubunit interactions. *J. Gen. Physiol.* 142, 3-22 (2013).

[54] Ma W, Hui H, Pelegrin P, Surprenant A. Pharmacological characterization of pannexin-1 currents expressed in mammalian cells. *J. Pharmacol. Exp. Ther*. 328, 409-418 (2009).

[55] Thompson RJ. Pannexin channels and ischaemia. *J. Physiol.* 593, 3463-3470 (2015).

[56] Wang F, Jiao C, Liu J *et al.* Oxidatives mechanisms contribute to nanosize silica dioxide-induced developmental neurotoxicity in PC12 cells. *Toxicol. In Vitro* 25, 1548 (2011).

• • Interesting study on the size-, dose- and time-dependent effect of SiO_2-nanoparticles on ROS production, lipid peroxidation and cell viability in a neuronal cell model.

[57] Karmakar A, Zhang Q, Zhang Y. Neurotoxicity of nanoscale materials. *J. Food. Drug Anal.* 22, 147-160 (2014).

[58] Song B, Zhang Y, Liu J, Feng X, Zhou T, Shao L. Is Neurotoxicity of Metallic Nanoparticles the Cascades of Oxidative Stress? *Nanoscale Res. Lett.* 11, 291 (2016).

[59] Liu Z, Liu S, Ren G, Zhang T, Yang Z. Nano-CuO inhibited voltage-gated sodium current of hippocampal CA1 neurons via reactive oxygen species but independent from G-proteins pathway. *J. Appl. Toxicol*. 31, 439-445 (2011).

[60] Zhao J, Xu L, Zhang T, Ren G, Yang Z. Influences of nanoparticle zinc oxide on acutely isolated rat hippocampal CA3 pyramidal neurons. *Neurotoxicology* 30, 220-230 (2009).

[61] Everaerts W, Nilius B, Owsianik G. The vanilloid transient receptorpotential channel TRPV4: from structure to disease. *Prog. Biophys. Mol. Biol*. 103, 2-17 (2010).

[62] Halliwell B, Gutteridge JM. Role of free radicals and catalytic metal ions in human desease: an overview. *Methods Enzymol.* 186, 1-85 (1990).

[63] Suresh K, Servinsky L, Jiang H *et al*. Reactive oxygen species induced Ca2+ influx via TRPV4 and microvascular endothelial dysfunction in the SU5416/hypoxia model of pulmonary arterial hypertension. *Am. J. Physiol. Lung Cell Mol. Physiol*. 314, L893-L907 (2018).

[64] Bubolz AH, Mendoza SA, Zheng X *et al*. Activation of endothelial TRPV4 channels mediates flow-induced dilation in human coronary arterioles: role of Ca2+ entry and mitochondrial ROS signaling. *Am. J. Physiol. Heart Circ. Physiol*. 302, H634-H642 (2012).

[65] Hong Z, Tian Y, Yuan Y *et al*. Enhanced Oxidative Stress Is Responsible for TRPV4-Induced Neurotoxicity. *Front. Cell Neurosci*. 10, 232 (2016).

[66] Hu F, Hui Z, Wei W *et al*. Hypotonic stress promotes ATP release, reactive oxygen species production and cell proliferation via TRPV4 activation in rheumatoid arthritis rat synovial fibroblasts. *Biochem. Biophys. Res. Commun.* 486, 108-115 (2017).

[67] Wu QF, Qian C, Zhao N *et al*. Activation of transient receptor potential vanilloid 4 involves in hypoxia/reoxygenation injury in cardiomyocytes. *Cell Death Dis.* 8, e2828 (2017).

- **Provides evidences that activation of TRPV4 channels induces in cardiomyocytes calcium influx, ROS release, depolarization of mitochondrial membrane potential and opening of mitochondrial permeability transition pore.**

[68] Muñoz MF, Puebla M, Figueroa XF. Control of the neurovascular coupling by nitric oxide-dependent regulation of astrocytic Ca(2+) signaling. *Front. Cell Neurosci.* 10, 9 (2015).

[69] Xu J, Chen L, Li L. Pannexin hemichannels: A novel promising therapy target for oxidative stress related diseases. *J. Cell Physiol*. 233, 2075-2090 (2018).

[70] Schneider B, Mutel V, Pietri M, Ermonval M, Mouillet-Richard S, Kellermann O. NADPH oxidase and extracellular regulated kinases 1/2 are targets of prion protein signaling in neuronal and nonneuronal cells. *Proc. Natl. Acad. Sci. U S A* 100, 13326-13331 (2003).

[71] Ma MW, Wang J, Zhang Q *et al*. NADPH oxidase in brain injury and neurodegenerative disorders. *Mol. Neurodegener.* 12, 7 (2017).

● ● Excellent review of NADPH-oxidases and their role in neurological disorders.

[72] Lehman SE, Morris AS, Mueller PS, Salem AK, Grassian VH, Larsen SC. Silica Nanoparticle-Generated ROS as a Predictor of Cellular Toxicity: Mechanistic Insights and Safety by Design. *Environ. Sci. Nano* 3, 56-66 (2016).

● ● Provides a correlation between ROS derived from SiO_2 nanoparticle surface-catalyzed reactions and cytotoxicity.

[73] White JP, Cibelli M, Urban L, Nilius B, McGeown JG, Nagy I. TRPV4: Molecular Conductor of a Diverse Orchestra. *Physiol. Rev*. 96, 911-973 (2016).

[74] Mendoza SA, Fang J, Gutterman DD *et al*. TRPV4-mediated endothelial Ca2+ influx and vasodilation in response to shear stress. *Am. J. Physiol. Heart Circ. Physiol.* 298, H466-H476 (2010).

[75] Shibukawa Y, Sato M, Kimura M *et al*. Odontoblasts as sensory receptors: transient receptor potential channels, pannexin-1, and ionotropic ATP receptors mediate intercellular odontoblast-neuron signal transduction. *Pflugers Arch*. 467, 843-863 (2015).

[76] Thoppil RJ, Cappelli HC, Adapala RK, Kanugula AK, Paruchuri S, Thodeti CK. TRPV4 channels regulate tumor angiogenesis via modulation of Rho/Rho kinase pathway. *Oncotarget* 7, 25849-25861 (2016).

[77] Chiu YH, Schappe MS, Desai BN, Bayliss DA. Revisiting multimodal activation and channel properties of Pannexin 1. *J. Gen. Physiol.* 150, 19-39 (2018).

[78] Chiacchiaretta M, Bramini M, Rocchi A *et al*. Graphene oxide upregulates the homeostatic functions of primary astrocytes and modulates astrocyte-to-neuron communication. *Nano Lett*. 18, 5827–5838 (2018).

[79] Rauti R, Lozano N, León V *et al.* Graphene oxide nanosheets reshape synaptic function in cultured brain networks. *ACS Nano* 10, 4459-4471 (2016).

[80] Bramini M, Sacchetti S, Armirotti A *et al.* Graphene oxide nanosheets disrupt lipid composition, Ca^{2+} homeostasis, and synaptic transmission in primary cortical neurons. *ACS Nano* 10, 7154-7171 (2018).

[81] Pampaloni NP, Lottner M, Giugliano M *et al.* Single-layer graphene modulates neuronal communication and augments membrane ion currents. *Nat Nanotechnol*. 13, 755-764 (2018).

[82] Ariano P, Zamburlin P, Gilardino A *et al*. Interaction of spherical silica nanoparticles with neuronal cells: size-dependent toxicity and perturbation of calcium homeostasis. *Small* 7, 766-774 (2011).

[83] Sanchez A, Alvarez JL, Demydenko K *et al*. Silica nanoparticles inhibit the cation channel TRPV4 in airway epithelial cells. *Part. Fibre Toxicol.* 14, 43 (2017).

Chapter 4

Oxaliplatin induces pH acidification in dorsal root ganglia neurons

Riva B.[1], Dionisi M.[1], Potenzieri A.[1], Chiorazzi A.[2], Cordero-Sanchez C[1], Rigolio R.[2], Carozzi VA.[2,3], Lim D.[1], Cavaletti G.[2], Marmiroli P.[2], Distasi C.[1], Genazzani AA[1].*

[1] Department of Pharmaceutical Sciences, University of Piemonte Orientale, Via Bovio 6, 28100, Novara, Italy. [2] Experimental Neurology Unit, School of Medicine and Surgery, University of Milano-Bicocca, Via Cadore 48, 20900, Monza, Italy.[3] Young Against Pain Group, Italy

Abstract

Oxaliplatin induced peripheral neurotoxicity is characterized by an acute cold-induced syndrome characterized by cramps, paresthesias/dysesthesias in the distal limbs and perioral region, that develops rapidly and lasts up to one week affecting nearly all the patients as well as by long-lasting symptoms. It has been previously shown that pharmacological or genetic ablation of TRPA1 responses reduces oxaliplatin-induced peripheral neurotoxicity in mouse models. In the present report, we show that treatment with concentrations of oxaliplatin similar to those

found in plasma of treated patients leads to an acidification of the cytosol of mouse dorsal root ganglia neurons in culture and this in turn is responsible for sensitization of TRPA1 channels, thereby providing a mechanistic explanation to toxicity of oxaliplatin. Reversal of the acidification indeed leads to a significantly reduced activity of TRPA1 channels. Last, acidification occurs also in vivo after a single injection of therapeutically-relevant doses of oxaliplatin.

4.1 Introduction

Chemotherapy-induced peripheral neurotoxicity is a dose-limiting toxicity of several anti-cancer agents, including platinum compounds, anti-tubulins and proteasome inhibitors. Management of peripheral neuropathy remains one of the most important unmet clinical needs in oncology practice since it compromises the quality of life and may limit the effectiveness of treatment (if doses need to be adjusted).

OHP induced peripheral neurotoxicity (OIPN) is characterized by an acute cold-induced syndrome characterized by cramps, paresthesias/dysesthesias in the distal limbs and perioral region, that develops rapidly and lasts up to one week affecting nearly all the patients[1,2,3]. In addition to these acute symptoms, most patients develop a chronic sensory neurotoxicity with enduring characteristics like ataxia, dysesthesias, paresthesias, burning and lancinating pain, that spreads from toes and fingers with a stocking-and-glove distribution[4]. The chronic symptoms are shared with other platinum-containing chemotherapeutics (*e.g.* cisplatin, carboplatin), while acute toxicity is a peculiarity of OHP. No therapies are available

to treat OIPN and patients often suffer from pain and sensory symptoms long after the end of the therapy[5].

DRG are thought to be the main target of OIPN, although the exact mechanism by which this occurs is still unknown. Since it is well established that intracellular calcium is a crucial second messenger that can induce short and long-term changes in the peripheral nervous system, the hypothesis that intracellular calcium-related events might play an important role in the onset of OIPN has been raised[6,7], but the mechanism by which changes in calcium signalling would occur are so far unknown. Hyper-excitability of neurons through triggering of voltage-operated sodium channels, which is not in contradiction with the Ca^{2+}-hypothesis, has also been postulated as a triggering event[8,9].

Transient receptor potential channels are non-selective cation channels that detect a vast array of signals. Given that they play an important role in DRG neurons[10], it is not surprising that some of its family members may be involved in OIPN[11]. For example, OHP-treated $TRPA1^{-/-}$ animals display reduced cold hypersensitivity[12], an effect which is also observable in $TRPM8^{-/-}$ animals[13].

In the present study, we set to investigate the relationship between OHP and TRPA1 activation in DRG neurons. We now report that OHP, in DRG neurons, induces cytosolic acidification and TRPA1 sensitization. This sensitization could be reversed if pH was restored to physiological pH, suggesting that it is acidification which leads to TRPA1 sensitization. Furthermore, acidification of intracellular pH was also observed in DRG cells excised from acutely or chronically OHP-treated animals, when measured within 24 hours after injection. In conclusion, our data demonstrate that OHP-induced cytosolic acidification is a key step in TRPA1 sensitization and may be related to acute toxicity.

4.2 Materials and Methods

Animals and husbandry. BALB/c male mice aged 5-10 weeks upon arrival were employed (Envigo, San Pietro al Natisone, Italy) both for DRG culture preparation and in vivo studies. Animals were maintained as previously reported[14]. Care and husbandry of animals were in conformity with the institutional guidelines in compliance with national and international laws and policies. The study plan was approved by the animal Ethics Committee of the University of Milano Bicocca and of the Università del Piemonte Orientale. The procedures were approved by the local animal-health and ethical committee (Università del Piemonte Orientale) and were authorized by the national authority (Istituto Superiore di Sanità; authorization number N. 22/2013). All mice were euthanized under deep isoflurane-induced anaesthesia for cell cultures and with CO_2 for *in vivo* experiments.

Chemicals. For *in vivo* studies OHP solution was prepared as reported by Renn and collaborators[15] and used as previously described[14].

For *in vitro* studies, OHP (5 mg/mL stock solution, Sigma-Aldrich Inc., Italy), cisplatin (5 mg/mL stock solution, Sigma-Aldrich Inc., Italy), sodium oxalate (10 mg/mL stock solution, Sigma-Aldrich Inc., Italy), capsaicin (1 mM stock solution, Sigma-Aldrich Inc., Italy), icilin (10 mM stock solution, Sigma-Aldrich Inc., Italy), BCTC (10 mM, stock solution, Sigma-Aldrich Inc., Italy), HC-030031 (50 mM stock solution, Sigma-Aldrich Inc., Italy), AITC (allyl isothiocyanate; 50 mM stock solution; Sigma-Aldrich Inc., Italy), BCECF ((2',7'-Bis-(2-Carboxyethyl)-5-(and-6)-Carboxyfluorescein, Acetoxymethyl Ester, 100 mM stock solution, Life Technologies, Italy), DIDS (4,4'-

Diisothiocyano-2,2'-stilbenedisulfonic acid; Sigma-Aldrich Inc., Italy) and nigericin (20 mM stock solution, Life Technologies, Italy) were used. These compounds, with the exception of capsaicin (reconstituted in 100% EtOH), were dissolved in 100% dimethyl sulfoxide (DMSO) and stored at -20 °C, according to manufacturers' specifications. Working concentrations of these drugs were freshly prepared for each experiment by diluting DMSO or EtOH to 0.1% in milliQ (MilliPore) water.

Experimental design for the *in vivo* study. For the evaluation of pH in chronically OHP-treated animals, animals (n=12 in two separate experiments) were injected intravenously in the tail vein with OHP 3.5 mg/Kg (10 mL/Kg) twice a week for 4 weeks, while control mice (n=12) were left untreated. The neurotoxicity of this chronic schedule and its capacity to mimic Human OIPN have already been reported in detail[15]. In a second experiment that evaluated the acute effect of OHP, eight animals (in two separate experiments) were injected intravenously in the tail vein with a single dose of OHP 3.5 mg/Kg (10 mL/Kg). Animals were sacrificed after 24 hours to investigate acute effects.

Isolation and Primary Cell Culture of Mouse DRG Neurons. DRG obtained from adult BALB/c mice (5/10-wk-old) were excised and collected in a dish containing cold F12 (Nutrient Mixture F12 Ham) medium (Sigma Aldrich Inc.). Working under a dissecting microscope and using fine forceps, the surrounding membranes were gently teased away from each DRG; nerves and sheath were cut. All de-sheathed DRG were then transferred into a sterile 35 mm dish containing collagenase from Clostridium hystoliticum 0.125% (Sigma Aldrich Inc.) and DNase (Sigma) in F12 (Nutrient Mixture F12 Ham) medium and incubated at 37 °C for 1 h. After

incubation, DRG were triturated using a 1000 µl tip. Myelin and nerve debris were eliminated by centrifugation through a bovine serum albumin (BSA) cushion. Cell pellets were re-suspended in Bottenstein and Sato medium (BS) (30% F12 (Nutrient Mixture F12 Ham medium), 40% DMEM (Dulbecco's Modified Eagle's medium (Sigma Aldrich Inc., Italy), 30% Neurobasal A medium (Life Technologies, Italy), 100 X N2 supplement (Life Technologies, Italy), penicillin 10 U/mL and streptomycin 100 mg/mL (Sigma Aldrich Inc., Italy), supplemented with Recombinant Human β-NGF, Recombinant Murine GDNF and Recombinant Human NT3 (Peprotech, USA) and plated onto 24 mm glass coverslips pre-coated with laminin (Sigma Aldrich Inc., Italy).

Real Time Quantitative PCR (QRT-PCR) . Total RNA was isolated from DRG using TRI-Reagent® and reverse transcribed according to the manufacturer's instructions (Im-Prom-II™ Reverse Transcription System, Promega, WI, USA). cDNA was then stored at -20°C until further used. qRT-PCRs were performed on 96-well plates (CFX96™ Real-Time PCR Detection Systems, Bio-Rad Inc), in triplicate and florescence intensity assessed using the CFX96™ Real-Time PCR Detection Systems (Bio-Rad Inc.). After an initial denaturation step at 95°C (10 min), each primer set was used (through 40 cycles of amplification) as follows: mouse TRPV1 5'-CCTGCATTGACACCTGTGAG-3' forward, 5'-AGAAGATGCGCTTGACAAATC-3' reverse; mouse TRPM8 5'-TGGAGCCAAAAACTTTGCTT-3' forward, 5'-TCATCAGGCCGTAGTGAGTG-3' reverse and mouse TRPA1 5'-TGTCACCCCTTCACATAGCT-3' forward, 5'-GTGGACATCAAAGCCGTGTT-3' reverse; 60°C annealing temperature. Transcripts were normalized to the expression of Ribosomal Protein S18 mRNAs, for each gene, the threshold cycle *(C_t)* was calculated. The C_t of treated cells was compared to the C_t generated by the control

cells and ΔC_t was calculated as the difference between C_t values, determined using the equation $2^{-\Delta Ct}$.

Cell lines. Human colorectal carcinoma LS180, HCT116, LoVo, HT29, HCT15 cell lines and SW620 colon cancer cells derived from metastatic site cell lines were obtained from ATCC (Rockville, MD, USA) and were cultured and grown according to the data sheets.

To evaluate viability, the 3-(4,5-Dimethylthiazol-2-Yl)-2,5-Diphenyltetrazolium Bromide (MTT) assay was used. Briefly, cells were plated at concentrations 2.5×10^4 per well in 24 well plates and treated with OHP and Na^+ oxalate. At the end of the treatments, the MTT reagent was added to cells at a final concentration of 0.25 mg/mL (Sigma-Aldrich Inc., Milan, Italy), for 90 min at 37°C. Reactions were stopped and the crystals were solubilized by adding isopropyl alcohol/HCL (1:1; vol:vol, Sigma-Aldrich Inc., Milan, Italy), before reading the absorbance at 570 nm, using the multi-plate reader Victor3 V (PerkinElmer, Milan, Italy). pH determinations with BCECF on LoVo and LS180 was performed as described in the relevant section below.

Fura-2 Ca^{2+} measurements and image analysis. For Ca^{2+} imaging, DRG cultures grown onto 24 mm round cover-slips were loaded with 5 μM Fura-2 AM in presence of 0.02% of Pluronic-127 (both from Life Technologies) and 10 μM sulfinpyrazone (Sigma Adrich Inc., Italy) in Krebs–Ringer buffer (KRB, 135 mM NaCl, 5 mM KCl, 0.4 mM KH_2PO_4, 1 mM $MgSO_4$, 5.5 mM glucose, 20 mM HEPES, pH 7.4) containing 2 mM $CaCl_2$ (30 min, room temperature). Cells were washed and incubated with KRB for other 15 min to allow de-esterification of Fura-2. During the experiments the

coverslips were mounted into acquisition chamber and places on the stage of a Leica DMI6000 epifluorescent microscope equipped with S Fluor ×40/1.3 objective. Cells were alternatively excited at 340/380 nm by the monochromator Polychrome IV (Till Photonics, Germany) and the fluorescent signal was collected by a CCD camera (Hamamatsu, Japan) through bandpass 510 nm filter; the experiments were controlled and images analysed with MetaFluor (Molecular Devices, Sunny-vale, CA, USA) software. Data in traces are expressed as 340/380 ratio while to quantify the differences in the amplitudes of Ca^{2+} transients the ratio values were normalized according to the formula $\Delta F/F0$ (referred to as normalized Fura-2 ratio, "Norm. Fura ratio").

To obtain the size of the neurons, images of fluorescent Fura-2 loaded neurons excited at 380 nm were analysed using ImageJ software (National Institutes of Health, Bethesda, MD, USA, http://imagej.nih.gov/ij). The size was estimated by the average soma diameter, calculated by measuring and averaging the length of the minimum and maximum Feret diameters of the neuronal cell body. TRPA1-positive neurons were determined by their ability to respond to icilin, without any prior selection. The diameter of these neurons is depicted in Suppl. Figure S2.

Measurement of intracellular pH in DRG cultures by epifuorescence microscopy with BCECF. DRG cultures or colorectal cancer cells grown onto 24 mm round cover-slips were incubated with 1 μM BCECF (Life Technologies, Italy) in Krebs–Ringer buffer (KRB, 135 mM NaCl, 5 mM KCl, 0.4 mM KH_2PO_4, 1 mM $MgSO_4$, 5.5 mM glucose, 20 mM HEPES, pH 7.4) containing 2 mM $CaCl_2$ (15 min, room temperature). Subsequently, cells were washed and re-suspended in KRB (pH 7.4). A Leica DMI6000 epifluorescent microscope equipped with S Fluor ×40/1.3 objective was used. Cells were alternatively excited at 490/450 nm (monochromator Polychrome

IV, Till Photonics, Germany) and the fluorescent signals were collected every 10 seconds (Hamamatsu, Japan); the experiments were controlled and images analysed with MetaFluor (Molecular Devices, Sunny-vale, CA, USA) software. Finally, intracellular pH was calculated by comparing 525/610 nm emission fluorescence ratios with *in vivo* calibration curves obtained by pH equilibration using the proton ionophore nigericin (20 μM) and Intracellular pH Calibration Buffer Kit (pH 7.5-5.5, Life Technologies).

Measurement of intracellular pH in DRG by flow cytometry with BCECF. After *in vivo* treatment and dissociation, DRG cells were incubated with 1 μM BCECF (Life Technologies, Italy) in Krebs–Ringer buffer (KRB, 135 mM NaCl, 5 mM KCl, 0.4 mM KH_2PO_4, 1 mM $MgSO_4$, 5.5 mM glucose, 20 mM HEPES, pH 7.4) containing 2 mM $CaCl_2$ (15 min, room temperature). Cells were washed, re-suspended in KRB (pH 7.4) and used for flow cytometry (FACSCanto I, Becton Dickinson,). Excitation was performed at 488 nm, using an air-cooled, 20-mW solid-state laser, the emission fluorescence was collected and the FITC and PE median fluorescence values and CV were determined using FACS Diva software. Approximately 10,000 cells were collected in a user-defined gate. A calibration curve was then prepared by suspending cells in high [K^+] buffers (pH 5.5-6.5-7.5) containing 20 μM of the proton ionophore nigericin (Intracellular pH Calibration Buffer Kit, Life Technologies). Finally, intracellular pH was calculated by comparing FITC/PE nm emission fluorescence ratios with the values obtained by the calibration curve.

Electrophysiology. Cell attached patch clamp recordings were performed at 22-25°C on control and OHP-treated neurons with a mean soma diameter < 25 □m.

Prior to the gigaseal formation, cells were continuously superfused with a standard physiological solution of the following composition (in mM): NaCl 154; KCl 4; $CaCl_2$ 2; $MgCl_2$ 1; 4-(2-hydroxyethyl)-1-piperazine ethane sulfonic acid (HEPES) 5; glucose 5.5; NaOH to pH 7.4. The patch electrodes prepared from borosilicate glass capillaries (World Precision Instruments) had a resistance of 5-7 MΩ. In most experiments the pipette solution contained (in mM): CsCl 130, TEACl 20, DIDS 1; 4-(2-hydroxyethyl)-1-piperazine ethane sulfonic acid (HEPES) 10, EGTA 2, BCTC 3 □M, Icilin 1 μM, CsOH to pH 7.4. In a set of experiments, we added 2 mM $CaCl_2$ in the absence of EGTA in the patch pipette solution. After seal formation (2-10 DRG cells were perfused with a solution containing KCl 150, $MgCl_2$ 2, $CaCl_2$ 1, EGTA 1.1, HEPES 5, KOH to pH 7.4, in order to set the membrane potential near 0 mV and to prevent intracellular calcium loading. Data were collected and filtered at 1 kHz with an Axopatch 200B amplifier (Molecular Devices, USA) and digitized continuously at a sampling frequency of 1 kHz with PClamp Axoscope software (Molecular Devices, USA). Steady state voltage clamp protocols were applied and digitized at 10 or 20 kHz with PClamp Clampex software Data analysis was performed with OriginPro (OriginLab, USA) and PClamp Clampfit software.

Statistical analysis. Data are presented as mean ± SEM or Median and IQR. Data points in the single channel current-voltage graphs represent mean ± S.D., estimated by fitting the amplitude histograms to a sum of Gaussian functions (OriginPro 9.1, OriginLab USA). The normality of data distributions was assessed using Shapiro–Wilk test. Parametric (unpaired t-test and One-way analysis of variance (ANOVA) followed by Tukey's post-hoc) or non parametric (Mann-Whitney U test and One-way Kruskal-Wallis H test followed by Dunn's post-hoc) statistical analysis was used for comparisons of data. All statistical assessments were two-

sided and a value of $P < 0.05$ was considered statistically significant. Statistical analyses were performed using GraphPad Prism software (GraphPad Software, Inc., USA). In *in vitro* experiments, the n number was calculated on the number of cells, and the number of independent experiments (defined as cultures from separate animals performed on different days) is given in the respective figure legends.

4.3 Results

Toxicity of OHP in dorsal root ganglia neuronal cultures.

Most *in vitro* studies so far performed to elucidate the mechanism of neurotoxicity have used concentrations of OHP in the range of 5-50 µg/mL[16,17]. In the present work, three different concentrations (0.1, 1, 10 µg/mL) of OHP were initially tested. Briefly, DRG neurons were exposed for 6 or 48 hours to OHP. Experiments were carried out after 48 hours of the treatment. Therefore, for the 6 hours exposure, cells were washed and grown for a further 42 hours in normal medium in the absence of OHP before the experiments. Immunostainings with GAP43[17] showed well-developed neurites when cells were exposed for only 6 hours with the lowest concentration of OHP (0.1 µg/mL), while other treatments showed a marked reduction both in neurite length and in the number of surviving neurons (Suppl. Figure S1). The concentration of 0.1 µg/mL for 48 hours leads only to minor alterations and was therefore also carried forward for calcium-signalling characterization together with the 6 hour treatment. It should be noted that the reported plasma concentrations of OHP in patients are in the range of 0.1 µg/mL[18].

OHP modifies responses to capsaicin and icilin

We first set out to investigate whether the above treatment conditions might affect TRPV1, TRPM8 and TRPA1 responses, in analogy to what observed by others with more aggressive protocols. DRG neurons exposed to OHP for 6 hours (0.1 μg/mL) challenged with capsaicin (TRPV1 agonist; 200 nM) showed a reduced Ca^{2+}-response compared to controls (median of CTRL: 1.98; median of OHP: 1.28; ****P= $1.4 \cdot 10^{-5}$). The reduction was more evident for neurons exposed for 48 hours to OHP (0.1 μg/mL; median of CTRL: 1.98; median of OHP: 0.37; P****$<10^{-6}$; Figure 1a).

Conversely, only a minority of the control DRG neurons responded to icilin (TRPA1 and TRPM8 agonist; 1 μM) with very small Ca^{2+}-rises (Figure 1b). DRG neurons pre-exposed for 6 hours to OHP, instead, unmasked a large icilin-induced Ca^{2+}-rise (median of CTRL: 0.05; median of OHP: 0.92; ****P$<10^{-6}$). DRG neurons treated for 48 hours with OHP also displayed an icilin-induced Ca^{2+}-rise although this was reduced compared to the shorter treatment (median of CTRL: 0.05; median of OHP: 0.23; P=$4 \cdot 10^{-6}$). Therefore, although the effect was evident both after 6 and 48 hours, the shortest treatment was chosen for all other experiments.

Responses to ATP were not affected by OHP in either treatment duration (Figure 1a, 1b), suggesting that cells were healthy and that our results were not a manifestation of an experimental artefact. Nonetheless, given the possibility that part of the effects elicited by OHP for 48 hours might have been attributed to neuronal suffering, we decided to focus our attention on the shorter treatment.

Given that OHP unmasked a response to icilin, we also investigated the neurons that were responsible for this response by measuring their average soma diameter (Suppl. Figure 2a for distributions). Briefly, our cell cultures were characterized by the presence of small size neurons (median of soma diameter for control neurons

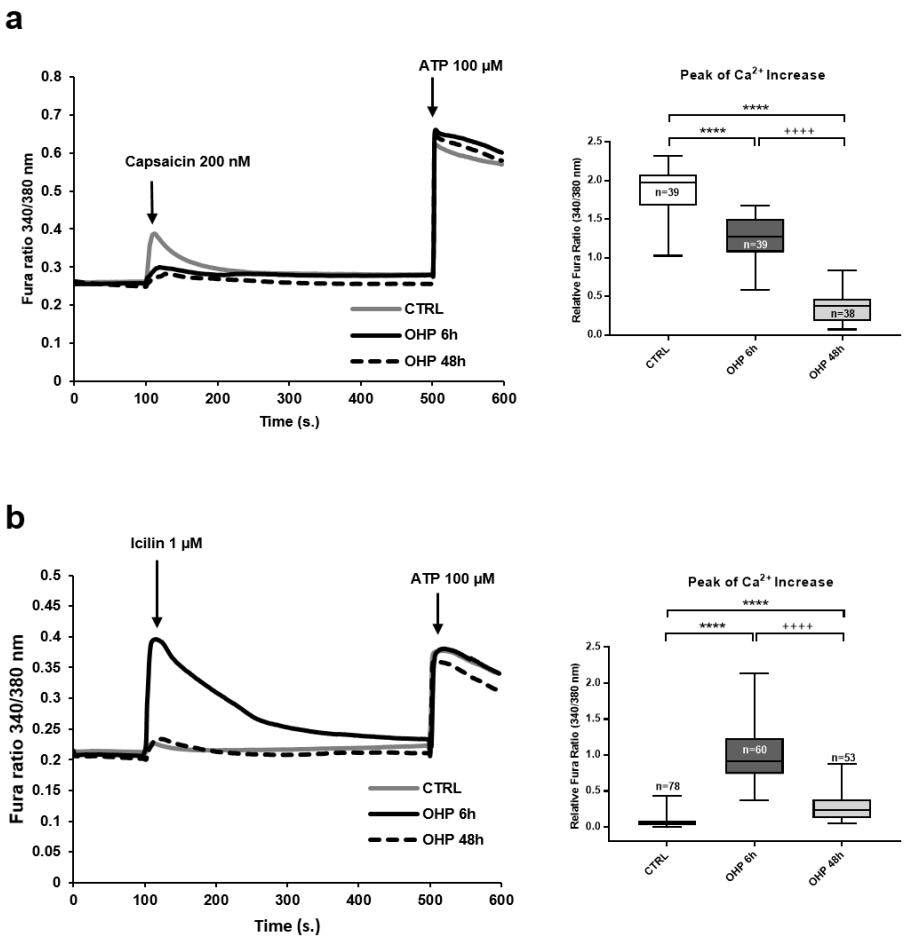

Figure 1. Calcium responses to capsaicin (a) and icilin (b). DRG neurons treated with OHP (0.1 µg/mL) for 6 or 48 hours or untreated (CTRL) were loaded with Fura2-AM and placed in an extracellular solution containing 2 mM calcium. Traces are the average of the cells indicated in the corresponding bar graphs, obtained from 3 independent experiments. Box and whisker plots show median and IQR of peak of calcium changes. Kruskal-Wallis H test followed by Dunn's post-hoc. ****$P < 10^{-6}$, $^{++++}P < 10^{-6}$. Calcium responses to AITC can be found in Suppl. Figure 3.

of 13.8 µm, n=278) and similar values were observable in OHP-treated neurons (13.1 µm, n= 223). The few cells that responded to icilin in control conditions (albeit with very small Ca^{2+}-rises) had a median soma diameter of 13.1 µm (n= 55) while the cells that responded to icilin in OHP-treated cultures had a median of 12.5 µm (n=172). There was no statistically significant difference between the groups (Kruskall Wallis test, P= 0.86, Suppl. Figure 2b). This would suggest that the observed unmasking of a Ca^{2+}-response to icilin might be relevant to the clinical manifestations.

Icilin responses are mediated by TRPA1 and not by TRPM8

Icilin has been reported to be an agonist of both TRPM8 and TRPA1 receptors[19,20]. To discriminate between the two, we used the specific inhibitors of TRPM8 (BCTC) or TRPA1 (HC-030031). As it can be observed in Figure 2a, icilin induced a response in OHP-treated DRG neurons both in the presence (3 µM; median: 0.71) or absence of BCTC (median: 1.01) suggesting that the TRPM8 was not involved. On the contrary, the response to icilin was completely abolished in the presence of HC-030031 (10 µM; median: 0.02) in OHP-treated neurons. In accord, in our conditions, preliminary experiments showed that menthol elicited very small responses (data not shown), suggesting that TRPM8 does not contribute to the icilin-response. This might be due to a number of factors, including the temperature at which we perform experiments.

Allyl isothiocyanate (AITC) is another well-known agonist of TRPA1 and we therefore evaluated whether the potentiation of the response by OHP treatment could be unmasked also by activation of the channel by this compound. As shown in Suppl. Figure 3, in control cells AITC induced only a modest response (median:

0.09), while in OHP-treated neurons the response was significantly potentiated (median: 0.39). The potentiated response was sensitive to HC-030031 (10 μM; median: 0.06).

These data would therefore suggest that, in our model, OHP modulates the response to TRPA1.

Sodium Oxalate or cisplatin do not mimic the effect of OHP

We next tested whether treatment for 6 hours with the close analogue cisplatin or sodium oxalate were able to mimic the sensitization of TRPA1. As it can be observed (Figure 3a), cisplatin (0.1 μg/mL; median: 0.05), unlike OHP (median: 0.81), was unable to potentiate the response to icilin in DRG neurons. Similarly, sodium oxalate, at the same molar concentration (0.3 μg/mL), was also unable to unmask a TRPA1-dependent Ca^{2+}-response (median: 0.14) (Figure 3b). We also evaluated whether sodium oxalate was able to modify the response to OHP and, to our surprise, co-treatment with equimolar concentrations of OHP and sodium oxalate led to the abolishment of the icilin response (median OHP: 0.82, median co-treatment: 0.10). Oxalate can chelate Ca^{2+}-ions, although it is unlikely that the low concentrations used (0.3 μg/mL; 2.2 μM) are able to mask Ca^{2+}-responses, also in light of the mM concentrations of Ca^{2+} in the extracellular medium. To verify that indeed oxalate does not affect Ca^{2+}-responses, we evaluated ATP-induced Ca^{2+}-mobilization in the same cells. As observed in the Suppl. Figure S4, the ATP induced Ca^{2+}-responses were not different in control, OHP-treated, and oxalate-treated cells (medians: 0.77; 0.91; 0.65, respectively).

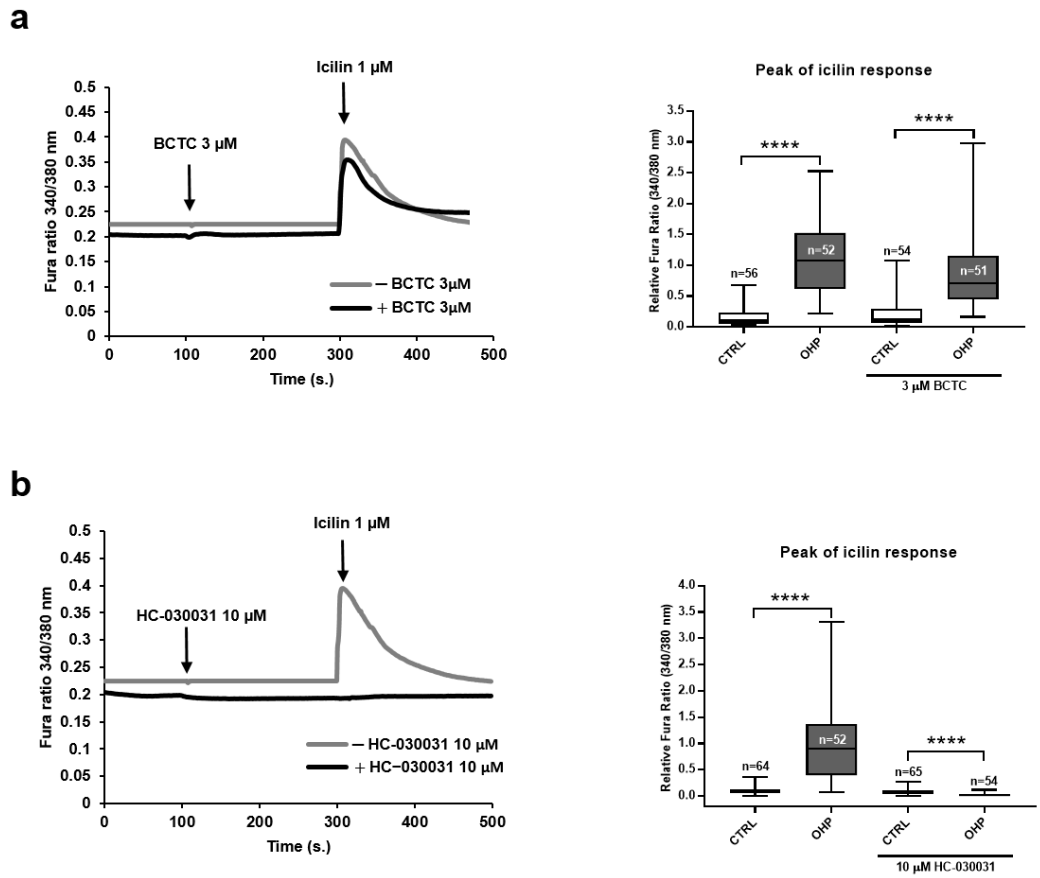

Figure 2. OHP increases icilin responses by a TRPA1-dependent mechanism. DRG neurons were treated with OHP (0.1 µg/mL) for 6 hours, loaded with 5 µM Fura2-AM and placed in an extracellular solution containing 2 mM calcium. Cells were pre-treated with BCTC (TRPM8 antagonist; **a**) or HC-030031 (TRPA1 antagonist; **b**) before being challenged with icilin. Traces are the average of the cells indicated in the corresponding bar graphs, obtained from 6 independent experiments. Box and whisker plots show median and IQR of peak calcium responses in the presence or in the absence of BCTC or HC-030031. Mann-Whitney U test; **** $P< 10^{-6}$.

The antagonistic effect of oxalate was unexpected and we therefore evaluated whether this also occurred for the cytotoxic effect of OHP. To this end, we treated 6 different colorectal cancer cell lines with OHP (3 µg/mL) in the presence or absence of equimolar concentrations of oxalate (9 µg/mL) for 24, 48 or 72 hours. The concentration of OHP was chosen based on the IC50 obtained in preliminary experiments for the 48h treatment. OHP was cytotoxic to the same degree in the presence or absence of oxalate (Suppl. Figure S5), suggesting that this antagonism is specific for TRPA1 calcium response in DRG neurons.

OHP does not modify mRNA levels for TRPA1 or TRPV1

After the 6 hour treatment with OHP, DRG cells are maintained for a further 42 hours in culture before experiments. Therefore, it is possible that gene expression changes may be responsible for the effects observed. Treatment with OHP did not induce any change in mRNA levels for TRPA1 (1.0± 0.1 of control; n=6), TRPV1 (1.1 ± 0.1 of control; n=6) or TRPM8. We also recently performed a microarray analysis with a validation set to investigate gene expression changes upon OHP treatment *in* vivo in DRG cells[14]. When interrogating the microarray results for these two genes, we confirmed that no significant changes occurred for either TRPA1 (|log2FC| 0.142) or TRPV1 (|log2FC| 0.016) *in vivo*. Similarly, RT-PCR data of the confirmation dataset performed on mRNA from DRG cells from a different set of animals confirmed that no significant changes occurred in these animals for these two channels (TRPA1 1.1 ± 0.2, TRPV1 1.0 ± 0.2; both normalized to control; n=8).

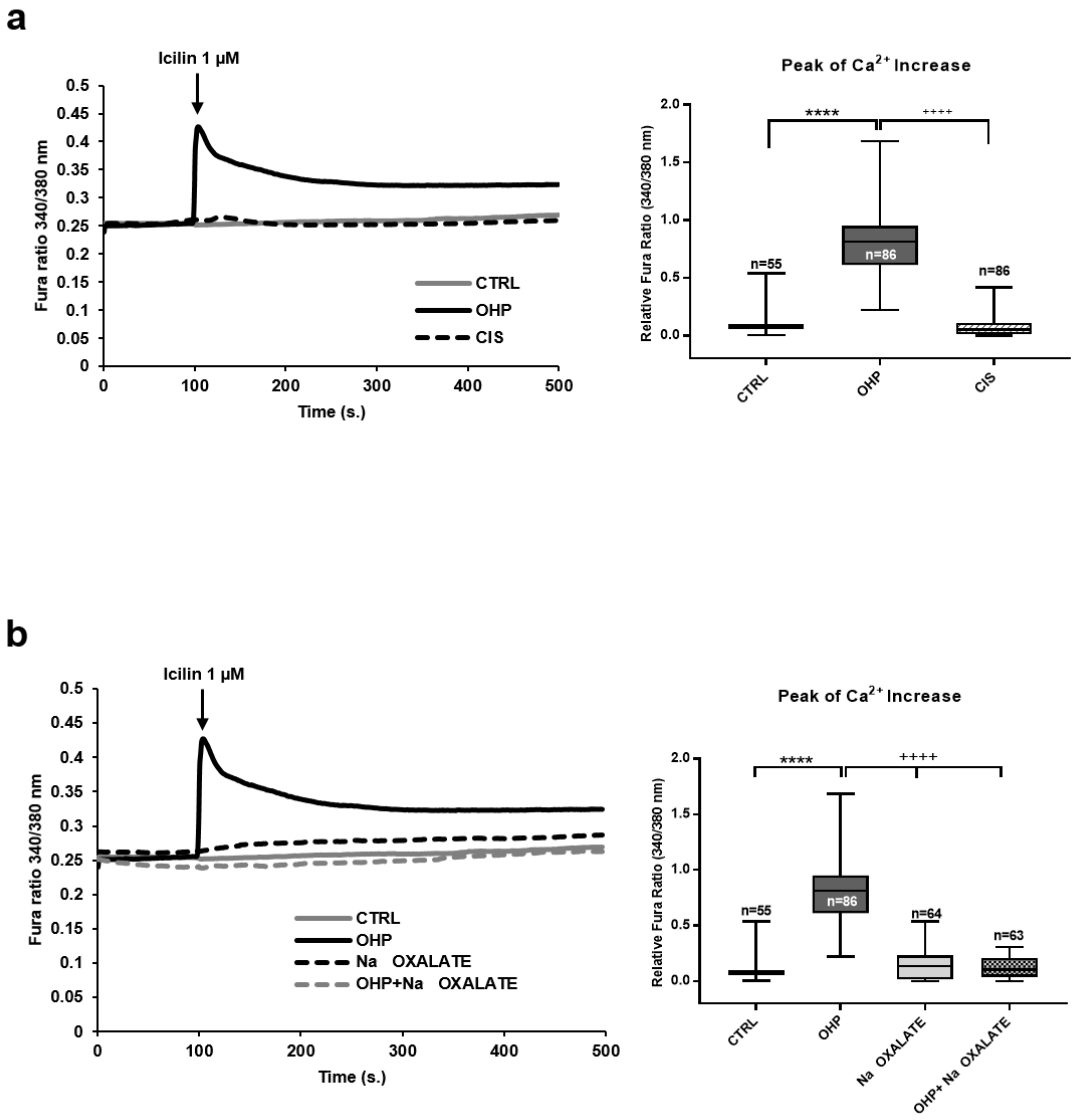

Figure 3. Icilin responses induced by cisplatin (a) or sodium oxalate (b). DRG neurons were treated with OHP (0.1 µg/mL), cisplatin (CIS; 0.1 µg/mL), or sodium oxalate (0.3 µg/mL) alone or in combination with OHP (0.1 µg/mL) for 6 hours. Traces are the average of the cells indicated in the corresponding bar graphs, obtained from 4 independent experiments. Box and whisker plots show median and IQR of peak of calcium changes after the addition of 1µM icilin. Kruskal-Wallis H test followed by Dunn's post-hoc. ****$P < 10^{-6}$ and $^{++++}P < 10^{-6}$.

pH changes occur upon OHP treatment in vitro and in vivo

If changes in channel expression cannot account for the change in icilin-response observed, *i.e.* the same number of channels are present in control and OHP-primed neurons, other explanations might account for the results observed. It is well known that TRP channels are multimodal receptors, able to detect a number of chemical and physical agents. In this respect, it has been reported that intracellular pH changes are able to modulate in opposite directions the effect of TRPV1 and TRPA1[21], which would be compatible with our Ca^{2+}-signalling results (Figure 1).

To investigate this aspect, we made use of BCECF, a specific ratiometric fluorescent pH probe[22,23]. As it can be observed (Figure 4a), a significant median drop from 7.23 to 6.49 occurred in cells exposed to OHP (****P < 10^{-6}). Paralleling the results obtained in calcium signalling (Figure 3), such changes did not occur upon exposure for the same length of time with either oxalate (7.55) or cisplatin (7.51). In line with what observed for calcium signalling, while devoid of any effect *per se*, oxalate was nonetheless able to revert the effect of OHP (7.36; Figure 4a).

While our protocol is translational (6-hour treatment followed by 42 hour recovery) it fails to disclose when this pH change takes place, *i.e.* in the first 6 hours or afterwards. To dissect the two, we then performed experiments at 6 hours. As shown in Figure 4b, 6 hours treatment with OHP was sufficient to reduce pH significantly (medians: control 7.37 and OHP 6.83). The effect on pH at 6 hours was paralleled by the sensitization to icilin (Figure. 4c, median of CTRL: 0.08; median of OHP: 0.28) and the reduction of the capsaicin response (Figure. 4d, median of CTRL: 0.96; median of OHP: 0.06).

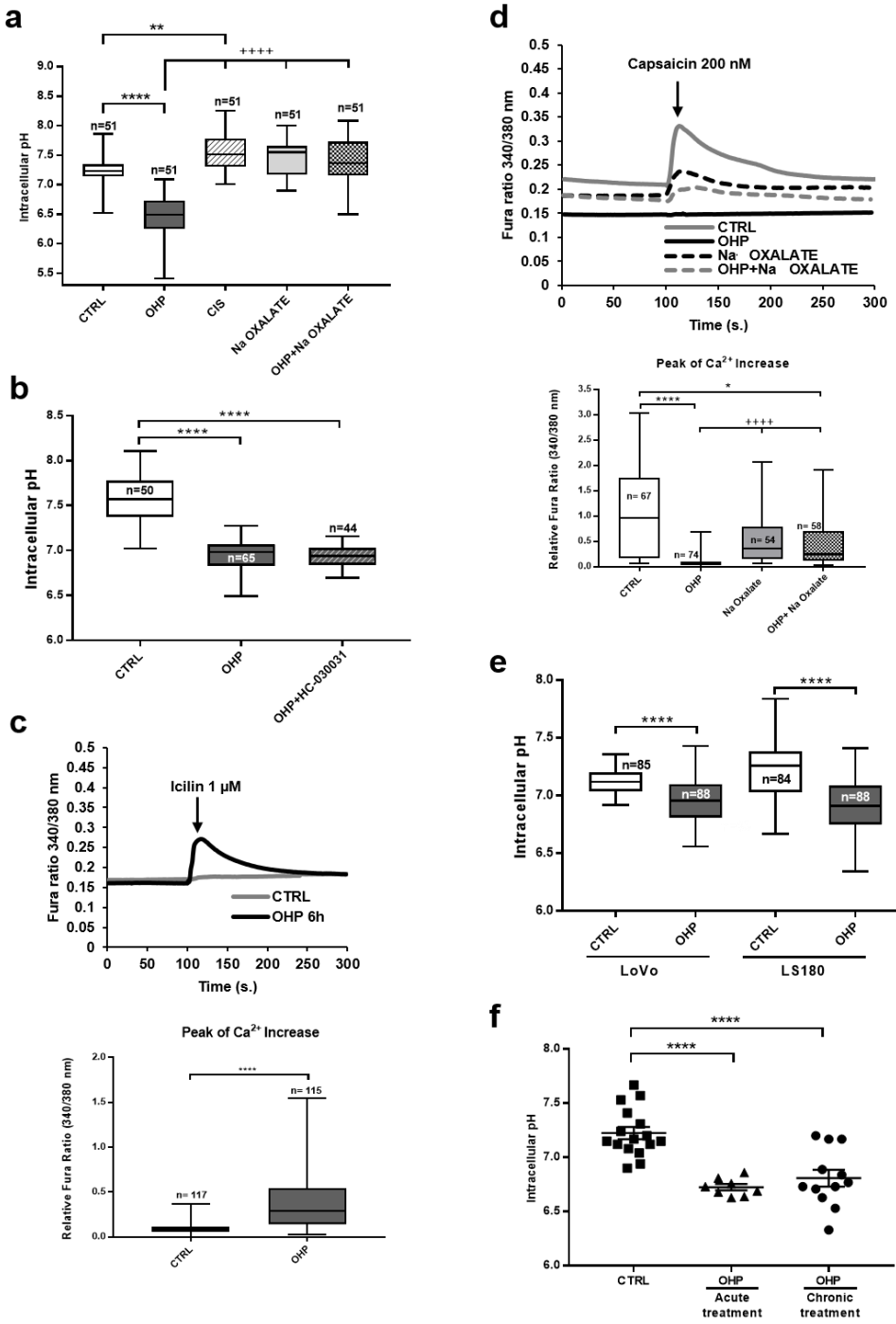
a
Intracellular pH
n=51
n=51
n=51
n=51
n=51
CTRL
OHP
CIS
Na OXALATE
OHP+Na OXALATE
b
Intracellular pH
n=50
n=65
n=44
CTRL
OHP
OHP+HC-030031
c
Fura ratio 340/380 nm
Icilin 1 µM
CTRL
OHP 6h
Time (s.)
Peak of Ca2+ Increase
Relative Fura Ratio (340/380 nm)
n= 117
n= 115
CTRL
OHP
d
Fura ratio 340/380 nm
Capsaicin 200 nM
CTRL
OHP
Na OXALATE
OHP+Na OXALATE
Time (s.)
Peak of Ca2+ Increase
Relative Fura Ratio (340/380 nm)
n= 67
n= 74
n= 54
n= 58
CTRL
OHP
Na Oxalate
OHP+ Na Oxalate
e
Intracellular pH
n=85
n=88
n=84
n=88
CTRL
OHP
CTRL
OHP
LoVo
LS180
f
Intracellular pH
CTRL
OHP
Acute treatment
OHP
Chronic treatment

Figure 4. Effects of OHP, cisplatin or sodium oxalate on intracellular pH. (**a**) pH evaluation in cultured DRG neurons treated with OHP (0.1 μg/mL), cisplatin (CIS; 0.1 μg/mL) or sodium oxalate (0.3 μg/mL) alone or in combination with OHP (0.1 μg/mL) for 6 hours. Box and whisker plots show median and IQR of pH_i values. For each treatment the number of cell is indicated in the corresponding bar; data are from 7 independent experiments. Kruskal-Wallis test followed by Dunn's post-hoc. ****P < 10^{-6}, **P= 0.0078; $^{+++}$P= P < 10^{-6} OHP vs. CIS, sodium oxalate and OHP+sodium oxalate; (**b**) pH evaluation of cultured DRG neurons treated with OHP (0.1 μg/mL) in the presence or absence of HC.030031 (10 μM) for 6 hours. Box and whisker plots show median and IQR of pH_i values. For each treatment the number of cell is indicated in the corresponding bar; data are from 2 independent experiments. Kruskal-Wallis test followed by Dunn's post-hoc. ****P < 10^{-6}; (c,d) Ca^{2+}-responses to icilin (1 μM; **c**) or capsacin (200 nM, **d**) in cells treated for 6 hours with the indicated compounds (OHP 0.1 μg/ml and oxalate 0.3 μg/ml). Box and whisker plots show median and IQR of peak of calcium changes after the addition of compounds. Kruskal-Wallis test followed by Dunn's post-hoc. ****P < 10^{-6}, *P= 0.031, $^{++++}$P<10^{-6}; (**e**) pH evaluation in the indicated colorectal cancer cells treated with OHP (0.1 μg/mL) for 6 hours and determined at 48 hours. Box and whisker plots show median and IQR of pH_i values. For each treatment the number of cell is indicated in the corresponding bar; data are from 2 independent experiments. Kruskal-Wallis test followed by Dunn's post-hoc. ****P < 10^{-6}; (**f**) freshly excised DRG cells from control or acutely or chronically OHP-treated BALB/c mice were loaded with 5 μM BCECF and placed in an extracellular physiological solution. Ratiometric measurements of pH_i and calibration curves were obtained by flow cytometry. Graphs show the mean ± S.E.M from n=16 controls, n= 12 chronic treatment, or n=8 acutely treated animals. One-way analysis of variance (F=19.38) followed by Tukey's post-hoc. **** P< 10^{-6}.

To confirm that the effects observed at this time-point were linked to those observed at 48 hours, we also co-treated for 6 hours DRG cultures with OHP and oxalate and tested the recovery of TRPV1 responses. As observed in Figure 4d, oxalate led to a partial recovery of TRPV1 responses, linking the two observations (median of oxalate: 0.36; median of OHP + oxalate: 0.25).

To understand whether pH changes were up-stream or down-stream of TRPA1-sensitization, we treated DRG cultures with OHP in the presence of HC-030031. In this manner, we tested whether acidification is the result of TRPA1 activation. As shown in Figure 4b, HC-030031 had no effect on OHP-induced acidification

(median: 6.84 compared to OHP 6.83), strongly suggesting that cytosolic acidification is an up-stream effect.

To investigate whether these OHP-induced pH changes were specific for DRG neurons or could be observed also in other cells, we tested, with the 48 hours protocol (6 hours treatment and further 42 hours in normal medium), two different colorectal cancer cells, LoVo and LS180. In both cells, OHP-treatment (0.1 μg/ml) led to a significant decrease in pH (medians for LoVo: control 7.12, OHP 6.81; for LS180 control 7.26 OHP 6.91) albeit of smaller entity compared to that observed in DRG neurons (Figure. 4e). This strengthens the notion that in DRG neurons, TRPA1 sensitization is down-stream of acidification, as these cells do not express TRPA1.

All the above data was obtained on DRG neurons or on cancer cell lines in culture, and, to test the relevance of these pH changes we felt necessary to explore the pH of DRG cells from OHP-treated animals. Briefly, BALB/c mice were treated either with OHP (3.5 mg/Kg) twice a week for four weeks[14] or only once (3.5 mg/Kg). Twenty-four hours after the last treatment, animals were sacrificed, DRG dissected, dissociated and FACS analysis with BCECF was performed as described in the materials and methods section. The average pH of cells (Figure 4f) from control animals was 7.22 $\pm$ 0.05 (n=16). The average pH of cells from animals treated chronically with OHP was 6.80 $\pm$ 0.07 (n=12) while average pH from animals treated once with OHP was 6.72 $\pm$ 0.03 (n=8). These data therefore correlate with what observed in DRG neurons in culture.

Restoration of physiological pH suppresses TRPA1 hyper-sensitivity

The above data would suggest that OHP acidifies the pH of DRG cells, both *in vitro* and *in vivo*, and this in turn modifies the activity of pH-sensitive channels, including TRPA1. If this were the case, it would be expected that experimental manipulations that restore pH of DRG neurons would normalize the channel activity.

To investigate this, we decided to perform electrophysiological patch clamp experiments in the cell attached mode, the recording configuration that less interferes with the intracellular milieu composition. In all experiments, DRG neurons were perfused with a bath solution containing 150 mM KCl and low [Ca^{2+}] (see methods), to set the membrane potential near zero and reduce the calcium load. Figure 5a shows two records of 30 s long showing the channel activity in an OHP treated neuron in the presence of icilin (1 µM in the presence of BCTC) and of 2 mM of $CaCl_2$ in the pipette solution at V_m= 40 mV (upper trace) and -40 mV (lower trace). Single channel currents were outwards at positive voltages and inwards at negative voltages as expected for a non-selective cationic channel. Figure 5b shows the I-V relationship obtained from the same experiment. Single channel conductance (γ) and reversal potential (V_r) were respectively of 109.3 ± 6.7 pS and of 3.9 ± 1.6 mV for outward currents and of 32.9 ± 3.3 pS and of -5.9 ± 3.4 mV for inward currents. Furthermore, the channel activity (NP_o, were N is the number of channels in the patch and P_o the open probability) was voltage-dependent, with high open probability at negative potentials and a voltage-dependent inactivation at positive potentials (Figure 5c). These channel properties are in good agreement with previously published data, and confirm that in OHP-treated neurons icilin robustly activates TRPA1 channels[24,25,26,27,28,29].

We next addressed the characterization of the channel biophysical properties in the absence of divalent ions in the pipette, with the purpose to attenuate calcium-dependent inactivation[25,28], a prerequisite for long duration experiments. Figure 5d shows a 30 s recording of the patch currents from an OHP treated neuron in the presence of 1 µM of icilin at Vm= 40 mV (upper trace) in which at least three channels were active. Moreover, the red open circles of Figure 5e represent the single channel current amplitudes recorded at different membrane potentials. In this condition, the fitted regression line yields a γ and a V_r respectively of 107.8 ± 7.6 pS and of 4.2 ± 2.0 mV. The lower trace of Figure 5d was obtained from an untreated neuron again in the presence of icilin in the pipette. Single channel current amplitudes at different V_m are represented as black open circles in Figure 5e. The values of the elementary conductance and the reversal potential were very similar for the two patches (γ 113.2 ± 5.0 pS and Vr =2.0 ± 1.4 mV). Moreover, Figure 5f compares the channel activity NP_o at Vm= 40 mV of the traces in D. We also obtained similar values in two other untreated (NP_o = 0.002 and 0.004) and treated neurons (NP_o = 0.13 and 0.05). This result suggests that NP_o is of one to two orders of magnitude greater in OHP-treated neuron compared to control.

Last, we assessed if the NP_o increase observed in treated neurons was dependent on the OHP-induced pH_i acidification. For this purpose, we added to the bathing solution 10 µM of the K^+/H^+ exchanger nigericin. In our ionic conditions, the insertion in the membrane of the ionophore should activate a net movement of H^+ outside the cell that will set the pH_i value close to the extracellular one. To validate this approach, using BCECF we evaluated the effect of nigericin on intracellular pH in DRG neurons pre-treated for 6 hours with OHP and then left for 42 hours in the same experimental conditions (i.e. high extracellular potassium, low calcium extracellular solution). As shown in Suppl. Figure S6, the addition of nigericin led to

an alkalinisation of intracellular pH, from approx. 6.8 to 7.5. We hypothesized that the change from an acidic to a slightly alkaline pH, should decrease TRPA1 channel activity, if the original hypothesis were true. We observed such effect in all the three neurons tested. In the experiment shown in Figure 5g and in another one, a complete inactivation of the channel occurred after about 2 min of nigericin perfusion. From the amplitude analysis of single channel recording obtained at different membrane potentials we obtained the I-V relationship (Figure 5f) for which the elementary conductance and the reversal potential were again very close to the expected values for TRPA1 channel (γ 121.1 ± 7.0 pS and Vr =-8.4 ± 1.8 mV). A complete channel inactivation after 7 min of nigerin perfusion was also observed in an experiment performed at V_m= -40 mV.

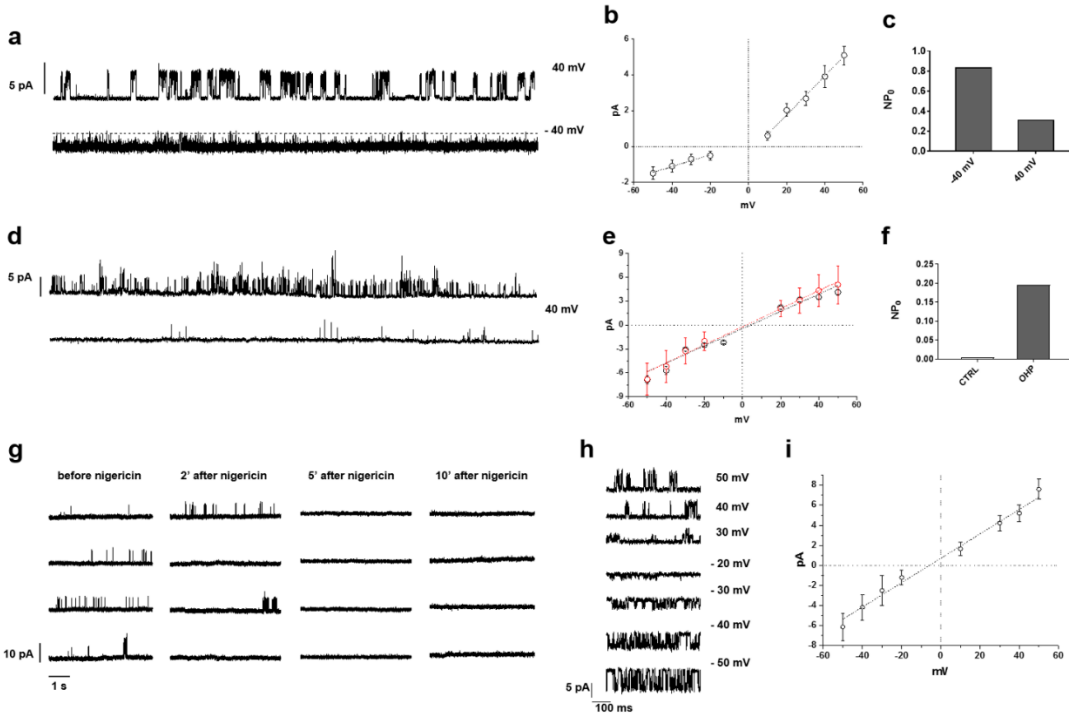

Figure 5. Restoration of physiological pH suppresses TRPA1 hyper-sensitivity to icilin in cell-attached patches. Single channel recordings at two different membrane potentials of a TRPA1 channel obtained in the presence of 2 mM $CaCl_2$ in the patch pipette from an OHP treated DRG neuron (**a**). *i-V* plot with linear regressions (b) and NP_o (**c**) for the same channel shown in (**a**). In this experiment and in all other shown in the figure, the patch pipette contained 1 μM icilin. (**d**) Two example of TRPA1 channel activity recorded in the absence of divalent ions in the patch pipette from an OHP-treated (upper trace) or untreated neuron (lower trace). *i-V* plot with linear regressions (**e**) and NP_o (**f**) for the channels shown in (**d**). Red symbols and line refer to treated neuron. (**g**) Single channel traces from an OHP-treated neuron before and during nigericin perfusion, that induces a pH_i shift towards a slightly alkaline value. (**h**) Elementary currents recorded for the channels shown in (**g**) at different membrane potentials and the corresponding *i-V* plot with linear regressions (**i**).

4.4 Discussion

In the present contribution we show that therapeutically-relevant OHP concentrations[18] induce an acidification of intracellular pH both in cultured DRG neurons and in DRG cells from treated animals. This pH change leads to a sensitization of TRPA1 channels which can be reversed by restoring pH to physiological level. Remarkably, acidification occurs even after a single injection of OHP in animals, suggesting its relevance for the occurrence of acute OIPN. This is strengthened by the observation that equi-molar concentrations of cisplatin, *in vitro*, are unable to induce any pH change.

It should be noticed that, while we do not see an effect of cisplatin at low concentrations on pH, higher concentrations (that we have not investigated) may be able to elicit an effect on DRG neurons. Indeed, this has been shown previously on colorectal cancer cells at approx 100-fold the concentrations used in the present study (20-30μM)[30, 31].

This may be indicative of the fact that all platinum containing drugs share this effect but have different potencies. Indeed, while it could be envisaged that its the oxalate molecule from oxaliplatin that is responsible for the effect observed, we believe this is not the case as: (i) the concentration of released oxalate would be too low; (ii) oxalate surprisingly reverts the effect of oxaliplatin; and (iii) cisplatin, at 100-fold higher concentrations, can elicit similar effects. It is interesting to speculate that the different relative potencies between the cytotoxic and pH effect may be responsible for the different neurotoxic potential of the drugs. In the present contribution, we indeed provide evidence that the effect on pH also occurs in colorectal cancer cells, at lower concentrations compared to the cytotoxic effect, thereby possibly dis-joining the two effects.

It should be noticed that the concentrations *in vitro* in the present manuscript are lower than those of previous reports attempting to elucidate the mechanism of OIPN[16,17], and therefore they are not in contradiction. Nonetheless, we believe that these lower concentrations more closely resemble those found in plasma of patients and of mice treated with OHP[32] compared to higher concentrations used in the literature.

In our hands, equimolar concentrations of oxalate were also unable to induce intracellular pH changes. Yet, to our surprise, co-treatment of equimolar concentrations of oxalate were able to abolish OHP-induced pH changes. At present, no explanation can be put forward for this, although it demonstrates that OHP-induced pH acidification occurs via a specific and saturable mechanism. It should be noted that oxalate antagonized the change in pH (and the relative sensitization of the channel), but did not antagonize the cytotoxic effects of OHP in any of the 6 colorectal cell lines tested, suggesting that the site of interaction might represent an exploitable pharmacological target in DRG to reduce OIPN. However,

since oxalate is *per se* toxic, it is unlikely that it could be directly used for OIPN prevention. In fact, oxalate is mainly nephrotoxic[33], and, at high doses, neurotoxic[11,34].

Our data are partly in contrast with earlier evidence that oxalate and OHP produce similar neurotoxic effects in rodents[34]. It should be nonetheless noticed that whether these two agents act via the same mechanism has never been investigated.

In the present contribution we have focused on TRPA1, a TRP channel that has been shown earlier to be involved in OIPN. For example, pharmacological inhibition of TRPA1 abolishes OHP-induced mechanical and cold-hypersensitivity and this effect is also abolished in TRPA1-null mice[12,35,36]. Furthermore, hypersensibility has also been shown upon pre-treatment *in vitro* in DRG neurons, in agreement with our data[12,36]. Remodelling of TRPA1 expression has been postulated as one the mechanisms that may underlie this hypersensitivity[13,16], but our data, obtained both *in vitro* and *in vivo*, failed to detect any mRNA change related to this channel[14] and this report. It has also been recently pointed out that while channel remodelling may explain chronic OIPN, it is unlikely that protein changes may explain hypersensitivity occurring within hours of exposure[36].

Our observation that intracellular pH acidification hyper-sensitizes the TRPA1 channel is supported by earlier data that report intracellular pH-dependent activation of this channel[37,38]. Indeed, this was postulated to be the mechanism by which humans detect some of the sensations from carbonated beverages[39]. Yet, it is likely that intracellular pH changes do not affect solely this channel, as other channels may also be affected. Indeed, TRPM8, the other TRP family member that has been postulated to be responsible for acute OIPN, has also been demonstrated to display pH sensitivity, although in this context acidification led to a decreased

sensitivity[40]. This observation is supported by the modest icilin-dependent BCTC-sensitive response in OHP-treated DRG neurons we observed. Also, TRPV1 has been shown[37] to be affected negatively by intracellular pH acidification, which is in agreement with the data obtained in the present manuscript (Figure 1).

In conclusion, our results suggest the OHP-induced cytosolic acidification as one of the key factors involved in the positive modulation of TRPA1 channels activity and this is related at least to the acute OHP neurotoxicity.

Acknowledgements

The Authors wish to acknowledge Fondazione Cariplo (2013.0842; grant to PM, AG), AIRC (Trideo 2014, Ref. 15942 grant to VC) and the Università del Piemonte Orientale (CD, Bando ricerca locale 2015) for financial support for this work.

References

1. Argyriou, A.A. et al. Peripheral neurotoxicity of oxaliplatin in combination with 5-fluorouracil (FOLFOX) or capecitabine (XELOX): a prospective evaluation of 150 colorectal cancer patients. Ann Oncol. **23**, 3116-3122 (2012).
2. Argyriou, A.A. et al. Clinical pattern and associations of oxaliplatin acute neurotoxicity: a prospective study in 170 patients with colorectal cancer. Cancer **119**, 438-444 (2013).
3. Lucchetta, M. et al. Incidence of atypical acute nerve hyperexcitability symptoms in oxaliplatin-treated patients with colorectal cancer. Cancer Chemother Pharmacol. **70**, 899-902 (2012).
4. Lehky, T.J., Leonard G.D., Wilson R.H., Grem J.L. & Floeter M.K. Oxaliplatin-induced neurotoxicity: acute hyperexcitability and chronic neuropathy. Muscle Nerve. **29**, 387-392 (2004).
5. Wolf S., Barton D., Kottschade L., Grothey A. & Loprinzi C. Chemotherapy-induced peripheral neuropathy: prevention and treatment strategies. Eur J Cancer. **44**, 1507-1515 (2008).
6. Scholz, J. & Woolf C.J. Can we conquer pain? Nat Neurosci. **5**, 1062-7 (2002).
7. Marmiroli, P. et al. Calcium-related Neurotoxicity of Oxaliplatin: Understanding the Mechanisms to Drive Therapy. Curr Med Chem. **22**, 3682-3694 (2015).
8. Grolleau, F. et al. A possible explanation for a neurotoxic effect of the anticancer agent oxaliplatin on neuronal voltage-gated sodium channels. J Neurophysiol. **85**, 2293-2297 (2001).
9. Adelsberger, H. et al. The chemotherapeutic oxaliplatin alters voltage-gated $Na^{(+)}$ channel kinetics on rat sensory neurons. Eur J Pharmacol. **406**, 25-32 (2000).
10. Woolf, C.J. & Ma Q. Nociceptors--noxious stimulus detectors. Neuron. **55**, 353-364. Review (2007).

11. Kawashiri, T. et al. L type Ca^{2}+ channel blockers prevent oxaliplatin-induced cold hyperalgesia and TRPM8 overexpression in rats. Mol Pain. **31**, 8-7 (2012).
12. Zhao, M. et al. Acute cold hypersensitivity characteristically induced by oxaliplatin is caused by the enhanced responsiveness of TRPA1 in mice. Mol Pain. **28**, 8-55 (2012).
13. Descoeur, J. et al. Oxaliplatin-induced cold hypersensitivity is due to remodelling of ion channel expression in nociceptors. EMBO Mol Med. **3**, 266-278 (2011).
14. Marmiroli, P., et al. Susceptibility of different mouse strains to oxaliplatin peripheral neurotoxicity: Phenotypic and genotypic insights. PLoS One. 12, e0186250 (2017).
15. Renn, C.L. et al. Multimodal assessment of painful peripheral neuropathy induced by chronic oxaliplatin-based chemotherapy in mice. Mol Pain. **26**, 7-29 (2011).
16. Ta, L.E., Espeset, L., Podratz, J. & Windebank, A.J. Neurotoxicity of oxaliplatin and cisplatin for dorsal root ganglion neurons correlates with platinum-DNA binding. Neurotoxicology. **27**, 992-1002 (2006).
17. Anand, U., Otto, W.R. & Anand, P. Sensitization of capsaicin and icilin responses in oxaliplatin treated adult rat DRG neurons. Mol Pain. **24**, 6-82 (2010).
18. Ehrsson ,H., Wallin, I. & Yachnin, J. Pharmacokinetics of oxaliplatin in humans. Med Oncol. **19**, 261-265 (2002).
19. Rawls, S.M., Gomez, T., Ding, Z. & Raffa, R.B. Differential behavioral effect of the TRPM8/TRPA1 channel agonist icilin (AG-3-5). Eur J Pharmacol. **575**, 103-4 (2007).
20. Bandell, M. Noxious cold ion channel TRPA1 is activated by pungent compounds and bradykinin. Neuron. **41**, 849-857 (2004).
21. Wang, Y.Y. et al. A TRPA1-dependent mechanism for the pungent sensation of weak acids. J Gen Physiol. 137, 493-505 (2011).
22. Lanz, E., Slavík, J., Kotyk, A. 2',7'-bis-(2-carboxyethyl)-5(6)-carboxyfluorescein as a dual-emission fluorescent indicator of intracellular pH suitable for argon laser confocal microscopy. Folia Microbiol (Praha) **44**, 429-434 (1999).

23. Franck, P. et al. Measurement of intracellular pH in cultured cells by flow cytometry with BCECF-AM. J Biotechnol. **46**, 187-195 (1996).
24. Macpherson, L.J. et al. Noxious compounds activate TRPA1 ion channels through covalent modification of cysteines. Nature. **445**, 541-545 (2007).
25. Cavanaugh, E.J., Simkin, D. & Kim, D. Activation of transient receptor potential A1 channels by mustard oil, tetrahydrocannabinol and GAP reveals different functional channel states. Neuroscience. **154**, 1467-1476 (2008).
26. Karashima, Y. et al. Modulation of the transient receptor potential channel TRPA1 by phosphatidylinositol 4,5-biphosphate manipulators. Pflugers Arch. **457**, 77-89 (2008).
27. Karashima, Y. et al. Agonist-induced changes in Ca (2+) permeation through the nociceptor cation channel TRPA1. Biophys J. 98, 773-783 (2010).
28. Nilius, B., Prenen, J. & Owsianik, G. Irritating channels: the case of TRPA1. J Physiol. **589**, 1543-1549.
29. Takahashi, N. et al. TRPA1 underlies a sensing mechanism for O_2. Nat Chem Biol. **28**, 701-711.
30. Milosavljevic, N. et al. Nongenomic effects of cisplatin: acute inhibition of mechanosensitive transporters and channels without actin remodeling. **70,** 7514-22 (2010).
31. Rebillard, A. et al. Cisplatin-induced apoptosis involves membrane fluidification via inhibition of NHE1 in human colon cancer cells. Cancer Res. **67**, 7865-74.
32. Pestieau, S.R., Belliveau, J.F., Griffin, H., Stuart, O.A. & Sugarbaker, P.H. Pharmacokinetics of intraperitoneal oxaliplatin: experimental studies. J Surg Oncol. **76**, 106-114 (2001).
33. Trinchieri, A., Castelnuovo, C., Lizzano, R. & Zanetti G. Calcium stone disease: a multiform reality. Urol Res. 33, 194-198 (2005).
34. Sakurai, M. et al. Oxaliplatin-induced neuropathy in the rat: involvement of oxalate in cold hyperalgesia but not mechanical allodynia. Pain. **147**, 165-174 (2009).

35. Nassini, R. et al. Oxaliplatin elicits mechanical and cold allodynia in rodents via TRPA1 receptor stimulation. Pain. **152**, 1621-31 (2011).
36. Nakagawa, T. & Kaneko, S. Roles of Transient Receptor Potential Ankyrin 1 in Oxaliplatin-Induced Peripheral Neuropathy. Biol Pharm Bull. **40**, 947-953 (2017).
37. Dhaka, A. et al. TRPV1 is activated by both acidic and basic pH. J Neurosci. **29**, 153-158 (2009).
38. Miyake, T. et al. Cold sensitivity of TRPA1 is unveiled by the prolyl hydroxylation blockade-induced sensitizationto ROS. Nat Commun. **7**, 12840 (2016).
39. Wang, Y.Y., Chang, R.B. & Liman, E.R. TRPA1 is a component of the nociceptive response to CO_2. J Neurosci. **30**, 12958-12963 (2010).
40. Andersson, D.A., Chase, H.W. & Bevan, S. TRPM8 activation by menthol, icilin, and cold is differentially modulated by intracellular pH. J Neurosci. **24**, 5364-5369 (2004).

Authors' contributions

BR designed and performed most of the experiments; MD performed the electrophysiological experiments; AP and CC-S performed in vitro experiments; AC performed in vivo experiments; RR performed in vivo experiments; VAC performed in vivo experiments; DL performed and supervised in vitro experiments; GC supervised in vivo experiments and contributed to design of the experimental plan; PM supervised and contributed to design of the experimental plan; CD designed, supervised and analyzed electrophysiological experiments; AAG designed the experimental plan, supervised in vitro and in vivo work and wrote the manuscript.

Chapter 5

Contribution of hyperpolarizing ion channels to acute cold hypersensitivity induced by oxaliplatin administration

Abstract

Oxaliplatin (OHP), a platinum-based chemotherapeutic agent, causes peripheral neurotoxicity (OIPN) characterized by an acute cold-induced syndrome accompanied by cramps, paresthesias/dysesthesias in the distal limbs and perioral region. No therapies are available to treat OIPN and patients often suffer from pain and sensory symptoms long after the end of the therapy. The molecular and cellular mechanisms that produce OIPN are not fully understood; however, one common mechanism appears to be changes in ion channels expression and/or function in primary afferent sensory neurons.

Here we have combined different electrophysiological approaches in order to investigate, in mice DRG neurons, the impact of OHP treatment on the molecular

targets that are known to participate in the processing of noxious stimuli as well as in the tuning of cold perception. Recently, we found that therapeutically-relevant OHP concentrations (0.1 μg mL^{-1}) lead to an acidification of the DRG cytosol neurons that modulate the activity of TRPA1 and TRPV1 channels. It is likely that other different classes of channels could be affected by this alteration in pH homeostasis. In particular, single channels recordings suggest the involvement of the two pore domain K^+ (K_2P) channel family members. These are background channels that contribute to the regulation of neuronal excitability hyperpolarizing the membrane potential of peripheral nerve terminals and that are tightly regulated by different stimuli, including variations of internal pH.

In light of this, the hyperexcitability underlying the OINP can be explained as the resultant effect of multiple regulations on different targets in response to the OHP alteration of pH homeostasis. This provides useful insights for the understanding of the pathogenesis behind this neuropathy in order to propose effective therapeutic pain management.

Keywords: oxaliplatin, K2P channels, neuropathic pain, pH, neurons

5.1 Introduction

Chemotherapy-induced peripheral neurotoxicity remains the most common side effect of several anticancer agents including vinca alkaloids, taxanes, platin derivates, bortezomib and thalidomide [13]. The relevant clinical hallmark of OHP is an acute sensory neuropathy characterized by alterations of sensitivity, dysesthesias, paresthesias and cramps, which are predominantly located in the extremities and in the face and, in most patients, last for hours or even days after

the first OHP injection. In addition, almost all patients that experience this acute cold-induced syndrome, develop chronic symptoms that are common to other platinum-based chemotherapies [16,37]. Currently, there have not been developed sufficiently effective agents for the prevention or treatment of OHP-induced peripheral neurotoxicity (OIPN) and thus patients' quality of life is affected long after the end of the therapy [13,15].

Even if there is an increasing knowledge of the cellular and molecular mechanisms by which anticancer agents induce such neurotoxicity, the pathogenesis of OIPN remains poorly understood. In this sense, OHP is known to induce hyperexcitability by remodelling the expression and/or altering the function of some molecular targets that participate in the transduction of the thermal sensation at a peripheral level [37]. Among them, transient receptor potential (TRP) channels are generally accepted as primary receptors for the detection of both physiological and noxious temperatures [92,93]. Cumulative genetic and pharmacological evidences suggest the involvement of cold-activated TRP members in the onset of OIPN [37,94]. However, there are other channels that modulate thermosensation. For instance, hyperpolarizing background K^+ channels (K_2P channels) work as regulators of the excitability of primary afferent fibers, and thus of pain signalling by tuning the excitation elicited by several stimuli including temperature [80,95,96]. In accordance with this idea, it has been proposed that all three components of the TREK-family channels (TREK-1, TREK-2 and TRAAK), which are widely expressed in DRG and TG, are also implicated in the mediation of cold hypersensitivity following the treatment with OHP[37,77].

Interestingly, a recent report has shown that therapeutically-relevant OHP concentrations induce cytosolic acidification in both cultured DRG neurons and DRG cells from treated animals [97]. In this line, the excitability of neurons is particularly

sensitive to intracellular pH (pH_i) and/or extracellular pH (pH_o) alterations since many surface channels, transporters and receptors present intra and/or extra pH-sensitive moieties [55]. In fact, as a consequence of the OHP-induced pH changes, a reversible hypersensitization of TRPA1 channels is observed [97]. In the present study, we have investigated the involvement of K_2P channels in this context since these channels also respond to, among other stimuli, intracellular pH [98–100]and strongly collaborate with TRP channels to generate the sensation of heat, cold and thermal pain [93]. We address this issue by means of an integrated approach that combines electrophysiological recordings in OHP-treated mice DRGs at both single cell level by using the patch clamp technique, and at population level by using multielectrode arrays (MEAs), as well as quantitative real-time polymerase chain reaction (qRT-PCR).

5.2 Material and methods

Animals. BALB/c male mice aged 5–10 weeks upon arrival were employed (Envigo, San Pietro al Natisone, Italy) both for DRG culture preparation and in vivo studies. Animals were maintained as previously reported14. Care and husbandry of animals were in conformity with the institutional guidelines in compliance with national and international laws and policies. The study plan was approved by the animal Ethics Committee of the University of Milano Bicocca and of the Università del Piemonte Orientale. The procedures were approved by the local animal-health and ethical committee (Università del Piemonte Orientale) and were authorized by the national authority (Istituto Superiore di Sanità; authorization number N. 22/2013). All mice were euthanized under deep isoflurane-induced anaesthesia for cell cultures and with CO_2 for in vivo experiments.

Chemicals. For in vivo studies OHP solution was prepared as reported by Renn and collaborators [101]and used as previously described [102].For in vitro studies, OHP (5 mg/mL stock solution, Sigma-Aldrich Inc., Italy), capsaicin (1 mM stock solution, Sigma-Aldrich Inc., Italy), DIDS (4,4'-Diisothiocyano-2,2'-stilbenedisulfonic acid; Sigma-Aldrich Inc., Italy), AA (Arachidonic acid; Sigma-Aldrich Inc., Italy) and nigericin (20 mM stock solution, Life Technologies, Italy) were used. These compounds, with the exception of capsaicin an AA (reconstituted in 100% EtOH and in water, respectively), were dissolved in 100% dimethyl sulfoxide (DMSO) and stored at −20 °C, according to manufacturers' specifications. Working concentrations of these drugs were freshly prepared for each experiment by diluting DMSO or EtOH to 0.1% in milliQ (MilliPore) water.

Experimental design for the *in vivo* study. For the evaluation of the expression of TREK and TRAAK channels in chronically OHP-treated animals, animals (n=12 in two separate experiments) were injected intravenously in the tail vein with OHP 3.5 mg/Kg (10 mL/Kg) twice a week for 4 weeks, while control mice (n=12) were left untreated. The neurotoxicity of this chronic schedule and its capacity to mimic Human OIPN have already been reported in detail [101].In a second experiment that evaluated the acute effect of OHP, eight animals (in two separate experiments) were injected intravenously in the tail vein with a single dose of OHP 3.5 mg/Kg (10 mL/Kg). Animals were sacrificed after 24 hours to investigate acute effects.

Isolation and Primary Cell Culture of Mouse DRG Neurons. DRG excised from adult BALB/c mice and (5/10-wk-old) were collected in a dish containing cold F12 (Nutrient Mixture F12 Ham) medium (Sigma Aldrich Inc.). The DRG, accurately de-sheathed, were transferred into a sterile 35 mm dish containing collagenase from Clostridium hystoliticum 0.125% (Sigma Aldrich Inc.) and DNase (Sigma) in F12 (Nutrient Mixture F12 Ham) medium and incubated at 37 °C. After 1 h incubation , DRG were triturated using a 1000 µl tip. Myelin and nerve debris were eliminated by centrifugation through a bovine serum albumin (BSA) cushion. Cell pellets were re-suspended in Bottenstein and Sato medium (BS) (30% F12 (Nutrient Mixture F12 Ham medium), 40% DMEM (Dulbecco's Modified Eagle's medium (Sigma Aldrich Inc., Italy), 30% Neurobasal A medium (Life Technologies, Italy), 100 X N2 supplement (Life Technologies, Italy), penicillin 10 U/mL and streptomycin 100 mg/mL (Sigma Aldrich Inc., Italy), supplemented with Recombinant Human β-NGF, Recombinant Murine GDNF and Recombinant Human NT3 (Peprotech, USA) and plated onto 24 mm glass coverslips pre-coated with laminin (Sigma Aldrich Inc., Italy).

Real Time Quantitative PCR (QRT-PCR) . Total RNA was isolated from DRG using TRI-Reagent® and reverse transcribed according to the manufacturer's instructions (Im-Prom-II™ Reverse Transcription System, Promega, WI, USA). Until using, cDNA was stored at -20°C. qRT-PCRs were performed on 96-well plates (CFX96™ Real-Time PCR Detection Systems, Bio-Rad Inc), in triplicate and florescence intensity assessed using the CFX96™ Real-Time PCR Detection Systems (Bio-Rad Inc.). The initial denaturation step was set at 95°C for 10 min, followed by 40 cycles of amplification using this set of primers: TREK-1 5'-TCACTCTGACGACCATTGGA-3'forward, 5'-GAGGATCCAGAACCACACCA-3' reverse; mouse TREK-2 5'-

CATCTGTGTGAGTCCCCAGG-3' forward, 5'-GACTGCTGCTGTTGGAAGAG-3' reverse and mouse TRAAK 5'-GTGTGAGCCAGAAGAGCCT-3' forward, 5'-GGTTGCTGCTATTGGTCCAG-3' reverse; 60°C annealing temperature. Transcripts were normalized to the expression of Ribosomal Protein S18 mRNAs, for each gene, the threshold cycle *(C_t)* was calculated. The C_t of treated cells was compared to the C_t generated by the control cells and ΔC_t was calculated as the difference between C_t values, determined using the equation $2^{-\Delta Ct}$.

Electrophysiology - Multielectrode Arrays (MEAs). Extracellular DRG action potentials were recorded by means of a commercial 60-channel multi-electrode array (MEA) setup. An external T-control unit (TC02) kept the temperature of the socket surface at 310 K. The digitalized output-data coming from the USB-ME64 unit were acquired, monitored and recorded on a PC through MC_Rack software (Version 4.6.2, Multi Channel Systems MCS GmbH). A channel was considered active for the analysis if it recorded at least 5 spikes in 60 s (time window of agonist application). Neuronal firing activity was evoked by 50 s applications of 1 µM capsaicin and later, after 16 min washing, of 40 mM KCl using continuous perfusion system (2 mL/min flux). Threshold was fixed at ±5 standard deviations from baseline noise (typically around 15 µV peak-to-peak). In general, according to the technical specifications of the device, one electrode does not correspond to a single cell. Rather, each electrode can detect all the electrical signals originating in the spatial region surrounding it, within a radius of tens of micrometers. NeuroExplorer (Nex Technologies, USA) was used to make raster plot from each channel. Only upward (positive) and downward (negative) spike cutouts from each of the available recording electrodes were stored. These waveforms consisted of 1 ms pre-spike and 4 ms post-spike fragments respect to the point of threshold crossing.

Electrophysiology - Patch-clamp *Cell attached* patch clamp recordings were performed at 22–25 °C on control and OHP-treated neurons with a mean soma diameter < 25 µm. During gigaseal formation DRG neurons were continuously superfused with a standard physiological solution of the following composition (in mM): NaCl 154; KCl 4; $CaCl_2$ 2; $MgCl_2$ 1; 4-(2-hydroxyethyl)-1-piperazine ethane sulfonic acid (HEPES) 5; glucose 5.5; NaOH to pH 7.4. The resistance of patch electrodes, prepared from borosilicate glass capillaries (World Precision Instruments), was 5–7 MΩ. In most experiments, pipette solution composition was (in mM): CsCl 130, TEACl 20, DIDS 1; 4-(2-hydroxyethyl)-1-piperazine ethane sulfonic acid (HEPES) 10, EGTA 2, BCTC 3 µM, Icilin 1 µM, CsOH to pH 7.4. In a second set of experiments, the pipette solution composition was (in mM): KCl 150, TEACl 20, DIDS 1; 4-(2-hydroxyethyl)-1-piperazine ethane sulfonic acid (HEPES) 10, EGTA 2, CsCl 1, BCTC 3 µM, KOH to pH 7.4. Once the seal was obtained (2–10 GΩ), cells were perfused with a solution containing KCl 150, $MgCl_2$ 2, $CaCl_2$ 1, EGTA 1.1, HEPES 5, KOH to pH 7.4, in order to set the membrane potential near 0 mV and to prevent intracellular calcium loading. *Inside out* experiments were performed on untreated DRG neurons. As describe above, standard physiological solution was used during gigaseal formation, and high potassium bath solution, once the seal was obtained and the patch excised. Pipettes were filled with the same 150 mM KCl pipette solution above described. Data were collected and filtered at 1 kHz with an Axopatch 200B amplifier (Molecular Devices, USA) and continuously digitized at 1 kHz sampling frequency with PClamp Axoscope software (Molecular Devices, USA). Steady state voltage clamp protocols were applied and digitized at 10 or 20 kHz with PClamp Clampex software Data analysis was performed with OriginPro (OriginLab, USA) and PClamp Clampfit software

Statistical Analysis. Data are presented as mean ± SEM or median and IQR, depending on the skewness of data distribution. Data points in the single channel current-voltage graphs represent mean ± SD, estimated by fitting the amplitude histograms to a sum of Gaussian functions (OriginPro 9.1, OriginLab USA). The normality of data distributions was assessed using Shapiro–Wilk test. Parametric (unpaired *t*-test and One-way analysis of variance (ANOVA) followed by Tukey's post-hoc) or nonparametric (Mann-Whitney *U* test) statistical analysis was used for data comparison.

5.3 Results

OHP effect on expression of TREK and TRAAK mRNA in DRG neurons

OHP promotes hyperexcitability by remodelling ion channel expression in cold-sensing nociceptors. Descoeur and collaborators (2011) [37] showed a drastic decrease of the expression of TREK and TRAAK channels in mice after four days post treatment with a single dose of OHP, just at the peak of pain hypersensitivity [37]. To investigate the effect of the treatment with OHP on the expression of TREK / TRAAK channels on DRG neurons, in our experimental conditions, we performed RT-PCR both *in vitro* and *in vivo*. In *in vitro* experiments, the mRNA levels were measured after a 6-h treatment with OHP, as well as, after removing the treatment, 42 hours later. In *in vivo* experiments, BALB/c mice were treated either with OHP (3.5 mg/Kg) twice a week for four weeks or only once (3.5 mg/Kg). Twenty-four hours after the

last treatment, animals were sacrificed, DRG dissected, and their mRNA levels measured as described in the materials and methods section.

We observed that the acute treatment with OHP induce a significant increase in the mRNA levels of K_2P channels both *in vitro* and *in vivo* (Fig. 1).

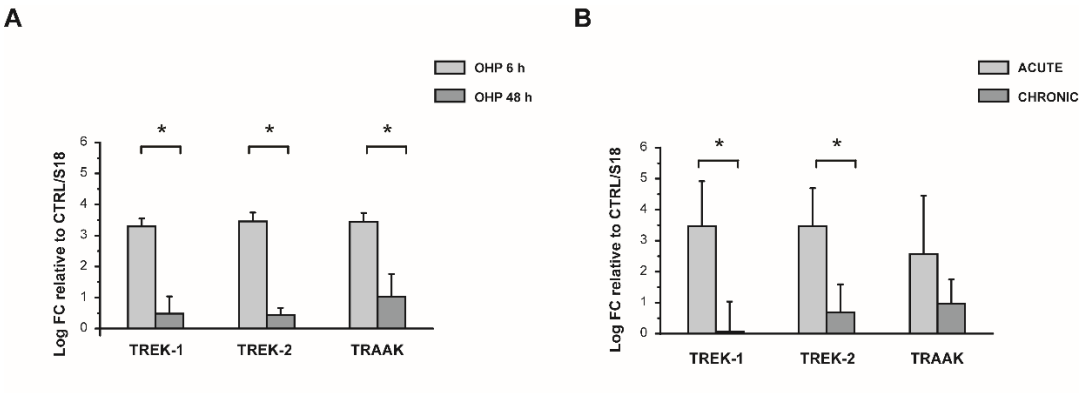

Fig 1. A Oxaliplatin affects in vitro the transcription of TREK-1, TREK-2 and TRAAK channels. The mRNA levels were measured after the 6 hour treatment with OHP and after 48 hours (upon 6 hour treatment with OHP), by RT-PCR. Values for both conditions were normalized against the expression of the same transcripts as evaluated in control (untreated) samples. Data show a significant increase of all K2P channels considered in this analysis after 6 hour treatment (*p-value<0.05, Bonferroni-adjusted). **B** These data were confirmed by the analysis performed on mRNA from DRG cells from a different set of animals upon OHP treatment in vivo (*p-value<0.05, Bonferroni-adjusted).

OHP effect on electrical activity in DRG neurons

The magnitude of the K^+ leak current is a primary determinant of neuronal resting V_m [92]. An increase of TREK/TRAAK channel expression and activity is expected to induce membrane hyperpolarization and decreased excitability. To provide such information on electrical activity elicited by OHP, we performed extracellular recordings from DRG neurons on MEAs.

Previous studies have shown that DRG neurons, even if representing a heterogeneous population of different sensory cells, have a very limited and sporadic spontaneous electrical activity [89]. For this reason, we evoked transitory activity in these primary cultures by adding 1 µM capsaicin and 40 mM KCl (Fig. 2).Full recordings sampled at 25 kHz were filtered using a voltage threshold (see Methods) in order to extract extracellular action potential (EAP) waveforms from raw data and build raster plots showed in Fig. 2a.

Three different time points were investigated, after 6-h treatment with OHP, 30 h and 42 h later, after removing the treatment (from now on they will be indicated as 24h and 48h respectively). We measured the average number of EAPs in a temporal window of 50 s both for capsaicin and KCl. Within these temporal borders, active channels changed their firing rate according to Fig. 2a.

For capsaicin, the average firing rate under control conditions, expressed as median and interquartile range, was respectively M_f = 0.701 Hz, IQR_f = [0.258; 1.148] Hz at 6 h (65 different channels, from n=4 independent experiments), M_f = 1.062 Hz, IQR_f = [0.506; 1.583] Hz at 24 h (54 different channels, from n=2 independent experiments) and M_f = 0.621 Hz, IQR_f = [0.346; 1.566] Hz at 48 h (76 different channels, from n=2 independent experiments). While for treated neurons the average firing rate was M_f = 0.255 Hz, IQR_f = [0.137; 0.484] Hz at 6 h (61 different channels, from n=4 independent experiments), M_f = 0.458 Hz, IQR_f = [0.236; 0.935]

Hz at 24 h (64 different channels, from n=2 independent experiments), and M_f = 0.580 Hz, IQR_f = [0.350; 1.917] Hz at 48 h (76 different channels, from n=2 independent experiments) . The OHP-treatment elicited a statistically significant median decrease in firing rate compared to the control electrical activity, both at 6 h ($p = 1.173 \cdot 10^{-4}$, Fig. 2B) and at 24 h ($p = 5.646 \cdot 10^{-5}$,Fig. 2B). No significant differences was observed at 48 h. For this reason, an analysis of statistical power was conducted to determine the minimum detectable effect in our experimental conditions. In particular, statistical sensitivity was computed in terms of absolute (difference in firing rate, Δf) and relative (Cohen's *d*) effect needed for having a significant *p*-value with a level of $\alpha = 0.05$ and a power of $\pi = 0.8$ (results of such an analysis are reported in Table 1).

For KCl, the average firing rate under control conditions, expressed as median and interquartile range, was respectively M_f = 0.188 Hz, IQR_f = [0.098; 0.288] Hz at 6 h (30 different channels, from n=4 independent experiments), M_f = 0.078 Hz, IQR_f = [0.039; 0.145] Hz at 24 h (11 different channels, from n=2 independent experiments) and M_f = 0.163 Hz, IQR_f = [0.111; 0.530] Hz at 48 h (7 different channels, from n=2 independent experiments). While for treated neurons the average firing rate was M_f = 0.128 Hz, IQR_f = [0.065; 0.179] Hz at 6 h (18 different channels, from n=4 independent experiments), M_f = 0.076 Hz, IQR_f = [0.041; 0.344] Hz at 24 h (12 different channels, from n=2 independent experiments) and M_f = 0.308 Hz, IQR_f = [0.185; 0.422] Hz at 48 h (14 different channels, from n=2 independent experiments)

In this case, the effect induced by OHP led to significant differences only in the 6-hour after-treatment group (p = 0.022, Fig. 2C). Even for this agonist a statistical power analysis was carried out (see Table 2).

Table 1.

Capsaicin (1 µM)	Effect size (Cohen's d)	Pooled Sd	Effect size (Δf)
6 h	0.468	1.481	0.693
24 h	0.515	1.588	0.818
48 h	0.534	0.963	0.514

Table 2.

KCl (40 M)	Effect size (Cohen's d)	Pooled Sd	Effect size (Δf)
6 h	0.874	0.089	0.078
24 h	1.258	0.192	0.241
48 h	1.403	0.219	0.308

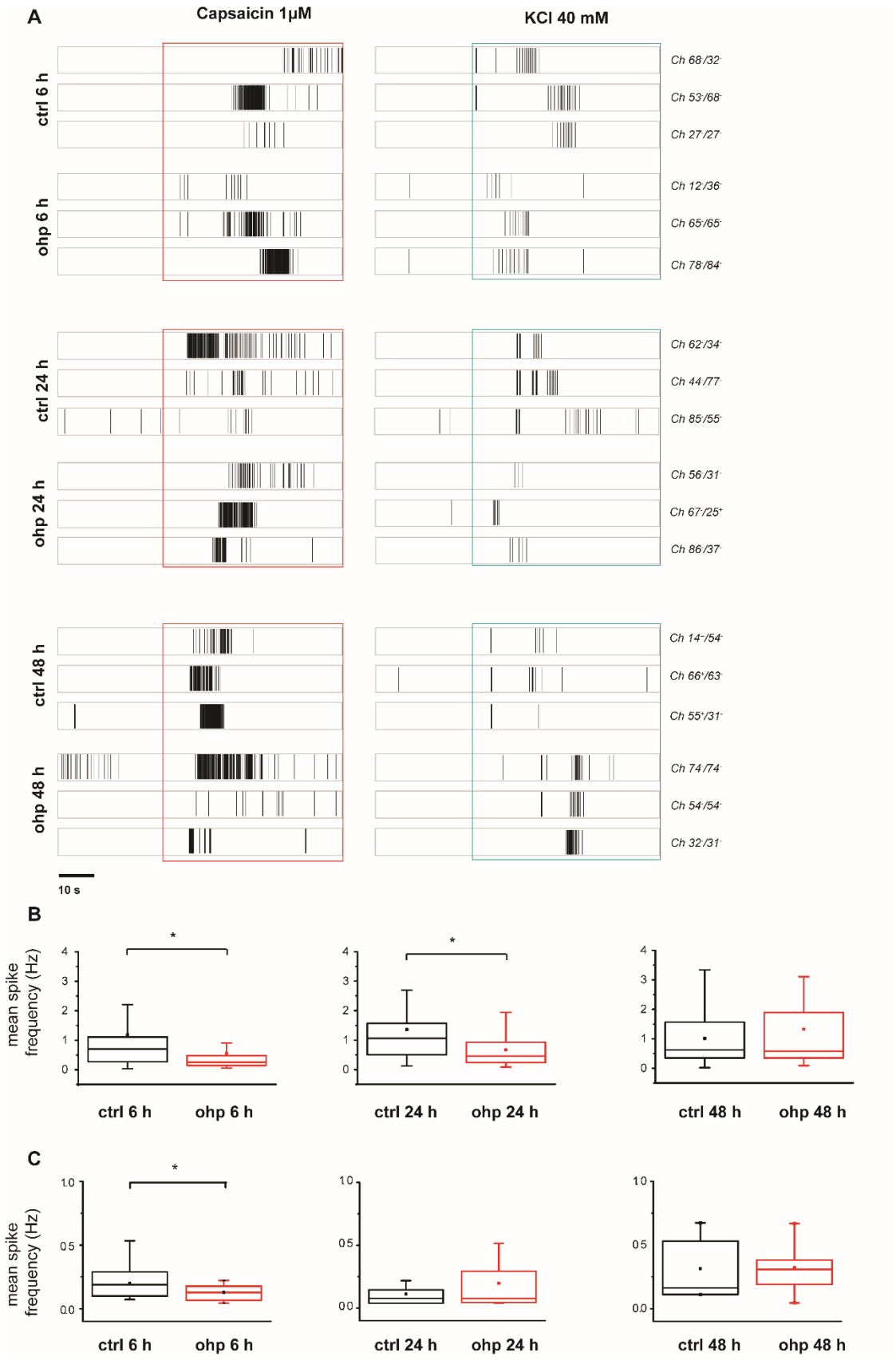
A
Capsaicin 1µM
KCl 40 mM
ctrl 6 h
ohp 6 h
ctrl 24 h
ohp 24 h
ctrl 48 h
ohp 48 h
Ch 68/32
Ch 53/68
Ch 27/27
Ch 12/36
Ch 65/65
Ch 78/84
Ch 62/34
Ch 44/77
Ch 85/55
Ch 56/31
Ch 67/25
Ch 86/37
Ch 14/54
Ch 66/63
Ch 55/31
Ch 74/74
Ch 54/54
Ch 32/31
10 s
B
mean spike frequency (Hz)
ctrl 6 h
ohp 6 h
ctrl 24 h
ohp 24 h
ctrl 48 h
ohp 48 h
C
mean spike frequency (Hz)
ctrl 6 h
ohp 6 h
ctrl 24 h
ohp 24 h
ctrl 48 h
ohp 48 h

Fig. 2. A Three representative raster plots for each condition (control and OHP treated neurons) and each time point considered during the application of 1 µM capsaicin and 40 mM KCl. On the right side of each raster is the channel identifier. Symbols + and – represent the direction (upward or downward respectively) of the EAPs detected. **B** Box plots show median and IQR of mean spike frequency (Hz) in the presence of capsaicin (at 6 h $p = 1.173 \cdot 10^{-4}$, Mann-Whitney *U* test, $m_{ctrl} = 61$ and $m_{OHP} = 65$ different channels, from n=4 independent experiments; at 24 h $p = 5.646 \cdot 10^{-5}$, Mann-Whitney *U* test, $m_{ctrl} = 54$ and $m_{OHP} = 64$ different channels, from n=2 independent experiments; at 48 h $p = 0.806$, Mann-Whitney *U* test, $m_{ctrl} = 76$ and $m_{OHP} = 76$ different channels, from n=2 independent experiments Mann-Whitney *U* test). **C** Box plots show median and IQR of mean spike frequency (Hz) in the presence of KCl (at 6 h $p = 0.022$, $m_{ctrl} = 30$ and $m_{OHP} = 18$ different channels, from n=4 independent experiments; at 24 h $p = 0.975$, $m_{ctrl} = 11$ and $m_{OHP} = 12$ channels, from n=2 independent experiments; at 48 h p= 0.975, $m_{ctrl} = 7$ and $m_{OHP} = 14$ different channels, from n=2 independent experiments; Mann-Whitney *U* test).

OHP effect on TREK-2 channel

Riva *et al.* (2018)[97] showed that OHP-induced intracellular acidification sensitize TRPA1 channels activity. This effect was abolished by using the K^+/H^+ exchanger nigericin to clamp pH_i to physiological levels, the effect of the ionophore being to mediate H^+ equilibration across the plasma membrane. On the other hand, a large amount of literature claims that intracellular protons influence TREK channels in different ways: TREK1 and TREK2 are both activated by acidification; while TRAAK is stimulated by alkalinization from pH 7.3, but without undergoing to any modification by cytoplasmic acidosis [103]. In light of this, we hypothesized that the reduced excitability in OHP-treated neurons depends on an increase of TREK1 and TREK2 channels activity that make the resting membrane potential more hyperpolarized.

To obtain a more direct evidence on the involvement of TREK channels, we performed single-channel patch clamp experiments in the recording configuration

that less interferes with the intracellular composition, i.e. the cell attached mode. To achieve a stable membrane potential near zero without inducing intracellular free calcium increases, we perfused DRG neurons with a bath solution containing 150 mM KCl and low [Ca^{2+}]. Furthermore, the pipette solution contained TEA chloride, CsCl and DIDS (see Material and methods) to exclude any contribution of other K^+-selective channels (inward-rectifying (Kir), voltage-gated (K_V), and calcium-activated K^+ channels (K_{Ca})) and Cl^--selective channels, which are known to be expressed in DRGs (ref).

Interestingly, in most cell attached patches (6 out of 11 cells) we observed a similar modulation as it is described for TRPA1 by Riva *et al.* (2018)[97], of a channel characterized by two different current levels at positive membrane potentials (+40 mV). Figure 3A shows the channel activity in an OHP-treated neuron before and during the perfusion of the high potassium solution containing 10 µM nigericin. With the ionic solution used in the experiments, nigericin activates a net efflux of H^+ and stabilizes the intracellular pH near 7.4. The channel activity (NP_o, were N is the number of channels in the patch and Po the open probability) changes from NP_o= 0.57 ± 0.19 to NP_o= 0.08 ± 0.11 following the perfusion with nigericin, evidencing a high sensitivity of this channel to acidic intracellular pH. In the insets (FIG 3A), as well as in the trace with an expanded scale shown in Figure 3B, it can be observed the small current level (S) and the larger one (L) more clearly. From the best fit of the amplitude histogram distribution of the single channel trace shown in Figure 3C there can be extracted the values for S and L, 1.68 pA and 5.21 pA at Vm=+40 mV, respectively.

Figure 3D, from the same experiment, shows the single channel I-V relationship obtained by plotting the mean amplitudes of the two current levels at different membrane potentials. Single channel slope conductance (γ) and negative reversal

potential (V_{rev}) values were, for the small phenotype, 15 ± 1.5 pS and -49 ± 7.5 mV, respectively, while 62 ±6 pS and -35 ±4 mV for the large one, on the basis of linear regression of current versus voltage. The biophysical properties described above are in agreement with previously published data for TREK2 channels [104]. Furthermore, V_{rev} values are less negative than expected for a K^+ selective channel, suggesting that the channel is slightly permeable to cesium ions [78]. On the other hand, in our ionic conditions the actual reversal potential is very difficult to evaluate from the current-voltage relationship. To overcome this difficulty and to better characterize the I-V properties and shape we performed a series of experiments replacing 130 mM CsCl with 150 mM KCl in the pipette solution. These conditions would allow us to observe the inward rectifying behaviour that characterises TREK2 channels [104,105]The red and blue traces in figure 3E represent examples of the channel activity recorded in a OHP-treated neuron during a voltage ramp from -120 mV to 100 mV. To obtain the I-V relationship and the reversal potential of the channel, we subtracted the recorded trace representing the closed state of the channel (baseline; black trace in Fig 3E) to the red one. The resulting curve in figure 3G (red trace) show that the channel is weakly inward rectifier with a V_{rev} = 0mV. Finally, we performed inside-out experiments in an untreated neuron in which we added arachidonic acid (AA; 10 μM), which is known to be a potent activator of TREK2 [106]. Although the open state shows high background noise, the inward rectifying behaviour of currents activated by the agonist can be observed (Fig. 3F). This evidence is well illustrated in Figure 3G. Here, the average current obtained from a series of ten ramp currents recorded during the administration of AA is showed (black trace) and superimposed with the I-V curve obtained in cell-attached experiments (red curve).

In conclusion, these data provide evidence that expressed cell-membrane TREK2 channels are functional at 48 h post OHP-treatment and that their activity is positively modulated by OHP-induced pH_i changes.

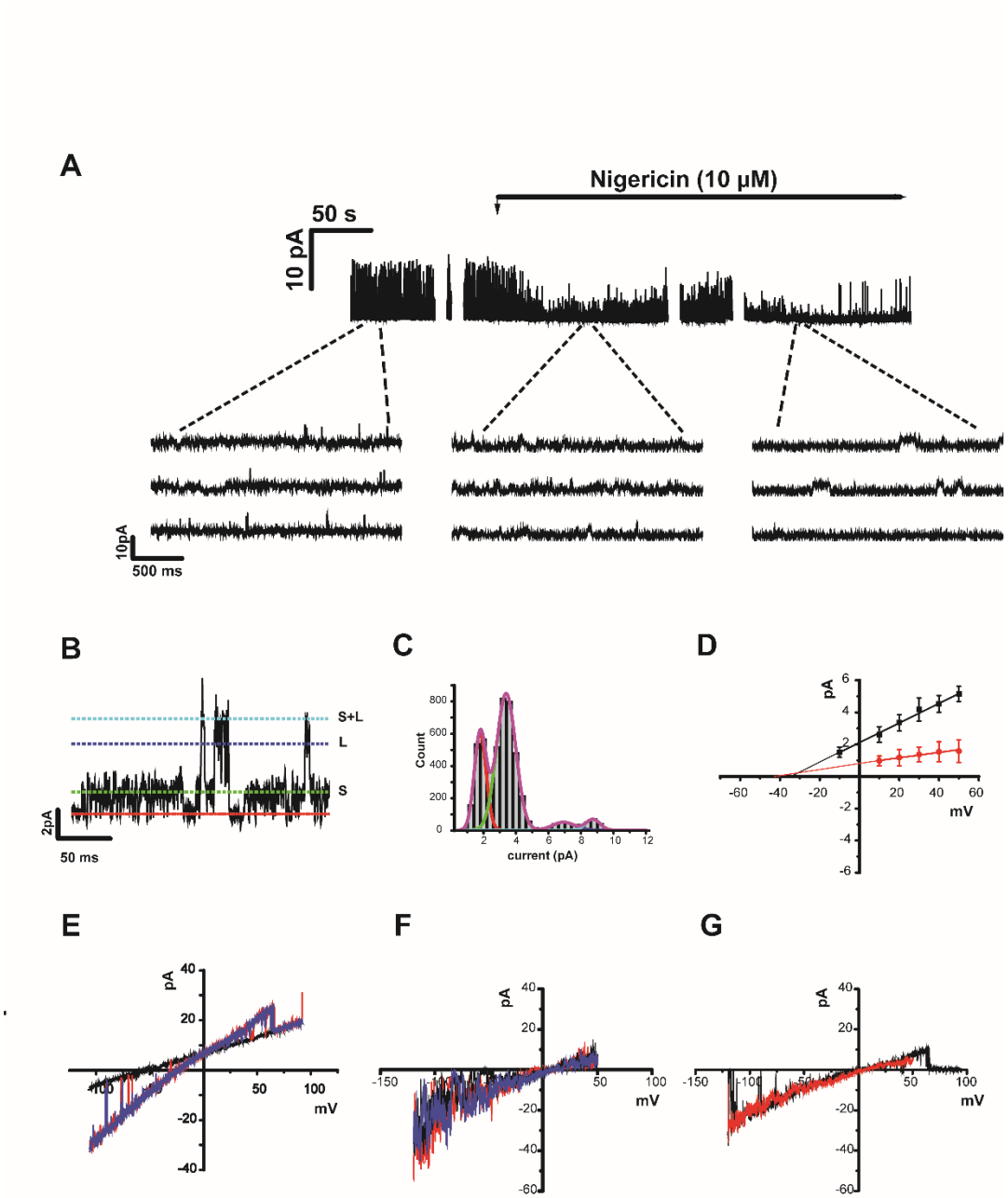

Fig 3. **A** Single channel recording at V_{hold}=+40 mV from an OHP treated DRG neuron, before and during nigericin perfusion. Insets show a magnification in three different time recording points (2 min before nigericin perfusion; 1 and 4 min after nigericin perfusion, respectively). **B** Single channel recorded in cell attached configuration at V_{hold}=+40 mV from an OHP treated DRG neuron. The two different levels of conductance could be observed: the smaller one (S) and the larger one (L). **C** Amplitude histograms of the two conductance levels shown in B. **D** I-V plot with linear regressions, for the channels shown in B. **E** I-V curve obtained from another experiment recorded in cell attached mode with high K^+ solution in the pipette. The black trace is the baseline level, while the blue and red traces representing I-V currents during the channel opening. **F** three examples of I-V recorded in inside out configuration during the stimulation with Arachidonic Acid (2 μM) in symmetrical K+ concentrations. **G** merge of the average of 10 I-V curve recorded in the presence of Arachidonic Acid with single channel I-V curve shown in E.

5.4 Discussion

The data presented in this work show that therapeutically-relevant OHP concentrations [97] induce a transiently overexpression of TREK-1, TREK-2 and TRAAK both in cultured DRG neurons and in DRG cells from treated animals. Moreover, MEA recordings provide evidence for a parallel decrease in the firing rate of both capsaicin- and KCl-triggered action potentials. Specifically, statistical significance emerged when comparing OHP-treated and control groups at 6 h and 24 h after-treatment in capsaicin-induced firing rates and at 6 h after-treatment in those KCl-induced.

Interestingly, power analysis revealed that the lack of statistical significance at 48 h after-treatment time point in capsaicin-induced firing rates cannot be ascribed to a lack of sensitivity (i.e. insufficient sample size). In other words, notwithstanding the impossibility of accepting the null hypothesis of no difference in frequency rates at

this time point, a biologically relevant effect can be ruled out. On the contrary, when considering the effect on firing triggered by KCl administration at 24 and 48 hours, a type II error (false negative) can be suspected. According to Table 2, the reduction in the estimated statistical sensitivity does not allow us to exclude the presence of an effect similar to the one detected after the first 6 hours. Therefore, more experiments are needed in order to increase the sample size of these two conditions and the accuracy of the related firing rate measurement.

In this regard, the lack of effect at 48 h after capsaicin triggering may be related to the restoring of expression similar to control conditions. These findings suggest that the K^+ leak current are likely to be transiently augmented in our experimental models. This could lead in turn in a shift of V_m towards the potassium Nernst potential (E_K) making the cells less excitable, that is larger depolarizations are required to initiate action potentials.

The most effective way to identify and characterize individual TREK channels involved in the responses OHP-induced is by recording single-channel openings from cell-attached patches. These recordings have evidenced that the activity of a channel with biophysical properties that can be associated with those described in literature for TREK-2 channels [78,104,107], was enhanced by OHP-treatment. In a previous work [97] we reported that the same concentrations of OHP, are able to induce an acidification of intracellular pH that, in turn, leads to a sensitization of TRPA1 channels. By restoring pH to physiological level the hyperactivity of this channel could be reversed. In this line, we performed cell attached recordings following the same experimental procedures reported in Riva et *al*[97]. A modulation of the TREK-2 channel activity similar to that recorded for TRPA1 in the previous work was observed. However, the contribution of the other members of the family, in particular TRAAK and TREK1, is not excluded [37,78,107]. In this regard, the

characterization of this family of channels is limited by the lack of specific agonist and antagonist. The identification of TREK-2 has been possible thanks to its unique biophysical properties, widely described in literature [99].

This is, to our knowledge, the first description of transient increase in the levels of the expression of TREK and TRAAK channels after OHP treatment. The decrease showed by Descoeur and collaborators [37] is related to a different time point, after four days post treatment with a single dose and higher dose of OHP.

In conclusion, the transient overexpression of the background K^+ channels could be interpreted as a tentative of neurons to restore the homeostasis condition. In detail, the hyperpolarizing currents carried by K_2P channels counteract the depolarization triggered by the positive modulation of non-selective cationic channels like TRPA1.

References

1. Chepelev, N. L., Moffat, I. D., Bowers, W. J. & Yauk, C. L. Neurotoxicity may be an overlooked consequence of benzo[a]pyrene exposure that is relevant to human health risk assessment. *Mutat. Res. - Rev. Mutat. Res.* **764**, 64–89 (2015).

2. Teleanu, D., Chircov, C., Grumezescu, A., Volceanov, A. & Teleanu, R. Impact of Nanoparticles on Brain Health: An Up to Date Overview. *J. Clin. Med.* **7**, 490 (2018).

3. Ge, D. *et al.* The neurotoxicity induced by engineered nanomaterials. *Int. J. Nanomedicine* **14**, 4167–4186 (2019).

4. Lovisolo, D., Dionisi, M., A. Ruffinatti, F. & Distasi, C. Nanoparticles and potential neurotoxicity: focus on molecular mechanisms. *AIMS Mol. Sci.* **5**, 1–13 (2018).

5. Bannunah, A. M., Vllasaliu, D., Lord, J. & Stolnik, S. Mechanisms of nanoparticle internalization and transport across an intestinal epithelial cell model: Effect of size and surface charge. *Mol. Pharm.* **11**, 4363–4373 (2014).

6. Lin, J. & Alexander-Katz, A. Cell membranes open 'doors' for cationic nanoparticles/ biomolecules: Insights into uptake kinetics. *ACS Nano* **7**, 10799–10808 (2013).

7. Zanella, D. *et al.* The direct permeation of nanoparticles through the plasma membrane transiently modifies its properties. *Biochim. Biophys. Acta - Biomembr.* **1861**, 182997 (2019).

8. Narayan, R., Nayak, U. Y., Raichur, A. M. & Garg, S. Mesoporous silica nanoparticles: A comprehensive review on synthesis and recent advances. *Pharmaceutics* **10**, 1–49 (2018).

9. Ariano, P. *et al.* Interaction of spherical silica nanoparticles with neuronal cells: Size-dependent toxicity and perturbation of calcium homeostasis. *Small* **7**, 766–774 (2011).

10. Gilardino, A. *et al.* Interaction of SiO<inf>2</inf> nanoparticles with neuronal cells: Ionic mechanisms involved in the perturbation of calcium homeostasis. *Int. J. Biochem. Cell Biol.* **66**, 101–111 (2015).

11. Zajaczkowską, R. *et al.* Mechanisms of chemotherapy-induced peripheral neuropathy. *Int. J. Mol. Sci.* **20**, (2019).

12. Aromolaran, K. A. & Goldstein, P. A. Ion channels and neuronal hyperexcitability in chemotherapy-induced peripheral neuropathy: Cause and effect? *Mol. Pain* **13**, 1–24 (2017).

13. Grisold, W., Cavaletti, G. & Windebank, A. J. Peripheral neuropathies from chemotherapeutics and targeted agents : *Neuro. Oncol.* **14**, 45–54 (2012).

14. Park, S. B. *et al.* <CA CANCER J CLIN 2013_Park_peripheral neuropathy cisplatin.pdf>. *CA Cancer J. Clin.* **63**, 419–437 (2013).

15. Chiorazzi, A., Semperboni, S. & Marmiroli, P. Current view in platinum drug mechanisms of peripheral neurotoxicity. *Toxics* **3**, 304–321 (2015).

16. Paola Marmiroli, Guido Cavaletti, Valentina Carozzi, Beatrice Riva, Dmitry Lim, A. A. G. Calcium-related Neurotoxicity of Oxaliplatin: Understanding the Mechanisms to Drive Therapy. Current Medicinal Chemistry Volume 22, Issue 32 , (2015).

17. Kaufman, M. A. *Environmental Neurotoxicology. The Committee on Neurotoxicology and Models for Assessing Risk, Board on Environmental Studies and Toxicology, Commission on Life Sciences, National Research Council* . *The Quarterly Review of Biology* vol. 69 (1994).

18. Harris, J. B. & Blain, P. G. Neurotoxicology: What the neurologist needs to know. *Neurol. Pract.* **75**, (2004).

19. Kann, O. & Kovács, R. Mitochondria and neuronal activity. *Am. J. Physiol. - Cell Physiol.* **292**, (2007).

20. Schwarz, T. L. Mitochondrial trafficking in neurons. *Cold Spring Harb. Perspect. Med.* **3**, 1–16 (2013).

21. Schmidt, B. Z. *et al.* In vitro acute and developmental neurotoxicity screening: an overview of cellular platforms and high-throughput technical possibilities. *Arch. Toxicol.* **91**, 1–33 (2017).

22. Podratz, J. L. *et al.* Cisplatin induced Mitochondrial DNA damage in dorsal root ganglion neurons. *Neurobiol. Dis.* **41**, 661–668 (2011).

23. Lee, J., Giordano, S. & Zhang, J. Autophagy, mitochondria and oxidative stress: Cross-talk and redox signalling. *Biochem. J.* **441**, 523–540 (2012).

24. Luo, Y. H. *et al.* Cadmium-based quantum dot induced autophagy formation for cell survival via oxidative stress. *Chem. Res. Toxicol.* **26**, 662–673 (2013).

25. Xia, T., Kovochich, M., Liong, M., Zink, J. I. & Nel, A. E. Cationic Polystyrene Nanosphere. *ACS Nano* **2**, 85–96 (2008).

26. Yang, Z. *et al.* A review of nanoparticle functionality and toxicity on the central nervous system. *Nanotechnology, Brain, Futur.* 313–332 (2013) doi:10.1007/978-94-007-1787-9_18.

27. Xu, F., Piett, C., Farkas, S., Qazzaz, M. & Syed, N. I. Silver nanoparticles (AgNPs) cause degeneration of cytoskeleton and disrupt synaptic machinery of cultured cortical neurons. *Mol. Brain* **6**, 1 (2013).

28. Hong, F. *et al.* Suppression of neurite outgrowth of primary cultured hippocampal neurons is involved in impairment of glutamate metabolism and NMDA receptor function caused by nanoparticulate TiO<inf>2</inf>. *Biomaterials* **53**, 76–85 (2015).

29. Liu, Z., Ren, G., Zhang, T. & Yang, Z. The inhibitory effects of nano-Ag on voltage-gated potassium currents of hippocampal CA1 neurons. *Environ. Toxicol.* **26**, 552–558 (2011).

30. Tang, M. *et al.* Mechanisms of unmodified CdSe quantum dot-induced elevation of cytoplasmic calcium levels in primary cultures of rat hippocampal neurons. *Biomaterials* **29**, 4383–4391 (2008).

31. Wei, H. *et al.* Ultrafine carbon black induces glutamate and ATP release by activating connexin and pannexin hemichannels in cultured astrocytes. *Toxicology* **323**, 32–41 (2014).

32. Lolignier, S. *et al.* The Nav1.9 Channel Is a Key Determinant of Cold Pain Sensation and Cold Allodynia. *Cell Rep.* **11**, 1067–1078 (2015).

33. Argyriou, A. A. *et al.* Voltage-gated sodium channel polymorphisms play a pivotal role in the development of oxaliplatin-induced peripheral neurotoxicity: Results from a prospective multicenter study. *Cancer* **119**, 3570–3577 (2013).

34. Ta, L. E. *et al.* Transient Receptor Potential Vanilloid 1 is essential for cisplatin-induced heat hyperalgesia in mice. *Mol. Pain* **6**, 1–15 (2010).

35. Zhao, M. *et al.* Acute cold hypersensitivity characteristically induced by oxaliplatin is caused by the enhanced responsiveness of TRPA1 in mice. *Mol. Pain* **8**, 1–11 (2012).

36. Poupon, L. *et al.* Targeting the TREK-1 potassium channel via riluzole to eliminate the neuropathic and depressive-like effects of oxaliplatin. *Neuropharmacology* **140**, 43–61 (2018).

37. Descoeur, J. *et al.* Oxaliplatin-induced cold hypersensitivity is due to remodelling of ion channel expression in nociceptors. *EMBO Mol. Med.* **3**, 266–278 (2011).

38. Furtado, D. *et al.* Overcoming the Blood–Brain Barrier: The Role of Nanomaterials in Treating Neurological Diseases. *Adv. Mater.* **30**, (2018).

39. Görlach, A., Bertram, K., Hudecova, S. & Krizanova, O. Calcium and ROS: A mutual interplay. *Redox Biol.* **6**, 260–271 (2015).

40. Nayernia, Z., Jaquet, V. & Krause, K. H. New insights on NOX enzymes in the central nervous system. *Antioxidants Redox Signal.* **20**, 2815–2837 (2014).

41. Demaurex, N. & Scorrano, L. Reactive oxygen species are NOXious for neurons. *Nat. Neurosci.* **12**, 819–820 (2009).

42. Genestra, M. Oxyl radicals, redox-sensitive signalling cascades and antioxidants. *Cell. Signal.* **19**, 1807–1819 (2007).

43. Dayem, A. A. *et al.* The role of reactive oxygen species (ROS) in the biological activities of metallic nanoparticles. *Int. J. Mol. Sci.* **18**, 1–21 (2017).

44. Brandes, R. P., Weissmann, N. & Schröder, K. Nox family NADPH oxidases: Molecular mechanisms of activation. *Free Radic. Biol. Med.* **76**, 208–226 (2014).

45. Bedard, K. & Krause, K. H. The NOX family of ROS-generating NADPH oxidases: Physiology and pathophysiology. *Physiol. Rev.* **87**, 245–313 (2007).

46. Ott, M., Gogvadze, V., Orrenius, S. & Zhivotovsky, B. Mitochondria, oxidative stress and cell death. *Apoptosis* **12**, 913–922 (2007).

47. Gaschler, M. M. & Stockwell, B. R. Lipid peroxidation in cell death. *Biochem. Biophys. Res. Commun.* **482**, 419–425 (2017).

48. Berridge, M. J., Bootman, M. D. & Roderick, H. L. Calcium signalling: Dynamics, homeostasis and remodelling. *Nat. Rev. Mol. Cell Biol.* **4**, 517–529 (2003).

49. Raffaello, A., Mammucari, C., Gherardi, G. & Rizzuto, R. Calcium at the Center of Cell Signaling: Interplay between Endoplasmic Reticulum, Mitochondria, and Lysosomes. *Trends Biochem. Sci.* **41**, 1035–1049 (2016).

50. Zecchini, E. & Pinton, P. NIH Public Access. **1787**, 1342–1351 (2010).

51. Berridge, M. J., Lipp, P. & Bootman, M. D. 2000-Review-Calcium Signalling. **1**, (2000).

52. Schwaller, B. Ca2+ buffers. *Handb. Cell Signaling, 2/e* **2**, 955–962 (2010).

53. Boron, W. F. Regulation of intracellular pH. *Am. J. Physiol. - Adv. Physiol. Educ.* **28**, 160–179 (2004).

54. Casey, J. R., Grinstein, S. & Orlowski, J. Sensors and regulators of intracellular pH. *Nat. Rev. Mol. Cell Biol.* **11**, 50–61 (2010).

55. Ruffin, V. A., Salameh, A. I., Boron, W. F. & Parker, M. D. Intracellular pH regulation by acid-base transporters in mammalian neurons. *Front. Physiol.* **5 FEB**, 1–11 (2014).

56. Deitmer, J. W., Theparambil, S. M., Ruminot, I. & Becker, H. M. The role of membrane acid/base transporters and carbonic anhydrases for cellular pH and metabolic processes. *Front. Neurosci.* **9**, (2015).

57. Montell, C. The TRP superfamily of cation channels. *Sci. STKE* **2005**, (2005).

58. Ramsey, I. S., Delling, M. & Clapham, D. E. A i trp c. *October* (2006) doi:10.1146/annurev.physiol.68.040204.100431.

59. Nilius, B. & Owsianik, G. The transient receptor potential family of ion channels. *Genome Biol.* **12**, (2011).

60. Venkatachalam, K. & Montell, C. TRP Channels TRP: Transient Receptor Potential. *Annu Rev Biochem.* **76**, 387–417 (2007).

61. Nilius, B. *et al.* Gating of TRP channels: A voltage connection? *J. Physiol.* **567**, 35–44 (2005).

62. Nilius, B., Mahieu, F., Karashima, Y. & Voets, T. Regulation of TRP channels: A voltage-lipid connection. *Biochem. Soc. Trans.* **35**, 105–108 (2007).

63. Hong, Z. *et al.* Enhanced oxidative stress is responsible for TRPV4-induced neurotoxicity. *Front. Cell. Neurosci.* **10**, 1–8 (2016).

64. Becker, D., Blase, C., Bereiter-Hahn, J. & Jendrach, M. TRPV4 exhibits a functional role in cell-volume regulation. *J. Cell Sci.* **118**, 2435–2440 (2005).

65. Wang, Y. Y., Chang, R. B., Allgood, S. D., Silver, W. L. & Liman, E. R. A TRPA1-dependent mechanism for the pungent sensation of weak acids. *J. Gen. Physiol.* **137**, 493–505 (2011).

66. Dhaka, A. *et al.* TRPV1 is activated by both acidic and basic pH. *J. Neurosci.* **29**, 153–158 (2009).

67. Startek, J. B., Boonen, B., Talavera, K. & Meseguer, V. TRP channels as sensors of chemically-induced changes in cell membrane mechanical properties. *Int. J. Mol. Sci.* **20**, (2019).

68. Kaneko, Y. & Szallasi, A. Transient receptor potential (TRP) channels: A clinical perspective. *Br. J. Pharmacol.* **171**, 2474–2507 (2014).

69. Willebrords, J., Maes, M., Crespo Yanguas, S. & Vinken, M. Inhibitors of connexin and pannexin channels as potential therapeutics. *Pharmacol. Ther.* **180**, 144–160 (2017).

70. Retamal, M. A. Connexin and Pannexin hemichannels are regulated by redox potential. *Front. Physiol.* **5 FEB**, 1–9 (2014).

71. Giaume, C., Leybaert, L., Naus, C. C. & Sáez, J. C. Connexin and pannexin hemichannels in brain glial cells: Properties, pharmacology, and roles. *Front. Pharmacol.* **4 JUL**, 1–17 (2013).

72. Patel, D., Zhang, X. & Veenstra, R. D. Connexin hemichannel and pannexin channel electrophysiology: How do they differ? *FEBS Lett.* **588**, 1372–1378 (2014).

73. Chiu, Y.-H., Schappe, M. S., Desai, B. N. & Bayliss, D. A. Revisiting multimodal activation and channel properties of Pannexin 1. *J. Gen. Physiol.* **150**, 19–39 (2018).

74. Bond, S. R. & Naus, C. C. The pannexins: Past and present. *Front. Physiol.* **5 FEB**, 1–24 (2014).

75. Makarenkova, H. P., Shah, S. B. & Shestopalov, V. I. The two faces of pannexins: New roles in inflammation and repair. *J. Inflamm. Res.* **11**, 273–288 (2018).

76. Niemeyer, M. I., Cid, L. P., Gonzalez, W. & Sepulveda, F. V. Gating, Regulation, and Structure in K2P K+ Channels: In Varietate Concordia? *Mol. Pharmacol.* **90**, 309–317 (2016).

77. Gada, K. & Plant, L. D. Two-pore domain potassium channels: emerging targets for novel analgesic drugs: IUPHAR Review 26. *Br. J. Pharmacol.* **176**, 256–266 (2019).

78. Schewe, M. *et al.* A Non-canonical Voltage-Sensing Mechanism Controls Gating in K2P K+Channels. *Cell* **164**, 937–949 (2016).

79. Li, X. Y. & Toyoda, H. Role of leak potassium channels in pain signaling. *Brain Res. Bull.* **119**, 73–79 (2015).

80. Waxman, S. G. & Zamponi, G. W. Regulating excitability of peripheral afferents: Emerging ion channel targets. *Nat. Neurosci.* **17**, 153–163 (2014).

81. Levitz, J. *et al.* Heterodimerization within the TREK channel subfamily produces a diverse family of highly regulated potassium channels. *Proc. Natl. Acad. Sci.* **113**, 4194–4199 (2016).

82. Radio, N. M. & Mundy, W. R. Developmental neurotoxicity testing in vitro: Models for assessing chemical effects on neurite outgrowth. *Neurotoxicology* **29**, 361–376 (2008).

83. Posimo, J. M. *et al.* Viability assays for cells in culture. *J. Vis. Exp.* **2**, 1–14 (2014).

84. Präbst, K., Engelhardt, H., Ringgeler, S. & Hübner, H. Colorimetric Proliferation Assays. *Basic Color. Prolif. Assays MTT, WST, Resazurin* **1601**, 1–17 (2017).

85. Kumar, P., Nagarajan, A. & Uchil, P. D. Analysis of cell viability by the lactate

dehydrogenase assay. *Cold Spring Harb. Protoc.* **2018**, 465–468 (2018).

86. Tong, Z. Bin *et al.* Characterization of three human cell line models for high-throughput neuronal cytotoxicity screening. *J. Appl. Toxicol.* **37**, 167–180 (2017).

87. McConnell, E. R., McClain, M. A., Ross, J., LeFew, W. R. & Shafer, T. J. Evaluation of multi-well microelectrode arrays for neurotoxicity screening using a chemical training set. *Neurotoxicology* **33**, 1048–1057 (2012).

88. Wheeler, B. C. & Nam, Y. In Vitro Microelectrode Array Technology and Neural Recordings. *Crit. Rev. Biomed. Eng.* **39**, 45–61 (2012).

89. Newberry, K. *et al.* Development of a spontaneously active dorsal root ganglia assay using multiwell multielectrode arrays. *J. Neurophysiol.* **115**, 3217–3228 (2016).

90. Massobrio, P., Tessadori, J., Chiappalone, M. & Ghirardi, M. In vitro studies of neuronal networks and synaptic plasticity in invertebrates and in mammals using multielectrode arrays. *Neural Plast.* **2015**, (2015).

91. Neher, E. & Sakmann, B. Single-channel currents recorded from membrane of denervated frog muscle fibres. *Nature* **260**, 799–802 (1976).

92. Plant, L. D. A Role for K2P Channels in the Operation of Somatosensory Nociceptors. *Front. Mol. Neurosci.* **5**, 1–11 (2012).

93. Lamas, J. A., Rueda-Ruzafa, L. & Herrera-Pérez, S. Ion Channels and Thermosensitivity: TRP, TREK, or Both? *Int. J. Mol. Sci.* **20**, (2019).

94. Zhao, M. *et al.* Acute cold hypersensitivity characteristically induced by oxaliplatin is caused by the enhanced responsiveness of TRPA1 in mice. *Mol. Pain* **8**, 1–11 (2012).

95. Alloui, A. *et al.* TREK-1, a K+ channel involved in polymodal pain perception. *EMBO J.* **25**, 2368–2376 (2006).

96. Noël, J. *et al.* The mechano-activated K±channels TRAAK and TREK-1 control both warm and cold perception. *EMBO J.* **28**, 1308–1318 (2009).

97. Riva, B. *et al.* Oxaliplatin induces pH acidification in dorsal root ganglia neurons. *Sci. Rep.* **8**, 1–12 (2018).

98. Patel, A. J. *et al.* A mammalian two pore domain mechano- gated S- like K + channel. *EMBO J.* **17**, 4283–4290 (1998).

99. Braun, G., Lengyel, M., Enyedi, P. & Czirják, G. Differential sensitivity of TREK-1, TREK-2 and TRAAK background potassium channels to the polycationic dye

ruthenium red. *Br. J. Pharmacol.* **172**, 1728–1738 (2015).

100. Lesage, F., Terrenoire, C., Romey, G. & Lazdunski, M. Human TREK2, a 2P Domain Mechano-sensitive K+Channel with Multiple Regulations by Polyunsaturated Fatty Acids, Lysophospholipids, and Gs, Gi, and GqProtein-coupled Receptors. *J. Biol. Chem.* **275**, 28398–28405 (2000).

101. Renn, C. L. *et al.* Multimodal assessment of painful peripheral neuropathy induced by chronic oxaliplatin-based chemotherapy in mice. *Mol. Pain* **7**, 29 (2011).

102. Marmiroli, P. *et al.* Susceptibility of different mouse strains to oxaliplatin peripheral neurotoxicity: Phenotypic and genotypic insights. *PLoS One* **12**, 1–25 (2017).

103. Noël, J., Sandoz, G. & Lesage, F. Molecular regulations governing TREK and TRAAK channel functions. *Channels* **5**, 402–409 (2011).

104. Kang, D., Choe, C., Cavanaugh, E. & Kim, D. Properties of single two-pore domain TREK-2 channels expressed in mammalian cells. *J. Physiol.* **583**, 57–69 (2007).

105. Fernández-Fernández, D. *et al.* Activation of TREK currents by riluzole in three subgroups of cultured mouse nodose ganglion neurons. *PLoS One* **13**, 1–24 (2018).

106. Kang, D., Choe, C. & Kim, D. Thermosensitivity of the two-pore domain K+ channels TREK-2 and TRAAK. *J. Physiol.* **564**, 103–116 (2005).

107. Kang, D. & Kim, D. TREK-2 (K 2P 10 . 1) and TRESK (K 2P 18 . 1) are major background K ƨ channels in dorsal root ganglion neurons. **2**, 138–146 (2006).

108. Feng, X. *et al.* Central nervous system toxicity of metallic nanoparticles. *Int. J. Nanomedicine* **10**, 4321–4340 (2015).

109. Golbamaki, N. *et al.* Genotoxicity of metal oxide nanomaterials: Review of recent data and discussion of possible mechanisms. *Nanoscale* **7**, 2154–2198 (2015).

110. Wang, Z. *et al.* Silver nanoparticles induced RNA polymerase-silver binding and RNA transcription inhibition in erythroid progenitor cells. *ACS Nano* **7**, 4171–4186 (2013).

111. Lehman, S. E. *et al.* Silica nanoparticle-generated ROS as a predictor of cellular toxicity: mechanistic insights and safety by design. *Environ. Sci. Nano* **3**, 56–66 (2016).

112. Wu, Q. F. *et al.* Activation of transient receptor potential vanilloid 4 involves in hypoxia/reoxygenation injury in cardiomyocytes. *Cell Death Dis.* **8**, e2828 (2017).

113. White, J. P. M. *et al.* TRPV4: Molecular conductor of a diverse orchestra. *Physiol.*

Rev. **96**, 911–973 (2016).

114. Chuang, H. H. & Lin, S. Oxidative challenges sensitize the capsaicin receptor by covalent cysteine modification. *Proc. Natl. Acad. Sci. U. S. A.* **106**, 20097–20102 (2009).

115. Andersson, D. A., Gentry, C., Moss, S. & Bevan, S. Transient receptor potential A1 is a sensory receptor for multiple products of oxidative stress. *J. Neurosci.* **28**, 2485–2494 (2008).

116. Nazıroğlu, M. Activation of TRPM2 and TRPV1 Channels in Dorsal Root Ganglion by NADPH Oxidase and Protein Kinase C Molecular Pathways: a Patch Clamp Study. *Journal of Molecular Neuroscience* vol. 61 425–435 (2017).

117. Descoeur, J. *et al.* Oxaliplatin-induced cold hypersensitivity is due to remodelling of ion channel expression in nociceptors. *EMBO Mol. Med.* **3**, 266–278 (2011).

118. Miyake, T. *et al.* Cold sensitivity of TRPA1 is unveiled by the prolyl hydroxylation blockade-induced sensitization to ROS. *Nat. Commun.* **7**, (2016).

119. Piechotta, P. L. *et al.* The pore structure and gating mechanism of K2P channels. *EMBO J.* **30**, 3607–3619 (2011).

120. Potenzieri, A. *et al.* Oxaliplatin-induced neuropathy occurs through impairment of haemoglobin proton buffering and is reversed by carbonic anhydrase inhibitors. *Pain* **161**, 405–415 (2020).

121. Bucci, E., Fronticelli, C. & Ragatz, B. The proton-binding behavior of human hemoglobin and its subunits in their native state. *J. Biol. Chem.* **243**, 241–249 (1968).

Chapter 6

Concluding Remarks

The central idea of my thesis project during these three years has been to study the role of specific ionic channels and to identify the main mechanisms in which they are involved regarding two cases of neurotoxicity, which were widely documented but not completely understood: 1) the potential neurotoxicity induced by SiO_2 NP and 2) the one induced by OHP.

The control of Ca^{2+} homeostasis is a key point for neuronal physiological and pathological processes. Any single step in neuronal functioning is linked to a tight control of intracellular Ca^{2+} levels and all the mechanisms involved in its regulation[48]. In both cases of neurotoxicity I studied, a dysregulation of Ca^{2+} signalling appears to be a critical starting point [10,15,16].

The two papers by Distasi et al. from 2018 and 2019 (corresponding to Chapters 2 and 3 of this thesis, respectively) give together a detailed electrophysiological characterization of the Ca^{2+} signals elicited by the interaction of 50 nm SiO_2 NPs with the neuronal plasma membrane.

Combining patch-clamp recordings from single neuroendocrine cells (GT1-7) together with population recordings by means of MEAs (Chapter 2) we have correlated oscillatory and reversible changes in $[Ca^{2+}]_i$ in GT1-7, as previously described by Gilardino et al. (2015)[10] for the modulation of the electrical activity elicited by the same non-toxic doses of 50 nm SiO_2 NPs. Three major classes of

channel types are involved: TRPV4 channels, Cx and Panx-like channels. All of these components are known to be involved in a wide spectrum of physiological and pathological processes and characterized by multiple activating mechanisms[60,62,70].

In the last decade, research on the potential toxic effects of NPs have focused on targets such as cell genome[108], as well as mitochondria and the following interruption of the respiratory chain function[23–25].

Ultrastructural and ICP-MS provide evidence that these SiO_2 NPs could be internalized by the activation of an endocytic process after the interaction with plasma membrane. These findings suggest the possibility that also intracellular organelles could represent potential targets. In contrast, the time course of internalization is slower than the onset of the calcium signals [10]. Further evidences that confirm we are describing a membrane-delimited pathway are 1) the fast transient increase in the firing rate of action potentials recorded with MEA early after the administration of SiO_2 NPs, and that 2) the activation of three classes of channels involved has been also observed in excised membrane patches.

The direct role of Ca^{2+} in controlling the transcriptional events were the rational for carrying out the analysis of the whole transcriptome. Interestingly, SiO_2 NPs do not induce transcriptional changes, in our experimental conditions, at any of the analyzed time points (30 min, 1, 6 and 24 hrs). In addition, evidences for DNA damage induced by SiO_2 NPs are limited, and confined to relatively high doses (in most cases over 100 $\mu g\ mL^{-1}$) [109].However, it cannot be excluded a transcriptional or genotoxic effect of these NPs whether a prolonged time window is considered, as described for other nanoparticles [109,110]. Furthermore, NPs toxicity can be influenced by the presence of serum. The different biomolecules which compose the serum may form a complex adsorption layer surrounding the NPs, the so-called protein corona, that may strongly modify the interaction of NP-membrane and

consequently the cellular uptake, cytotoxicity and genotoxicity. It has been described that the toxic doses can change even of a few orders of magnitude when evaluated in the presence or in the absence of serum [109]. In our experimental conditions, even in the absence of FBS, the lack of effects on expression profile are paralleled by a lack in reduction of cell survival.

Several reviews report that NPs induce cytotoxicity by increasing ROS production that, in turn, activate subsequent pathways such as the oxidation of proteins that leads to their aggregation, the oxidation of mitochondrial DNA, and also the perturbation of Ca^{2+} homeostasis[4]. A recent paper has reported that the generation of ROS can be stimulated by SiO_2 NPs in the extracellular environment[111]; however, no specific evidence for neuronal cells can be found in the literature. In this line, we showed (Chapter 3) that lipid peroxidation is significantly increased after 30 minutes exposures with NPs and that the NP-induced [Ca2+]i increases were strongly reduced when the cells were preincubated with the antioxidant NAC. This observation points out that the most relevant mechanism by which SiO_2 NPs elicit the activation of TRPV4 channels and Cx and Panx-like channels is likely related to the production of ROS. As described in the section 1.5 of the Introduction section, all these channels are activated by ROS. In the case of TRPV4, a potential amplification mechanism may be involved, since ROS production has been also observed downstream the TRPV4-mediated Ca^{2+} influx[63,112]. This is also supported by the fact that the same NPs when functionalized with amine groups did not catalyze the production of ROS. This result is in solid agreement with the lack of detectable increases in $[Ca^{2+}]_i$ by aminated NPs[10] and the lack of inward currents in most cells tested (Chapter 3).

However, our explanation does not exclude the possibility that more than one mechanism may coexist. TRPV4, as well as the other two components, is activated

by different chemical and physical stimuli, so for example, mechanotransduction, following membrane stretch due to the interaction with the NP, represents a possible candidate[73,113].

These findings are not limited to the GT1-7 experimental model. Electrophysiological recordings in current clamp mode (Chapter 2) have evidenced that 50 nm SiO_2 NPs elicit similar depolarizing responses also on primary adult neurons. Since each cell type expresses a different set of membrane proteins depending on its needs, in addition to TRPV4, connexin and pannexin-like channels, likely other calcium permeable channels may contribute to the onset of these responses NP-induced in DRG. In particular, TRPV1, TRPA1 and TRPM2, highly expressed channels in these neurons, are known to be activated by oxidizing agents[114–116].

As described in the Introduction section (Chapter 1) TRP channels are an heterogenous class of ion channels that detect a wide variety of external environment stimuli. For this reason, they are considered cellular sensors that mediate a broad range of pato-physiological processes[68].

The peripheral nervous system is one of the regions of the NS more sensible to structural and functional injury in response to toxicants because it is only partially protected by BBB. In detail, the BBB in this area just comprises capillaries with fenestrated walls that allow the free passage of molecules between the bloodstream and the extracellular fluid[18]. This feature explains, in part, why sensory neurons located in DRG and TG are common targets of chemotherapeutic agents like platinum-based drugs[11].

Although the pathomechanism by which these chemotherapeutic agents induce peripheral neurotoxicity was considered multifactorial, alteration of Ca^{2+} signalling seems to be one of the most important factors. Especially in the onset of the OHP-

induced acute syndrome, in which changes in the expression of ion channels and/or their function in primary afferent sensory neurons have been reported[15].

The involvement of TRPV1, TRPA1, TRPM8, known as the main receptors participating in the transduction and generation of pain, was confirmed in OIPN [54]. Among them, we have focused on TRPA1 (Chapter 4). Reported Ca^{2+} imaging data indicate that therapeutically relevant OHP concentrations induce, in our conditions, an hypersensitization of this channel. Although the remodelling of TRPA1 expression has been postulated as one of the mechanisms that may underlie this hypersensitivity[117], our data, obtained by both *in vitro* and *in vivo* assays, failed to detect any mRNA change related to this channel. The same observation was recently obtained by Marmiroli et *al.* (2017)[102]. In light of this, we have correlated the positive modulation of the activity of TRPA1 channels after the treatment with OHP with an alteration of a fundamental parameter for maintaining of neuronal homeostasis, the pH_i. The ionization state and, therefore, the structure and function of virtually all proteins of the cells depends on pH. Intracellular and extracellular moieties of membrane proteins (such as channels, transporters, receptors and even ATPase pumps) provide them extreme sensitivity to pH changes. Thus, a straight correlation between the excitability of the neurons and alterations of this functional parameter exists[55]. In this regard, the resultant hyper-excitability observed in DRG neurons can be interpreted as the effect of multiple adjustments on different molecular targets whose activity is altered by changes in the pH induced by OHP.

Apart from TRPA1, we have evidenced (Chapter 5) the involvement of other molecular targets belonging to TREK-family channels that are widely expressed in DRG and TRG, and also implicated in the mediation of cold hypersensitivity following the treatment with OHP[77,117].

Cell attached recordings showed in Chapter 4 and in Chapter 5 have confirmed that the observed sensitization of TRPA1 and TREK-2-like channels can be reversed by restoring pH to physiological levels. Moreover, these findings are also supported by previous data reporting intracellular pH-dependent activation for both TRPA1[118] and TREK-2[78,119].

Interestingly, in contrast to what happens to TRPA1, OHP promotes a significant increase in the mRNA levels of TREK / TRAAK channels that, in our experimental conditions, is limited to the period right after the OHP treatment (6 h). Such changes in transcript expression are confirmed also *in vivo*. Finally, MEA recordings provide evidence for a parallel decrease in the firing rate of action potentials. Since the augmentation of K^+ leak currents moves V_m closer to potassium Nernst potential (E_K), the cells become less excitable and a larger depolarization is required to generate an action potential. The members of this class of channels work as regulators of the excitability of primary afferent fibers and, thus, of pain signalling by tuning the excitation elicited by several stimuli, including temperature[77,117].

In this regard, the transient overexpression of the background K^+ channels could be interpreted as a tentative of neurons to restore a condition of homeostasis. In detail, the hyperpolarizing currents curried by K_2P channels are counteracting the high depolarization triggered by hyperactivity of TRPA1 OHP-induced.

To study the mechanisms involved in these two cases of neurotoxicity, we have worked under the threshold for toxicity, which were established previously by testing the cell viability. The information presented here may be valuable, particularly for contributing to current knowledge on this subject mainly regarding cells of the nervous system, as some evidence and mechanistic suggestions are provided. Nevertheless, there are some aspects that needs further investigation:

1) The fact that the same NPs can elicit quite similar responses in more than one neuronal cell model, showing different functional properties and different expression of membrane channels, provides evidence that the mechanisms involved may be quite general. Therefore, it could be interesting to study whether analogous responses can be observed with different types of nano-objects on selected cellular models and whether the molecular players involved are the same. Several other reports are available regarding the perturbation of neuronal excitability and synaptic transmission (ref) induced by NPs but, to our knowledge, this is the first detailed electrophysiological description of the changes in electrical activity of neurons following exposure to a nanoparticle, and of its evolution in time.

More information on the specific channels and mechanisms responsible for the observed effects would be useful for a better design of safe and efficient tools for nanomedicine.

2) At present, no explanation for the pH homeostasis alteration can be done. We observed that oxalate antagonized the change in pH (Chapter 4), without any negative impact on the cytotoxic effects of OHP (in any of the 6 colorectal cell lines tested). This finding suggests that OHP-induced pH acidification occurs via a specific and saturable mechanism.

A recent report[120] shows that OHP creates adducts with neuronal haemoglobin (HB) that acts as a proton-buffer, as reported for the red blood cells[121]. However, more players are probably involved in the mechanism underlying the intracellular acidification.

The pH_i homeostasis is a complex process. At any instant in time, the rate of pH_i change depends on the total intracellular buffering power and the balance between acid-loading and acid-extruding rates and the way to alter steady-state pH_i is to alter the fundamental kinetics of JE and JL[53].

Therefore, it could be interesting to study whether OHP directly interferes with the activity of proton pumps, transporters and channels.

References

1. Chepelev, N. L., Moffat, I. D., Bowers, W. J. & Yauk, C. L. Neurotoxicity may be an overlooked consequence of benzo[a]pyrene exposure that is relevant to human health risk assessment. *Mutat. Res. - Rev. Mutat. Res.* **764**, 64–89 (2015).
2. Teleanu, D., Chircov, C., Grumezescu, A., Volceanov, A. & Teleanu, R. Impact of Nanoparticles on Brain Health: An Up to Date Overview. *J. Clin. Med.* **7**, 490 (2018).
3. Ge, D. *et al.* The neurotoxicity induced by engineered nanomaterials. *Int. J. Nanomedicine* **14**, 4167–4186 (2019).
4. Lovisolo, D., Dionisi, M., A. Ruffinatti, F. & Distasi, C. Nanoparticles and potential neurotoxicity: focus on molecular mechanisms. *AIMS Mol. Sci.* **5**, 1–13 (2018).
5. Bannunah, A. M., Vllasaliu, D., Lord, J. & Stolnik, S. Mechanisms of nanoparticle internalization and transport across an intestinal epithelial cell model: Effect of size and surface charge. *Mol. Pharm.* **11**, 4363–4373 (2014).
6. Lin, J. & Alexander-Katz, A. Cell membranes open 'doors' for cationic nanoparticles/ biomolecules: Insights into uptake kinetics. *ACS Nano* **7**, 10799–10808 (2013).
7. Zanella, D. *et al.* The direct permeation of nanoparticles through the plasma membrane transiently modifies its properties. *Biochim. Biophys. Acta - Biomembr.* **1861**, 182997 (2019).
8. Narayan, R., Nayak, U. Y., Raichur, A. M. & Garg, S. Mesoporous silica nanoparticles: A comprehensive review on synthesis and recent advances. *Pharmaceutics* **10**, 1–49 (2018).
9. Ariano, P. *et al.* Interaction of spherical silica nanoparticles with neuronal cells: Size-dependent toxicity and perturbation of calcium homeostasis.

Small **7**, 766–774 (2011).

10. Gilardino, A. *et al.* Interaction of SiO<inf>2</inf> nanoparticles with neuronal cells: Ionic mechanisms involved in the perturbation of calcium homeostasis. *Int. J. Biochem. Cell Biol.* **66**, 101–111 (2015).
11. Zajaczkowską, R. *et al.* Mechanisms of chemotherapy-induced peripheral neuropathy. *Int. J. Mol. Sci.* **20**, (2019).
12. Aromolaran, K. A. & Goldstein, P. A. Ion channels and neuronal hyperexcitability in chemotherapy-induced peripheral neuropathy: Cause and effect? *Mol. Pain* **13**, 1–24 (2017).
13. Grisold, W., Cavaletti, G. & Windebank, A. J. Peripheral neuropathies from chemotherapeutics and targeted agents : *Neuro. Oncol.* **14**, 45–54 (2012).
14. Park, S. B. *et al.* <CA CANCER J CLIN 2013_Park_peripheral neuropathy cisplatin.pdf>. *CA Cancer J. Clin.* **63**, 419–437 (2013).
15. Chiorazzi, A., Semperboni, S. & Marmiroli, P. Current view in platinum drug mechanisms of peripheral neurotoxicity. *Toxics* **3**, 304–321 (2015).
16. Paola Marmiroli, Guido Cavaletti, Valentina Carozzi, Beatrice Riva, Dmitry Lim, A. A. G. Calcium-related Neurotoxicity of Oxaliplatin: Understanding the Mechanisms to Drive Therapy. Current Medicinal Chemistry Volume 22, Issue 32 , (2015).
17. Kaufman, M. A. *Environmental Neurotoxicology. The Committee on Neurotoxicology and Models for Assessing Risk, Board on Environmental Studies and Toxicology, Commission on Life Sciences, National Research Council* . *The Quarterly Review of Biology* vol. 69 (1994).
18. Harris, J. B. & Blain, P. G. Neurotoxicology: What the neurologist needs to know. *Neurol. Pract.* **75**, (2004).
19. Kann, O. & Kovács, R. Mitochondria and neuronal activity. *Am. J. Physiol. - Cell Physiol.* **292**, (2007).

20. Schwarz, T. L. Mitochondrial trafficking in neurons. *Cold Spring Harb. Perspect. Med.* **3**, 1–16 (2013).
21. Schmidt, B. Z. *et al.* In vitro acute and developmental neurotoxicity screening: an overview of cellular platforms and high-throughput technical possibilities. *Arch. Toxicol.* **91**, 1–33 (2017).
22. Podratz, J. L. *et al.* Cisplatin induced Mitochondrial DNA damage in dorsal root ganglion neurons. *Neurobiol. Dis.* **41**, 661–668 (2011).
23. Lee, J., Giordano, S. & Zhang, J. Autophagy, mitochondria and oxidative stress: Cross-talk and redox signalling. *Biochem. J.* **441**, 523–540 (2012).
24. Luo, Y. H. *et al.* Cadmium-based quantum dot induced autophagy formation for cell survival via oxidative stress. *Chem. Res. Toxicol.* **26**, 662–673 (2013).
25. Xia, T., Kovochich, M., Liong, M., Zink, J. I. & Nel, A. E. Cationic Polystyrene Nanosphere. *ACS Nano* **2**, 85–96 (2008).
26. Yang, Z. *et al.* A review of nanoparticle functionality and toxicity on the central nervous system. *Nanotechnology, Brain, Futur.* 313–332 (2013) doi:10.1007/978-94-007-1787-9_18.
27. Xu, F., Piett, C., Farkas, S., Qazzaz, M. & Syed, N. I. Silver nanoparticles (AgNPs) cause degeneration of cytoskeleton and disrupt synaptic machinery of cultured cortical neurons. *Mol. Brain* **6**, 1 (2013).
28. Hong, F. *et al.* Suppression of neurite outgrowth of primary cultured hippocampal neurons is involved in impairment of glutamate metabolism and NMDA receptor function caused by nanoparticulate TiO<inf>2</inf>. *Biomaterials* **53**, 76–85 (2015).
29. Liu, Z., Ren, G., Zhang, T. & Yang, Z. The inhibitory effects of nano-Ag on voltage-gated potassium currents of hippocampal CA1 neurons. *Environ. Toxicol.* **26**, 552–558 (2011).
30. Tang, M. *et al.* Mechanisms of unmodified CdSe quantum dot-induced

elevation of cytoplasmic calcium levels in primary cultures of rat hippocampal neurons. *Biomaterials* **29**, 4383–4391 (2008).

31. Wei, H. *et al.* Ultrafine carbon black induces glutamate and ATP release by activating connexin and pannexin hemichannels in cultured astrocytes. *Toxicology* **323**, 32–41 (2014).
32. Lolignier, S. *et al.* The Nav1.9 Channel Is a Key Determinant of Cold Pain Sensation and Cold Allodynia. *Cell Rep.* **11**, 1067–1078 (2015).
33. Argyriou, A. A. *et al.* Voltage-gated sodium channel polymorphisms play a pivotal role in the development of oxaliplatin-induced peripheral neurotoxicity: Results from a prospective multicenter study. *Cancer* **119**, 3570–3577 (2013).
34. Ta, L. E. *et al.* Transient Receptor Potential Vanilloid 1 is essential for cisplatin-induced heat hyperalgesia in mice. *Mol. Pain* **6**, 1–15 (2010).
35. Zhao, M. *et al.* Acute cold hypersensitivity characteristically induced by oxaliplatin is caused by the enhanced responsiveness of TRPA1 in mice. *Mol. Pain* **8**, 1–11 (2012).
36. Poupon, L. *et al.* Targeting the TREK-1 potassium channel via riluzole to eliminate the neuropathic and depressive-like effects of oxaliplatin. *Neuropharmacology* **140**, 43–61 (2018).
37. Descoeur, J. *et al.* Oxaliplatin-induced cold hypersensitivity is due to remodelling of ion channel expression in nociceptors. *EMBO Mol. Med.* **3**, 266–278 (2011).
38. Furtado, D. *et al.* Overcoming the Blood–Brain Barrier: The Role of Nanomaterials in Treating Neurological Diseases. *Adv. Mater.* **30**, (2018).
39. Görlach, A., Bertram, K., Hudecova, S. & Krizanova, O. Calcium and ROS: A mutual interplay. *Redox Biol.* **6**, 260–271 (2015).
40. Nayernia, Z., Jaquet, V. & Krause, K. H. New insights on NOX enzymes in the

central nervous system. *Antioxidants Redox Signal.* **20**, 2815–2837 (2014).

41. Demaurex, N. & Scorrano, L. Reactive oxygen species are NOXious for neurons. *Nat. Neurosci.* **12**, 819–820 (2009).
42. Genestra, M. Oxyl radicals, redox-sensitive signalling cascades and antioxidants. *Cell. Signal.* **19**, 1807–1819 (2007).
43. Dayem, A. A. *et al.* The role of reactive oxygen species (ROS) in the biological activities of metallic nanoparticles. *Int. J. Mol. Sci.* **18**, 1–21 (2017).
44. Brandes, R. P., Weissmann, N. & Schröder, K. Nox family NADPH oxidases: Molecular mechanisms of activation. *Free Radic. Biol. Med.* **76**, 208–226 (2014).
45. Bedard, K. & Krause, K. H. The NOX family of ROS-generating NADPH oxidases: Physiology and pathophysiology. *Physiol. Rev.* **87**, 245–313 (2007).
46. Ott, M., Gogvadze, V., Orrenius, S. & Zhivotovsky, B. Mitochondria, oxidative stress and cell death. *Apoptosis* **12**, 913–922 (2007).
47. Gaschler, M. M. & Stockwell, B. R. Lipid peroxidation in cell death. *Biochem. Biophys. Res. Commun.* **482**, 419–425 (2017).
48. Berridge, M. J., Bootman, M. D. & Roderick, H. L. Calcium signalling: Dynamics, homeostasis and remodelling. *Nat. Rev. Mol. Cell Biol.* **4**, 517–529 (2003).
49. Raffaello, A., Mammucari, C., Gherardi, G. & Rizzuto, R. Calcium at the Center of Cell Signaling: Interplay between Endoplasmic Reticulum, Mitochondria, and Lysosomes. *Trends Biochem. Sci.* **41**, 1035–1049 (2016).
50. Zecchini, E. & Pinton, P. NIH Public Access. **1787**, 1342–1351 (2010).
51. Berridge, M. J., Lipp, P. & Bootman, M. D. 2000-Review-Calcium Signalling. **1**, (2000).

52. Schwaller, B. Ca2+ buffers. *Handb. Cell Signaling, 2/e* **2**, 955–962 (2010).
53. Boron, W. F. Regulation of intracellular pH. *Am. J. Physiol. - Adv. Physiol. Educ.* **28**, 160–179 (2004).
54. Casey, J. R., Grinstein, S. & Orlowski, J. Sensors and regulators of intracellular pH. *Nat. Rev. Mol. Cell Biol.* **11**, 50–61 (2010).
55. Ruffin, V. A., Salameh, A. I., Boron, W. F. & Parker, M. D. Intracellular pH regulation by acid-base transporters in mammalian neurons. *Front. Physiol.* **5 FEB**, 1–11 (2014).
56. Deitmer, J. W., Theparambil, S. M., Ruminot, I. & Becker, H. M. The role of membrane acid/base transporters and carbonic anhydrases for cellular pH and metabolic processes. *Front. Neurosci.* **9**, (2015).
57. Montell, C. The TRP superfamily of cation channels. *Sci. STKE* **2005**, (2005).
58. Ramsey, I. S., Delling, M. & Clapham, D. E. A i trp c. *October* (2006) doi:10.1146/annurev.physiol.68.040204.100431.
59. Nilius, B. & Owsianik, G. The transient receptor potential family of ion channels. *Genome Biol.* **12**, (2011).
60. Venkatachalam, K. & Montell, C. TRP Channels TRP: Transient Receptor Potential. *Annu Rev Biochem.* **76**, 387–417 (2007).
61. Nilius, B. *et al.* Gating of TRP channels: A voltage connection? *J. Physiol.* **567**, 35–44 (2005).
62. Nilius, B., Mahieu, F., Karashima, Y. & Voets, T. Regulation of TRP channels: A voltage-lipid connection. *Biochem. Soc. Trans.* **35**, 105–108 (2007).
63. Hong, Z. *et al.* Enhanced oxidative stress is responsible for TRPV4-induced neurotoxicity. *Front. Cell. Neurosci.* **10**, 1–8 (2016).
64. Becker, D., Blase, C., Bereiter-Hahn, J. & Jendrach, M. TRPV4 exhibits a functional role in cell-volume regulation. *J. Cell Sci.* **118**, 2435–2440 (2005).
65. Wang, Y. Y., Chang, R. B., Allgood, S. D., Silver, W. L. & Liman, E. R. A TRPA1-

dependent mechanism for the pungent sensation of weak acids. *J. Gen. Physiol.* **137**, 493–505 (2011).

66. Dhaka, A. *et al.* TRPV1 is activated by both acidic and basic pH. *J. Neurosci.* **29**, 153–158 (2009).
67. Startek, J. B., Boonen, B., Talavera, K. & Meseguer, V. TRP channels as sensors of chemically-induced changes in cell membrane mechanical properties. *Int. J. Mol. Sci.* **20**, (2019).
68. Kaneko, Y. & Szallasi, A. Transient receptor potential (TRP) channels: A clinical perspective. *Br. J. Pharmacol.* **171**, 2474–2507 (2014).
69. Willebrords, J., Maes, M., Crespo Yanguas, S. & Vinken, M. Inhibitors of connexin and pannexin channels as potential therapeutics. *Pharmacol. Ther.* **180**, 144–160 (2017).
70. Retamal, M. A. Connexin and Pannexin hemichannels are regulated by redox potential. *Front. Physiol.* **5 FEB**, 1–9 (2014).
71. Giaume, C., Leybaert, L., Naus, C. C. & Sáez, J. C. Connexin and pannexin hemichannels in brain glial cells: Properties, pharmacology, and roles. *Front. Pharmacol.* **4 JUL**, 1–17 (2013).
72. Patel, D., Zhang, X. & Veenstra, R. D. Connexin hemichannel and pannexin channel electrophysiology: How do they differ? *FEBS Lett.* **588**, 1372–1378 (2014).
73. Chiu, Y.-H., Schappe, M. S., Desai, B. N. & Bayliss, D. A. Revisiting multimodal activation and channel properties of Pannexin 1. *J. Gen. Physiol.* **150**, 19–39 (2018).
74. Bond, S. R. & Naus, C. C. The pannexins: Past and present. *Front. Physiol.* **5 FEB**, 1–24 (2014).
75. Makarenkova, H. P., Shah, S. B. & Shestopalov, V. I. The two faces of pannexins: New roles in inflammation and repair. *J. Inflamm. Res.* **11**, 273–

288 (2018).

76. Niemeyer, M. I., Cid, L. P., Gonzalez, W. & Sepulveda, F. V. Gating, Regulation, and Structure in K2P K+ Channels: In Varietate Concordia? *Mol. Pharmacol.* **90**, 309–317 (2016).

77. Gada, K. & Plant, L. D. Two-pore domain potassium channels: emerging targets for novel analgesic drugs: IUPHAR Review 26. *Br. J. Pharmacol.* **176**, 256–266 (2019).

78. Schewe, M. *et al.* A Non-canonical Voltage-Sensing Mechanism Controls Gating in K2P K+Channels. *Cell* **164**, 937–949 (2016).

79. Li, X. Y. & Toyoda, H. Role of leak potassium channels in pain signaling. *Brain Res. Bull.* **119**, 73–79 (2015).

80. Waxman, S. G. & Zamponi, G. W. Regulating excitability of peripheral afferents: Emerging ion channel targets. *Nat. Neurosci.* **17**, 153–163 (2014).

81. Levitz, J. *et al.* Heterodimerization within the TREK channel subfamily produces a diverse family of highly regulated potassium channels. *Proc. Natl. Acad. Sci.* **113**, 4194–4199 (2016).

82. Radio, N. M. & Mundy, W. R. Developmental neurotoxicity testing in vitro: Models for assessing chemical effects on neurite outgrowth. *Neurotoxicology* **29**, 361–376 (2008).

83. Posimo, J. M. *et al.* Viability assays for cells in culture. *J. Vis. Exp.* **2**, 1–14 (2014).

84. Präbst, K., Engelhardt, H., Ringgeler, S. & Hübner, H. Colorimetric Proliferation Assays. *Basic Color. Prolif. Assays MTT, WST, Resazurin* **1601**, 1–17 (2017).

85. Kumar, P., Nagarajan, A. & Uchil, P. D. Analysis of cell viability by the lactate dehydrogenase assay. *Cold Spring Harb. Protoc.* **2018**, 465–468 (2018).

86. Tong, Z. Bin *et al.* Characterization of three human cell line models for high-

throughput neuronal cytotoxicity screening. *J. Appl. Toxicol.* **37**, 167–180 (2017).

87. McConnell, E. R., McClain, M. A., Ross, J., LeFew, W. R. & Shafer, T. J. Evaluation of multi-well microelectrode arrays for neurotoxicity screening using a chemical training set. *Neurotoxicology* **33**, 1048–1057 (2012).
88. Wheeler, B. C. & Nam, Y. In Vitro Microelectrode Array Technology and Neural Recordings. *Crit. Rev. Biomed. Eng.* **39**, 45–61 (2012).
89. Newberry, K. *et al.* Development of a spontaneously active dorsal root ganglia assay using multiwell multielectrode arrays. *J. Neurophysiol.* **115**, 3217–3228 (2016).
90. Massobrio, P., Tessadori, J., Chiappalone, M. & Ghirardi, M. In vitro studies of neuronal networks and synaptic plasticity in invertebrates and in mammals using multielectrode arrays. *Neural Plast.* **2015**, (2015).
91. Neher, E. & Sakmann, B. Single-channel currents recorded from membrane of denervated frog muscle fibres. *Nature* **260**, 799–802 (1976).
92. Plant, L. D. A Role for K2P Channels in the Operation of Somatosensory Nociceptors. *Front. Mol. Neurosci.* **5**, 1–11 (2012).
93. Lamas, J. A., Rueda-Ruzafa, L. & Herrera-Pérez, S. Ion Channels and Thermosensitivity: TRP, TREK, or Both? *Int. J. Mol. Sci.* **20**, (2019).
94. Zhao, M. *et al.* Acute cold hypersensitivity characteristically induced by oxaliplatin is caused by the enhanced responsiveness of TRPA1 in mice. *Mol. Pain* **8**, 1–11 (2012).
95. Alloui, A. *et al.* TREK-1, a K+ channel involved in polymodal pain perception. *EMBO J.* **25**, 2368–2376 (2006).
96. Noël, J. *et al.* The mechano-activated K±channels TRAAK and TREK-1 control both warm and cold perception. *EMBO J.* **28**, 1308–1318 (2009).
97. Riva, B. *et al.* Oxaliplatin induces pH acidification in dorsal root ganglia

neurons. *Sci. Rep.* **8**, 1–12 (2018).

98. Patel, A. J. *et al.* A mammalian two pore domain mechano- gated S- like K + channel. *EMBO J.* **17**, 4283–4290 (1998).

99. Braun, G., Lengyel, M., Enyedi, P. & Czirják, G. Differential sensitivity of TREK-1, TREK-2 and TRAAK background potassium channels to the polycationic dye ruthenium red. *Br. J. Pharmacol.* **172**, 1728–1738 (2015).

100. Lesage, F., Terrenoire, C., Romey, G. & Lazdunski, M. Human TREK2, a 2P Domain Mechano-sensitive K+Channel with Multiple Regulations by Polyunsaturated Fatty Acids, Lysophospholipids, and Gs, Gi, and GqProtein-coupled Receptors. *J. Biol. Chem.* **275**, 28398–28405 (2000).

101. Renn, C. L. *et al.* Multimodal assessment of painful peripheral neuropathy induced by chronic oxaliplatin-based chemotherapy in mice. *Mol. Pain* **7**, 29 (2011).

102. Marmiroli, P. *et al.* Susceptibility of different mouse strains to oxaliplatin peripheral neurotoxicity: Phenotypic and genotypic insights. *PLoS One* **12**, 1–25 (2017).

103. Noël, J., Sandoz, G. & Lesage, F. Molecular regulations governing TREK and TRAAK channel functions. *Channels* **5**, 402–409 (2011).

104. Kang, D., Choe, C., Cavanaugh, E. & Kim, D. Properties of single two-pore domain TREK-2 channels expressed in mammalian cells. *J. Physiol.* **583**, 57–69 (2007).

105. Fernández-Fernández, D. *et al.* Activation of TREK currents by riluzole in three subgroups of cultured mouse nodose ganglion neurons. *PLoS One* **13**, 1–24 (2018).

106. Kang, D., Choe, C. & Kim, D. Thermosensitivity of the two-pore domain K+ channels TREK-2 and TRAAK. *J. Physiol.* **564**, 103–116 (2005).

107. Kang, D. & Kim, D. TREK-2 (K 2P 10 . 1) and TRESK (K 2P 18 . 1) are major

background K ƨ channels in dorsal root ganglion neurons. **2**, 138–146 (2006).

108. Feng, X. *et al.* Central nervous system toxicity of metallic nanoparticles. *Int. J. Nanomedicine* **10**, 4321–4340 (2015).
109. Golbamaki, N. *et al.* Genotoxicity of metal oxide nanomaterials: Review of recent data and discussion of possible mechanisms. *Nanoscale* **7**, 2154–2198 (2015).
110. Wang, Z. *et al.* Silver nanoparticles induced RNA polymerase-silver binding and RNA transcription inhibition in erythroid progenitor cells. *ACS Nano* **7**, 4171–4186 (2013).
111. Lehman, S. E. *et al.* Silica nanoparticle-generated ROS as a predictor of cellular toxicity: mechanistic insights and safety by design. *Environ. Sci. Nano* **3**, 56–66 (2016).
112. Wu, Q. F. *et al.* Activation of transient receptor potential vanilloid 4 involves in hypoxia/reoxygenation injury in cardiomyocytes. *Cell Death Dis.* **8**, e2828 (2017).
113. White, J. P. M. *et al.* TRPV4: Molecular conductor of a diverse orchestra. *Physiol. Rev.* **96**, 911–973 (2016).
114. Chuang, H. H. & Lin, S. Oxidative challenges sensitize the capsaicin receptor by covalent cysteine modification. *Proc. Natl. Acad. Sci. U. S. A.* **106**, 20097–20102 (2009).
115. Andersson, D. A., Gentry, C., Moss, S. & Bevan, S. Transient receptor potential A1 is a sensory receptor for multiple products of oxidative stress. *J. Neurosci.* **28**, 2485–2494 (2008).
116. Nazıroğlu, M. Activation of TRPM2 and TRPV1 Channels in Dorsal Root Ganglion by NADPH Oxidase and Protein Kinase C Molecular Pathways: a Patch Clamp Study. *Journal of Molecular Neuroscience* vol. 61 425–435

(2017).

117. Descoeur, J. *et al.* Oxaliplatin-induced cold hypersensitivity is due to remodelling of ion channel expression in nociceptors. *EMBO Mol. Med.* **3**, 266–278 (2011).

118. Miyake, T. *et al.* Cold sensitivity of TRPA1 is unveiled by the prolyl hydroxylation blockade-induced sensitization to ROS. *Nat. Commun.* **7**, (2016).

119. Piechotta, P. L. *et al.* The pore structure and gating mechanism of K2P channels. *EMBO J.* **30**, 3607–3619 (2011).

120. Potenzieri, A. *et al.* Oxaliplatin-induced neuropathy occurs through impairment of haemoglobin proton buffering and is reversed by carbonic anhydrase inhibitors. *Pain* **161**, 405–415 (2020).

121. Bucci, E., Fronticelli, C. & Ragatz, B. The proton-binding behavior of human hemoglobin and its subunits in their native state. *J. Biol. Chem.* **243**, 241–249 (1968).

Abbreviations

NPs = nanoparticles

SiO_2 NP = silica nanoparticles

OHP = Oxaliplatin

NMs = Nanomaterials

ISO = The International Organization for Standardization

CNS = Central nervous system

QDs = Quantum dots (QDs)

CIPN = Chemotherapy-induced peripheral neuropathy

TNF-α = tumor necrosis factor alpha

NF-kB = nuclear factor kappa B

b-FGF = basic fibroblast growth factor

VEGF = vascular endothelial growth factor

BBBs = blood–brain barriers

mtDNA = mitochondrial DNA

ROS = reactive oxygen species

PM10 = particulate matter 10

DNA = deoxyribonucleic acid

ATP = adenosine triphosphate

TRP = transient receptor potential channels

Na_V = voltage-gated sodium channels

K_2P = two-pore domain potassium channels

BCSFB = blood–cerebrospinal fluid barrier

CSF = cerebrospinal fluid

BMECs = brain microvessel endothelial cells

ISF = interstitial fluid

NVU = neurovascular unit

EC = endothelial cells

NADPH = nicotinamide adenine dinucleotide phosphate

ER = endoplasmic reticulum

FADH2 = Flavin adenine dinucleotide

NOX = nicotinamide adenine dinucleotide phosphate oxidases

O^{2-} = superoxide anion

SOD = superoxide dismutase

H_2O_2 = hydrogen peroxide

OH = hydroxyl radicals

MPT = mitochondrial permeability transition

PTP = permeability transition pores

PMCA = plasma membrane Ca^{2+} ATPase

NCX = sodium-calcium exchanger

VOCCs = Voltage-operated Ca^{2+} channels

NMDA = N-methyl-D-aspartate

NMDARs = NMDA receptors

ROCs = receptor-operated channels

SMOCs = second-messenger-operated channels

SR = sarcoplasmatic reticulum

Ins(1,4,5)P3 = inositol-1,4,5-trisphosphate

cADPR = cyclic ADP ribose

NAADP = nicotinic acid adenine dinucleotide phosphate

S1P = sphingosine-1-phosphate

RYR = ryanodine receptors

Ins (1,4,5) P_3R = inositol (1,4,5) trisphosphate receptors

CICR = Ca^{2+}-induced Ca^{2+} release

V-ATPase = vacuolar H^+-ATPase

NHE = Na^+-H^+ exchangers

NCBTs = Na^+-coupled HCO_3^- transporters

PtdIns (4,5) P_2 = phosphatidylinositol (4,5) bisphosphate

PLCs = phospholipases C

GPCRs = G protein–coupled receptors

DAG = diacylglycerol

PUFAs = polyunsaturated fatty

AA = arachidonic acid

SOCE = store-operated Ca^{2+} entry

CCE = capacitative Ca^{2+} entry

ALS-G = guamanian amyotrophic lateral sclerosis

GJs = Gap junctions

HCs = hemichannels

Cx = connexin

EL = extracellular loops

CL = cytoplasmic loop

CT = cytoplasmic C-terminal tail

NAD^+ = nicotinamide adenine dinucleotide

ODDD = oculodentodigital dysplasia

Panx = pannexin

K_V = voltage-gated potassium channels

Kir = inwardly rectifying potassium channels

SF = selectivity filter

LDH= lactate dehydrogenase

MEAs = Multielectrode arrays

APC = automated patch-clamp

NAC = N-acetyl-L-cysteine

BCTC = 4-(3-Chloro-2-pyridinyl)-*N*-[4-(1,1-dimethylethyl)phenyl]-1-piperazinecarboxamide

OIPN = oxaliplatin-induced peripheral neuropathy

TEOS = tetraethylorthosilicate

HRTEM = high resolution transmission electron microscopy

DLS =dynamic light scattering

GnRH = gonadotropin-hormone releasing hormone

DMEM = Dulbecco's modified eagle's medium

NGF = nerve growth factor

GDNF = glial derived neurotrophic factor

NT3 = neurotrophin-3 factor

TEM = transmission electron microscopy

ICP-MS = inductively coupled plasma mass spectrometry

EAPs = extracellular action potentials

SEM = scanning electron microscope

LAA = linoleamide alkyne

CCD = charge-coupled device camera

CBX = carbenoxolone

RR = ruthenium red

BCECF = 2',7'-Bis-(2-Carboxyethyl)-5-(and-6)-Carboxyfluorescein, Acetoxymethyl Ester

DIDS = 4,4’-Diisothiocyano-2,2’-stilbenedisulfonic acid

DMSO = dimethyl sulfoxide

Ringraziamenti

Un doveroso, ma soprattutto sentito, ringraziamento va alla Prof. Carla Distasi, per la disponibilità che mi ha sempre mostrato e per tutti i suoi insegnamenti che hanno guidato la mia attività in questi anni e di cui farò tesoro per il futuro.
Vorrei inoltre ringraziare il Prof. Davide Lovisolo, coordinatore della mia tesi durante il corso di Laurea Magistrale in Biologia molecolare e cellulare, è stato un punto di riferimento costante anche durante questi anni di dottorato.
Un ringraziamento va anche al Dottor Federico Alessandro Ruffinatti e alla Dottoressa Beatrice Riva, il loro aiuto e supporto è stato fondamentale per la stesura di questa tesi.

Ed infine un grazie a tutti gli amici e parenti che, da vicino e lontano, hanno contribuito a mantenere la giusta atmosfera di serenità intorno a me.